The Role of Mesenchymal G Proteins in Pulmonary Fibrosis and Lung Development

Amanda Tracie Goodwin, MBChB MSc

Thesis submitted to the University of Nottingham for the degree of Doctor of Philosophy

January 2021

For Quinn Rose

Abstract

The maintenance of lung homeostasis is complex and involves the concerted actions of numerous cell types and signalling pathways. Any disturbance to these intricate processes and interactions can result in lung disease, such as pulmonary fibrosis. In pulmonary fibrosis, an abnormal wound healing response involving the abnormal recapitulation of developmental signalling pathways occurs, resulting in scarring of the lungs. An understanding of normal lung developmental pathways, and how they become abnormally reactivated in pulmonary fibrosis, may hold the key to creating regenerative strategies to benefit patients with this condition.

Mesenchymal cells, including fibroblasts, myofibroblasts, and pericytes, play several roles in maintaining lung homeostasis, including the manipulation of extracellular matrix (ECM) properties such as content and mechanical stiffness, cellular crosstalk and transdifferentiation, and transforming growth factor-β (TGFβ) activation. These cells can respond to both chemical and mechanical stimuli, and any disturbance to these external influences can result in an imbalance between lung repair and cellular quiescence, as seen in pulmonary fibrosis. In the developing lung abnormal mesenchymal cell function can halt or disturb normal

developmental processes resulting in structural lung abnormalities, for example as seen in bronchopulmonary dysplasia (BPD). An understanding of how mesenchymal cells detect chemical and mechanical stimuli in lung development and disease could inform the treatment of both pulmonary fibrosis and BPD.

G proteins are essential signalling mediators in numerous physiological processes, mammalian organ development and in the pathogenesis of pulmonary fibrosis. However, the exact roles of these proteins in mesenchymal cell function have not been determined. The aim of this study was to understand the role of the mesenchymal cell G protein families $G_{\alpha q/11}$ and $G_{\alpha 12/13}$ in the pathogenesis of pulmonary fibrosis and provide insight into the manipulation of these signalling mediators as a therapeutic strategy for this condition. This study also aimed to assess the potential adverse effects associated with G protein inhibition *in vivo*.

Mice lacking mesenchymal $G_{\alpha q/11}$ (*Pdgfrb-Cre*$^{+/-}$*;Gnaq*$^{fl/fl}$*;Gna11*$^{-/-}$) from conception had a severely detrimental phenotype, which included growth restriction and abnormal lung appearances consistent with disturbed alveolarisation and reminiscent of BPD. Furthermore, mice lacking mesenchymal $G_{\alpha 12/13}$ from conception (*Pdgfrb-Cre/ERT2;Gna12*$^{-/-}$*;Gna13*$^{fl/fl}$) were born abnormally infrequently, suggesting that this genotype resulted in death *in utero*. While it was hypothesised that mesenchymal cell $G_{\alpha q/11}$ or $G_{\alpha 12/13}$ inhibition may be protective against pulmonary fibrosis, the physical condition of these transgenic mice precluded their use for *in vivo* pulmonary fibrosis models.

In vitro experiments demonstrated that breathing-related cyclical stretch induced TGFβ signalling in fibroblasts, and this response was elevated in human lung fibroblasts from donors with pulmonary fibrosis. Furthermore, fibrotic human lung fibroblasts were more contractile than non-diseased cells, implying that these cells have greater ECM-organising abilities. Further experiments revealed that $G_{\alpha q/11}$, but not $G_{\alpha 12/13}$, is essential for stretch-mediated TGFβ activation through the generation of TGFβ2. When the response to matrix stiffness was assessed, this study found that $G_{\alpha q/11}$ also modulates the myofibroblast phenotype in response to ECM stiffness. Conversely, a contraction assay showed that $G_{\alpha 12/13}$, but not $G_{\alpha q/11}$, is essential for fibroblast contractility at baseline and in response to the G protein coupled receptor (GPCR) agonist lysophosphatidic acid (LPA). Both $G_{\alpha q/11}$ and $G_{\alpha 12/13}$ were found to be important mediators of LPA-induced TGFβ signalling in fibroblasts. As stretch, cellular contraction, ECM properties, and TGFβ signalling are all important in the pathogenesis of pulmonary fibrosis and for normal alveolarisation processes, this study highlights the roles of $G_{\alpha q/11}$ and $G_{\alpha 12/13}$ as shared signalling pathway components between development and disease.

When a tamoxifen-inducible conditional gene knockout model was used mice with mesenchymal $G_{\alpha q/11}$ knockdown induced in adulthood developed emphysema. These data indicate that mesenchymal $G_{\alpha q/11}$ is responsible for maintaining lung homeostasis, probably via TGFβ signalling, and this represents a shared pathway between pulmonary

fibrosis and normal lung development. The breeding of mice with tamoxifen-inducible knockdown of mesenchymal $G_{\alpha 12/13}$ (*Pdgfrb-Cre/ERT2;Gna12*$^{-/-}$*;Gna13*$^{fl/fl}$) in adulthood was also found to be feasible. These animals may be suitable for *in vivo* models of pulmonary fibrosis in future studies.

Overall, the findings of this study demonstrate that mesenchymal cell $G_{\alpha q/11}$ and $G_{\alpha 12/13}$ play essential roles in the pathogenesis of pulmonary fibrosis, normal lung development, and lung homeostasis through responses to mechanical stimuli, cellular contraction, and TGFβ signalling. Further dissection of the processes involved, including the role of specific TGFβ isoforms, could lead to the development of lung regenerative strategies that will benefit patients with a range of respiratory diseases including pulmonary fibrosis and BPD.

Publications

Goodwin AT, John AE, Joseph C, Habgood A, Tatler AL, Offermanns S, Henderson NS, Jenkins G. Stretch Regulates Alveologenesis Via Mesenchymal $G_{\alpha q/11}$-Mediated TGFβ2 Activation. **Revisions ongoing for *Development*** (Preprint on BioRxiv: **doi:** https://doi.org/10.1101/2020.09.06.284778).

Goodwin AT, Saini G. "Supportive Care of Patients with Fibrosing Interstitial Lung Disease: Answering a Great Clinical Need". ***Breathe* 2020;16:200066**

Pakshir, P., Noskovicova, N., Lodyga, M., Son, D.O., Schuster, R., Goodwin, A., Karvonen, H., and Hinz, B. The myofibroblast at a glance. ***J Cell Sci* 2020; *133*.**

Goodwin AT, Jenkins G. Molecular Endotyping of Pulmonary Fibrosis. ***Chest* 2016 Jan;149(1):228-37**

Conference Presentations

National Oral Presentations:

"Cyclical Mechanical Stretch Regulates Alveologenesis Via Mesenchymal Gαq/11-Mediated TGFβ2 Signalling" **Accepted for oral presentation at BTS Winter Feb 2021, online**

"The G Proteins $G_{\alpha q/11}$ and $G_{\alpha 12/13}$ Drive Unique Myofibroblast Functions to Promote Pulmonary Fibrosis" **Accepted for oral presentation at BTS Winter Feb 2021, online**

"Mesenchymal $G_{\alpha q/11}$ Signalling promotes pulmonary fibrosis, but is also essential for normal lung development and tumour suppression: A shared pathway across disease themes" **British Association for Lung Research Summer Meeting 2019.**

"Deletion of mesenchymal $G_{\alpha q/11}$ results in abnormal lung development and renal abnormalities: a transgenic mouse study" ***Thorax* 2018: 73 (Supp 4); A40. Presented at the British Thoracic Society Winter Meeting, London, 2018**

"Cyclical Stretch induces Gaq/11 mediated TGFβ activation in lung fibroblasts" ***Thorax* 2017; 72 (Suppl 3); A47. Presented at the British Thoracic Society Winter Meeting, London, 2017**

International Oral Presentations

"Molecular Endotyping of Pulmonary Fibrosis". Interstitial Lung Disease Featured Lecturer. **American College of Chest Physicians CHEST 2017 conference**, **Toronto, Canada.**

International Poster Presentations

"Mesenchymal $G_{\alpha q/11}$ promotes profibrotic signalling and the myofibroblast phenotype, but is essential for normal organ development and tumour suppression" **Presented at the International Colloquium of Lung and Airway Fibrosis Meeting 2018, Monterey CA, USA.**

“Mice Deficient in Mesenchymal Gαq/11 Signalling Have Airspace Enlargement and Increased Alveolar Wall Thickness Consistent with Defective Alveolarisation” ***Am J Respir Crit Care Med*** **2018;197:A7791. Presented at the American Thoracic Society Meeting 2018, San Diego, USA.**

“Cyclical stretch induces transforming growth factor-β signalling via $G_{\alpha q/11}$ in fibroblast, but does not increase myofibroblast differentiation” **Presented at the European Respiratory Society Lung Science Conference 2018, Estoril, Portugal.**

“Cyclical stretch of lung fibroblasts induces TGFβ activation via $G_{\alpha q/11}$-mediated signalling”. **Presented at the Gordon Research Conference in Lung Repair and Regeneration, New Hampshire, USA**

Acknowledgements

I would firstly like to thank the National Institute for Health Research (NIHR) and the Medical Research Council (MRC) for providing the funding for my NIHR Academic Clinical Fellowship and MRC Clinical Research Training Fellowship, respectively. Without this financial support my project would not have been possible, and these fellowships have given me valuable opportunities to travel, learn new skills, and to complete this PhD.

Throughout this project I was supported by numerous members of the Respiratory Medicine Division at the University of Nottingham. To Prof Gisli Jenkins, my long-term mentor, thank you for the guidance and encouragement that you have given to me over the years, from conducting my first laboratory project in 2009, to applying for my MRC Fellowship, to finally finishing this thesis. I would also like to thank Dr Alison John, Dr Amanda Tatler, Dr Rachel Clifford, Ms Jo Porte, and Professor Alan Knox for supporting me in preparing conference talks, manuscripts, experiments, and general life issues over the years. Also special thanks to Dr Tony Habgood and Ms Rochelle Edwards-Pritchard for their assistance with the *in vivo* work, and to Dr Chitra Joseph for her valuable contribution to the immunohistochemistry work in this project.

I am incredibly grateful to Prof Boris Hinz (University of Toronto) for hosting me as a visiting research fellow to his laboratory for 6 months in 2018, during which time I conducted the contraction assays that form an integral part of this thesis. Prof Hinz's group immediately made me feel

very welcome in Toronto, and I would particularly like to thank Dr Monika Lodyga, Mr Trong Shen, Ms Michelle Im, and Dr Pardis Pakshir for kindly teaching me new techniques that will serve me well for years to come, as well as showing me the best places to visit in Toronto.

I would also not have been able to complete this project without many collaborators from outside of the University of Nottingham. Many thanks to Prof Neil Henderson (University of Edinburgh) for providing the *Pdgfrb-Cre*$^{+/-}$ mice that formed an integral part of this project. Prof Stefan Offermanns (Max Planck Institute for Heart and Lung Research, Bad Nauheim, Germany) kindly provided the *Gnaq*$^{fl/fl}$*;Gna11*$^{-/-}$ and *Gna12*$^{-/-}$*;Gna13*$^{fl/fl}$ mice, in addition to the *Gnaq*$^{-/-}$*;Gna11*$^{-/-}$ and *Gna12*$^{-/-}$*;Gna13*$^{-/-}$ murine embryonic fibroblasts that were used for the experiments in this thesis. I would also like to thank Prof Katalin Susztak and Dr Mathew Palmer (University of Pennsylvania, USA) who kindly gave their time and expertise to help me with interpreting the kidney histology, and Dr Tim Kendall (University of Edinburgh) for his valuable insights into the liver histology.

Last but certainly not least, I would like to thank my family for their support throughout my PhD. To my husband Peter, thank you for holding me up through the hard times, grounded during the good times, and for being my travel buddy during our Canadian adventure. Finally, to my daughter Quinn, who will have her own story to tell from 2020, you have changed my life for the better and are the best thing that happened during my PhD. Keep smiling baby girl.

Contents

List of Abbreviations

4-OH-TAM	4-hydroxytamoxifen
ABC	Avidin biotin complex
AEBSF	Aminoethylbenzenesulfonyl fluoride hydrochloride
AECI	Type I alveolar epithelial cell
AECII	Type II alveolar epithelial cell
Alk5	Activin receptor-like kinase
ANOVA	Analysis of variance
αSMA	Alpha smooth muscle actin
AT1R	Angiotensin II receptor 1
AU	Arbitrary units
B2M	β2-microglobulin
B2R	Bradykinin receptor
BAC	Bacterial artificial chromosome
BCA	Bicinchoninic acid
BIPF	Bleomycin induced pulmonary fibrosis
bp	Basepairs
BPD	Bronchopulmonary dysplasia

BSA	Bovine serum albumin
cAMP	Cyclical adenosine monophosphate
cDNA	Complementary DNA
CTGF	Connective tissue growth factor
CMS	Cyclical mechanical stretch
COPD	Chronic obstructive pulmonary disease
Cre^{ERT2}	Tamoxifen-inducible Cre recombinase
Ct	Cycle threshold
DAG	Diaglycerol
DAPI	4′,6-diamidino-2-phenylindole
DC	Dendritic cell
df	Degrees of freedom
DMEM	Dulbecco’s Modified Eagles Medium
DNA	Deoxyribonucleic acid
dNTP	Deoxynucelotide triphosphates
ECL	Enhanced chemilluminescence
ECM	Extracellular matrix
EDTA	Ethylenediaminetetraacetic acid

ELISA	Enzyme-linked immunosorbent assay
END	Endoxifen
ESC	Embryonic stem cell
ET-1	Endothelin-1
F	Female
FAK	Focal adhesion kinase
FGF	Fibroblast growth factor
FITC	Fluorescein isothiocyanate
Fl	Floxed
GAP	GTPase activating protein
GAPDH	Glyceraldehyde 3-phosphate dehydrogenase
GDP	Guanosine disphosphate
GEF	Guanine nucleotide exchange factor
GnRH	Gonadotropin releasing hormone
GPCR	G protein coupled receptor
GTP	Guanosine triphosphate
H5R	Histamine receptor 1
H&E	Haematoxylin and Eosin

HLF	Human lung fibroblast
Hprt	Hypoxanthine-guanine phophoribosyltransferase
IC_{50}	Half maximal inhibitory concentration
IHC	Immunohistochemistry
ILC	Innate lymphatic cell
IP	Intraperitoneal
IP_3	Inositol-1,4,5 triphosphate
IPF	Idiopathic pulmonary fibrosis
IQR	Interquartile range
KO	Knockout
LAP	Latency associated peptide
Lbc	Lymphoid blast crisis
LBD-ER	Ligand binding domain of the oestrogen receptor
LARG	Leukaemia-associated RhoGEF
LLC	Large latent complex
LTBP	Latent TGFβ binding protein
LPA	Lysophosphatidic acid
LPI	Lysophosphatidylinositol

M	Male
MAPK	Mitogen activated protein kinase
MEF	Murine embryonic fibroblast
MLI	Mean linear intercept
MMP	Matrix metalloproteinase
Mono	Monocyte
mRNA	Messenger RNA
MRTF	Myocardin related transcription factor
MTT	3-(4,5-dimethylthiazol-2-yl)-2,5-diphenyltetrazolium bromide
NADPH	Nicotinamide adenine dinucleotide phosphate
NeoR	Neomycin resistance
NG2	Nerve glial antigen-2
NL	Non-diseased
NOX	NADPH oxidase
P	Postnatal day
PAGE	Polyacrylamide gel electrophoresis
PAH	Pulmonary arterial hypertension
PAI-1	Plasminogen activator inhibitor-1

PAR1	Protease activated receptor
PAS	Periodic acid Schiff
PBS	Phosphate buffered saline
PCR	Polymerase chain reaction
PDGF	Platelet derived growth factor
PDGFRβ	Platelet derived growth factor receptor β
PIP_2	Phosphatidylinositol-4,5-bisphosphate
PKC	Protein kinase C
PLC	Phospholipase C
PMSF	Phenylmethylsulfonyl fluoride
Poly A	Poly adenosine
pSmad	Phosphorylated Smad protein
PR	Picrosirius red
Pro-SPC	Pro surfactant protein C
PTH	Parathyroid hormone
PTH1R	Parathyroid hormone receptor 1
PVDF	Polyvinylidene
PYK2	Protein tyrosine kinase 2

qPCR	Quantitative polymerase chain reaction
RGD	Arginine-Glycine-Aspartate motif
RISC	RNA-induced silencing complex
RNA	Ribonucleic acid
RNASeq	RNA sequencing
ROCK	Rho-associated coiled-coil containing kinase
RT-PCR	Reverse transcription PCR
S1P	Sphinghosine-1-phosphate
SARA	Smad anchor for receptor activation
scRNASeq	Small cell RNA sequencing
SDS	sodium dodecyl sulphate
SEM	Standard error of the mean
Shh	Sonic hedgehog
siRNA	Small interfering RNA
SLC	Small latent complex
SPC	Surfactant protein C
SRF	Serum response factor
SSIV	Superscript IV reverse transcriptase

TAZ	Transcriptional coactivator with PDZ-binding motif
TBST	Tris buffered saline Tween20
TCP	Tissue culture plastic
TGFβ	Transforming growth factor-β
TFM	Traction force microscopy
TGFBR	TGFβ receptor
Tk	Thymidine kinase
TMLCs	Transformed mink lung cells
TX-100	Triton X-100
UMAP	Uniform manifold approximation and projection
VE	Vascular endothelial
VSMC	Vascular smooth muscle cell
VVG	Verhoeff van Gieson
Wnt	Wingless integrated
WT	Wild-type
YAP	Yes-activated protein

1 Introduction

1.1 Introduction

G protein coupled receptor (GPCR) signalling drives multiple physiological processes across every mammalian organ system, and aberrant GPCR signalling has been implicated in many diseases. Mesenchymal cells play key roles in maintaining lung structure and function through a series of complex signalling pathways and interactions with the mechanical environment. This thesis will explore the role of mesenchymal cell G protein signalling in idiopathic pulmonary fibrosis (IPF) and bronchopulmonary dysplasia (BPD and evaluate how G protein signalling may regulate disease in these two distinct patient populations.

1.2 Idiopathic Pulmonary Fibrosis

1.2.1 Epidemiology

Pulmonary fibrosis is a condition characterised by scarring of the lung and encompasses multiple heterogeneous conditions with a range of aetiologies. Idiopathic pulmonary fibrosis (IPF), the commonest form of pulmonary fibrosis, is a progressive and debilitating chronic condition. The incidence of IPF is increasing worldwide, an observation that is likely to be related to the aging population and increasing exposure to inhaled injurious stimuli (1, 2), resulting in a growing disease burden from this condition. Unfortunately, the prognosis of IPF is poor and this disease is associated with a median survival time from diagnosis of just 3 years, which is worse than many malignancies (3).

The significant and increasing mortality burden associated with IPF has driven a dramatic increase in research over recent years, aiming to both

examine the pathophysiological mechanisms that drive this disease and assess methods of manipulating these processes as therapeutic measures (2, 4). However, the results from clinical trials have generally been disappointing and there is still no cure for IPF other than lung transplantation, which many patients with IPF are unsuitable for because of their advanced age and comorbidities (5). Therefore, more research to enhance our understanding of the molecular mechanisms that drive IPF is essential to identify new targets for novel therapeutic approaches.

1.2.2 Pathophysiology of IPF

The pathophysiological processes that drive IPF involve several cell types and signalling pathways, and ultimately cause the replacement of normal lung parenchyma with scar tissue. The current paradigm is that alveolar epithelial injury, for example from inhaled dusts or gastro-oesophageal reflux disease, in an individual who is susceptible because of genetic factors or advanced age triggers an abnormal wound healing response (Figure 1-1) (5). The recruitment of inflammatory cells and release of profibrotic cytokines by immune and injured epithelial cells promotes vascular leak and attracts fibroblasts into the area (5). These fibroblasts differentiate into myofibroblasts, and accumulations of these cells form fibroblastic foci, the classic histopathological feature of IPF (6). Together, the abnormally active fibroblasts and myofibroblasts create “scarred” (fibrotic) areas in the lung by depositing excessive amounts of extracellular matrix (ECM) proteins and through cellular contraction (7).

The subsequent architectural distortion of the lung results in impaired gas exchange and culminates in respiratory failure (5).

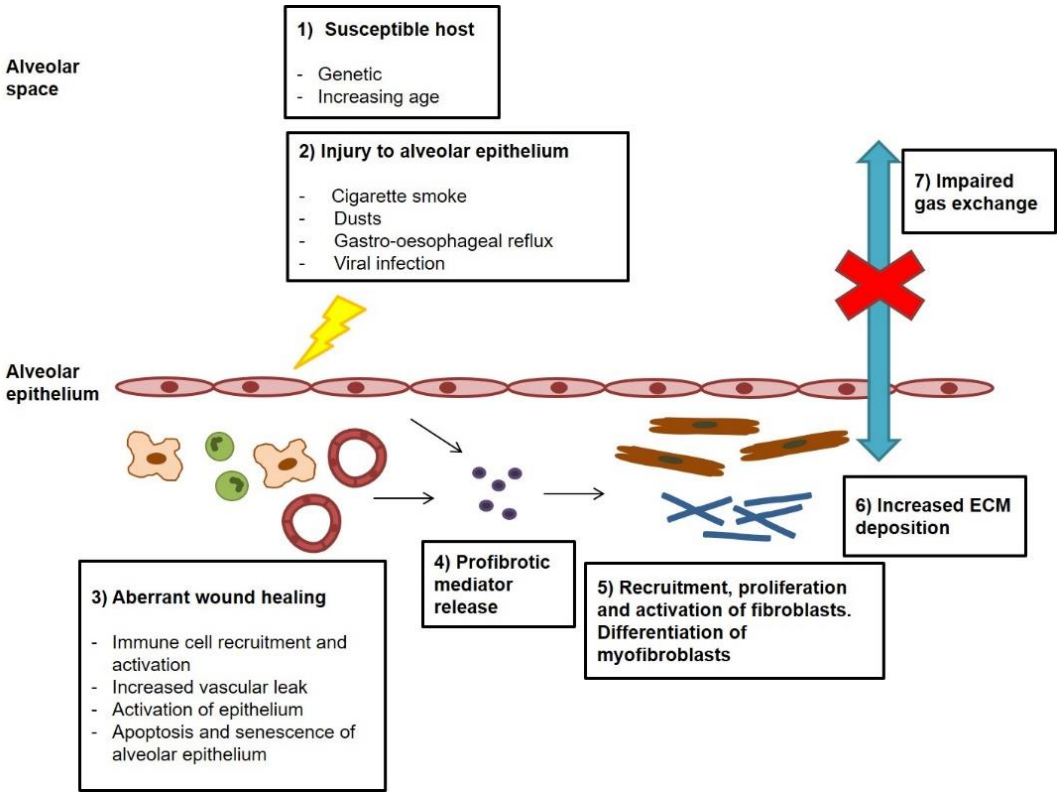

Figure 1-1: The pathogenesis of IPF

In a susceptible individual, alveolar epithelial injury initiates an exaggerated wound healing response. The resulting accumulation and activity of fibroblasts and myofibroblasts causes the formation of fibrotic tissue through excessive ECM protein deposition and cellular contraction. This impairs gas exchange across the blood-alveolar barrier, resulting in respiratory failure. Adapted from Goodwin & Jenkins 2016 (5).

ECM = extracellular matrix

In contrast to normal wound healing following an injury, where myofibroblasts undergo apoptosis when the intact epithelium is restored, IPF is characterised by uncontrolled fibroblast and myofibroblast

persistence and activity (7). This may be perpetuated by a failure of re-epithelisation due to recurrent injury or ageing, driving the persistent and abnormal mesenchymal activation (8). While epithelial injury is thought to be the initiating factor in IPF, it is the dysregulated fibroblast and myofibroblast response that propagates fibrosis, making these cells attractive therapeutic targets. However, the development of specific fibroblast- and myofibroblast-directed therapies has proven challenging (9). A greater understanding of the molecular pathways that become dysregulated in IPF, including normal developmental and regenerative processes, may help to identify new treatments for this condition.

1.3 Lung development

1.3.1 The five stages of lung development

Mammalian lung development occurs in five well characterised stages. These phases are common across all mammals, however the timing of each stage varies between species. The stages of normal lung development are described below, with the timing relevant to human gestation included in brackets.

1. **Embryonic stage (4-7 weeks)**: Lung development begins as the primitive trachea and lung buds emerge as an outgrowth of the embryonic foregut endoderm (10, 11).
2. **Pseudoglandular stage (5-16 weeks)**: During this phase the conducting airways are formed through branching morphogenesis, a process of highly regulated and repeated branching of airways from the two lung buds (8, 10, 11).

3. **Canalicular stage (16-25 weeks)**: The respiratory bronchioles form during this stage (10, 11). Capillaries, which previously formed a loose network within the mesenchyme, begin to arrange around the developing distal airspaces (12).
4. **Saccular stage (24-40 weeks)**: Throughout this stage the saccules, which are the sac-shaped distal airways that form the primitive basis for the alveoli, develop (13). The developing epithelium and vasculature become closer together to facilitate gas exchange, and bilayer capillaries become embedded in the thick primary septa that divide the saccules (12). Differentiation of type I (AECI) and type II (AECII) alveolar epithelial cells also begins during the canalicular stage (10).
5. **Alveolar stage (36 weeks gestation – 8 years old):** The final structure of the alveoli is established during this stage through a process called alveolarisation. Alveolarisation occurs through secondary septation, a process where thin walls develop within and subdivide the saccules, dramatically increasing the surface area for gas exchange (10, 11). The double capillary layer that was originally present in the saccular walls condenses to form a single capillary layer within the alveolar septa (12, 13). The fully formed air-blood barrier is composed of a thin epithelial layer, the basement membrane, and a thin layer of endothelial cells (8).

Mouse models are frequently used to study lung development, and the timings of mouse and human lung developmental stages are shown in

Figure 1-2. It should be noted that these timings are approximate, and there is some overlap between the lung developmental stages. Additionally, when born at term humans are in the alveolar stage of lung development, whereas mice are born in the saccular stage (13), which is relevant to studies of BPD and alveolarisation.

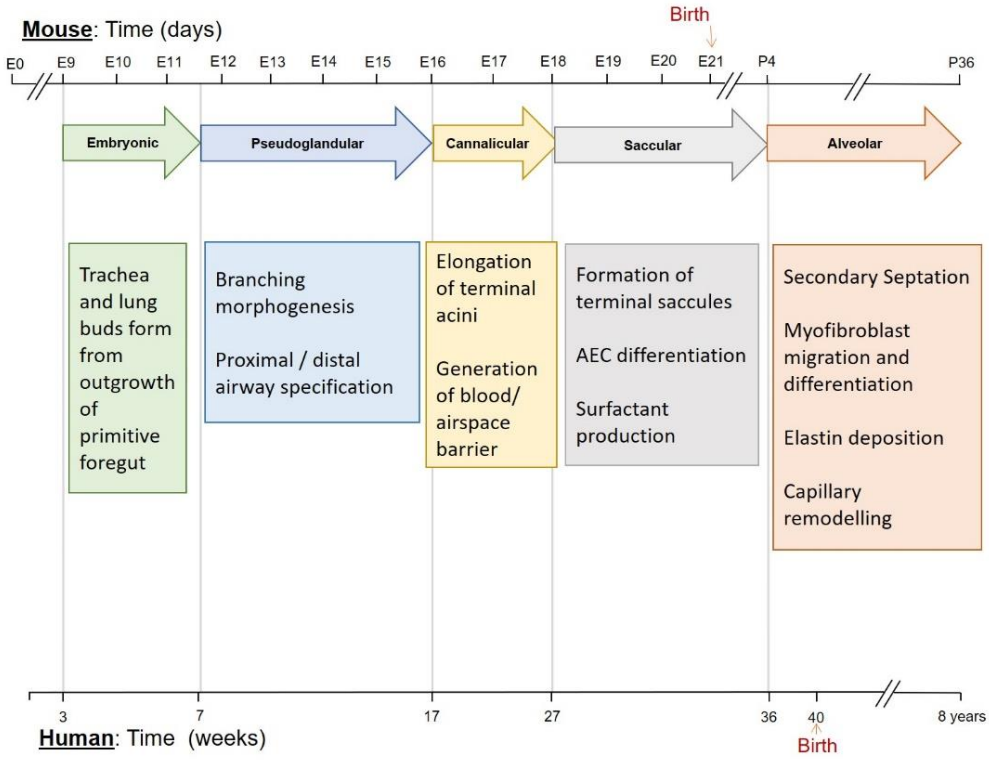

Figure 1-2: Mammalian lung development
The events of the five stages of mammalian lung development, with approximate timings in mice (top) and humans (bottom). Figure adapted from Donahoe et al 2016 (11) and Beauchemin et al 2016 (14).
AEC = alveolar epithelial cell

1.3.2 Alveolarisation

An understanding of the cells involved with and the signalling pathways that drive alveolarisation is essential if regeneration of injured gas

exchange areas in adult lungs is ever to be achieved. This late process in normal lung development will be discussed in detail here.

Major structural changes to the primitive saccules occur during alveolarisation (Figure 1-3). At the end of the saccular stage, the gas exchange regions of the lung contain thick septa containing two layers of blood capillaries separated by connective tissue (15). The physical distance between the alveolar air and capillary blood, as well as the multiple layers to traverse, would make gas exchange inefficient at this stage *ex utero*. During alveolarisation, saccules are subdivided through secondary septation, increasing the surface area for gas exchange (15). Additionally, the bilayer capillaries fuse to form a single capillary layer, and the septa become thinner (15). These processes form vastly increase the efficiency of the respiratory units for gas exchange, and support the transition of the foetus from the *in utero* to *ex utero* environments.

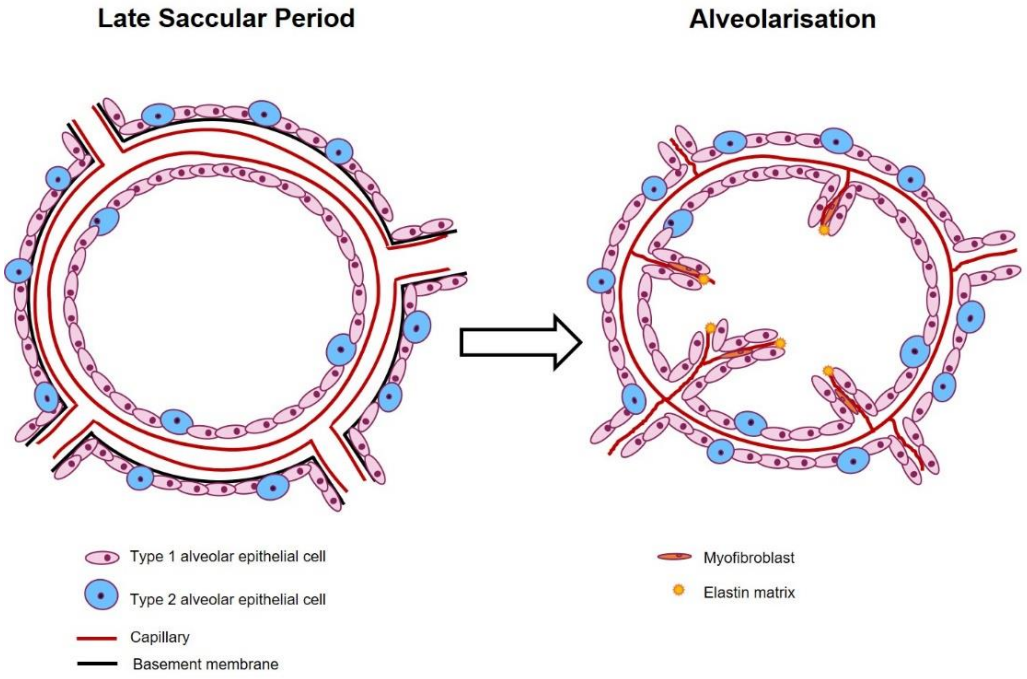

Figure 1-3: The physical changes in the structure of the gas exchange region in late lung development
At the end of the saccular period the gas exchange areas of the lungs contain thick septa and a double capillary layer (left). During alveolarisation, myofibroblast elastin deposition drives secondary septation, and the thinning of pulmonary septa and the formation of a single capillary layer increases the efficiency of gas exchange at the alveoli. Figure adapted from Donahoe et al 2016 (11).

The coordinated activity of multiple different cell types and formation of various structures is required for proper alveolar development. Growth factor signalling, the lung vasculature, the ECM, and several cell types are all known to be integral to alveolar development (13). Some of the individual cellular roles in alveolarisation are summarised in Table 1-1, however it should be emphasised that the cooperation and crosstalk between multiple cell and tissue types is essential for normal alveolar development (16).

Table 1-1: The roles of different cell types and structures in alveolarisation (17-20)

Structures	Cell	Function
Epithelial	AECI	Cover 95% of the distal lung and form the major gas exchange area between air and blood.
	AECII	Secrete surfactant, which reduces surface tension and increases lung compliance. Function as alveolar stem cells able to differentiate into AECIs.
Mesenchyme	Myofibroblasts	Produce elastin and other ECM proteins. ECM organisation via contraction.
	Lipofibroblasts	Store vitamin A. Supply substrate for surfactant production. Maintain pulmonary epithelial cell growth and differentiation.
Microvasculature	Endothelium	Formation of blood-air barrier. Drive vasculogenesis.
	Lymphatics	Fluid drainage.
AECI = type I alveolar epithelial cell; AECII = type II alveolar epithelial cell		

Myofibroblasts are essential cells in normal alveolar formation as they drive secondary septation. Myofibroblasts generate and organise the ECM protein elastin, which is a critical step in secondary septation (21). Myofibroblast-induced elastin deposition elevates the secondary crests

that form ridges along the saccular wall, dividing the saccule into a greater number of units (22, 23). Furthermore, myofibroblasts also produce other ECM components in addition to elastin such as collagen and proteoglycans, the balanced production of which gives structural support and elasticity to the growing septa (24). Properly deposited elastin and collagen fibres in the secondary crests tether areas of the primary saccular wall, allowing the remaining portions of the wall expand further outwards (22), therefore myofibroblasts play key roles in alveolarisation. Given their roles in both alveolar development and IPF, myofibroblasts are a major focus of this study.

1.3.3 Developmental pathways are reactivated in IPF

Many of the abnormal repair processes that drive IPF occur due to the aberrant reactivation of signalling pathways that drive normal developmental processes (25). However, in contrast normal lung development where there is tight spatiotemporal regulation of molecular signalling pathways and cellular activity, in IPF these developmental processes are activated in a chaotic and uncontrolled manner (26). Transforming growth factor-β (TGFβ), Wingless Integrated (Wnt), Sonic hedgehog (Shh), Notch, and fibroblast growth factor (FGF) signalling all regulate the specialised branching and patterning that occurs during the earlier stages of lung development, and dysregulation of these signalling pathways has been implicated in the pathophysiology of IPF (8).

The induction of alveolar regeneration in diseased adult lungs is an exciting potential therapeutic strategy for numerous conditions, including

IPF (27). For this approach to translate into an effective treatment for lung disease, including IPF, an understanding of the processes that drive alveologenesis is essential. Several pathways that drive alveolarisation, including Wnt and Shh signalling, have been found to be dysregulated in IPF (24, 28), however shared profibrotic and late lung developmental pathways are not as well established as with the earlier stages of lung development. A better understanding of normal alveologenesis, and the pathophysiological conditions where this process is disturbed, could identify key molecular signalling pathways that could be manipulated to induce alveolar regeneration in adult lung disease.

1.4 Bronchopulmonary dysplasia

1.4.1 Epidemiology

Bronchopulmonary dysplasia (BPD) is a developmental lung disease that affects premature neonates. BPD is a major cause of death in extremely premature infants (84 deaths per 1000 of these live births) (29), and is the second commonest cause of paediatric respiratory disease after asthma (30). In addition to the significant early life mortality rate, which is occurs due to respiratory failure, pulmonary hypertension and cor pulmonale (31), BPD can cause life-long morbidity secondary to chronic respiratory failure, increased susceptibility to respiratory tract infections, impaired lung function, and reduced quality of life (30, 32-35). BPD therefore has significant effects on patients at every stage of their lives.

14.9 million babies are born earlier than 37 weeks gestation worldwide every year, and the rate of premature birth is stable or increasing in most

countries (36). Although it is unclear how many preterm babies develop BPD, these statistics suggest that there is a significant and increasing rate of a major risk factor (preterm birth) for BPD. Furthermore, due to advances in neonatal intensive care the proportion of premature infants that survive has increased considerably over recent decades, and the lung abnormalities associated with BPD do not resolve with time (30). BPD is therefore responsible for an increasing disease burden worldwide, and is a growing clinical problem.

Unfortunately, the medical management of BPD is largely supportive and has a limited evidence base (32). There are no treatments for BPD that are targeted against the aberrant molecular pathways that drive this condition, and regenerative medical approaches are not used for this disease. Hence, work to identify the molecular mechanisms that drive BPD has been identified as a research priority, and this may promote the development of new targeted therapeutics (32).

1.4.2 Definition

BPD is diagnosed according to clinical criteria and is defined by the need for supplementary oxygen and/ or positive pressure ventilation at 36 weeks post-menstrual age in infants that required supplementary oxygen at 28 days old (30, 37, 38). BPD has been described in two forms, “old” and “new” BPD, according to the histological pattern, although histology does not form part of the diagnostic criteria as lung biopsies are not performed in routine clinical practice. With advances in neonatal care,

the pathology and clinical presentation of BPD has changed, and “old” BPD is now very rarely seen (38).

1.4.3 Pathology

Northway published the first description of BPD in 1967, and his observations were based on post-mortem samples (39). This “old” form of BPD occurred prior to the establishment of the modern medical management of premature neonates, which includes surfactant therapy, maternal steroids, and protective ventilation strategies that protect against the sequelae of fibrosis and pulmonary hypertension (30, 33). While “new” BPD is often regarded to be less severe than “old” BPD, both forms of the these have the common features of alveolar simplification and abnormal capillary morphology (40) (Table 1-2). From here, the term BPD refers to new BPD unless otherwise stated.

Table 1-2: Pathological features of old and new BPD

“Old” BPD (39)	**“New” BPD (30)**
Alveolar simplification and enlargement	Alveolar simplification and enlargement
Smooth muscle hyperplasia	Vascular simplification
Pulmonary artery lesions	
Extensive interstitial fibrosis	
Right ventricular hypertrophy	

The outcomes for infants born extremely prematurely (earlier than 27 weeks gestation) are highly variable, with some babies developing severe lung disease complicated by pulmonary hypertension, and others having no serious sequelae (31), and there is considerable heterogeneity in the clinical manifestations of patients diagnosed with BPD (41). The reasons for this phenotypic variation are unclear, although genetic factors and variable circulating cytokine profiles have been proposed as contributing factors (42). Given the heterogeneity of BPD it has been proposed that this disease results from several different pathophysiological processes with a common risk factor, premature birth (41). While the clinical and pathological definitions of BPD do not consider how these disease-driving pathways cause this condition, a greater understanding these processes and how they relate to disease complications could lead to the identification of novel therapeutic targets and biomarkers for risk stratification to benefit patients with BPD.

1.4.4 Pathophysiology

The pathophysiology of BPD is complex, but the primary risk factor is preterm birth. The premature initiation of pulmonary gas exchange that occurs with preterm birth interrupts the normal processes of alveolarisation, impairing alveolar and distal lung vasculature development (40, 41). Other perinatal insults such as sepsis, mechanical ventilation and hyperoxia contribute to the oxidant injury, barotrauma, volutrauma, inflammation, and disordered repair processes that disturb or arrest normal alveolarisation (12), resulting in alveolar simplification.

While the molecular mechanisms that cause BPD are incompletely understood, disturbances to elastin production and vascular formation are central features in this condition. In BPD alveolar elastin fibres are disorganised and located in abnormal positions away from the alveolar septa, resulting in disturbed secondary septation, reduced lung elastance, and increased effort of breathing (17, 22). Dysmorphic alveolar microvessels that are immature and distributed abnormally are also found in BPD and are thought to result from the disordered expression of angiogenic growth factors (12, 40). The molecular pathways that govern elastin production and vasculogenesis in alveolarisation are incompletely understood, but mesenchymal cells are likely to play key roles in these processes.

1.4.5 IPF and BPD have several common features

While IPF and BPD affect patients at opposite ends of the age spectrum and are associated with distinct histopathological patterns, they also share several clinical and pathophysiological characteristics.

IPF and BPD have both been identified as heterogeneous conditions, where the histopathological manifestations are increasingly being thought to be driven by distinct pathophysiological mechanisms in individual patients (5, 41). Additionally, genetic polymorphisms are thought to account for much of the population variability in the risk of developing either IPF or BPD, should an initiating insult occur (5, 43). Many potential initiating and perpetuating factors have been identified that are shared between IPF and BPD including oxidant injury,

barotrauma and volutrauma from mechanical ventilation, inflammation, and disordered repair processes (5, 12, 44). Furthermore, IPF and BPD are both characterised by the existence of abnormal ECM composition and structure (5, 22). These shared characteristics suggest that IPF and BPD may be driven by disturbances to similar molecular pathways. Precise definition of these shared disease pathways could lead to the development of therapies that restore normal lung structure and function in both IPF and BPD.

Several growth factors are known to drive the pathogenesis of IPF as well as normal alveolar septation, including platelet-derived growth factor (PDGF), fibroblast growth factor (FGF), connective tissue growth factor (CTGF) and TGFβ (13, 24). Myofibroblasts respond to all of these signalling mediators, but TGFβ is particularly important in governing myofibroblast activity and differentiation from mesenchymal progenitors (5, 22). This study will focus on the mechanisms of TGFβ signalling in mesenchymal cells, and how this influences normal alveolar development and IPF.

1.5 Mesenchymal cells

1.5.1 Pulmonary mesenchymal cells

The pulmonary mesenchymal cell population comprises a diverse range of cells that develop into connective tissue, blood vessels and lymphatic tissue (25), and examples include fibroblasts, myofibroblasts, smooth muscle cells, and pericytes (45). The study of mesenchymal cell lineages is a complex and evolving field, and the evidence suggests the existence

of numerous mesenchymal cell subpopulations, which vary in anatomical location, gene expression, and cell surface markers (45). Combinations of cellular markers are usually required for mesenchymal cell subtype identification, but there is a lack of consensus on these defining cellular markers, the precursor cells from which these cells derive, and their biological properties (45). This is particularly problematic for the increasing number of mesenchymal cell subtypes that are being identified in the developing and adult lung (45). The mesenchymal cell subtypes important to myofibroblast function in lung development and repair will be reviewed in the following section.

1.5.2 Defining mesenchymal cell subtypes

While there are numerous markers used to identify mesenchymal cell subtypes, the expression of two platelet-derived growth factor receptors (PDGFR), PDGFRα and PDGFRβ, is frequently used to define broad mesenchymal cell subtypes.

During lung development, PDGFRα$^+$ cells display either lipofibroblastic (lipid-containing, αSMA-negative) or myofibroblastic (α-smooth muscle actin (αSMA)-expressing) phenotypes (46). As the lungs form, PDGFRα$^+$ progenitors can be found around the distal lung epithelial tubules and buds, and they then spread to the terminal saccules during the canalicular and saccular stages (23, 47). These cells eventually become alveolar myofibroblasts, which are essential for secondary septation (16, 23, 47). By the end of the alveolar stage, few PDGFRα$^+$ cells contain either αSMA or lipid, implying a dynamic change in mesenchymal cellular

phenotype and function during lung development (46). Both pericytes and resident lung fibroblasts have been found to express PDGFRα (25).

PDGFRβ expression has been demonstrated in adult fibroblasts, myofibroblasts, smooth muscle cells, pericytes and neurones, as well as developing, but not adult, endothelial cells (48, 49). PDGFRβ^{+} cells are thought to be particularly important in the wound-healing response to injury, particularly myofibroblasts which derive from pericytes, and are therefore important in fibrogenesis (48). Cells with high PDGFRβ expression are increased in fibrotic lungs (45), and the deletion of αv integrins, key mediators of fibrosis, in Pdgfrb^{+} cells has been reported to protect mice from pulmonary and renal fibrosis (48). This evidence suggests that PDGFRβ^{+} cells are key drivers of fibrogenesis, however their role in alveolar development is not known. This study will focus on the roles of PDGFRβ-expressing cells in normal lung development and pulmonary fibrosis.

1.5.3 Myofibroblasts

Myofibroblasts are characterised by their contractility and the expression and incorporation of α-smooth muscle actin (αSMA) into stress fibres (9). These cells contribute significantly to lung development and fibrosis through the generation and organisation of the ECM (9, 25, 50).

The pulmonary ECM is a dynamic structure that provides physical support for lung integrity and elasticity, and consists of proteins, such as collagens, fibronectin, and elastin, and proteoglycans (21). In addition to

the structural components, the ECM contains sequestered growth factors, which are released in response to cellular activity and can influence cell behaviour (21). The activities of local cells modify the ECM, and there is constant remodelling of the ECM through component synthesis, degradation, reassembly, and chemical modification (21).

The ECM has different characteristics depending on the physiological or pathophysiological context. During lung development, the ECM acts as a structural scaffold that supports branching morphogenesis and regulates diverse cellular features, such as shape, motility, and growth, which drive organogenesis (21). ECM remodelling, particularly of elastin, is essential for normal alveolarisation, and insufficient ECM deposition negatively impacts lung development (13). Conversely, in IPF the ECM is excessive in amount and highly organised, and signalling by the ECM-sequestered growth factor TGFβ becomes excessive.

Myofibroblast activity is central to both normal alveologenesis and IPF. These cells produce the ECM proteins, including the collagen and fibronectin that predominate in the abnormal IPF ECM, as well as the elastin that drives secondary septation during lung development (9, 25, 47). Additionally, myofibroblast contraction is central to both the excessive organisation of the lung ECM in IPF, and the normal arrangement of elastin fibres that is required for alveologenesis (47). An understanding of the stimuli that drive myofibroblast differentiation and activity in the lung is therefore essential to understand both IPF and normal alveolar development.

Lineage tracing studies have demonstrated that myofibroblasts originate from pericytes and resident fibroblasts during lung development and after injury (25), although epithelial- and endothelial-to-mesenchymal transition and differentiation from bone marrow-derived fibrocytes have also been suggested to contribute to the myofibroblast population in pulmonary fibrosis (51, 52). Myofibroblast differentiation from precursor cells is triggered by numerous mediators, including TGFβ, lysophosphatidic acid (LPA), platelet derived growth factor (PDGF), connective tissue growth factor (CTGF), and endothelin-1 (ET-1) (7). Furthermore, mechanical stimuli are important regulators of myofibroblast differentiation, as the increased ECM stiffness found in IPF promotes myofibroblast differentiation and activity (53). Manipulation of the mechanisms by which myofibroblasts detect and respond to these chemical and mechanical stimuli could lead to the development of approaches that modify myofibroblast differentiation and activity to the benefit of fibrotic and developmental diseases.

1.5.4 Pulmonary pericytes

Pericytes are multipotent cells that are found in every vascularised tissue in the body, and they are thought to be precursors for multiple cell types, including fibroblasts, myofibroblasts, neural cells, adipocytes (48, 54). Pericytes are contractile, found in close contact with capillaries, and are defined anatomically by the presence of cellular processes that contact endothelial cells and the capillary basement membrane (25, 55). In addition to maintaining vascular structure and function, pericytes have

been postulated to play roles in immune surveillance and the recruitment of immune cells (25). The extent of pericyte vascular coverage, and thus the number of cells, varies by organ but is relatively high in the lung (25), indicating potentially important roles for these cells in lung physiology.

In the lung, pericytes are necessary for the patterning and cellular differentiation that drives a number of developmental processes (25). Furthermore, these cells contribute to the pathological inflammation and tissue remodelling that can occur in response to injury, but they may also be capable of initiating tissue regeneration with resolution of the injurious stimulus (25). In pulmonary fibrosis, pericytes migrate away from the endothelium, contributing to the vascular leak observed in this condition (56), and these cells are a major source of the myofibroblasts that drive the expansion of fibrotic tissue within the lung (54, 57). These reports indicate that pericytes may have essential roles in the maintenance of lung homeostasis.

In addition to the anatomical definition described above, pericytes are identified by the presence of molecular markers such as PDGFRβ and nerve glial antigen 2 (NG2) (54), alongside an absence of leukocyte, endothelial, and parenchymal markers (25). However, it should be noted that the expression of PDGFRβ and PDGFRα expression overlaps in some cell types, and pericytes have also been reported to express PGDFRα in adult lung tissue (25). PDGFRβ-expressing cells have been used as targets for gene modification in animal models investigating the

role of pericytes in adult lung disease (48, 55), however the role of this cell population in lung development is unknown.

1.6 TGFβ signalling is a key physiological and pathophysiological mediator

TGFβ is a pleiotropic cytokine that influences a multitude of cellular functions, including cellular proliferation and differentiation, wound healing, ECM homeostasis, haematopoiesis, and immune regulation (8, 58, 59). In the lung, TGFβ signalling is essential for organ development, the maintenance of tissue homeostasis, and responses to tissue injury (8). Dysregulated TGFβ signalling can therefore lead to a variety of pathological manifestations. TGFβ signalling will be reviewed in the next section, followed by a review of how dysregulated TGFβ signalling contributes to pulmonary disease.

1.6.1 TGFβ signalling

In canonical TGFβ signalling, active TGFβ binds to TGFβ receptor 1 (TGFBR1), which forms a complex with TGFβ receptor 2 (TGFBR2). This receptor complex then phosphorylates serine residues of the intracellular receptor Smad proteins, Smad2 and Smad3, which subsequently heterodimerise and bind to co-Smad Smad4 (7). The resulting Smad complex translocates to the nucleus, binds to Smad binding elements in gene promoter regions, and recruits transcriptional co-activators, co-repressors and transcription factors to modulate gene expression, which may be specific to the cell type (7, 60). Dephosphorylated Smad proteins

shuttle back into the nucleus and can be targeted for proteasomal degradation by the inhibitory Smad7 (60) (Figure 1-4).

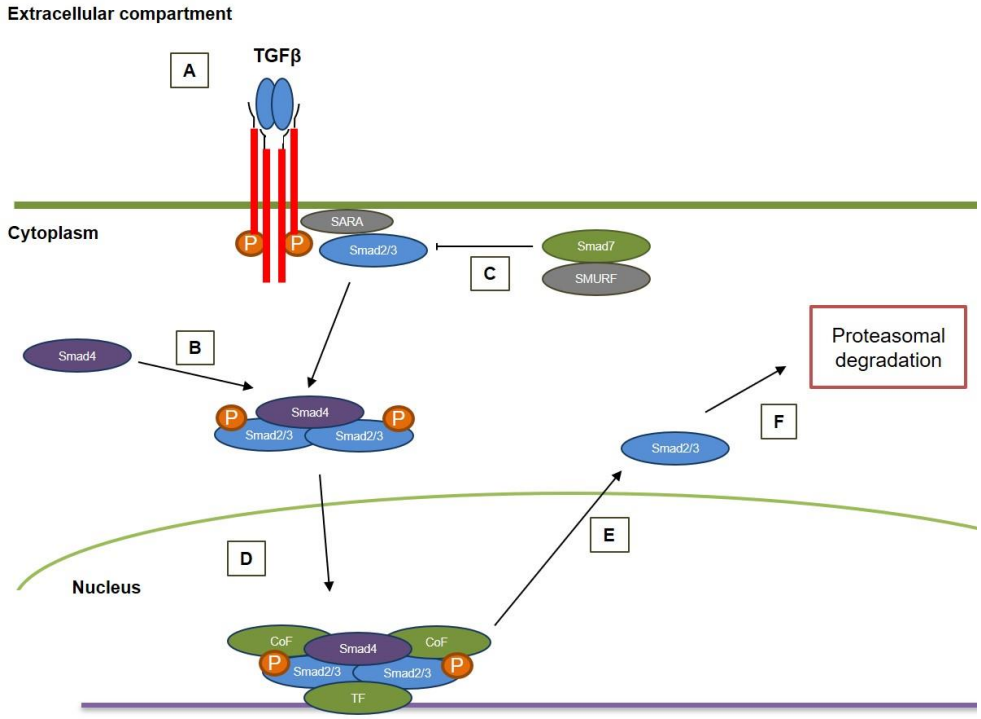

Figure 1-4: Canonical TGFβ signalling

A) TGFβ homodimers engage with the heterotetrameric TGFBRI and TGFBRII receptors, resulting in the phosphorylation of intracellular Smad2 and Smad3.

B) Smad4 forms a heterotrimeric complex with the phosphorylated receptor-regulated Smads.

C) Smad7 and the Smad-specific E3 ubiquitin protein ligases (Smurf) targets the receptor complex for ubiquitination and proteasomal degradation, and acts as an inhibitor of Smad signalling.

D) The activated Smad complex associates with transcription factors and cofactors within the nucleus to promote transcription of target genes

E) Dephosphorylated Smad proteins shuttle back into the cytoplasm

F) In the cytoplasm, Smads may be targeted for ubiquitination and proteasomal degradation.
Figure adapted from Piersma 2015 (60).
SARA= Smad anchor for receptor activation

TGFβ also induces non-canonical signalling cascades, including the MAPK and PI3K pathways, demonstrating the wide-ranging effects that this cytokine can exert (7). While direct modulation of TGFβ signalling is possible, the vital roles that this cytokine plays in physiological processes such as wound healing and immune regulation explain why toxicity prohibits complete TGFβ blockade (61). The upstream mechanisms that lead to dysregulated TGFβ activation in disease are an active area of research, as interrupting these processes may be a less toxic therapeutic approach for TGFβ-associated conditions.

1.6.2 TGFβ isoforms

There are three mammalian TGFβ isoforms: TGFβ1, TGFβ2 and TGFβ3. All three isoforms are expressed in the lung and TGFβ1 is thought to be the most important in pulmonary fibrosis (62), however there are few studies investigating the role of individual TGFβ isoforms in the healthy and diseased lung. Signalling downstream of all TGFβ isoforms is thought to be identical once the cytokine is activated, therefore unique roles for these mediators may be driven by differences in activation mechanisms and spatiotemporal expression profiles (61, 63, 64).

1.6.3 TGFβ activation

TGFβ is produced by numerous cell types including endothelial, epithelial, immune, and mesenchymal cells (60). All three TGFβ isoforms are synthesised as homodimeric proproteins, and the propeptide dimer is cleaved from the mature cytokine prior to secretion (65). This latency associated peptide (LAP) remains bound to TGFβ by non-covalent interactions, and the complex is secreted as the small latent complex (SLC) (62, 65). The latent TGFβ binding protein (LTBP) associates with the SLC via disulphide bonds between the LAP and LTBP, and tethers latent TGFβ to the ECM in the large latent complex (LLC) (65).

For TGFβ to be activated and exert any biological effects, its association with the LAP must be altered so that it can interact with TGFβ receptors. This can occur via several mechanisms, including the action of proteases, extremes of heat or pH, oxidation or via integrin-mediated activation (62, 66, 67).

Integrins are heterodimeric transmembrane proteins that consistent of α and β subunits. Integrins are key mediators of communication between the intracellular and extracellular environments, and can interact with a range of molecules including cell surface ligands, transmembrane proteins, proteases, and growth factors (66). Several integrins, including the αv integrins, bind ligands with an arginine-glycine-aspartate (RGD) sequence (66). The LAPs of TGFβ1 and TGFβ3 contain an RGD motif, and integrins are key activators of these TGFβ isoforms via traction-induced alterations to the LLC, or via the facilitation of protease activity

in the case of the αvβ8 integrin (66). Conversely, the LAP of TGFβ2 does not contain an RGD motif, and this isoform is therefore predominantly activated via integrin-independent mechanisms (66, 68). Work to identify the role of these mechanisms of TGFβ activation in lung development and disease is ongoing.

1.6.4 TGFβ in pulmonary fibrosis

TGFβ is a well-established driver of fibrotic diseases and exerts multiple profibrotic effects on numerous different cell types. TGFβ induces AEC apoptosis, inhibits AEC proliferation, promotes myofibroblast proliferation, differentiation and survival, and enhances ECM production (8, 62, 69, 70), all of which are central features of the pathogenesis of IPF. Furthermore, TGFβ is found at elevated levels in the lungs of IPF patients and in animal models of pulmonary fibrosis (71, 72), and TGFβ blockade ameliorates pulmonary fibrosis in animal models (73). These studies affirm the critical role of TGFβ in this disease and explain the great interest in the mechanisms of abnormal TGFβ activation as a treatment strategy for fibrotic diseases.

An example of a strategy to modify the abnormal activation of TGFβ in pulmonary fibrosis is STX-100, a humanised monoclonal antibody that can block the αvβ6 integrin. The αvβ6 integrin is highly expressed in the alveolar epithelium of patients with IPF, and can induce TGFβ activation (74). Antibody-mediated blockade of αvβ6 signalling can inhibit TGFβ activation *in vivo* (75), however the clinical trial of STX-100 in IPF was halted due to safety concerns (ClinicalTrials.gov NCT03573505). While

this was a disappointing end to work on a potentially disease-modifying compound, these studies demonstrate that the mechanisms that cause abnormal TGFβ activation can be modulated *in vivo*. Further work is required to further examine the molecular mechanisms of abnormal TGFβ activation in fibrosis, to develop new therapeutic compounds that modify the abnormal activation of this cytokine while maintaining its physiological functions.

1.6.5 TGFβ in lung development

TGFβ is broadly expressed during development, and marked increases in expression are generally observed in areas undergoing morphogenetic events such as epithelial-mesenchymal interactions or cellular differentiation (58). TGFβ signalling is integral to a number of processes that drive normal lung development, including branching morphogenesis (76-78), angiogenesis (79), and epithelial cell differentiation (80, 81). The wide-ranging effects of TGFβ may be contextual and concentration-dependent during lung development (8).

All three TGFβ isoforms are highly expressed in the developing lung, but they have discrete cell-specific expression patterns at different developmental stages (82, 83). The phenotypes of *Tgfb1*$^{-/-}$, *Tgfb2*$^{-/-}$, and *Tgfb3*$^{-/-}$ mice demonstrate the potential unique roles for the TGFβ isoforms in development. *Tgfb1*$^{-/-}$ mice develop widespread inflammation and die within 2-3 weeks of birth (61). *Tgfb3*$^{-/-}$ mice die within hours of birth and have craniofacial abnormalities and evidence of delayed pulmonary development (64). *Tgfb2*$^{-/-}$ mice die shortly after birth from a

range of developmental defects that do not overlap with *Tgfb1*$^{-/-}$ or *Tgfb3*$^{-/-}$ mice (61, 63, 64). Although *Tgfb2*$^{-/-}$ mice have no gross lung morphological abnormalities at late gestation, collapsed conducting airways are found postnatally (63). These genetic studies of the roles of TGFβ isoforms in development are complicated by the potential compensation for the genetic defects by maternal TGFβ production during pregnancy. For example, while *Tgfb2*$^{-/-}$ mice have normal branching morphogenesis, inhibition of TGFβ2, but not TGFβ1 or TGFβ3, inhibits branching morphogenesis *in vitro* (84, 85). This raises the possibility that maternal TGFβ2 compensates for the genetic deficiency of any offspring during pregnancy (84). Additionally, as TGFβ signalling is broadly involved in the development and function of all organs, any lung-specific phenotypes may be confounded by the existence of extrapulmonary pathology which may also negatively impact lung development (86). Therefore, the isoform-specific roles of TGFβ in lung development remain unclear.

1.6.5.1 TGFβ in alveolarisation

The importance of tightly regulated TGFβ signalling in late lung development is well established, with both over- and under-activity being implicated in disturbances to alveolarisation (87-97). In addition to regulating ECM production, TGFβ signalling controls an early pathway that regulates the commitment and differentiation of mesenchymal precursors to myofibroblasts or lipofibroblasts (98), and is thus essential for normal secondary septation to occur. Furthermore, TGFβ is involved

in pericyte-endothelial crosstalk during vascular development, a process that is closely related to alveolar development (54).

While TGFβ isoform-specific roles have been suggested in branching morphogenesis (85), the role of the different isoforms in alveolarisation is unknown. The expression of all three TGFβ isoform genes increases dramatically during alveolarisation in rat lung (99), suggesting that all TGFβ isoforms have important roles in this process. Genetic reduction of TGFβ2 in *Ltbp4*$^{-/-}$ mice, which already have abnormal alveolar septation before any manipulations to TGFβ signalling, restores a normal lung appearance (100, 101). However, this approach was taken to reduce overall TGFβ signalling and because of practical difficulties in targeting the other isoforms, rather than implying an isoform-specific effect (100, 101). Therefore, any unique roles for the TGFβ isoforms in alveolarisation remain to be determined.

1.6.6 TGFβ in BPD

Dysregulation of TGFβ signalling has been described in BPD, suggesting an important role for TGFβ in the pathophysiology of this disease. Elevated pulmonary TGFβ expression levels have been found in animal models of BPD (102), and overexpression of TGFβ1 in neonatal mouse lung recapitulates the histological appearance of BPD (95). Furthermore, TGFβ is elevated in the lungs of premature human neonates with lung injury, and this correlates with BPD severity (103). While altered TGFβ signalling could be both a driver and result of the pathophysiological processes in BPD, inhibition of TGFβ signalling rescues the abnormal

alveolar and microvascular appearance of mice in the hyperoxia model of BPD (88). This finding raises the possibility of modulating TGFβ signalling as a therapeutic approach in BPD. However, more work is required to dissect the exact roles of TGFβ in BPD.

1.7 G protein signalling activates TGFβ

1.7.1 G protein coupled receptor signalling

G protein coupled receptors (GPCRs) are widely expressed in every mammalian tissue. There are over 800 GPCRs, which comprise approximately 5% of the human genome (104), and the stimuli that activate GPCRs consist of a diverse array of molecules including biogenic amines, amino acids, ions, peptides, proteins, and photons (104). Given this diversity, GPCRs are involved in numerous physiological processes, including neurotransmission, cellular metabolism, cellular differentiation, proliferation, inflammation, and immune responses (104). The study of GPCR signalling is therefore relevant to numerous physiological and pathophysiological conditions.

GPCRs consist of a polypeptide chain that crosses the plasma membrane seven times, and they are associated with heterotrimeric guanosine triphosphate (GTP)-binding proteins (G proteins) on the intracellular aspect, which consist of α, β, and γ subunits (105). Ligand binding to a GPCR results in a conformational change in the receptor, stimulating the exchange of guanosine diphosphate (GDP) for GTP on the α subunit, and the dissociation of the α and βγ subunits from the GPCR (105). Both α and βγ subunits induce downstream signalling

pathways. These signals are terminated when the intrinsic GTPase activity of the α subunit hydrolyses GTP to GDP, reverting the GPCR to an inactive state (105) (Figure 1-5). G protein signalling is also modulated by regulatory proteins which alter the GTP binding status of the α subunit. GTPase activating proteins (GAPs) enhance hydrolysis of G protein-bound GTP to GDP, and guanine nucleotide exchange factors (GEFs) promote G protein-GTP binding, driving G proteins into “off” and “on” states, respectively (106).

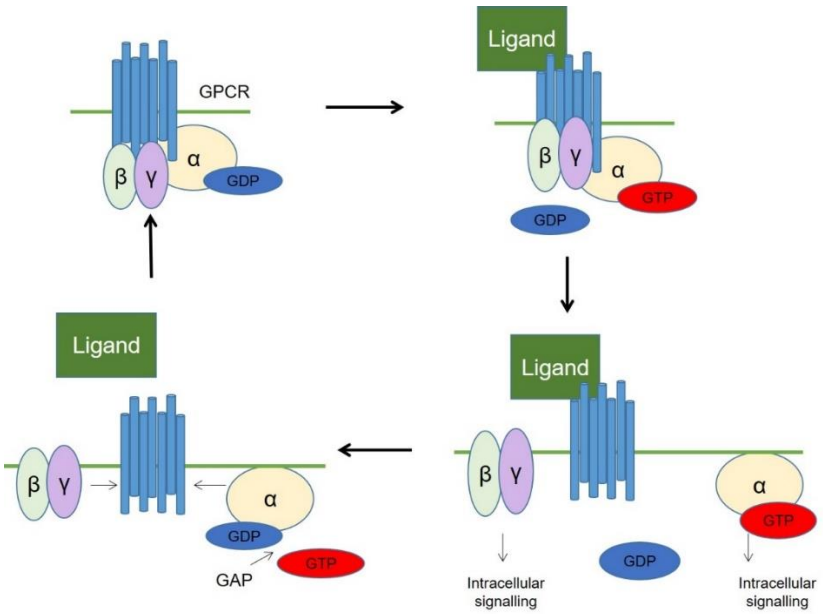

Figure 1-5: Heterotrimeric G protein signalling
In the inactive form, the α, β, and γ subunits are associated with the GPCR, and the α subunit is GDP-bound (top left). GPCR activation by ligand binding results in the exchange of GDP for GTP on the α subunit (top right). The βγ and α subunits then dissociate and initiate downstream signalling pathways (bottom right). Signalling is terminated when the α subunit-bound GTP is hydrolysed to GDP, and the heterotrimeric G protein components return to the inactive form (bottom left). Figure adapted from Kamato et al 2017 (105).

While there are hundreds of mammalian GPCRs, these converge on just four G_{α} subunit protein families which propagate downstream signalling. These G_{α} subunits are thought to determine the main properties of a GPCR (107). Therefore, focussing on the study of G_{α} families rather than individual GPCRs could enhance our understanding of numerous diseases and physiological processes.

1.7.1.1 Heterotrimeric G protein families

The four mammalian heterotrimeric G proteins families, $G_{\alpha i}$, $G_{\alpha s}$, $G_{\alpha 12}$, and $G_{\alpha q}$, are classified according to the sequences and functional homology of the α subunit (107). The tissue expression of the members of the G_{α} subunit families is widespread, however this does vary between individual G_{α} subunits (Table 1-3).

Table 1-3: Mammalian G protein α subunits and tissue expression. Adapted from Offermanns 2001 (107)

G Protein Family	Subtype	Gene	Expression
$G_{\alpha s}$	$G_{\alpha s}$	*Gnas*	Ubiquitous
	$G_{\alpha olf}$	*Gna1*	Brain, olfactory epithelium
$G_{\alpha i}$	$G_{\alpha i1}$	*Gnai-1*	Widely expressed
	$G_{\alpha i2}$	*Gnai-2*	Ubiquitous
	$G_{\alpha i3}$	*Gnai-3*	Widely expressed
	$G_{\alpha o}$	*Gnao*	Neuronal, neuroendocrine
	$G_{\alpha z}$	*Gnaz*	Neuronal, platelets
	$G_{\alpha gust}$	*Gnag*	Taste cells, brush cells
	$G_{\alpha t\text{-}r}$	*Gnat-1*	Retinal rods, taste cells
	$G_{\alpha t\text{-}c}$	*Gnat-2*	Retinal cones
$G_{\alpha q}$	$G_{\alpha q}$	*Gnaq*	Ubiquitous
	$G_{\alpha 11}$	*Gna-11*	Almost Ubiquitous
	$G_{\alpha 14}$	*Gna-14*	Kidney, lung spleen, testis
	$G_{\alpha 15}$	*Gna-15*	Haematopoietic cells
$G_{\alpha 12}$	$G_{\alpha 12}$	*Gna-12*	Ubiquitous
	$G_{\alpha 13}$	*Gna-13*	Ubiquitous

The four G_{α} subunit families are reviewed below.

1.7.1.2 The $G_{\alpha i}$ and $G_{\alpha s}$ families

The $G_{\alpha i}$ and $G_{\alpha s}$ families influence adenylyl cyclase activity and cyclic adenosine monophosphate (cAMP) levels (107). $G_{\alpha i}$- and $G_{\alpha s}$–coupled GPCRs detect a variety of stimuli, but are predominantly associated with special senses and the nervous system (107), and have not been heavily implicated in myofibroblast activity, pulmonary fibrosis, or lung development. Conversely, the $G_{\alpha q}$ family members $G_{\alpha q}$ and $G_{\alpha 11}$, and the

$G_{\alpha 12}$ members $G_{\alpha 12}$ and $G_{\alpha 13}$ have been implicated in GPCR-mediated profibrotic pathways, and therefore will be the focus of this study.

1.7.1.3 The $G_{\alpha q}$ family

$G_{\alpha q}$ and $G_{\alpha 11}$ are the most widely expressed members of the $G_{\alpha q}$ family. They have 88% amino acid sequence homology, share many functions, and have similar tissue expression profiles apart from in platelets and the central nervous system (107-110) (Table 1-3). Due to these overlapping functions and cellular co-expression, $G_{\alpha q}$ and $G_{\alpha 11}$ are usually studied together and are collectively referred to as $G_{\alpha q/11}$ (109).

Upon activation by upstream GPCR stimulation, $G_{\alpha q/11}$ triggers phospholipase C (PLC) signalling, which hydrolyses membrane bound phosphatidylinositol-4,5-bisphosphate (PIP_2) to diaglycerol (DAG) and inositol-1,4,5 triphosphate (IP_3). IP_3 induces the release of calcium ions (Ca^{2+}) from the endoplasmic reticulum, and DAG and Ca^{2+} activate protein kinase C (PKC) (105, 111). The subsequent changes in cytosolic calcium concentration and phosphorylation of other molecules by PKC induce several downstream signalling pathways that alter cellular activity (Figure 1-6). In addition to this classical $G_{\alpha q/11}$ signalling pathway, $G_{\alpha q/11}$ also activates the small GTPase Rho and its target, the serine-threonine kinase Rho-associated, coiled-coil containing kinase (ROCK) via PLC- and calcium-dependent and -independent mechanisms (112). As will be discussed in detail later, Rho-ROCK signalling is thought to be important for TGFβ activation in the lung (74, 113).

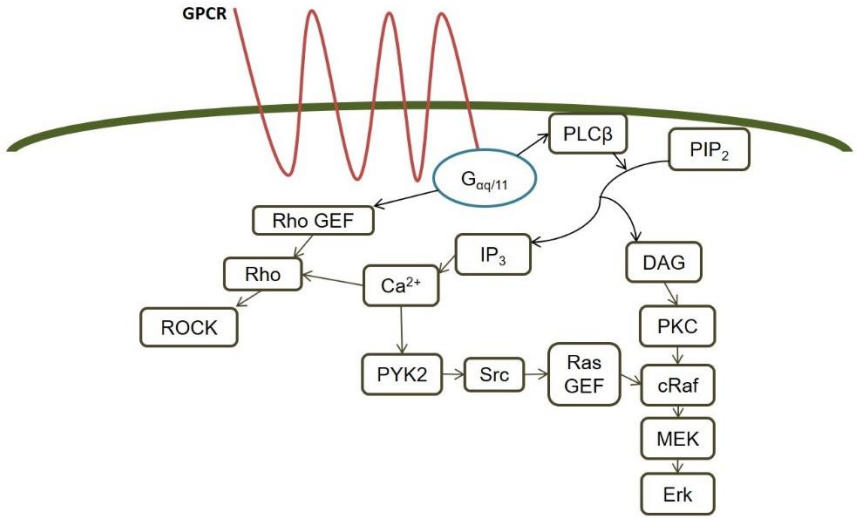

Figure 1-6: $G_{\alpha q/11}$ signalling

$G_{\alpha q/11}$ signalling activates PLCβ, leading to the hydrolysis of PIP_2 into IP_3 and DAG. IP_3 induces calcium release, which activates MAPK signalling via PYK2, Src, and Ras GEF. MAPK signalling also occurs directly downstream of DAG. $G_{\alpha q/11}$ can also directly activate Rho/ROCK signalling, independent of PLC activity. Figure adapted from Kamato et al 2015 (114).

PLC = phospholipase C; PIP_2 = phosphatidylinositol-4,5-bisphosphate; DAG = diaglycerol; IP_3 = inositol-1,4,5 triphosphate; MAPK = mitogen-activated protein kinase; ROCK = Rho-associated, coiled-coil containing kinase; PYK2 = protein tyrosine kinase 2; PKC = protein kinase C; MEK = MAPK/ERK kinase; Erk = extracellular signal-regulated kinase;

1.7.1.4 The $G_{\alpha 12}$ family

Similar to $G_{\alpha q}$ and $G_{\alpha 11}$, $G_{\alpha 12}$ and $G_{\alpha 13}$ are usually studied in a pair, although the sequence homology is lower between $G_{\alpha 12}$ and $G_{\alpha 13}$ than it is between $G_{\alpha q}$ and $G_{\alpha 11}$ (67% vs 88%) (115). $G_{\alpha 12/13}$ expression is ubiquitous, and the primary signalling pathway downstream of this G protein family is the Rho-ROCK cascade. $G_{\alpha 12/13}$ activates Rho/ROCK

signalling through the activation of RhoGEFs including p115RhoGEF, PDZ-RhoGEF, leukaemia-associated RhoGEF (LARG), and lymphoid blast crisis (Lbc)-RhoGEF, in addition to other pathways (106, 116-118).

$G_{\alpha 12/13}$ and $G_{\alpha q/11}$ can both activate Rho/ROCK signalling, which is an essential mediator of cellular contraction, and thus ECM remodelling and TGFβ activation. This indicates a potential key role for $G_{\alpha 12/13}$ and $G_{\alpha q/11}$ in myofibroblast function, which is discussed below.

1.7.1.5 Rho-ROCK signalling occurs downstream of $G_{\alpha q/11}$ and $G_{\alpha 12/13}$

Rho is activated when bound to GTP, a process catalysed by Rho guanine nucleotide exchange factors (RhoGEFs) (106). GTP-bound RhoA activates ROCK, which triggers further downstream signalling via the reorganisation of the actin cytoskeleton (Figure 1-7). Activated ROCK stimulates the conversion of globular (G) actin monomers to filamentous (F) actin polymers, which form the F-actin stress fibres. During this process, G-actin releases the associated myocardin related transcription factor –A and -B (MRTF-A, MRTF-B), allowing these transcription factors to translocate to the nucleus and coactivate serum response factor (SRF)-mediated gene expression (119-121).

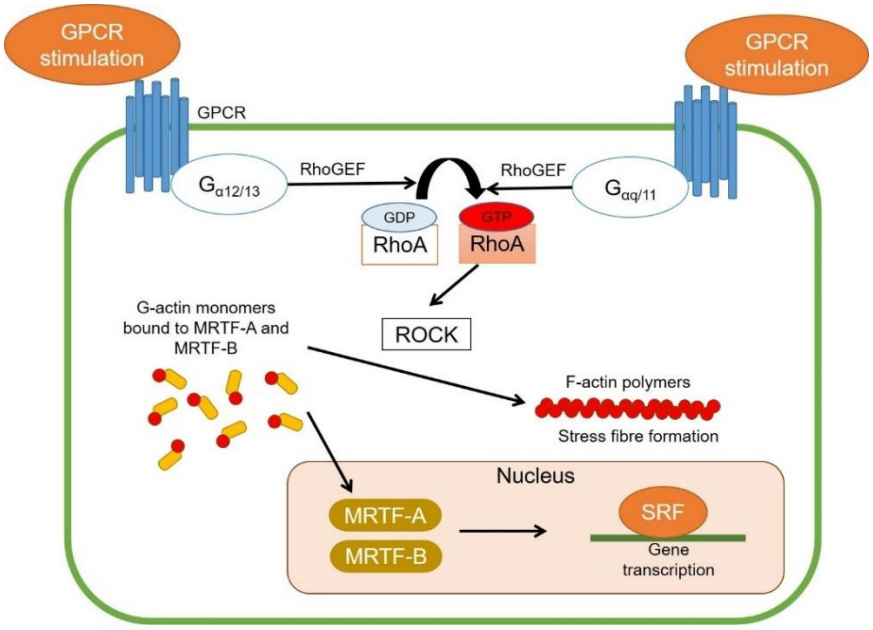

Figure 1-7: Rho-ROCK signalling occurs downstream of $G_{\alpha q/11}$ and $G_{\alpha 12/13}$

Stimulation of GPCRs linked to $G_{\alpha12/13}$ and $G_{\alpha q/11}$ results in the activation of RhoGEFs. RhoGEFs stimulate the exchange of GDP for GTP on RhoA, which induces ROCK activation. ROCK stimulates the formation of F actin polymers, which form F-actin stress fibres from G actin monomers. This liberates MRTF-A and MRTF-B from G-actin. MRTF-A and MRTF-B translocate to the nucleus and induce SRF-mediated gene transcription. Genes transcribed by SRF-mediated gene transcription include the genes for connective tissue growth factor (CTGF), αSMA, and collagens (7, 120), all of which are important in the myofibroblast phenotype.

Figure adapted from Xiang et al 2014 (106)

GPCR = G protein coupled receptor; MRTF = myocardin-related transcription factor; SRF = serum response factor

In addition to influencing gene expression, ROCK-generated actin stress fibres are contiguous with focal adhesion complexes, which exist at the cell membrane and are composed of talin, vinculin, paxillin, and other

accessary proteins (122). Focal adhesion complexes associate with integrins to provide a transmembrane link between the intracellular and extracellular environments, and are essential signalling components in the crosstalk between myofibroblasts and the ECM (122).

Rho-ROCK signalling-induced αSMA expression, actin cytoskeletal reorganisation, stress fibre formation, and focal adhesion assembly are all key components of the myofibroblast phenotype (119, 120, 123). As myofibroblasts play key roles in pulmonary fibrosis and fibrosis, Rho-ROCK signalling also likely to play key roles in these processes.

The Rho-ROCK pathway is upregulated in pulmonary fibrosis (123, 124), and inhibition of ROCK signalling is protective against animal models of pulmonary fibrosis (123, 125). However, no developmental lung abnormalities have been reported in mice with genetic deficiency of either ROCK isoform (125). Therefore, while Rho-ROCK signalling is central to pulmonary fibrosis, the role of this key myofibroblast pathway in lung development is less clear.

1.7.2 GPCR signalling in pulmonary fibrosis

Given the widespread expression and physiological functions of GPCRs, it is unsurprising that disturbed GPCR signalling has been described in multiple pathophysiological states, including fibrosis. Several GPCR agonists have been implicated as drivers in IPF through fibroblast activation, including endothelin, thrombin, lysophosphatidic acid (LPA), serotonin, angiotensin, and spinghosine-1-phosphate (S1P) (74, 118,

126-132). In this thesis, LPA will be discussed as the prototypical GPCR agonist.

1.7.2.1 LPA in pulmonary fibrosis

LPA is a bioactive phospholipid released following injury, and is produced either from the membrane phospholipids of cells or platelets or from surfactant phospholipids (133, 134). LPA is generated via two enzyme-mediated pathways involving autotaxin or phospholipases A1 or A2 (135). Different species of LPA exist and have different biological activities (135). In this study, the oleoyl form of LPA was used, which is felt to be a predominant and bioactive form in the lung (135).

LPA is elevated in the lungs of mice subject to bleomycin-induced pulmonary fibrosis and humans with IPF (127, 129, 134, 136). LPA can induce many of the key pathophysiological mechanisms of IPF, such as alveolar epithelial cell apoptosis, fibroblast recruitment and persistence, vascular leak, and activation of latent TGFβ (74, 127, 129, 133). LPA also promotes alterations in shape, contraction, and migration of numerous cell types (137-139), processes which often occur via activation of Rho-ROCK signalling (121) and may be relevant to the tissue remodelling observed in pulmonary fibrosis.

LPA activates seven known GPCRs (LPA_{1-7}), and both LPA_1 and LPA_2 have been implicated in the pathogenesis of pulmonary fibrosis. LPA_1 is the predominant LPA receptor on lung fibroblasts and is thought to be responsible for the promotion of epithelial and inhibition of fibroblast

apoptosis (127). LPA_2 has been shown to mediate LPA-induced TGFβ activation in epithelial cells (74) and fibroblast-to-myofibroblast transition (140). Furthermore, blockade of LPA_1 or LPA_2 is protective against bleomycin-induced pulmonary fibrosis (127, 140, 141). Importantly, LPA signalling induces TGFβ activation in lung epithelial cells (74), suggesting that modulation of LPA signalling has therapeutic potential in pulmonary fibrosis.

$G_{\alpha q/11}$, $G_{\alpha 12/13}$, $G_{\alpha s}$ and $G_{\alpha i/o}$ all signal downstream of LPA receptors (111), and $G_{\alpha q/11}$ signalling has been found to mediate LPA-induced TGFβ signalling in lung epithelial cells (74). However, the role of G_α subunit signalling downstream of LPA receptors in mesenchymal cells in pulmonary fibrosis is unknown.

1.7.2.2 LPA in development

LPA may play a role in late lung development, as mice lacking the LPA_1 receptor exhibit alveolar simplification, disorganised alveolar elastin, and altered tropoelastin production by fibroblasts and myofibroblasts (142), all of which are hallmarks of disturbed alveolarisation. This effect is not common to all LPA receptor knockouts, as developmental lung abnormalities have not been reported in mice lacking LPA_2 (140). These findings, along with the observations that both mice lacking LPA_1 and LPA_2 are protected from pulmonary fibrosis (127, 140, 141), imply both overlapping and distinct roles for the LPA receptors in different biological processes. This may be explained by different G_α subunit signalling

pathways downstream of different LPA receptors, which warrants further investigation.

1.7.3 Heterotrimeric G proteins are essential for survival

The fundamental role of $G_{\alpha 12/13}$ and $G_{\alpha q/11}$ in a number of physiological processes is exemplified by the phenotypes of transgenic mice lacking the genes for these G proteins (107). Germline knockouts of $G_{\alpha 12/13}$ and $G_{\alpha q/11}$ (*Gna12*$^{-/-}$;*Gna13*$^{-/-}$ and *Gnaq*$^{-/-}$;*Gna11*$^{-/-}$, respectively) die *in utero* with a range of defects (Table 1-4). While these studies of global gene deletion indicate that $G_{\alpha q/11}$ and $G_{\alpha 12/13}$ play essential roles in development, their functions in cell- and organ-specific processes could not be determined by these studies.

Table 1-4: Phenotypic characteristics of mice deficient in G protein α-subunits (107)

Mouse genotype	Phenotype
***Gnaq*$^{-/-}$**	Cerebellar ataxia (109) Defective platelet activation, increased bleeding times (108)
***Gna11*$^{-/-}$**	No phenotype observed (143)
***Gnaq*$^{-/-}$ *; Gna11*$^{-/-}$**	Myocardial hypoplasia, die embryonic day 11 (143)
***Gnaq*$^{+/-}$ *;* *Gna11*$^{-/-}$**	Cardiac malformations, die shortly after birth (143)
***Gnaq*$^{-/-}$ *;* *Gna11*$^{+/-}$**	Craniofacial defects, cardiac malformations, die shortly after birth (143)
***Gnaq*$^{+/-}$ *;* *Gna11*$^{+/-}$**	No phenotype observed (143)
***Gna12*$^{-/-}$**	No phenotype observed (117)
***Gna13*$^{-/-}$**	Defective angiogenesis, embryonically lethal day 10 (144)
***Gna12*$^{+/-}$ *;* *Gna13*$^{-/-}$**	Embryonically lethal day 9.5 (117)
***Gna12*$^{-/-}$ *;* *Gna13*$^{+/-}$**	Embryonically lethal day 10.5 (117)
***Gna12*$^{+/-}$ *;* *Gna13*$^{+/-}$**	No phenotype observed (117)
***Gna12*$^{-/-}$ *;* *Gna13*$^{-/-}$**	Embryonically lethal day 8.25 (117)

The transgenic mouse studies summarised in Table 1-4 also demonstrate the functional redundancy and compensatory function of G_{α} subunit pairs. For example, *Gna12*$^{-/-}$ animals are viable and show no

abnormal phenotype, but at least one *Gna12* allele must be present for a *Gna13*$^{+/-}$ animal to survive (117), suggesting some functional interaction between $G_{\alpha 12}$ and $G_{\alpha 13}$. This observed compensation and redundancy is not restricted to within G protein families, as mice lacking both $G_{\alpha 12}$ and $G_{\alpha q}$ die *in utero* at embryonic day 13, whereas mice lacking just one of these G proteins are viable at birth (117). Many individual G protein functions are unclear because of this functional redundancy and compensation. Studies using tissue specific G_{α} subunit deletions may identify roles for individual G proteins in specific developmental and pathophysiological processes.

1.7.4 GPCR signalling as a therapeutic target

1.7.4.1 GPCR inhibition

Several clinical trials have investigated the inhibition of individual GPCRs (Table 1-5). Unfortunately, many of the promising antifibrotic effects observed in preclinical studies have not been recapitulated in humans. This may be due to differences between human IPF and animal models of pulmonary fibrosis such as stage of disease, different pathophysiological mechanisms, and disease complexity (5). Furthermore, given the convergence of GPCR signalling onto just four G_{α} subunit families, inhibition of a single GPCR may still allow other GPCRs to activate the same downstream pathways, blunting any antifibrotic effects of individual GPCR inhibition. In addition, IPF is a complex disease where the lungs are likely to be affected by a plethora of profibrotic mediators simultaneously, many of which signal via GPCRs

(145), and it is likely that multiple GPCRs are abnormally active simultaneously. Finally, GPCR signalling may be active to different degrees in patients with different IPF endotypes, making single GPCR inhibition an over-simplistic therapeutic approach for these patients. Alternative approaches to GPCR inhibition must therefore be considered to enhance the antifibrotic effects of this approach.

Table 1-5: GPCR-targeting drugs tested in pulmonary fibrosis. Adapted from Haak et al 2020 (145)

GPCR agonist	Activity	Drug	Outcome	Phase	Trial reference
Endothelin	ET_A and ET_B agonist	Bosentan	No benefit	II/ III III	NCT00071461 (146) NCT00391443 (147)
		Macitentan	No benefit	II	NCT00903331 (148)
	ET_A agonist	Ambresentan	Detrimental	III	NCT00768300 (149)
LPA	LPA1 agonist	BMS-986020	FVC improved. Study terminated, adverse effects	II	NCT01766817 (150)
Fatty acids	GPR40 agonist / GPR84 antagonist	PBI-4050	Drug well tolerated	II	NCT02538536 (151)
Fatty acids	GPR84 antagonist	GLPG1205	Not reported	II	NCT03725852 (152)

Angiotensin	AT_1 antagonist	Losartan	FVC improved	Pilot	NCT00879879 (153)
Adrenaline	β_2 agonist	Formoterol	Improved FEV1	Pilot	EudraCT:2013-004404-19 (154)
Leukotriene	Leukotriene antagonist	Tipelukast	Not reported	II	NCT02503657 (152) (recruiting)

Approaches to enhance to efficacy of GPCR blockade in IPF may also have significant limitations. While polypharmacy, where several GPCR inhibitors are used simultaneously, could reduce compensatory GPCR signalling, this is likely to increase side effects and would be associated with a significant pill burden for patients (145). Personalised medicine, where therapy is tailored to the overactive disease pathways in an individual, will become more common in the coming years but is not currently in widespread clinical use (5, 145), thus this method does not yet benefit patients. As a solution to these issues, therapeutic targeting of signalling pathways downstream of GPCRs has been proposed, and may be a feasible approach in IPF.

1.7.4.2 Targeting downstream mediators of GPCR signalling

A key antifibrotic approach in the management of pulmonary fibrosis may be to reduce the abnormally elevated TGFβ signalling that drives the disease. While abnormal GPCR signalling contributes to TGFβ activation, TGFβ blockade is likely to be very toxic given the broad physiological functions of TGFβ, and individual GPCR inhibition has

proven to be ineffective (Table 1-5). There are several other signalling pathway components between GPCR activation and TGFβ signalling that could serve as effective targets for antifibrotic drugs (Figure 1-8). For example, ROCK1 and ROCK2 inhibition blocks fibroblast activation and experimental pulmonary fibrosis in mice (125), although the widespread expression and pleiotropic effects of ROCK is cause for concern regarding side effects with ROCK inhibition (145). Furthermore, ROCK can be activated by non-GPCR-related signalling, increasing the likelihood of unintended off-target effects. Alternative GPCR downstream signalling pathway components should therefore be considered for therapeutic targeting.

The G_{α} subunits, which act directly downstream of GPCRs, have not been inhibited therapeutically in humans, although this is a theoretically promising approach for pulmonary fibrosis (Figure 1-8). A single GPCR can activate multiple G_{α} subunit families, which induce different biological effects. For example, the thrombin receptor protease activated receptor-1 (PAR1) couples to $G_{\alpha i/o}$, $G_{\alpha q}$, or $G_{\alpha 12/13}$, but only $G_{\alpha q}$ is important for thrombin-induced CCL2 expression in fibroblasts (155). Additionally, LPA induces fibroblast migration via $G_{\alpha i}$, but if $G_{\alpha i}$ is inhibited LPA inhibits cell migration through $G_{\alpha 12/13}$-coupled signalling (127). These studies suggest that the activity of the G_{α} subunits themselves should be studied to improve our knowledge of IPF and develop novel therapeutics.

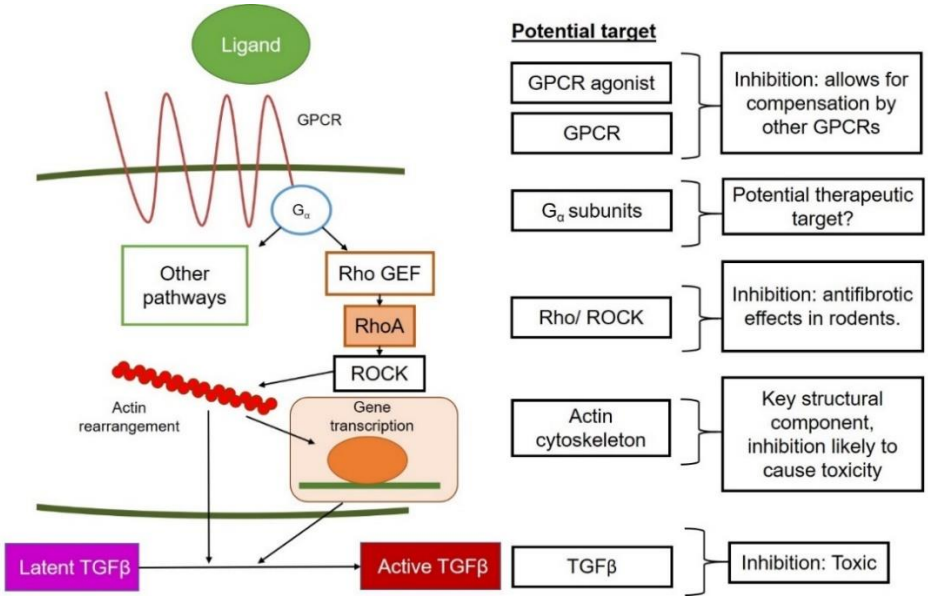

Figure 1-8: Potential benefits and limitations of inhibiting GPCR signalling components

Inhibition of several components of GPCR signalling pathways could have antifibrotic effects. This figure shows the signalling pathway components that could be targeted in pulmonary fibrosis, and the potential problems with these approaches.

GCPRs relevant to fibroblast profibrotic activity signal via $G_{i/o}$, $G_{\alpha q/11}$, and $G_{\alpha 12/13}$ (145, 156), although $G_{\alpha q/11}$ and $G_{\alpha 12/13}$ are the best studied G_α subunits in fibrosis. While small molecular $G_{\alpha q}$ inhibitors exist, they have not been assessed in humans or pulmonary fibrosis animal models (114). Furthermore, there are no chemical inhibitors of $G_{\alpha 12/13}$. Although the animal models of G_α subunit knockdown suggest that caution should be exercised with this approach, G_α subunit inhibition, particularly if restricted to certain organs, tissues, or cell types, may be an effective antifibrotic approach. As mesenchymal cells are so fundamental to pulmonary fibrosis, research into the roles of mesenchymal cell $G_{\alpha q/11}$ and $G_{\alpha 12/13}$ signalling in fibrosis-related signalling may reveal new

therapeutic approaches for this disease. Furthermore, these studies may also clarify the roles of G_{α} subunit signalling in lung development, which may share common G protein-mediated signalling pathways with IPF.

1.8 Mechanical signals in lung fibrosis and development

1.8.1 Mechanical forces in the lung

Research investigating the pathogenesis of pulmonary fibrosis has traditionally focussed on the effect of chemical signals on fibrogenesis. These studies are usually performed by using cells grown on rigid and static tissue culture plastic. This artificial environment is very different to that found in the lungs, where the cellular surroundings are softer and there is constant mechanical force generated by breathing-related cyclical mechanical stretch (CMS) and contraction of nearby cells. These mechanical forces are known to influence multiple cellular processes, including cellular differentiation, adhesion, proliferation, migration, and gene expression (157-159). There is increasing evidence to suggest that myofibroblasts are exquisitely mechanosensitive and can both respond and contribute to mechanical stimuli, influencing both lung development and fibrogenesis, which will be reviewed in the following section.

1.8.2 ECM stiffness influences fibrogenesis

The ECM consists of proteins, such as elastin, collagen, and fibronectin, which act as load-bearing molecules than transmit mechanical stress (160). The elastic modulus (stiffness) of the ECM is defined as the force per unit area (stress) required to deform (strain) the material (161), and is influenced by the composition, organisation, and degree of cross

linking of ECM components (160). There is increasing evidence that the elastic modulus of the ECM is not only increased by profibrotic signalling, but also acts as a fibrosis-promoting stimulus itself.

In pulmonary fibrosis, areas of fibrotic lung have a higher elastic modulus that normal lung parenchyma (100kPa in fibrotic lung compared to 3-5kPa in healthy lung), resulting in in “stiffening” of the lungs and a restrictive ventilatory defect (113, 162, 163). The increased ECM stiffness in fibrosis primarily results from fibroblast- and myofibroblast-generated excessive ECM protein production and cellular contraction, however there is increasing evidence indicating that increased tissue stiffness itself contributes to fibrosis. For example, fibroblasts cultured in stiff environments have enhanced myofibroblast differentiation (164-166), higher ECM protein synthetic activity (162, 163), and reduced matrix degradation enzyme production (162) compared with cells exposed to softer environments. Additionally, fibroblast contractility is enhanced in stiff environments (167), which promotes the activation of TGFβ sequestered in the ECM and generates further profibrotic signalling (168). In addition to being more active in stiff environments, fibroblasts preferentially accumulate in stiff areas when cultured on a stiffness gradient through a process called durotaxis (162, 169). The increased tissue stiffness in fibrosis is therefore both a driver of fibrogenesis and a result of cell-driven processes, and this feedback loop of increased tissue stiffness and enhanced myofibroblast activity drives the progression of pulmonary fibrosis.

Exposure to stiff environments also has lasting effects on the activity of myofibroblasts, which retain a “memory” of the high stiffness-driven phenotype even when returned to environments with physiological mechanical properties. Cells primed on stiff tissue culture substrates behave in a more fibrotic manner even when transferred to softer substrates (53). Furthermore, cells primed on soft substrates and transferred to stiffer substrates are partially protected from developing a high stiffness-induced fibrotic phenotype (53). These data demonstrate how the mechanical environment can cause lasting changes to cellular behaviour, even if resolution of scarring occurs. However, the mechanisms by which cells detect matrix stiffness are incompletely understood.

1.8.3 Cellular contractility modifies ECM organisation

Fibroblasts and myofibroblasts are essential modulators of ECM organisation, which is another key driving factor in IPF. ECM organisation occurs secondary to small repetitive low-force fibroblast contractions, which increase with matrix stiffness and myofibroblast activation (161). Myofibroblasts activate latent TGFβ sequestered in the ECM via contraction of the actin cytoskeleton and integrin tethering to the large latent TGFβ complex, and these cells are more efficient at these processes than the fibroblasts that they differentiate from (168, 170). Highly organised ECM provides greater mechanical resistance to cellular contraction, further enhancing TGFβ activation. Active TGFβ promotes myofibroblast differentiation, a process that is increased in stiffer

environments (165), creating a positive feedback loop of heightened ECM stiffness, increased myofibroblast activity, and TGFβ activation (Figure 1-9).

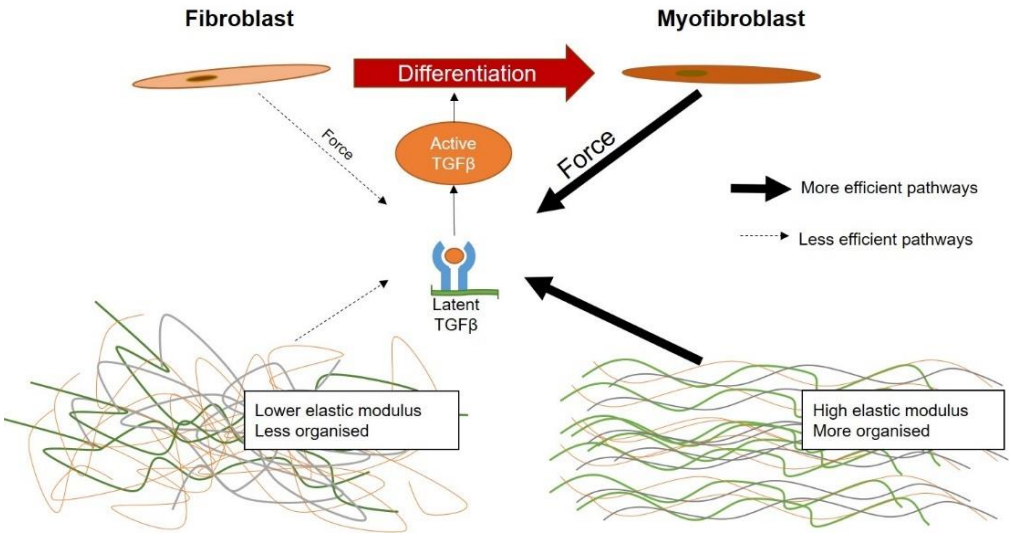

Figure 1-9: Myofibroblast activation results in a positive feedback loop of TGFβ activation enhanced by myofibroblast contractility and ECM properties

TGFβ stimulates fibroblast-to-myofibroblast differentiation. Myofibroblasts are more contractile than fibroblasts, and create stiffer and more organised ECM than fibroblasts, thus are more efficient at liberating active TGFβ from the latent TGFβ complex. This results in a positive feedback loop of myofibroblast differentiation, ECM deposition, and TGFβ activation.

GPCRs may be involved in this self-sustaining loop of fibrosis. For example, the profibrotic GPCR agonist LPA has been found to induce cellular contraction *in vitro*, and this promotes TGFβ activation (74, 137, 171). Previous studies have shown that $G_{\alpha q/11}$ and $G_{\alpha i/o}$ mediate LPA-induced cellular contractility in epithelial cells (74, 171). However, the role

of LPA in fibroblast and myofibroblast contractility and TGFβ activation, and the G_{α} subunits that drive this, is unknown.

1.8.4 Cyclical stretch may promote pulmonary fibrosis

Breathing-related cyclical mechanical stretch (CMS) is a ubiquitous and physiologically relevant force in the lungs that may contribute to pulmonary fibrosis. Breathing-induced CMS forces are heterogeneously distributed in the lung, with the greatest forces occurring in the posterior and basal areas of the lung. These areas also correspond to the locations where fibrotic changes are first seen in patients with IPF, raising the possibility that stretch itself may initiate or propagate pulmonary fibrosis (172).

While no specific studies of lung CMS have been performed in patients with IPF, these patients are prone to acute exacerbations of their disease and worsening lung function if they receive mechanical ventilation (173-175), an intervention associated with repetitive stretch of the lungs. This is thought to occur secondary to alveolar collapse in areas of fibrosis, with overdistension of the remaining, non-collapsed alveoli with breathing (176), resulting in considerable force on epithelial cells secondary to the repeated alveolar opening and collapse (177). This could be exacerbated by the surfactant abnormalities reported in IPF, which may cause perturbations to surface tension and alterations in stretch force distribution (178). Breathing-related CMS is therefore a common stimulus that may contribute to the self-perpetuating lung injury and progression of pulmonary fibrosis.

TGFβ is likely to be a key driving molecule in CMS-related fibrogenesis. Lung stretch via mechanical ventilation increases the expression of mesenchymal cell markers in the lung (179), a process likely to involve TGFβ as stretch increases TGFβ activation in fibrotic lung tissue (113). Stretch also promotes TGFβ expression and activation in a number of different cells types, including vascular and airway smooth muscle cells (180-182), chondrocytes (183, 184), trabecular meshwork cells (185), gingival and dermal fibroblasts (186, 187), renal tubular epithelial cells (188), hepatic stellate cells (189), and Achilles tenocytes (77). The presence of high levels of active TGFβ may also modulate the cellular response to stretch (190), further driving the fibrotic response. Therefore, stretch is a well-established stimulus of TGFβ activity. However, the role of breathing-related CMS in TGFβ signalling in lung fibroblasts, and the mechanisms of stretch detection in these cells, have not been investigated.

CMS is also likely to interact with the altered ECM properties found in pulmonary fibrosis to further promote disease progression. For example, the degree of stretch-mediated TGFβ activation has been reported to correlate with the stiffness of lung tissue (113). Furthermore, stretch-induced production of the ECM component α1 procollagen is influenced by the ECM protein used to coat cell culture plates (191), and cells unable to produce fibronectin have repressed stretch-induced RhoA activation (192). Matrix density is also an important factor in stretch-induced Rho-ROCK signalling (193), suggesting that ECM organisation modulates

cellular responses to CMS. The current hypothesis for the mechanisms underlying this apparent interaction between ECM properties and responses to stretch is that stiff fibrotic ECM provides more mechanical resistance to stretch-induced release TGFβ from the LLC (113). In addition, matrix components such as fibronectin may act as integrin ligands leading to Rho-ROCK signalling and TGFβ activation (113, 182). CMS should therefore be considered alongside ECM properties in studies of pulmonary fibrosis.

Existing studies on the role of CMS on pulmonary fibrosis-related signalling has focussed on whole lung models (113), whereas the effect of mechanical strain on mesenchymal cells specifically has not been investigated previously.

1.8.5 Mechanical forces are important in lung development

In addition to the potential pathophysiological roles that mechanical forces play in the lung, ECM properties and CMS are also essential for normal lung development. Mechanical forces are known to regulate cell fate decisions during organogenesis (194, 195), however are there currently few studies investigating the role of mechanical forces in lung development.

The ECM serves as a scaffold that directs lung development, and is constantly remodelled throughout organogenesis (22, 196). The ECM in foetal, neonatal, and adult lung is distinct, and temporally regulates the shape, migration, and differentiation of resident cells to drive

developmental processes (22). Important roles for ECM structural proteins and remodelling enzymes in alveolarisation have been identified using transgenic mice (196), and these components are known to influence the mechanical properties of the ECM. Traction forces, which increase with ECM rigidity, enhance branching during generation of the salivary glands (194), which undergo branching morphogenesis in a similar manner to the lungs, suggesting a role for ECM stiffness and cellular contraction in organogenesis. However, the role of ECM stiffness in lung development, in particular late lung development, has not been investigated.

Stretch of the lung is also an important stimulus of lung development and growth (191, 197, 198). Oligohydramnios, a condition where there is an abnormally low amniotic fluid volume, and congenital diaphragmatic hernia both result in lung hypoplasia (11, 22). This is thought to be due to restricted lung expansion, which usually begins *in utero* as the foetus inhales amniotic fluid (11, 22). Therefore, lung stretch is an important mechanical force in early lung development. As alveolarisation occurs predominantly postnatally, and breathing-related CMS increases dramatically at birth, it is reasonable to hypothesise that CMS is an important stimulus in alveolarisation.

Published data do indicate an important role for mechanical forces in alveolarisation. During normal development, mechanical stress exerted onto the elastic fibres found along the saccular walls of the developing lung is believed to induce the protrusion of elastin fibres, leading to new

septum formation (47). In BPD, the amount of lung elastin increases with increasing severity of respiratory distress, but this elastin is disorganised and found in aberrant sites away from the alveolar septa (22). These abnormal elastin locations, such as the saccular-alveolar duct junction, are thought to represent the sites of the highest mechanical stress (22), suggesting that force distribution contributes to this disease. Furthermore, mechanical ventilation may uncouple elastin synthesis and assembly, resulting in defective lung alveolarisation and vascular development (13), key features of BPD. These data indicate that stretch-related signalling is essential for normal alveolarisation and may be disturbed in BPD, however the exact mechanisms underlying this are unclear.

1.9 How are mechanical signals detected?

Mechanotransduction is the process by which cells sense and respond to mechanical stimuli (157). This process encompasses the receptors which detect mechanical signals and the communication of this information to produce a cellular response, which includes intracellular and extracellular signalling components. These processes often involve the conversion of mechanical forces to biochemical signals (199), and will be discussed here.

1.9.1 Cell surface mechanoreceptors

Receptor-mediated mechanosensing is essential for a plethora of cellular processes that drive normal development and disease, including cellular activation, differentiation, apoptosis, and proliferation (199). Mechanical

stimuli are usually applied to cell surface receptors that are in direct physical contact with the ECM or adjacent cells (199). A number of mechanically sensitive cell surface receptors (mechanoreceptors) have been identified, including ion channels, integrins, GPCRs, and membrane-associated enzymes such as phospholipase A2 (200, 201). It is beyond the scope of this thesis to discuss each of these extensively, and this work will focus on mechanical signalling mediators related to GPCRs.

Integrins associate with intracellular G proteins (202), and are key components of GPCR agonist-induced TGFβ activation (74). The integrin family consists of 18α and 8β subunits which combine to form 24 αβ heterodimeric membrane receptors that link the cytoskeleton to the ECM, and are key mechanosensors (159, 199, 203). Fibroblasts and myofibroblasts express the αvβ1, αvβ3, αvβ5 and αvβ8 integrins, all of which may be important in mechanosensation, and are able to activate latent TGFβ (9). Mechanical forces may induce conformational changes to integrins, altering ligand binding affinity and strengthening the bonds between integrins and ECM components (204-206), with important implications for profibrotic signalling. Furthermore, integrins have been found to be essential for stretch-induced TGFβ activation (113, 207), and therefore may be important in pulmonary fibrosis and lung development.

1.9.2 Intracellular mechanical signalling

A number of intracellular signalling mediators convert mechanical stimuli into biochemical signals including adaptor and scaffolding proteins, such

as talin, and vinculin, kinases and phosphatases, such as focal adhesion kinase (FAK), cytoskeletal components including actin filaments, myosin, and microtubules, and transcriptional coactivators, such as YAP/TAZ, and transcription factors, such as MRTF-A and MRTFB (157, 159). These will be discussed below in terms of their common effects on the actin cytoskeleton and Rho/ROCK signalling.

Components of the actomyosin cytoskeleton and associated proteins, such as vinculin and talin, constitute the “molecular clutch” (159). The molecular clutch is used to transmit forces to the surrounding matrix, resulting in the generation of biochemical signals. Increased matrix stiffness enhances activity of this molecular clutch via increased mechanical loading on talin, which intensifies its binding affinity for vinculin and elevates force transmission (203, 208). The actomyosin cytoskeleton is a critical mediator of both sensation of the mechanical environment and cellular propulsion towards stiff areas (209), and consideration of the mechanisms that induce cytoskeletal change is important to the study of mechanobiology.

Although a diverse array of signalling and transcriptional programmes is activated by mechanoreceptors, a common effect on RhoGTPases and actin cytoskeletal assembly is often seen (145). Rho-ROCK signalling increases matrix stiffness through activation of profibrotic genes transcription via YAP/TAZ and MRTF-A and -B activity (145), and is a key component in the detection of ECM stiffness. Stiff ECM increases the activity of RhoA and ROCK in fibroblasts (119), and knockdown of

both ROCK1 and ROCK2 abrogates αSMA fibre assembly in cells grown on stiff tissue culture matrices (120). In addition, RhoA/ ROCK inhibition abrogates stiff matrix-induced actin cytoskeletal reorganisation, MRTF nuclear translocation, myofibroblast differentiation, and contractile function of IPF fibroblasts (119, 167). Furthermore, Rho-ROCK signalling is required for CMS-induced stress fibre formation and stretch-induced TGFβ signalling in fibrotic lung (113, 193). This evidence suggests an important role for ROCK signalling in the detection of mechanical signals including matrix stiffness and CMS.

Given the key roles of Rho/ROCK signalling in mechanically-induced myofibroblast function, Rho/ROCK signalling is likely to be important in both lung fibrosis and development. However, the situation is complex, as ROCK may play different roles in the maintenance of the myofibroblast phenotype in different mechanical environments as, unlike the situation observed on stiff substrates, ROCK inhibition does not alter F-actin stress fibre formation on soft matrices (120). In addition, complete loss of αSMA stress fibre assembly is only seen when both the ROCK 1 and ROCK2 isoforms are absent, suggesting that each isoform plays independent roles in sustaining the myofibroblast phenotype (120). The balance between ROCK 1 and ROCK 2 isoforms is also significant, as knockout of one isoform paradoxically increases αSMA expression in myofibroblasts grown on stiff matrices (120). An understanding of how Rho/ROCK signalling is regulated in lung development and becomes

dysregulated in fibrosis may identify mechanisms by which lung regeneration can be induced following injury.

1.9.3 GPCRs as mechanosensors

There is growing evidence that GPCRs are mechanosensitive, and thus can transmit intracellular signals in response to mechanical stimuli. Mechanosensitive GPCRs include the angiotensin II receptor 1 (AT1R), bradykinin receptor (B2R), parathyroid receptor 1 (PTH1R), histamine receptor 1 (H5R), and the muscarinic receptor M5R (200). In addition, several GPCRs that have been implicated in the pathogenesis of pulmonary fibrosis, including those for thrombin, lysophosphatidic acid (LPA), and spinghosine-1-phosphate (S1P), have been found to activate RhoA signalling (74, 118, 126-128). The activation of this mechanosensitive pathway by the activation of fibrosis-related GPCRs suggests that GPCR mechanosensation may be important in pulmonary fibrosis.

G proteins may participate in mechanotransduction through interactions with cell surface molecules or GPCRs. Intracellular G proteins are involved in the integrin-mediated “outside-in” signalling by which integrins transmit signals from the extracellular area to the intracellular environment that stimulate cell spreading, retraction, migration, proliferation and survival (202). There is significant crosstalk between GPCR and integrin signalling, for example GPCR activation increases $G_{\alpha 13}$ binding to the integrin β1 and β3 subunits, which then augments integrin-mediated signalling (202). This evidence suggests that G

proteins may have a role in facilitating mechanosensitive pathways mediated by cell surface molecules.

In addition, GPCRs may be intrinsically mechanosensitive. Membrane tension resulting from mechanical forces is thought induce conformational changes in some GPCRs (200, 210), precluding the need for a GPCR agonist in GPCR activation. For example, the $G_{\alpha q/11}$-coupled angiotensin II receptor AT1 has been found to transduce signals involved in vascular constriction and cardiac hypertrophy in response to high intraluminal pressures in the absence of the GPCR agonist angiotensin II, in vascular smooth muscle cells and cardiomyocytes, respectively (211-215). The role of intrinsic GPCR mechanosenstivity in the lung has not been previously studied.

As the Rho-ROCK signalling pathway is integral to both the myofibroblast phenotype and mechanical signal transduction from cell stretch and matrix stiffness, and $G_{\alpha q/11}$ and $G_{\alpha 12/13}$ both signal via the Rho-ROCK cascade, $G_{\alpha q/11}$ and $G_{\alpha 12/13}$ could be hypothesised to be mechanical signalling components. $G_{\alpha 12/13}$ is traditionally thought of as a mechanosensitive G protein family because of its well-established relationship with Rho-ROCK signalling and the actin cytoskeleton. The role of $G_{\alpha 12/13}$ stretch-mediated signalling is best understood in cardiac fibrosis, where $G_{\alpha/13}$ mediates stretch-induced expression of fibrogenic factors (216, 217). In cardiomyocytes, stretch induces $G_{\alpha 12/13}$-mediated RhoGEF12 activity, which subsequently activates the Rho-ROCK cascade (217). In a pressure overload-induced cardiac fibrosis model,

$G_{\alpha 12/13}$ was found to mediate stretch-induced expression of collagen, CTGF, and TGFβ genes, as well as the TGFβ protein (216). In addition, $G_{\alpha 12/13}$ transmits signals in response to stretch in renal epithelial cells, via Rho and the actin cytoskeleton (218). However, the role of stretch mediated $G_{\alpha 12/13}$ in lung homeostasis and disease is not known.

While Rho-ROCK signalling is not the major pathway downstream of $G_{\alpha q/11,}$ these G proteins can also couple to specific RhoGEFs and induce RhoA signalling (118). In addition, many GPCRs that induce RhoA signalling via $G_{\alpha 12/13}$ also couple to $G_{\alpha q}$ and PLC, suggesting that collaborative signalling between the two G protein families may be common (118). Furthermore, mice lacking alveolar epithelial $G_{\alpha q/11}$ are protected from ventilator-induced lung injury through reduced stretch-mediated TGFβ activation (219), suggesting a role for $G_{\alpha q/11}$ in detecting CMS and the subsequent activation of a profibrotic signalling mediator. Loss of this mechanosensitive pathway results in loss of lung homeostasis, demonstrated by emphysema in mice deficient in alveolar epithelial $G_{\alpha q/11}$ signalling (219). Interestingly, mice lacking $G_{\alpha 12/13}$ signalling in alveolar epithelial cells exhibited no abnormal lung phenotype in this study (219), demonstrating different roles for lung epithelial $G_{\alpha 12/13}$ and $G_{\alpha q/11}$ *in vivo*. The role of mesenchymal cell $G_{\alpha q/11}$ and $G_{\alpha 12/13}$ in the detection of mechanical signals in the lung, and how this influences lung development and IPF, has not been investigated.

1.10 Animal models of lung disease

Much of our understanding of the pathophysiology of lung disease, such as IPF and BPD, and normal lung development has come from *in vivo* models. The following section will discuss the common animal models used in these areas.

1.10.1 Pulmonary fibrosis models

Rodent models of pulmonary fibrosis are commonly used to elucidate disease mechanisms and for early investigation of potential antifibrotic compounds. There are a number of methods used to induce pulmonary fibrosis in animals models including bleomycin, radiation, fluorescein isothiocyanate (FITC), and transgenic expression of profibrotic mediators (220). The bleomycin-induced pulmonary fibrosis (BIPF) model is the most commonly used and is considered by some to be the best available model, as it can be performed over a shorter timeframe and with less specialised equipment relative to other models (220, 221).

Bleomycin is a chemotherapeutic agent used for haematological malignancies, and its use in pulmonary fibrosis research is based on the lung toxicity that occurs in some patients that receive bleomycin chemotherapy. Bleomycin is thought to induce pulmonary fibrosis by enhancing free radical formation and overproduction of reactive oxygen species (222). BIBF is controversial as the evidence suggests that, unlike IPF, BIPF resolves with time (220), and many therapeutics tested with “prophylactic” timing in the BIBF model have proven to be ineffective in

IPF clinical trials (222). However, it should be noted that no animal model exactly recapitulates the pathogenesis of IPF (220).

Pathophysiological mechanisms of IPF have also been implied from studies of transgenic mice, where animals lacking a key profibrotic mediator are found to be protected from BIBF. BIPF is usually induced in mice aged 6-8 weeks, and animals must be sufficiently robust at this age to withstand the acute lung injury induced by bleomycin in order to get meaningful results from a study (74, 223). Therefore, the phenotyping and observation of any new transgenic mouse strains that are intended for use in the BIBF model, particularly for baseline lung abnormalities induced by gene manipulation, must be performed before the BIPF model is considered for this kind of study.

1.10.2 BPD models

There is no perfect animal model for BPD, as BPD is a clinical entity and the BPD animal models are defined by their ability to disturb lung alveolarisation (13). A common animal model used to recapitulate the abnormalities seen in BPD is the hyperoxia rodent model, where mice or rats are exposed to high FiO_2 (60-100%) for around 14 days after birth (40).

Mechanical ventilators may also be used to mimic the mechanical ventilation of the preterm neonate. These can be used in rodents, but lamb and baboon models allow long-term ventilation and are also used in BPD research (40). Larger mammal models also permit the

manipulation of other BPD risk factors, such as induction of chorioamnionitis by intraamniotic administration of E.Coli toxin during pregnancy, but require specialist skills and facilities.

1.10.3 Transgenic mouse models

Transgenic mice with alterations to the genes for various signalling components have been widely used to imply mechanism in both pulmonary fibrosis and BPD. However, relevant to this project, the global genetic deletion of $G_{\alpha q/11}$ or $G_{\alpha 12/13}$ is embryonically lethal (page 71), therefore the roles of these G proteins in normal lung development and fibrogenesis have not been determined *in vivo*.

Cell-specific expression of DNA recombinases allows gene knockout in specific cell types, which is useful when global gene deletion is unfeasible. The Cre-lox system is the most widely used method of cell-specific gene targeting in mice (224). In this system, loxP sites, which are 34bp DNA sequences containing two 13bp inverted repeated and an asymmetric 8bp spacer region, are the targets of DNA recombination (224). A gene with loxP sites either side of one or more essential exons is called a “floxed” (flanked by loxP) gene, and DNA sequences flanked by loxP sites will be excised in the presence of Cre recombinase, a DNA recombinase (224). In the conditional knockout model, Cre recombinase is expressed under the control of a gene expressed only by a certain cell type, and in cells where Cre recombinase is present floxed genes are deleted (225), resulting in cell type-specific gene knockout. Cell type-specific gene knockout can occur from conception, in germline Cre-Lox

models, or can be induced at a time point appropriate for the investigation, for example with tamoxifen-inducible Cre recombinase expression (226).

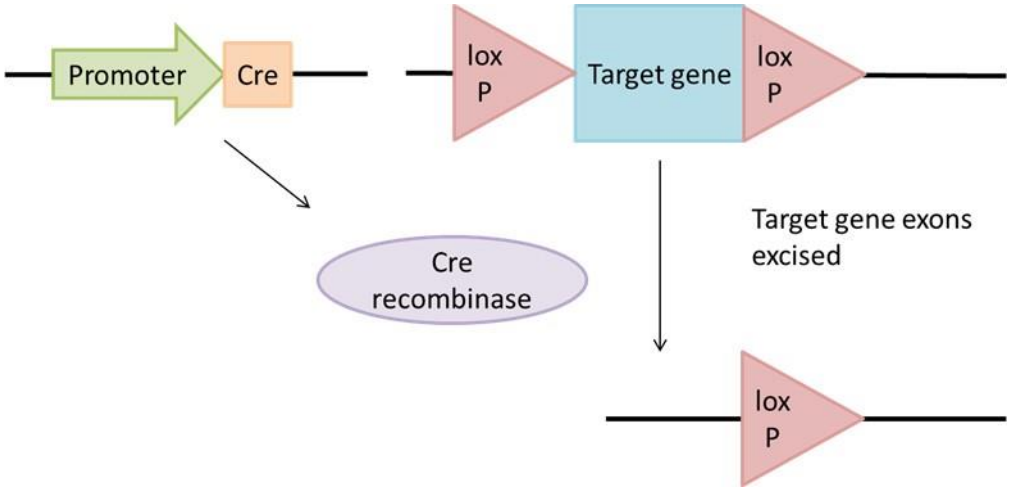

Figure 1-10: The Cre-lox method for cell type-specific gene knockout

Cre recombinase expression is driven by a cell-specific promoter, leading to cre recombinase expression only in certain cell types. The target gene is flanked by loxP site (floxed). Cre recombinase excises DNA between the loxP sites, resulting in inactivation of the target gene. Figure adapted from Kohan 2008 (224)

The Cre-lox system has previously been used to induce cell type-specific knockout of $G_{\alpha q/11}$ and $G_{\alpha 12/13}$ (219, 227). Given the key roles of mesenchymal cells in lung development and fibrogenesis, mesenchymal cell-specific $G_{\alpha q/11}$ and $G_{\alpha 12/13}$ knockout mice may be incredibly useful tools to assess the roles of $G_{\alpha q/11}$ and $G_{\alpha 12/13}$ in these processes.

1.11 Summary

Numerous pathways are shared between the pathogenesis of IPF and normal lung development, including those induced by both chemical and

physical stimuli. $G_{\alpha q/11}$ and $G_{\alpha 12/13}$ are G protein families that signal downstream of many GPCRs implicated in both lung development and IPF, and mesenchymal cells, particularly pericytes and myofibroblasts, are key cells in both of these processes. However, the exact roles of $G_{\alpha q/11}$ and $G_{\alpha 12/13}$ in the chemical and mechanical signalling pathways that drive mesenchymal cell differentiation and function, and how these affect lung development and pulmonary fibrosis, are unclear. A better understanding of these signalling pathways may identify novel therapeutic targets that could improve the outcomes for patients with IPF and BPD.

2 Aims and Hypothesis

2.1 Aims

The overall aims of this study were to:

1) Understand the roles of mesenchymal cell $G_{\alpha q/11}$ and $G_{\alpha 12/13}$ in mediating chemical and mechanical signals in the pathogenesis of pulmonary fibrosis.
2) Establish murine models of mesenchymal $G_{\alpha q/11}$ and $G_{\alpha 12/13}$ knockdown to investigate the roles of these molecules in the pathogenesis of pulmonary fibrosis.
3) Determine any potential toxic effects related to reductions in mesenchymal cell $G_{\alpha q/11}$ and $G_{\alpha 12/13}$ signalling that may occur if this approach is pursued as a therapeutic strategy for pulmonary fibrosis.

2.2 Hypothesis

The two hypotheses underlying the work presented in this thesis are:

Mesenchymal cell $G_{\alpha q/11}$ and $G_{\alpha 12/13}$ play central roles in the pathogenesis of pulmonary fibrosis, and these functions may occur via different molecular mechanisms.

Inhibition of mesenchymal cell $G_{\alpha q/11}$ and $G_{\alpha 12/13}$ in vivo may be protective against experimental pulmonary fibrosis, but this approach could be associated with adverse effects.

3 General methods

3.1 Methods

Techniques that were used to generate data for several results chapters are discussed here. Any chapter-specific methods are discussed in the relevant results chapters.

3.2 Materials

All materials and suppliers are listed in the Appendix (page 367).

3.3 *In vitro* experiments

3.3.1 Cells

3.3.1.1 Murine embryonic fibroblasts

Wild-type (WT), *Gnaq*$^{-/-}$; *Gna11*$^{-/-}$, and *Gna12*$^{-/-}$;*Gna13*$^{-/-}$ murine embryonic fibroblasts (MEFs) were a gift from Stefan Offermanns (Germany). These cells and were derived from mouse embryos with the appropriate genotypes at the founding laboratory (117, 228).

3.3.1.2 Human lung fibroblasts

Human lung fibroblasts (HLFs) from donors with and without pulmonary fibrosis were obtained from a cell bank at the University of Nottingham NIHR Respiratory Biomedical Research Centre. These cells were used at passage 5-6.

3.3.1.3 Transformed mink lung cells

Transformed mink lung cells (TMLCs) that express luciferase under the control of the TGFβ-induced gene plasminogen activator inhibitor (Pai-1) were used for the luciferase reporter assays (229).

3.3.2 Cell culture

3.3.2.1 Cell culture media recipes

The cell culture media recipes used for *in vitro* experiments are shown in Table 3-1.

3.3.2.2 Cell culture

All cells were cultured at 37ºC and 5% CO_2 and confirmed to be mycoplasma negative prior to experiments. Cell culture media was changed every 2-3 days to ensure removal of waste products and adequate supply of growth mediators.

Cells were passaged when 80% confluent. At passage, cells were detached from cell culture flasks with trypsin-EDTA solution and the trypsin was neutralised with full media. The cell suspension was then centrifuged at 11000rpm for 5 minutes, and cells resuspended at the desired concentration in full media.

Prior to experiments, cells were growth arrested for 24 hours in either 0% foetal calf serum (FCS) or 1% FCS in Dulbeccos Modified Eagles Medium (DMEM), according to the specific protocols. Growth arrest was performed to ensure that all cells were at the same stage of the cell cycle, and to remove confounding by signalling mediators present in full media.

Table 3-1: Cell culture media recipes

Culture media	Components
Full media	DMEM supplemented with 10% FCS, L-glutamine (4nM), penicillin (100 units/ml), streptomycin (0.1 mg/ml)
0% FCS DMEM	DMEM supplemented with L-glutamine (4nM), penicillin (100 units/ml), streptomycin (0.1 mg/ml)
1% FCS DMEM	DMEM supplemented with 1% FCS, L-glutamine (4nM), penicillin (100 units/ml), streptomycin (0.1 mg/ml)
TMLC media	DMEM supplemented with 10% FCS, L-glutamine (4nM), penicillin (100 units/ml), streptomycin (0.1 mg/ml), G418 (25µg/ml)
Antibiotic-free full media	DMEM supplemented with 10% FCS, L-glutamine (4nM)
Transfection media	DMEM supplemented with L-glutamine (4nM), transfection reagent (assay-dependent concentration), siRNA (assay-dependent concentration)
Antibiotic-free 1% FCS DMEM	DMEM supplemented with 1% FCS, L-glutamine (4nM),
Antibiotic-free 0% FCS DMEM	DMEM supplemented with L-glutamine (4nM)
Freezing media	90% full media, 10% DMSO
FCS= foetal calf serum; DMEM = Dulbeccos modified eagles medium	

3.3.2.3 Preparation of cells from donated human lung tissue

HLFs were originally derived from donated human lung tissue, from either living surgical lung biopsy or post-mortem tissue samples. Non-diseased human lung fibroblasts were obtained from donors without pulmonary fibrosis, from areas of lung with a normal appearance.

Lung tissue was cut into 1mm^3 fragments which were placed 10mm apart on the surface of 10cm tissue culture dishes. These fragments were allowed to dry for 5 minutes to encourage adherence to the culture surface, then a small volume of full media with 2.5µg/ml amphotericin B added to each tissue fragment. 2ml full media with amphotericin B was added to each culture dish, and the fragments were left in a humidified incubator at 5% CO_2 overnight. After 24 hours, when the tissue fragments were firmly adhered to the dishes, a further 8ml full media with amphotericin B was added to each dish. Media was changed every 3-5 days, and tissue fragments removed and disposed of when they detached from the plate.

Fibroblasts could be observed growing from tissue fragments after around 7 days. When they reached 80% confluency, cells were detached from the dish surface using 0.25% Trypsin/ Ethylenediaminetetraacetic acid (EDTA). Cell suspensions were centrifuged at 300 x g for 5 minutes, the supernatant discarded, and pellet resuspended in 30ml full media. This suspension was split equally between two T150 flasks and marked as passage 1 (P1).

When the P1 cells reached 80% confluency each T150 flask was split into 3 T150 flasks and designated P2, and for each subsequent passage each T150 flask was divided into 3 T150 flasks. Cells were frozen for long term storage at P1 or P2.

3.3.2.4 Cryopreservation of cells

As primary cells can undergo only a finite number of passages before becoming senescent, cell stocks were frozen to a temperature of -180^{o}C in liquid nitrogen until they were needed. In this process, the cyropreservative agent dimethyl sulphoxide (DMSO) is included in the freezing media to lower the freezing point of the solution and to prevent the formation of intracellular ice crystals, which would result in cell death (230). A specialised freezing chamber, such as the “Mr Frosty” is used, which is filled with isopropanol. The isopropanol cools at a rate of around 1^{o}C per minute when placed in a -80^{o}C freezer, which is within the 1-3^{o}C per minute cooling rate that is optimal for cell cryopreservation.

Prior to freezing, cells were suspended in freezing media at 5 x 10^{5} cells per cryogenic vial. Vials containing cell suspension were placed into a “Mr Frosty” containing isopropanol. This was kept at -80^{o}C overnight, then cells were transferred for long-term storage in liquid nitrogen.

When frozen cells were to be thawed, the vials were placed in a water bath at 37^{o}C for 1-2 minutes. When the cell suspension had defrosted, this was added to 30ml of warm media in a T150 flask, and the cells incubated as normal.

3.3.2.5 Cell counting

The cell number in a cellular suspension was determined using a haemocytometer. 10µl of cell suspension was distributed under the coverslip of the haemocytometer. Cells were counted by viewing the haemocytometer under a light microscope, and counting the number of cells in each of the four corner squares. The mean cell number of the four corner squares was taken and multiplied by 1 x 10^4 to give the number of cells per ml of cell suspension.

3.3.2.6 Lung tissue donor characteristics

The demographic details for the donors of lung tissue from which the HLFs were derived are shown in Table 3-2.

Table 3-2: Demographic details of human lung fibroblast donors

Donor code	Condition	Sex (M/F)	Age (years)
RS11009	Non-fibrotic	M	Not recorded
RS11010	Non-fibrotic	F	73
RS11013	Non-fibrotic	M	75
ALS09002	Non-fibrotic	M	64
ALS09004	Non-fibrotic	M	68
RS10005	Non-fibrotic	M	57
RS09004	IPF	M	Not recorded
RS12017	IPF	F	59
RS10006	IPF	M	56
RS12020	IPF	M	43
AT260615	IPF	F	Not recorded
RS09001	IPF	F	Not recorded

3.3.3 Cell stimulation experiments

3.3.3.1 General principles

All *in vitro* experiments were performed on cells grown on six well cell culture plates, unless otherwise stated. Each experimental condition was performed in duplicate during every experimental replicate. For experiments where protein expression was measured, samples from two wells were pooled to generate a protein sample for analysis. For experiments where gene expression was measured, samples from each well were processed separately, and mean gene expression calculated from both wells.

For assays measuring the TGFβ activation response using pSmad2 expression, control wells were stimulated with 2ng/ml TGFβ1 for 1 hour to give a positive control sample for pSmad2 expression.

Prior to all experiments where cells underwent chemical or stretch stimulation, cells were growth arrested in either 0% or 1% FCS DMEM according to the assay. This process synchronises all cells into the same phase of the cell cycle, and removes any chemical mediators found within FCS that could alter cellular signalling.

3.3.3.2 LPA preparation

In this study, the oleoyl form of lysophosphatidic acid (LPA) was used as this is felt to be a predominant and bioactive form (135).

Solid LPA was dissolved to make a 11.4mM stock solution in 0.1% bovine serum albumin (BSA) in phosphate-buffered saline (PBS). This was

agitated on a roller at room temperature for 30 minutes, to ensure the dry compound had completely dissolved. Reconstituted LPA was stored at -20ºC.

3.3.3.3 Inhibitor experiments

For experiments involving the use of a chemical inhibitor, the inhibitor was applied in growth arrest media appropriate to the individual experimental protocol 30-60 minutes before the experimental stimulus was applied. If an inhibitor was reconstituted in DMSO, an equivalent concentration of DMSO without inhibitor was used as a negative control.

3.3.3.4 Chemical inhibitor preparation

Chemical inhibitors were prepared as described in Table 3-3.

Table 3-3: Chemical inhibitors

Inhibitor	Target	Diluent	Stock concentration	Storage
Y27632	ROCK	Water	10mM	-20ºC
YM-254890	$G_{\alpha q/11}$	DMSO	10mM	4ºC
SB-525334	Alk5	DMSO	50µM	-20ºC
U73122	PLC	DMSO	1.9mM	-20ºC
CWHM-12	αv integrins	DMSO	10mM	-20ºC
AEBSF	Serine proteases	Water	100mM	-20ºC
NOTT199SS	β1 integrins	DMSO	10mM	-20ºC
GM-60001	Matrix metalloproteinases	DMSO	2.5mM	-20ºC

3.3.4 siRNA transfections

3.3.4.1 Principle of method

RNA interference is a method used to induce transient posttranslational gene silencing *in vitro*. In this method, synthetic non-coding double stranded RNAs called small interfering RNAs (siRNAs) are designed to target mRNA sequences specific to the gene that is to be knocked down. SiRNAs consist of an antisense (guide) strand, which is the reverse complement the intended target mRNA, and a sense (passenger strand). These 21-nucleotide long RNAs form a duplex long with a two nucleotide overhang at the 3' end of each strand (231). The siRNA can be transfected into cells via a number of methods, including using cationic liposome- or polymer-based transfection reagents, electroporation, or viral-mediated delivery methods. Once within the cell, the siRNA becomes incorporated into the RNA-induced silencing complex (RISC) and is unwound to form single stranded RNA (231). The antisense single-stranded siRNA component then guides and aligns the RISC complex onto the target mRNA which is cleaved through the action of catalytic RISC protein (231). The target mRNA is thus temporarily unavailable for translation into protein.

3.3.4.2 Method

SiRNA was used to induce *GNAQ* and *GNA11* or *GNA12* and *GNA13* knockdown in HLFs. Commercially available pooled siRNAs for human *GNAQ*, *GNA11*, *GNA12* and *GNA13* were used. SiRNAs were applied to cells in pairs according to the G protein family under investigation (i.e.

$G_{\alpha q/11}$ or $G_{\alpha 12/13}$). Control (non-targeting) siRNA was applied to control cells at 25nM, as per the manufacturer's instructions.

Prior to first use, siRNA was resuspended in 1x siRNA buffer, which was diluted from a commercial 5 x siRNA buffer (Dharmacon) to make 5nmol stocks. Working stocks of 20µM siRNA were made in RNAse-free water prior to each experiment.

GNAQ, *GNA11*, *GNA12*, and *GNA13* siRNAs were used at assay-specific final concentrations, diluted in antibiotic-free 0% FCS DMEM. SiRNA suspensions were mixed with Dharmacon Transfection Reagent 1^{TM} diluted in antibiotic-free 0% FCS DMEM (final concentration of transfection reagent 4µl/ml), and incubated for 20 minutes at room temperature. 1.6ml of antibiotic-free 10% FCS DMEM was added to each well of a six well plate, and 400µl of the siRNA/ transfection mixture added to each well. After 24 hours, the transfection media was replaced with antibiotic-free 10% FCS DMEM. The growth arrest protocols for the siRNA experiments were assay-specific and are detailed in the relevant chapters.

3.3.5 Sample collection

3.3.5.1 Samples for protein analysis

The cell culture media was aspirated and cells were washed with ice cold PBS. The lysis buffer consisted of 10x lysis buffer diluted 1:10 in sterile water and supplemented with phosphatase inhibitors (Phos-stop, 1 tablet per 5ml of lysis buffer), protease inhibitors (Complete Mini, 1 tablet per

5ml of lysis buffer), and phenylmethane sulfonyl fluoride (PMSF, final concentration 2mM). Cells were lysed in 150µl lysis buffer per well of a six well plate, and samples immediately stored at -20^{o}C.

3.3.5.2 Sample collection for mRNA analysis

The cell culture media was aspirated and cells washed with PBS. Cells were lysed with RA1 lysis buffer supplemented with β-mercaptoethanol, and samples stored at -20^{o}C until RNA isolation. The RA1 buffer and RNA isolation columns and materials were from a commercially available kit (Machery-Nagel Nucleospin RNA isolation kit), and was used according to the manufacturer's instructions.

3.3.6 Western blotting

3.3.6.1 Principle of assay

Sodium dodecyl sulphate-polyacrylamide gel electrophoresis (SDS-PAGE) is a method for separating proteins within a sample according to the molecular weight by loading protein samples onto a polyacrylamide gel and applying a current. In this method, samples are boiled in lamellae buffer, during which SDS binds to and denatures the proteins, and β-mercaptoethanol reduces any disulphide bridges contributing to tertiary protein structure, resulting in fully-denatured and negatively-charged proteins in each sample. When a current is applied to the polyacrylamide gel, the negatively charged protein-SDS complexes move towards the anode, but as smaller proteins pass more easily through the pores of the resolving gel, the proteins become separated by molecular weight (232).

The separated proteins can then be transferred to a membrane by electroblotting, where the protein-containing polyacrylamide gel and a polyvinylidene fluoride (PVDF) membrane are arranged between two electrodes and a current passed through this “sandwich”. The protein within the gel moves towards the anode on application of this current, and is transferred onto the PVDF membrane (232).

Before the blot is probed with a primary antibody, it is incubated in a protein solution (e.g. 5% non-fat dried milk or BSA) to block any remaining hydrophobic binding sites on the PVDF membrane (232). The blot is then incubated with an IgG antibody that will bind to the protein of interest, which can then be detected by chemiluminescence and indicate whether the protein is present.

3.3.6.2 Western blot buffers

Western blot buffers were made in house, and the recipes for these are shown in the Appendix (page 376).

3.3.6.3 Protein quantification using the BCA assay

3.3.6.3.1 Principle of assay

The bicinchoninic acid (BCA) assay depends on colour changes created by incubating a protein sample with the BCA reagent. The peptide bonds of protein present in the sample being tested react with the copper ions (Cu^{2+}) in the BCA reagent to produce Cu^{+}, which reacts with bicinchoninic acid and creates a purple colour (233). The degree of colour change is determined by the concentration of protein within the sample. The colour

change is quantified by measuring absorbance of the sample/BCA at 560nm, and comparing these values to the absorbance of a standard curve of samples of known concentration.

3.3.6.3.2 Method

A commercial BCA protein assay kit was used, as per the manufacturer's instructions. The BCA working reagent was made by diluting Reagent A with Reagent B from the BCA assay kit at a 50:1 ratio. 5µl of each sample was incubated with 95µl BCA working for 30 minutes in a 96 well plate, and the absorbance at 560nm read on a BMG plate reader. The protein concentration was calculated from a bovine serum albumin (BSA) standard curve using Omega software (BMG Labtech). Each sample was analysed in duplicate and the absorbance value corrected to a "blank" sample consisting of water only, and the mean sample protein concentration calculated. The BCA assay was performed immediately before western blots were performed to avoid protein degradation secondary to freeze-thawing of samples.

3.3.6.4 Western blot gel casting

A BioRad Protean Tetra gel casting system was used for gel casting. A 10% resolving gel was prepared (components listed in the Appendix, page 378) and pipetted into the casting system, leaving approximately 2cm at the top of the casting system. Isopropanol carefully layered over the resolving gel solution to disperse any bubbles at the top of the gel. The gel was left to polymerise for 30 minutes at room temperature, and the isopropanol poured away. A stacking gel solution was prepared

(components listed in the Appendix, page 378) and poured on top of the resolving gel to fill the casting system, and a 10 or 15 well comb inserted. This was left to set for around 30 minutes, the comb removed, and the gels placed into the running tank in 1 x running buffer.

3.3.6.5 Sample preparation

4x lamellae buffer (components listed in the Appendix, page 376) was mixed with samples in a 1:3 ratio. The samples were then incubated at 100^{o}C for 5 minutes before being loaded onto the polyacrylamide gels.

3.3.6.6 Running

For experiments where pSmad2 was measured, the first lane of each gel was loaded with the TGFβ positive control sample. This was to ensure a distance between the positive control sample and experimental samples, so that any low-grade pSmad2 expression in the experimental samples was not masked by the positive control. 10µl of rainbow molecular marker was loaded into the second well, and the subsequent lanes loaded with experimental samples containing 15-25µg protein. For each experiment, all wells were loaded with an equal amount of protein as determined by the BCA assay.

The running tank was filled with 1x running buffer (components listed in the Appendix, page 376) to the indicator mark, and a voltage of 150V applied for 70 minutes. Adequate separation of the rainbow molecular marker, which give different coloured bands according to the molecular

weight of its components and can be viewed with the naked eye, was confirmed visually before moving to the transfer step.

3.3.6.7 Transfer

Gels were washed in 1x transfer buffer (components listed in the Appendix, page 377) for 5 minutes, then sandwiched into the transfer kit with foam, filter paper, and PVDF membrane. The PVDF was activated by soaking in methanol for 15-30 seconds. Protein was transferred from the gel to the PVDF by applying a voltage of 110V for 1 hour in 1x transfer buffer. Ice blocks were used to prevent the transfer buffer from overheating during the transfer process.

3.3.6.8 Blocking

For most western blots, the membrane was blocked with 5% blotto non-fat milk made up in Tris (tris(hydroxymethyl)aminomethane) buffered saline plus 0.1% Tween20 (TBST) (components listed in the Appendix, page 377) for one hour, then incubated with primary antibody in 5% non-fat milk in TBST overnight at 4^{o}C.

For $G_{\alpha 12}$ western blots, the membrane was blocked with 3% BSA in TBST rather than with milk.

3.3.6.9 Protein detection

In this study, horseradish peroxidase (HRP)-conjugated secondary antibodies and enhanced chemiluminescence (ECL) were used to detect protein on the PVDF membrane. In this method, the blot is incubated with an HRP-conjugated secondary antibody specific to the IgG of the species

of the primary antibody, resulting in HRP at the position where the protein of interest is found. When this blot is incubated with ECL solution, the HRP oxidises the luminol contained in the ECL, resulting the production of light (232). This light is detected by holding the blot against photographic film, which is then developed and shows dark bands where HRP activity occurred (232). The positions of these bands are compared to the position of the coloured bands created by the molecular weight marker on the PVDF membrane, and proteins identified according to their molecular weight.

3.3.6.9.1 Antibodies

The following primary antibodies were used for western blots, with the dilutions and concentrations, if available, in brackets: rabbit anti-phospho-Smad2 (pSmad2) antibody (1:1000), rabbit anti-Smad2/3 (1:1000), rabbit anti-αSMA (0.5µg/ml), rabbit anti-glyceraldehyde-3-phosphate dehydrogenase (GAPDH) antibody (1:10000, 0.1485µg/ml), rabbit anti-$G_{\alpha 12}$ antibody (1:100), rabbit anti-$G_{\alpha 13}$ antibody (1:1000), goat anti-$G_{\alpha q}$ antibody (0.1µg/ml), and rabbit anti-$G_{\alpha 11}$ antibody (1:1000, 0.63µg/ml).

Excess primary antibody was removed by washing the membrane in TBST, and secondary antibody applied in blocking solution (either 5% non-fat milk in TBST, or 3% BSA in TBST) for 1-2 hours at room temperature. The goat anti-rabbit and rabbit anti-goat secondary horseradish peroxidase-conjugated antibodies were used at a concentration of 0.25µg/ml.

3.3.6.9.2 Protein detection

Membranes probed for pSmad2 and Smad2/3 were incubated with BioRad Clarity enhanced chemiluminescence (ECL) western blotting substrate for 5 minutes. Membranes probed for all other proteins were incubated with ECL Western blotting detection reagent (Amersham) for 1 minute. Membranes were exposed to hyperfilm and developed using Carestream® Kodak® autoradiography developer/ replenisher and fixer/ replenisher solutions.

Where membranes were probed for two different proteins of the same molecular weight, i.e. the pSmad2 and Smad2/3, the membrane was stripped after analysis of pSmad2 using the commercial Western Restore Stripping Buffer™ for 1-2 minutes and re-blocked with 5% non-fat milk before application of the Smad2/3 antibody. Removal of the first antibody was confirmed after stripping by incubating the membrane with secondary antibody and exposing to hyperfilm as described above.

3.3.6.10 Densitometry of western blots

The densitometry method of western blot quantification depends on the principle that the size and intensity of a protein band is proportional to the amount of protein present. Image processing software can be used to detect the number of pixels in an area of interest, in this case over a protein band (232). The pixel counts for the protein of interest and a loading control protein can be used to calculate the relative protein expression for each sample.

Densitometry was performed using ImageJ software (National Institutes of Health) on scanned western blot films. Images were saved in JPEG format and converted into greyscale images. The “rectangle” tool was used to draw around each protein band and create densitometry plots. The software was used to calculate densitometry values for each protein band relative to the other bands analysed, i.e. a value of how much “density” each band contributes to the total amount of density created by all of the bands thought to represent the protein of interest on the film. These relative densitometry values were used to calculate the expression of pSmad2 relative to total Smad2 using the equation:

$$\text{pSmad2 relative to Smad2} = \frac{\text{pSmad2 densitometry value}}{\text{Smad2 densitometry value}}$$

The relative densitometry value was used rather than the absolute densitometry value as it is not possible to develop western blot films for pSmad2 and Smad2 simultaneously, thus differences in exposure would impact absolute densitometry values.

For proteins where the loading protein and protein of interest cold be visualised on the same film, absolute densitometry values could be used.

3.3.7 Molecular Biology

3.3.7.1 RNA extraction

RNA extraction was performed using the NucleoSpin RNA extraction kit according to the manufacturer’s protocol. Briefly, in this column-based assay cells are lysed, guanidinium thiocyanate used to inhibit RNAses

and promote protein denaturation, contaminating DNA removed, through a DNAse incubation step, and RNA precipitated in ethanol and bound to a silica membrane (234). Washing steps ensure the removal of contaminants such as salts and cellular components, and pure RNA is eluted in nuclease-free water (234).

3.3.7.2 Reverse transcriptase PCR

3.3.7.2.1 Principle of assay

The reverse transcription polymerase chain reaction (RT-PCR) is used to create complementary DNA (cDNA) from mRNA template through a reverse transcription reaction. In this process, the RNA isolated from cell lysates is incubated with and oligo-dT primer, which binds to the multiple adenosine residues (poly A tail) found at the 3' end of an RNA molecule (235). The synthesis of cDNA occurs by extension from the oligo-dT primer by deoxynucleotide triphosphates (dNTPs), and is catalysed by a reverse transcriptase enzyme (235). An RNAse inhibitor, such as RNAsin, is usually included in these reactions to inhibit RNA degradation.

3.3.7.2.2 Method

The concentration of isolated RNA was determined by UV spectrophotometry using a nanodrop. At 260nm 1 absorbance unit equates to 40µg/ml RNA. The following calculation is used to determine the concentration of RNA in a sample.

$$\text{RNA concentration } (\mu g/ml) = 40 \times A_{260}$$

RNA samples were diluted in nuclease-free water to make samples with 200ng RNA in 10µl. 1.25µl oligo-dT primer (200µg/ml), 1µl dNTPs (10mM), and 0.75µl nuclease-free water was added to each sample. Samples were incubated at 65^{o}C for 5 minutes, then incubated on ice for 1 minute.

The following RT reaction components were added to each reaction: 1µl RNAsin, 1µl DTT (0.1M), 1µl Superscript IV (SSIV) enzyme, and 4µl SSIV buffer (Superscript IV kit). The samples were then incubated at 55^{o}C for 10 minutes, then 80^{o}C for 10 minutes. Resulting cDNA samples were immediately used for qPCR analysis, or stored at -20^{o}C.

3.3.7.3 Quantitative PCR (qPCR)

3.3.7.3.1 Principle of assay

In quantitative PCR (qPCR), cDNA generated from mRNA template is amplified and quantified through the incorporation of a DNA-binding fluorescent dye, such as SYBR green. With each PCR cycle, the cDNA is denatured (at around 95^{o}C), annealed to primers designed according to the gene of interest (at around 60^{o}C), and extended in a buffer containing dNTPs (at around 72^{o}C). The amount of dye incorporated into DNA increases with each PCR cycle, and thus the degree of fluorescence emission from the dye correlates with the amount of DNA (235). When the fluorescence reaches the crossing threshold (Ct) value, this value is recorded by the machine, and used in later calculations to quantify mRNA expression. A melting curve, where the temperature of the PCR product is gradually increased until the double-stranded PCR

product denatures is used to ensure the amplification of a single PCR product.

3.3.7.3.2 Method

1.5µl cDNA was used for each qPCR analysis, and each sample was analysed in triplicate. Primers sequences are shown in Table 3-4, and were used at a final concentration of 0.2µM. Primers were confirmed to amplify specific genes by running the sequences through the Primer BLAST software (National Institutes of Health).

Amplification was performed using the MxPro3000 qPCR machine with MxPro software with Kapa SYBR fast Taq polymerase at a denaturation temperature of 95^{o}C, an annealing temperature of 60°C, and an elongation temperature of 72^{o}C, repeated for 40 cycles. A standard curve for each primer set was performed to confirm a primer efficiency of 90-110%. With each qPCR run, a “no template control” containing water in place of cDNA was run to ensure no cDNA contamination of the other reaction components.

Table 3-4: QPCR Primer Sequences

Mouse primers	
Gene	**Primer sequence**
Hprt F	5’ – TGA AAG ACT TGC TCG AGA TGT CA - 3’
Hprt R	5’ – CCA GCA GGT CAG CAA AGA ACT 3’
Tgfb1 F	5' TTG CTT CAG CAG CTC CAC AGA GA 3'
Tgfb1 R	5' TGG TTG TAG AGG GCA AGG AC 3'
Pai-1 F	5' AGT CTT TCC GAC CAA GAG CA 3'
Pai-1 R	5' ATC ACT TGC CCC ATG AAG AG 3'

Acta2 F	5’ - GGG ATC CTG ACG CTG AAG TA – 3’
Acta2 R	5’ – GAC AGC ACA GCC TGA ATA GC – 3’
Gnaq F	5’ – CAG ACA ATG AGA ACC GCA – 3’
Gnaq R	5’ – GGA ATA CAT GAT TTT CTC CTC T – 3’
Gna11 F	5’ – TCA AGA CGC TGT GGA GTG AC – 3’
Gna11 R	5’ AAA CGG GTA CTC GAT GAT GC – 3’
Gna12 F	5’ TGA ACA TCT TCG AGA CCA TCG – 3’
Gna12 R	5’ – ACA GAC TTC ACC TTC TCC ACC – 3’
Gna13 F	5’ – TGA TGG CAT TTG ATA CCC GC – 3’
Gna13 R	5’ – ACC ACT GTC CTC CCA TAA GGC T – 3’
Eln F	5' GAT GGT GCA CAC CTT TGT TG 3'
Eln R	5' CAG TGT GAG GAG CCA TCT CA 3'
Col1a1 F	5' AGC TTT GTG CAC CTC CGG CT 3'
Col1a1 R	5' ACA CAG CCG TGC CAT TGT GG 3'
Ctgf F	5' AGC AGC TGG GAG AAC TGT GT 3'
Ctgf R	5' TGG TAT TTG CAG CTG CTT TG 3'
Human primers	
Gene	**Primer sequence**
B2M F	5’ – AATCCAAATGCGGCATCT - 3’
B2M R	5’ – GAGTATGCCTGCCGTGTG - 3’
TGFB1 F	5’ – AAG GAC CTC GGC TGG AAG TG – 3’
TGFB1 R	5’ – CCC GGG TTA TGC TGG TTG TA – 3’
PAI-1 F	5′- TCTGCAGACCTGGTTCCCAC -3′
PAI-1 R	5′- AGCCCCGTAGTTCCATCCTG -3′
ACTA2 F	5’ – GCT AGG TGG GTG ACG AAG CAC – 3’
ACTA2 R	5’ – CAT AAT TTG AGT CAT TTT CTC – 3’
GNAQ F	5’ – GGACAGGAGAGGGTGGCAAG – 3’
GNAQ R	5’ – TGGGATCTTGAGTGTGTCCA – 3’
GNA11 F	5’ – CCACTGCTTTGAGAACGTGA – 3’
GNA11 R	5’ GCAGGTCCTTCTTGTTGAGG – 3’
GNA12 F	5’ TGA ACA TCT TCG AGA CCA TCG – 3’

GNA12 R	5’ – ACA GAC TTC ACC TTC TCC ACC – 3’
GNA13 F	5’ – TGA TGG CAT TTG ATA CCC GC – 3’
GNA13 R	5’ – ACC ACT GTC CTC CCA TAA GGC T – 3’
F = forward; R = reverse	

3.3.7.4 Gene expression quantification

The ΔΔCt method was used to quantify gene expression normalised to a control sample. Expression values for the gene of interest were normalised to the housekeeping genes hypoxanthine-guanine phophoribosyltransferase (Hprt) or β2-microglobulin (B2M) in mouse and human samples, respectively, using the following formula:

$$\Delta Ct_{sample} = Ct_{gene} - Ct_{housekeeper}$$

The ΔΔCt was calculated using the following formula:

$$\Delta\Delta Ct = Ct_{sample} - Ct_{control}$$

Relative gene expression was calculated using the following formula:

$$\text{Relative gene expression} = 2^{-\Delta\Delta Ct}$$

3.4 *In vivo* methods

3.4.1 Animals

Pdgfrb-Cre$^{+/-}$ mice were a gift from Neil Henderson (University of Edinburgh). Mice with a germline *Gna11* knockout and floxed alleles for *Gnaq* (*Gnaq*$^{fl/fl}$*;Gna11*$^{-/-}$), and mice with a germline knockout of *Gna12* and floxed alleles for *Gna13* (*Gna12*$^{-/-}$*; Gna13*$^{fl/fl}$) were supplied by Stefan Offermanns (Max-Planck Institute of Heart and Lung Research,

Germany). *Pdgfrb-Cre/ERT2*$^{+/-}$ mice were purchased from Jackson Laboratories. All mice were bred onto a C57BL/6 background for at least 6 generations.

Animal work was performed in accordance with the Animals (Scientific Procedures) Act 1986 and approved by the Animal Welfare and Ethical Review Board at the University of Nottingham.

3.4.2 Generation of transgenic mice

The generation of *Pdgfrb-Cre*$^{+/-}$, *Pdgfrb-Cre/ERT2*$^{+/-}$, *Gnaq*$^{fl/fl}$*;Gna11*$^{-/-}$, and *Gna12*$^{-/-}$*;Gna13*$^{fl/fl}$ mice has been reported previously (55, 117, 143) (236, 237), and will briefly be discussed here.

3.4.2.1 *Gnaq*$^{fl/fl}$*;Gna11*$^{-/-}$ mice

To generate *Gna11*$^{-/-}$ mice, a *Gna11*-targetting construct designed to replace exons 3,4, and a portion of exon 5 with the Pgk::Neo transgene was introduced to mouse embryonic stem cells (ESCs). *Gna11*$^{+/-}$ ESCs were then injected into C57BL6 blastocysts to generate chimeric mice, which were then bred with C57BL6 or 129/Sv mice to generate *Gna11*$^{+/-}$ offspring. Intercrosses of these heterozygous mice resulted in *Gna11*$^{-/-}$ mice (143).

A *Gnaq* allele containing three loxP sites and a cassette containing a neomycin resistance (NeoR) gene and the thymidine kinase (tk) (*Gnaq*^{ta}) was created by gene targeting of ESCs. Cre-mediated recombination in these ESCs converted the *Gnaq*^{ta} allele to *Gnaq*^{fl}, which lacks the *neoR/ta* sites and contains just two loxP sites which flank exon 6 of *Gnaq*.

Gnaq$^{fl/fl}$ mice were then generated through a similar breeding process to that described for *Gna11*.

Gnaq$^{fl/fl}$*;Gna11*$^{-/-}$ mice were generated by cross breeding *Gnaq*$^{fl/fl}$ and *Gna11*$^{-/-}$ animals in the founding laboratory (Offermanns lab, Max Planck Institute for Heart and Lung Research, Germany).

3.4.2.2 *Gna12*$^{-/-}$*;Gna13*$^{fl/fl}$ mice

A targeting construct for *Gna12* was generated by replacing a 701-bp fragment of exon 4 with a *Pgk*::*Neo* gene in the reverse orientation. The construct was introduced into mouse ESCs by electroporation. ES cells with the null mutation in one *Gna12* allele were injected into C57BL/6 blastocysts, and chimeras were bred with C57BL/6 and 129/Sv mice to generate *Gna12*$^{+/-}$ mice. Further intercrosses of the heterozygous mice produced *Gna12*$^{-/-}$ mice (117).

For *Gna13*$^{fl/fl}$ mice, a similar method to that described for the generation of *Gnaq*$^{fl/fl}$ mice was used. A *Gna13*^{ta} allele containing three loxP sites and a cassette containing the *NeoR* and *tk* genes was generated by gene targeting of ESCs (236). The *Gna13*^{ta} allele was converted into the *Gna13*^{fl} allele, in which exon 2 is flanked by loxP sites, and *Gna13*$^{fl/fl}$ mice generated by interbreeding as described above.

Gna12$^{-/-}$*;Gna13*$^{fl/fl}$ mice were generated by cross breeding *Gna12*$^{-/-}$ and *Gna13*$^{fl/fl}$ animals in the founding laboratory (Offermanns lab, Max Planck Institute for Heart and Lung Research, Germany).

3.4.2.3 *Pdgfrb-Cre*$^{+/-}$ mice

Pdgfrb-Cre$^{+/-}$ mice were generated by pronuclear injection of a *Pdgfrb* gene fragment and a cDNA encoding Cre recombinase followed by an SV40 polyadenylation signal, a process involving the injection of DNA into the pronucleus of a fertilised oocyte (55). The animals used were of a mixed 129/ C57BL6 genetic background (55).

3.4.2.4 *Pdgfrb-Cre/ERT2*$^{+/-}$ mice

A bacterial artificial chromosome (BAC) containing the entire murine *Pdgfrb* gene was modified by the insertion of a Cre^{ERT2} fusion gene into the start codon of *Pdgfrb* (237). This BAC was microinjected into fertilised mouse oocytes, resulting in a *Pdgfrb-Cre/ERT2*$^{+/-}$ founder line with a transgenic insertion on Chromosome 5 (237). This transgenic mouse line was maintained through several generations of inbreeding (237).

3.4.3 Animal husbandry

Mice were housed in specific pathogen free conditions, with a 12-hour light/ dark cycle, in temperature- and humidity-controlled conditions. Food and water were available *ad libitum*. Standard rodent chow was used, unless specified for tamoxifen-induced gene knockout experiments.

At the end of each study, or if humane endpoints were reached, mice were humanely killed by intraperitoneal (IP) injection of pentobarbital (Euthatal) and exsanguination.

3.4.4 Mouse genotyping

3.4.4.1 DNA extraction

3.4.4.1.1 Principle of technique

In this method, DNA is recovered from cells within a tissue sample using a detergent- and proteinase-containing extraction buffer that will cause cell rupture without DNA breakdown. DNA is then precipitated in alcohols, and redissolved in 10mM Tris (pH 8) for storage until analysis (234).

3.4.4.1.2 Method

Ear biopsies were taken from mice at the age of 2 weeks. DNA was extracted by incubating these tissue samples in DNA extraction buffer (recipe shown in the Appendix, page 379) at 56^{o}C overnight.

DNA was precipitated in 100% isopropanol, then 75% ethanol, with centrifugation at 21,000g for 5 minutes after each precipitation step. The DNA pellet was dissolved in 75µl 10mM Tris pH 8 and stored at 4^{o}C.

3.4.4.2 Genotyping PCRs

3.4.4.2.1 Principle of assay

The polymerase chain reaction (PCR) is a method used to amplify a precise fragment of DNA relevant to a specific gene from a sample of DNA. Using the known sequence of the target gene or DNA region, two oligonucleotide primers are designed to be complementary to a stretch of DNA to the 3' side of the DNA region of interest (one for each DNA strand). In the denaturation step, the double stranded DNA template is

denatured by heating the reaction to over 90°C, making the target DNA region accessible (235). In the annealing step, the reaction is cooled to a reaction-specific temperature of 40-60°C, which allows the oligonucleotide primers to bind to their complementary sites that flank the target DNA (235). The primers provide a free 3' hydroxyl group for the thermostable Taq DNA polymerase to act upon. In the extension step, the temperature of the reaction is increased to 72°C, and DNA synthesis from the primers and along beyond the target DNA occurs, catalysed by the thermostable Taq DNA polymerase (235). This process is repeated for 30-40 cycles, resulting in exponential amplification of the target DNA. The amplified target DNA will have a defined length, facilitating later detection methods.

3.4.4.2.2 Method

The genotype of each mouse was determined by PCR using allele-specific primers (Table 3-5), PCR reaction components (Table 3-6), and thermocycler conditions (Table 3-7). For each PCR run, a negative control containing no DNA sample and a positive control of known genotype was included.

Table 3-5: Primer sequences for genotyping PCRs

Gene	Primer	Primer Sequence	PCR Product
Cre	olMR1084	5'- GCG GTC TGG CAG TAA AAA CTA TC – 3'	Cre transgene = 100bp
	olMR4085	5' - GTG AAA CAG CAT TGC TGT CAC TT – 3'	
	olMR7338	5' - CTA GGC CAC AGA ATT GAA AGA TCT – 3'	Internal positive control = 324bp
	olMR7339	5' - GTA GGT GGA AAT TCT AGC ATC ATC C – 3'	
Gna12	12INC	5' - GTG CTC ATC CTT CCT GGT TTC C - 3'	WT (from 12INC and 1092R) = 441 bp KO (from 12INC and NeoB) = 314bp
	1092R	5'- CGG GTC GCC CTT GAA ATC TGG – 3'	
	Neo B	5' – GGC TGC TAA AGC GCA TGC TCC – 3'	
Gna13	Lox 3.2	5' – GCC ACA GAG GGA TTC AGC AC – 3'	WT = 400bp Floxed allele = 470bp
	13 Seq 1	5' – GCA CTC TTA CAG ACT CCC AC – 3'	
***Gna11* WT**	TW24	5' – AGC ATG CTG TAA GAC CGT AG - 3'	WT = 820bp
	TW25	5' – GCC CCT TGT ACA GAT GGC AG – 3'	
***Gna11* KO**	116EXAS	5' - CAG GGG TAG GTG ATG ATT GTG – 3'	KO= 450bp
	Neo A	5' – GAC TAG TGA GAC GTG CTA CTT CC - 3'	

Gnaq	TVQFL1	5’ – GCA TGC GTG TCC TTT ATG TGA G 3’	WT = 600bp Floxed allele = 700bp
	QIN6C	5’ – AGC TTA GTC TGG TGA CAG AAG – 3’	
WT = wild-type, KO = knockout, bp = basepairs			

Table 3-6: PCR reaction components

Allele	**Cre**	***Gna12***	***Gna13***	***Gna11* WT**	***Gna11* KO**	***Gnaq***
PCR buffer (5X Green GoTaq Flexi Buffer, Promega)	5µl	5µl	5µl	5µl	5µl	5µl
25mM $MgCl_2$ (Promega)	1.7µl	1.7µl	1.7µl	2.1µl	1.5µl	2.1µl
10mM dNTPs (Promega)	0.5µl	0.5µl	0.5µl	0.5µl	0.5µl	0.5µl
10mM primers (Table 3-5, Eurofins)	1µl	1µl	1µl	1µl	1µl	1µl
Go-taq enzyme (Promega)	0.125 µl	0.125µl	0.125µl	0.125µl	0.125µl	0.125µl
Water	11.675µl	12.675µl	13.675µl	13.275 µl	13.875 µl	13.275µl
DNA	2µl	2µl	2µl	2µl	2µl	2µl
Total volume	25µl	25µl	25µl	25µl	25µl	25µl
WT= wild-type, KO = knockout						

Table 3-7: Thermocycler conditions for PCR reactions

Gene	Stage	Temperature	Number of cycles
Cre	1	94ºC - 3 minutes	1
	2	94ºC – 30 seconds 56ºC – 1 minute 72ºC – 1 minute	35
	3	72ºC – 2 minutes	1
Gna12	1	94ºC - 5 minutes	1
	2	94ºC – 30 seconds 65ºC – 30 seconds 72ºC – 1 minute, 30 seconds	35
	3	72ºC – 2 minutes	1
Gna13	1	94ºC - 5 minutes	1
	2	94ºC – 30 seconds 56ºC – 30 seconds 72ºC – 1 minute	35
	3	72ºC – 10 minutes	1
Gna11 **WT**	1	94ºC - 3 minutes	1
	2	94ºC – 30 seconds 60ºC – 1 minute 72ºC – 1 minute	30
	3	72ºC – 10 minutes	1
Gna11 **KO**	1	94ºC - 3 minutes	1
	2	94ºC – 30 seconds 57ºC – 30 seconds 72ºC – 1 minute	30
	3	72ºC – 10 minutes	1
Gnaq	1	94ºC - 5 minutes	1
	2	94ºC – 30 seconds 60.5ºC – 30 seconds	35

		72°C – 1 minute 30 seconds	
	3	72°C – 10 minutes	1

For the tamoxifen-inducible Cre recombinase mouse colonies a commercial genotyping service (Transnetyx, USA) was used. Identical primers and PCR conditions were used for *Gna11*, *Gnaq*, *Gna12*, and *Gna13*, as described in Table 3-5, Table 3-6, and Table 3-7.

Pdgfrb-Cre^{ERT2} genotyping was performed as recommended by Jackson Laboratories, using the primer sequences shown in Table 3-8, PCR reaction components shown in Table 3-9, and thermocycler protocol shown in Table 3-10.

Table 3-8 – Primer sequences for *Cre/ERT2* genotyping

Gene	Primer name	Primer sequence	PCR product
Cre/ERT2	30968	5'- GAA CTG TCA CCG GGA GGA - 3'	400bp
	oIMR9074	5' - AGG CAA ATT TTG GTG TAC GG – 3'	
Internal positive control	oIMR8744	5' - CAA ATG TTG CTT GTC TGG TG – 3'	200bp
	oIMR8745	5' - GTC AGT CGA GTG CAC AGT TT – 3'	

Table 3-9: PCR reaction components for *Cre/ERT2* genotyping

Reaction component	Volume
PCR buffer (5X Green GoTaq Flexi Buffer, Promega)	5µl
25mM $MgCl_2$ (Promega)	2.6µl
10mM dNTPs (Promega)	0.5µl
10mM primers (4 primers, Table 3-8, Eurofins)	1µl
Go-taq enzyme (Promega)	0.125µl
Water	10.775µl
DNA	2µl
Total volume	25µl

Table 3-10: Thermocycler protocol for *Cre/ERT2* PCR reaction

Step	Temperature (°C)	Duration	Special notes
1	94	2 min	
2	94	20 sec	
3	65	15 sec	↓ 0.5°C per cycle
4	68	10 sec	
5	**Repeat steps 2-4 for 10 cycles**		
6	94	15 sec	
7	60	15 sec	
8	72	10 sec	
9	**Repeat steps 6-8 for 28 cycles**		
10	72	2 min	
11	10	hold	

3.4.4.3 Electrophoresis of DNA samples

3.4.4.3.1 Principle

Electrophoresis is used to separate DNA molecules within an agarose gel according to size. In a similar principle to SDS-PAGE, when a current is applied across the gel the negatively charged DNA travels towards the anode at a rate proportional to the size of the DNA molecule, creating distinct bands of DNA of different sizes (238). The gel contains ethidium bromide, which binds to DNA and fluoresces when illuminated with ultraviolet light (238). Samples are run alongside a “ladder” sample which contains DNA of defined lengths. The position of the bands is compared to the bands of known size of the ladder sample to identify the size of the PCR product.

3.4.4.3.2 Method

The buffer recipes for the electrophoresis of PCR products are detailed in the Appendix (page 379). Agarose was dissolved in 1x Tris base, acetic acid and EDTA (TAE buffer, components listed in Appendix page 379) by heating in a microwave to make a 1% agarose solution in TAE. 5µl ethidium bromide was added per 100ml of 1% agarose in TAE solution. The 1% agarose solution was poured onto the gel casting system, a comb inserted into the apparatus, and the gel allowed to set at room temperature. The gel was then submerged in 1 x TAE in the electrophoresis apparatus. 7.5µl of a 100 basepair (100bp) DNA ladder was added to the first well, and the entire PCR product of each sample added to subsequent wells. The electrophoresis equipment was run at

100V for 30 minutes. DNA bands were illuminated using UV light in a G:BOX gel docking system, and images acquired using GeneSnap (Syngene) software.

3.4.5 Organ collection

Organs were collected immediately after mice had been humanely killed. Organs were placed in an aqueous 4% formaldehyde solution (10% formalin, commercial reagent from VWR) immediately following collection, a process which kills the cells within the organs but maintains the tissue structure for histological staining.

The internal organs were exposed by a midline incision and cutting through the sternum. The lungs were cleared of blood by injecting heparin (40 units/ml in PBS) into the right ventricle. Lungs were inflated by cannulating the trachea and filling the lungs with 10% formalin under gravity. The trachea was tied off with thread to keep the formalin within the airways, and the heart and lungs removed *en bloc*. Livers, hearts and kidneys were dissected from surrounding tissues. Organs were kept in 10% formalin for 24 hours before being paraffin embedded (service provided by Nottingham Biobank, and the Translational Medicine department, Nottingham University Hospitals). Fine slices of the paraffin embedded tissue (3-5µm) were cut using a microtome, and tissue slices were mounted onto glass slides and dried in an oven overnight.

3.4.6 Histology

3.4.6.1.1 Principle

Histological staining protocols use the principle that different dyes bind to different tissue components with variable affinities, thus allowing certain tissue components to be highlighted in different colours to facilitate the identification of different structures when the tissue is viewed microscopically.

3.4.6.1.2 General method

3µm (lung and kidney), and 5µm (liver and heart) formalin-fixed paraffin embedded tissue sections were used for staining. Haematoxylin and eosin (H&E), Verhoeff van Gieson, and picrosirius red staining were performed using buffers and stains prepared in house (components described in the Appendix, page 380). Periodic acid Schiff (PAS) staining was performed using a commercially available kit.

For all protocols, paraffin embedded tissue sections were deparaffinised in two changes of xylene and rehydrated in graded alcohols (100% ethanol x 2 for 3 minutes, 70% ethanol x 2 for 3 minutes, distilled water 1 minute). Following staining, tissue sections were dehydrated in graded alcohols (75% ethanol x 1, 100% ethanol x 2) and cleared in two changes of xylene (3 minutes each). Slides were mounted using a distyrene, plasticiser, and xylene -containing resin (DPX mountant), and covered with glass coverslips, and allowed to dry overnight before being viewed.

3.4.6.2 Histology buffers

The components of the histology solutions made in house are listed in the Appendix (page 380).

3.4.6.3 Haematoxylin and eosin (H&E) stain

3.4.6.3.1 Principle

This staining method is commonly used to show the general structure of the tissue sections. Haematoxylin stains nuclei blue, and eosin stains the cytoplasm pink, allowing the general tissue structure of histological sections to be visualised.

3.4.6.3.2 Method

After being deparaffinised and rehydrated, tissue sections were submerged in Mayers haematoxylin for 2 minutes, then acid/alcohol solution to remove excess alcohol and further define the nuclei for 1 minute, then 1% eosin solution for 3 minutes. Sections were rinsed with tap water between each step, then dehydrated and mounted as described above.

3.4.6.4 Elastin (Verhoeff Van Gieson) stain

3.4.6.4.1 Principle

In this technique, the Iron(III) chloride and iodine within the Verhoeff's stain oxidise haematoxylin to haematin, which is retained by elastin in the tissue being stained (239). Excess iron (III) chloride is used to differentiate the tissue, then sodium thiosulphate is used to remove excess iodine (239). The van Gieson counterstain stains muscle and

collagen fibres, and further differentiates the tissue (239). In this method, elastin fibres and nuclei stain black.

3.4.6.4.2 Method

Lung sections were deparaffinised and hydrated to distilled water, then stained in Verhoeff's solution for 1 hour until the tissue was completely black. Sections were differentiated in an aqueous 2% ferric chloride solution until elastin fibres were seen on a grey background under the microscope, incubated in 5% sodium thiosulphate for 1 minute, then washed in running tap water for 5 minutes. Sections were then counterstained in Van Gieson's solution for 5 minutes, then dehydrated and mounted as described above.

3.4.6.5 Periodic Acid Schiff (PAS) stain

3.4.6.5.1 Principle

In this method, periodic acid oxidises polysaccharides, resulting in the formation of aldehyde groups. These aldehyde groups react with the Schiff reagent to give a purple colour to "PAS-positive" areas (240). Haematoxylin is used to stain nuclei blue. PAS-positive structures include polysaccharides and glycoproteins, and mucins, and the PAS stain is useful for the demonstration of basement membranes (240).

In liver staining, diastase (α-amylase) is used to break down glycogen prior to the periodic acid step. The diastase digestion step removes glycogen stores in the liver, to allow the differentiation between glycogen and other PAS-positive components of the liver (240).

3.4.6.5.2 Method

Kidney and liver sections were PAS stained using the Abcam PAS stain kit according to the manufacturer's instructions, with the omission of the bluing reagent and light green stain steps. Briefly, sections were submerged in periodic acid for 10 minutes, rinsed in four changes of distilled water, then submerged in Schiff's solution for 30 minutes. Sections were rinsed in running hot tap water, then distilled water. Tissue sections were counterstained in haematoxylin for 3 minutes, washed in distilled water, then dehydrated and mounted as described above.

Liver sections were stained with and without diastase digestion, which was performed by incubating slides in 0.5% diastase solution for 20 minutes at room temperature prior to the periodic acid step.

3.4.6.6 Picrosirius red stain

3.4.6.6.1 Principle

Picrosirius red is an anionic dye that associates with cationic collagen fibres and enhances their natural birefringence under cross-polarized light. Under normal light microscopy, collagen fibres appear red, but under polarised light collagen fibres appear yellow or green on a black background, allowing visualisation of the collagen network (241).

3.4.6.6.2 Method

Lung, kidney, and heart sections were deparaffinised and hydrated. Nuclei were stained with Weigert's haematoxylin for 8 minutes, then washed in running tap water for 5 minutes. Sections were incubated in

picrosirius red for 1 hour, washed in two changed of acidified water, then dehydrated and mounted.

3.4.6.7 Immunohistochemistry (IHC)

3.4.6.7.1 Principle

In IHC, a primary IgG antibody incubated with tissue sections will bind to the protein of interest if present in the tissue. A biotinylated secondary antibody against the IgG of the primary antibody species is then incubated with the tissue and will bind to the primary antibody (242). The avidin peroxidase within the avidin-biotin complex (ABC) binds to the biotin on the secondary antibody, as well as other avidin-biotin complexes within this reagent, and amplifies the signal to be detected in the next step (242). Diaminobenzidine (DAB) is then added, and acts as a substrate for avidin peroxidase, resulting in a brown colour change at the positions where antibody is bound to the tissue (242).

In IHC, several steps are taken to facilitate antibody binding and reduce non-specific staining. Heat-mediated antigen retrieval is performed by boiling tissue sections in citric acid. This process exposes the antigenic sites on the fixed tissue that will have been masked by the fixation process, facilitating later antibody binding (242). To reduce non-specific background staining, tissue sections are incubated in hydrogen peroxide to block endogenous peroxidases within the tissue (242). Non-specific antibody binding is reduced by incubating tissue sections in serum from the same species as the secondary antibody to be used (242).

3.4.6.7.2 Method

Tissue sections were deparaffinised and rehydrated as described above. Heat-mediated antigen retrieval was performed by boiling sections in a microwave for 20 minutes in 10mM citric acid buffer (pH 6.0). Endogenous peroxidase activity was blocked by incubating sections in 3% hydrogen peroxide in methanol for 30 minutes. Nonspecific binding was blocked with 5% goat serum in 0.1% BSA/PBS. Sections were incubated with primary antibody in 5% goat serum overnight at 4^{o}C, followed by incubations for 60 minutes with secondary antibody, and 30 minutes with avidin-biotin complex. Sections were then stained with diaminobenzidine, counterstained with Mayers haematoxylin, and mounted in DPX. Slides were washed in PBS) between incubation steps. Primary and secondary antibodies are detailed in Table 3-11.

Table 3-11: Immunohistochemistry Antibodies

Target	Primary antibody	Primary antibody dilution	Secondary antibody	Secondary antibody dilution	Blocking reagent
αSMA	Ab5694 (Abcam)	1:500	Biotinylated goat anti-rabbit IgG (BA1000, Vector)	1:200	Goat serum
Ki67	Ab15580 (Abcam)	1:1000		1:200	
CD31	Ab182981 (Abcam)	1:2000		1:200	
SPC	Ab3786 (Sigma)	1:2000		1:200	
TGFβ2	Proteintech Cat# 19999-1-AP	1:3000		1:200	

3.4.6.8 Microscopy

Images of H&E, elastin, IHC, and PAS staining were taken using a Nikon 90i microscope and NIS-Elements software v3.2. Polarised light and matched brightfield imaging of picrosirius red stained samples was performed using a Zeiss Axioplan microscope and MicroManager 1.4 software.

3.4.7 Histology image analysis

For quantification of histological staining, 5-10 images were assessed per set of lungs, covering all lobes and avoiding major airways, large

blood vessels, and tissue cutting artefacts. All quantification was performed by an observer blinded to genotype.

For all analyses, *Pdgfrb-Cre*$^{+/-}$;*Gnaq*$^{fl/fl}$;*Gna11*$^{-/-}$ or *Pdgfrb-Cre/ERT2*$^{+/-}$;*Gnaq*$^{fl/fl}$;*Gna11*$^{-/-}$ mice were compared with *Pdgfrb-Cre*$^{-/-}$;*Gnaq*$^{fl/fl}$;*Gna11*$^{-/-}$ or *Pdgfrb-Cre/ERT2*$^{-/-}$;*Gnaq*$^{fl/fl}$;*Gna11*$^{-/-}$ control littermates, and four animals per genotype were assessed. Control mice (*Pdgfrb-Cre*$^{-/-}$;*Gnaq*$^{fl/fl}$;*Gna11*$^{-/-}$ or *Pdgfrb-Cre/ERT2*$^{-/-}$;*Gnaq*$^{fl/fl}$;*Gna11*$^{-/-}$) are referred to as *Gna11*$^{-/-}$ controls throughout this thesis. These control groups were chosen because *Gnaq*$^{fl/fl}$;*Gna11*$^{-/-}$ mice that do not possess an allele for Cre recombinase expression express *Gnaq* normally and do not express an abnormal phenotype (219). Furthermore, *Gna11*$^{-/-}$ littermates would have the same genetic background and environmental exposures as mice with the genotypes of interest, reducing potential confounding factors. Male and female mice were included in the analyses.

Morphometric analyses were performed using NIS Elements software v3.2, except for peripheral pulmonary vessel and cardiac wall thickness measurements and TGFβ2 staining quantification, which were performed using CaseViewer 2.3 software. For quantification of other immunohistochemistry and elastin staining, the “count” feature of ImageJ was used.

3.4.7.1 Mean linear intercept (MLI) distance

Mean linear intercept (MLI) analysis of airspace size was performed as previously described (219). Briefly, 10x magnification images were taken and overlaid with a 100μm grid, and “intercepts” between gridlines and airspace walls counted. The length of each gridline was divided by the intercept count to calculate the MLI value. The mean MLI value was calculated from all measurements across all images from an individual mouse and used for data presentation.

3.4.7.2 Alveolar wall thickness

Images were taken at 40x magnification. Five equally spaced horizontal lines were overlaid across each image, and the alveolar wall thickness measured at points where lung tissue crossed the line. Mean alveolar wall thickness values were calculated from all measurements across all images and used for data presentation.

3.4.7.3 Quantification of secondary crests

Ten images were taken at 20 x magnification. The counting tool was used to quantify the number of secondary crests per image. Secondary crests were defined as tissue projections from the alveolar walls into the alveolar space.

3.4.7.4 Quantification of Elastin Stain

Ten 40x magnification images were analysed per mouse. Elastin fibres, identified as thin black fibres, and elastin positive secondary crests, identified as any secondary crest with black staining that was not a cell

nucleus, were counted. If there was any doubt about whether an area of staining was elastin or a cell nucleus, the area was not included in the count. The proportion of elastin-positive secondary crests was calculated relative to the total number of secondary crests.

3.4.7.5 Pulmonary vessel wall thickness

Ten randomly selected peripheral pulmonary vessels were analysed per mouse. Vessels were identified as circular hollow structures with an inner layer staining positively for CD31. Large central pulmonary vessels were excluded. Maximum and minimum wall thickness was measured for each blood vessel, and the mean value of each lung recorded per lung.

3.4.7.6 Cardiac wall measurements

The left and right cardiac ventricles were identified on H&E stained tissue. The left ventricle was identified as having a thicker wall, and having the interventricular septum bulge away from it and towards the right ventricle. Left and right ventricular wall thickness was measured, and the right: left ventricular wall thickness ratio calculated.

3.4.7.7 αSMA IHC

Ten 40 x magnification images were per mouse. αSMA positive secondary crests were identified by brown staining, and the proportion of secondary crests that were αSMA positive was calculated.

3.4.7.8 Ki67

Five 40x magnification images were taken per mouse. Ki67-positive nuclei were identified by brown staining and counted. The proportion of Ki67-positive nuclei relative to the total number of nuclei was calculated.

3.4.7.9 Pro-SPC

Five 40x magnification images were taken per mouse. Pro-SPC-positive cells were identified by brown staining and counted. The total number of was quantified by counting the number of cell nuclei. The proportion of pro-SPC-positive cells was calculated relative to the total number of cells for each image.

3.4.7.10 TGFβ2

For quantification of TGFβ2 staining, the scoring system in Table 3-12 was used. 7 fields (20x magnification) per mouse were analysed.

Table 3-12: TGFβ2 Scoring System

Cells stained per 20x field	Staining intensity	Score
No staining	-	0
1-25	Low	0.5
1-25	High	1
26-50	Low	1.5
26-50	High	2
>50	Low	2.5
>50	High	3

3.4.7.11 External assistance with histology interpretation

Lung histology was interpreted in house at the Division of Respiratory Medicine at the University of Nottingham. Kidney histology was interpreted with the assistance of Prof Katalin Susztak and Dr Mathew Palmer (University of Pennsylvania). Liver histology was interpreted with the assistance of Dr Tim Kendall (University of Edinburgh).

3.5 Statistical analyses

Statistical tests were performed using GraphPad Prism software version 8.2. For comparisons between two groups, a Students T test was performed for parametric data of sample sizes of six or more, or a Mann-Whitney U test for nonparametric data or for sample sizes of fewer than six. For comparisons between multiple groups, a one-way ANOVA was performed if the data followed a normal distribution and for samples sizes of six or more. For comparisons between multiple groups of non-parametric data or with sample sizes of less than six, a Kruskal Wallis test was performed. A Wilcoxon signed rank test was performed to test for differences between matched samples if the data were non-parametric or the sample size lower than six. A Chi squared test was used to assess whether mouse birth frequencies were different to the expected Mendelian frequencies. A result was considered statistically significant with a p value <0.05.

4 The *In Vivo* Roles of Mesenchymal $G_{\alpha q/11}$ and $G_{\alpha 12/13}$ in Development

4.1 Introduction

Several lines of evidence suggest that $G_{\alpha q/11}$ and $G_{\alpha 12/13}$ may play important roles in fibrogenesis, as discussed in the Introduction (Chapter 1). However, the embryonic lethality of *Gnaq*$^{-/-}$;*Gna11*$^{-/-}$ and *Gna12*$^{-/-}$;*Gna13*$^{-/-}$ mice means that the study of the *in vivo* roles of $G_{\alpha q/11}$ and $G_{\alpha 12/13}$ in health and disease has been limited, as these animals do not survive to an age appropriate for inclusion in disease models (143, 243).

Conditional gene knockout systems, where cell-specific expression of DNA recombinases results in gene knockout in defined cell types, can be useful when global gene knockout proves to be embryonically lethal, as is the case with *Gnaq*$^{-/-}$;*Gna11*$^{-/-}$ and *Gna12*$^{-/-}$;*Gna13*$^{-/-}$ mice. Cre-lox systems involving mice with floxed *Gnaq* and deleted *Gna11* alleles (*Gnaq*$^{fl/fl}$;*Gna11*$^{-/-}$), or deleted *Gna12* and floxed *Gna13* alleles (*Gna12*$^{-/-}$;*Gna13*$^{fl/fl}$), have been used to generate mice with cell type-specific $G_{\alpha q/11}$ or $G_{\alpha 12/13}$ knockout, respectively (236, 244, 245). These models utilise the fact that *Gna11*$^{-/-}$ and *Gna12*$^{-/-}$ mice develop normally and do not differ phenotypically from wild-type mice(107). The floxed *Gnaq* and *Gna13* alleles allow for full $G_{\alpha q/11}$ and $G_{\alpha 12/13}$ deletion in predetermined cell types only, defined by the Cre driver gene.

Mesenchymal cell-specific gene knockouts have been generated for *in vivo* fibrosis models using *Pdgfrb-Cre*$^{+/-}$ mice, which express Cre recombinase under the control of the platelet-derived growth factor-β (*Pdgfrb*) promoter (48, 246). These animals express Cre recombinase in *Pdgfrb*-expressing cells, including myofibroblasts, pericytes and smooth

muscle cell lineages (48, 247-249). However, mice with mesenchymal cell specific knockdown of $G_{\alpha q/11}$ and $G_{\alpha 12/13}$ have not previously been studied, and the role of mesenchymal $G_{\alpha q/11}$ and $G_{\alpha 12/13}$ *in vivo* in development and disease is unknown.

4.2 Aims and Hypothesis

This work aimed to:

- Understand the effects of germline mesenchymal $G_{\alpha q/11}$ and $G_{\alpha 12/13}$ knockout on normal development *in vivo*
- Establish the suitability of germline mesenchymal $G_{\alpha q/11}$ and $G_{\alpha 12/13}$ knockout mice for use in the bleomycin model of pulmonary fibrosis

The hypothesis underlying this work was:

> *Mesenchymal cell-specific knockout of $G_{\alpha q/11}$ and/ or $G_{\alpha 12/13}$ will protect against pulmonary fibrosis, but may be associated with developmental abnormalities*

4.3 Methods

4.3.1 Breeding strategy

Pdgfrb-Cre$^{+/-}$ mice were crossed with *Gna12*$^{-/-}$*; Gna13*$^{fl/fl}$ or *Gnaq*$^{fl/fl}$*; Gna11*$^{-/-}$ mice in two-stage breeding strategies.

For the $G_{\alpha q/11}$ colony, *Pdgfrb-Cre*$^{+/-}$ mice were mated with *Gnaq*$^{fl/fl}$*;Gna11*$^{-/-}$ mice to produce *Pdgfrb-Cre*$^{+/-}$*;Gnaq*$^{+/fl}$*;Gna11*$^{+/-}$ offspring (F1 generation). F1 mice were bred back onto the *Gnaq*$^{fl/fl}$*;Gna11*$^{-/-}$ founder

mouse generation, which resulted in eight possible genotypes in the offspring (F2 generation) (Figure 4-1). These genotypes were expected to have an equal probability of occurring.

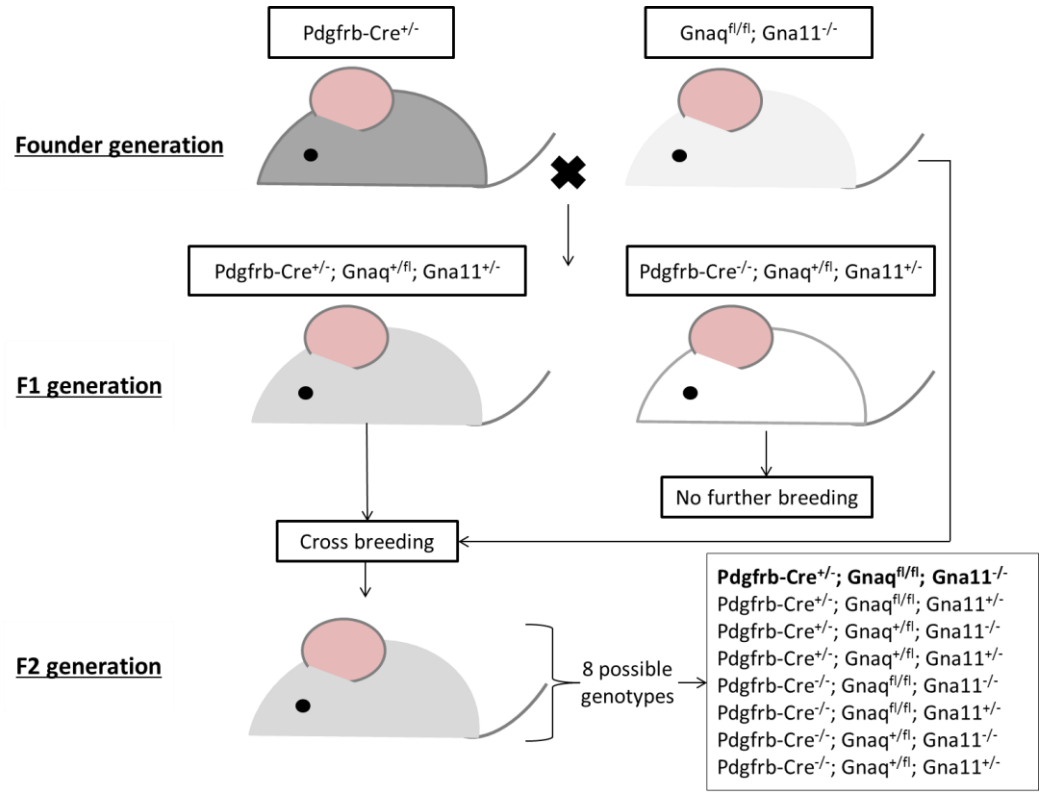

Figure 4-1: Breeding strategy to generate *Pdgfrb-Cre$^{+/-}$;Gnaq$^{fl/fl}$;Gna11$^{-/-}$* mice

A two stage breeding strategy was used to generate mice lacking mesenchymal $G_{\alpha q/11}$ (*Pdgfrb-Cre$^{+/-}$;Gnaq$^{fl/fl}$;Gna11$^{-/-}$*). This strategy generates eight possible genotypes of F2 mice (box bottom right).

A similar strategy was used to generate *Pdgfrb-Cre$^{+/-}$;Gna12$^{-/-}$;Gna13$^{fl/fl}$* mice, however founder animals were heterozygous for *Gna12* and homozygous for the *Gna13* floxed allele (*Gna12$^{+/-}$;Gna13$^{fl/fl}$*) due to poor breeding of *Gna12$^{-/-}$* animals. Twelve different genotypes were possible in the F2 generation from this breeding strategy (Figure 4-2), which were expected to occur at equal frequencies.

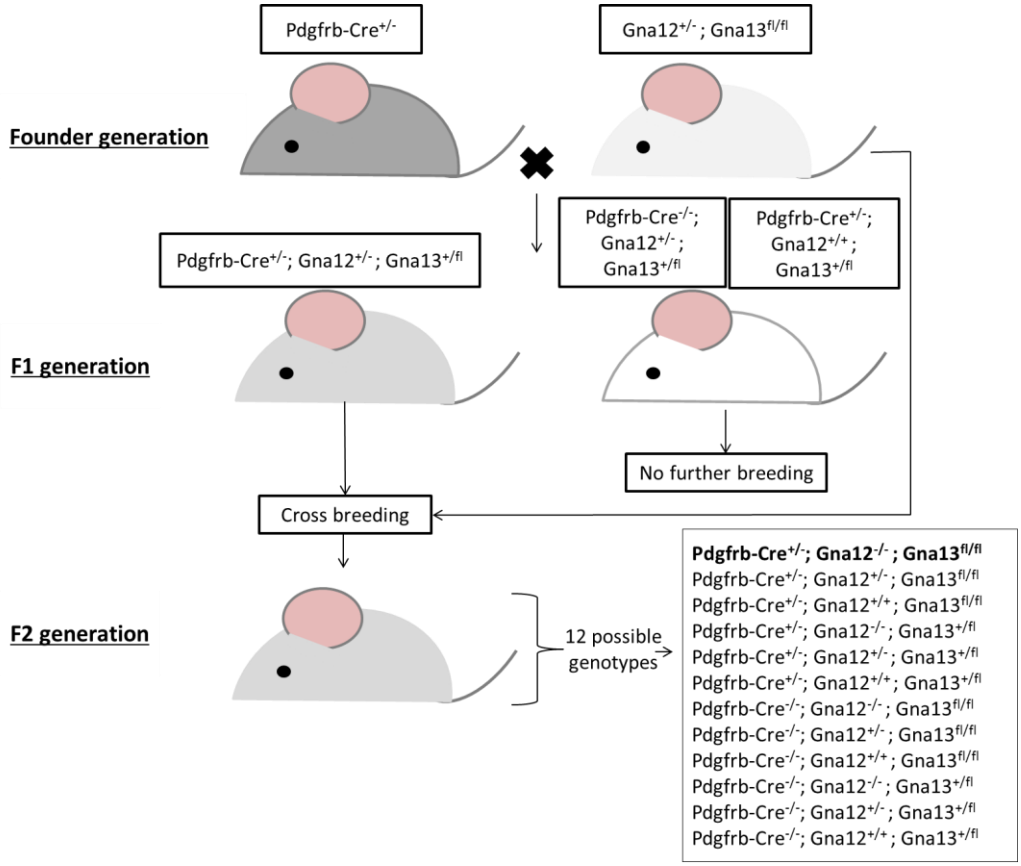

Figure 4-2: Breeding strategy to generate *Pdgfrb-Cre$^{+/-}$;Gna12$^{-/-}$;Gna13$^{fl/fl}$* mice

A two stage breeding strategy was used to generate mice lacking mesenchymal $G_{\alpha 12/13}$ (*Pdgfrb-Cre$^{+/-}$;Gna12$^{-/-}$;Gna13$^{fl/fl}$*). 12 different genotypes were possible in the F2 generation from this breeding strategy (box).

The genotype ratios from each colony were compared with the expected Mendelian frequencies (12.5% and 8.3% per genotype in the $G_{\alpha q/11}$ and $G_{\alpha 12/13}$ colonies, respectively).

4.3.2 Germline mesenchymal $G_{\alpha q/11}$ and $G_{\alpha 12/13}$ mouse phenotyping

Phenotyping assessments were performed by an observer blinded to genotype.

F2 mice from the *Gnaq*$^{fl/fl}$;*Gna11*$^{-/-}$ x *Pdgfrb-Cre*$^{+/-}$ colony were weighed and disease severity scored at 2 weeks of age. These mice were humanely killed at 2 weeks old and organs were collected as described in the General Methods (Chapter 3). Lungs and kidneys were weighed, and organ weights corrected to total body weight to give a relative organ weight using the following calculation:

Relative organ weight = organ weight (mg) / total body weight (g)

All F2 mice from the *Gna12*$^{-/-}$;*Gna13*$^{fl/fl}$ x *Pdgfrb-Cre*$^{+/-}$ colony, and a small portion of F2 mice from the *Gnaq*$^{fl/fl}$;*Gna11*$^{-/-}$ x *Pdgfrb-Cre*$^{+/-}$ colony, were observed twice weekly from weaning age (3 weeks old), with weight monitoring and disease severity scoring. At 8 weeks of age, organs were collected from these mice for histological analysis as described in the General Methods (Chapter 3).

4.4 Results

4.4.1 Mesenchymal $G_{\alpha q/11}$ deletion causes a detrimental phenotype

To establish the impact of germline mesenchymal $G_{\alpha q/11}$ knockout *in vivo*, the genotype ratios from the F2 generation of the *Pdgfrb-Cre*$^{+/-}$ x *Gnaq*$^{fl/fl}$;*Gna11*$^{-/-}$ breeding were analysed. It was assumed that a birth rate less than the expected Mendelian frequency (1 in 8) for any genotype indicated death *in utero* or in early life. There were fewer *Pdgfrb-Cre*$^{+/-}$;*Gnaq*$^{fl/fl}$;*Gna11*$^{-/-}$ mice than any other genotype with at least one intact *Gnaq* or *Gna11* allele (Figure 4-3). *Pdgfrb-Cre*$^{+/-}$;*Gnaq*$^{fl/fl}$;*Gna11*$^{-/-}$ mice were born at less than the expected frequency of

12.5% (6.6% vs 12.5%, χ^2 = 22.03, p<0.005, Figure 4-3). Conversely, mice with at least one functional mesenchymal *Gnaq* or *Gna11* allele reached genotyping age at rates closer to the expected Mendelian frequencies (Figure 4-3). *Pdgfrb-Cre*$^{+/-}$;*Gnaq*$^{fl/fl}$;*Gna11*$^{-/-}$ mice were not viable beyond 3 weeks old (n=2), therefore further analyses were performed in 2 week old mice.

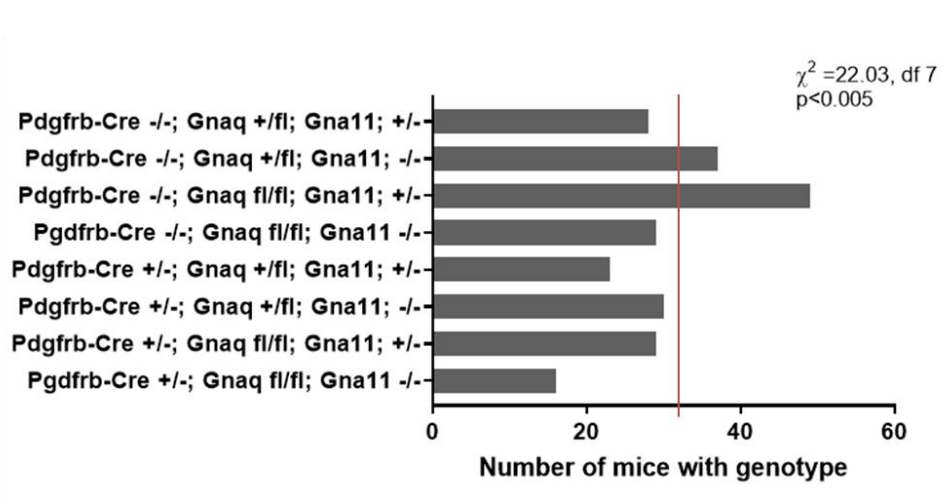

Figure 4-3: Mice lacking mesenchymal $G_{\alpha q/11}$ are born at less than the expected frequency

A) Frequency of mice born with each genotype from the *Pdgfrb-Cre*$^{+/-}$ x *Gnaq*$^{fl/fl}$;*Gna11*$^{-/-}$ mouse crosses. Red line indicates the expected number of mice calculated from an expected Mendelian frequency of 12.5% per genotype. Total number of mice 241, 34 litters, mean litter size 7.4. χ^2 = 22.03, degrees of freedom (df)=7, p<0.005.

In addition to being born less frequently than expected, *Pdgfrb-Cre*$^{+/-}$;*Gnaq*$^{fl/fl}$;*Gna11*$^{-/-}$ mice were significantly smaller than littermates with at least one intact mesenchymal *Gna11* or *Gnaq* allele (Figure 4-4A, C). *Pdgfrb-Cre*$^{+/-}$;*Gnaq*$^{fl/fl}$;*Gna11*$^{-/-}$ mice had a mean weight 1.9-3.2g lower than all other genotypes (5.4g vs 7.3-8.4g, p<0.03, Figure 4-4A). This

difference was not be explained by the slightly different proportions of male and female mice between genotypes, as the weights of 2 week old male and female mice from this colony did not differ significantly (p=0.65, Figure 4-4B). On gross examination, *Pdgfrb-Cre*$^{+/-}$*;Gnaq*$^{fl/fl}$*;Gna11*$^{-/-}$ pups were also visibly smaller in physical size compared with control animals (Figure 4-4C).

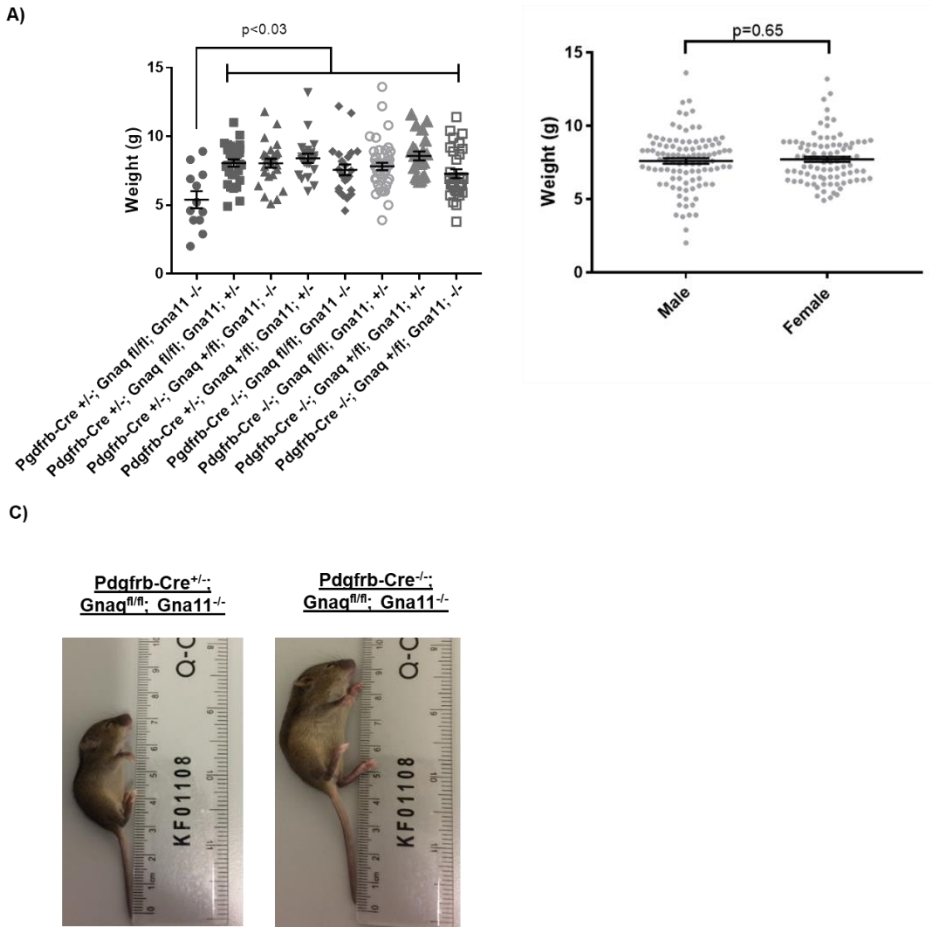

Figure 4-4: Mice lacking mesenchymal $G_{\alpha q/11}$ are growth restricted

A) Body weights of F2 pups from the *Gnaq$^{fl/fl}$;Gna11$^{-/-}$* x *Pdgfrb-Cre$^{+/-}$* colony by genotype at 2 weeks old. Data shown as mean ± standard error of the mean (SEM). Statistical analysis performed using a one-way ANOVA with Tukey's multiple comparisons test, n = 12-43 per group).

B) Body weights of all pups from *Pdgfrb-Cre$^{+/-}$* x *Gnaq$^{fl/fl}$;Gna11$^{-/-}$* crosses by sex. Data shown as mean ± SEM. Statistical analysis performed using an unpaired Students T test. 88 female and 102 male mice.

C) Photographs of a representative *Pdgfrb-Cre$^{+/-}$;Gnaq$^{fl/fl}$;Gna11$^{-/-}$* mouse (left) and a *Pdgfrb-Cre$^{+/-}$;Gnaq$^{fl/fl}$;Gna11$^{-/-}$* littermate (right).

A proportion of F2 mice with at least one intact mesenchymal *Gnaq* or *Gna11* allele, i.e. those with genotypes other than *Pdgfrb-Cre*$^{+/-}$*;Gnaq*$^{fl/fl}$*;Gna11*$^{-/-}$, were observed until 8 weeks of age. No gross phenotype or evidence of ill health was identified in 33 out of 34 of these animals (3-6 mice per genotype, Figure 4-5). One *Pdgfrb-Cre*$^{+/-}$*;Gnaq*$^{+/fl}$*:Gna11*$^{+/-}$ mouse was humanely killed at 34 days old due to abdominal distension and respiratory distress, and was found to have evidence of a bowel obstruction on necropsy. However, two other mice with the same genotype survived to the end of the observation period without evidence of ill health, and no similar observations were made in *Pdgfrb-Cre*$^{+/-}$*;Gnaq*$^{fl/fl}$*;Gna11*$^{-/-}$ mice, suggesting that this may have been a coincidental occurrence unrelated to genotype.

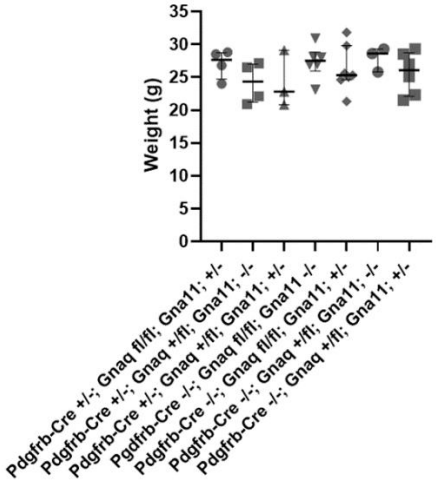

Figure 4-5: Mice with at least one intact *Gnaq* or *Gna11* allele in mesenchymal cells do not have evidence of ill health at 8 weeks old

Weights of F2 mice from the *Pdgfrb-Cre x Gnaq*$^{fl/fl}$*;Gna11*$^{-/-}$ breeding programme at 8 weeks old, by genotype.

Overall, these data indicate that mesenchymal $G_{\alpha q/11}$ deletion causes a detrimental phenotype compared with mice than possess at least one intact mesenchymal *Gnaq* or *Gna11* allele. Subsequent work aimed to identify the underlying reason for the poor condition of the *Pdgfrb-Cre*$^{+/-}$*;Gnaq*$^{fl/fl}$*;Gna11*$^{-/-}$ mice.

4.4.2 Mice lacking mesenchymal $G_{\alpha q/11}$ have abnormal lungs

To assess for pulmonary abnormalities in *Pdgfrb-Cre*$^{+/-}$*;Gnaq*$^{fl/fl}$*;Gna11*$^{-/-}$ mice, histological analysis of lung tissue was performed. *Pdgfrb-Cre*$^{+/-}$*;Gnaq*$^{fl/fl}$*;Gna11*$^{-/-}$ mice had an abnormal lung appearance (Figure 4-6A). This included enlarged airspaces (mean linear intercept distance of 63.47µm vs 36.43µm in controls, p=0.03, Figure 4-6C), thickened alveolar walls (12.2µm vs 7.0µm, p=0.03, Figure 4-6D, and a reduced number of secondary crests (53.7 vs 107.2 per field, p=0.03, Figure 4-6B) compared with *Pdgfrb-Cre*$^{-/-}$*;Gnaq*$^{fl/fl}$*;Gna11*$^{-/-}$ (from here referred to as *Gna11*$^{-/-}$) controls. Furthermore, *Pdgfrb-Cre*$^{+/-}$*;Gnaq*$^{fl/fl}$*;Gna11*$^{-/-}$ mice had increased lung weight relative to total body weight compared with *Gna11*$^{-/-}$ controls (16.5 vs 14.3mg/g total body weight, p<0.01, Figure 4-6E).

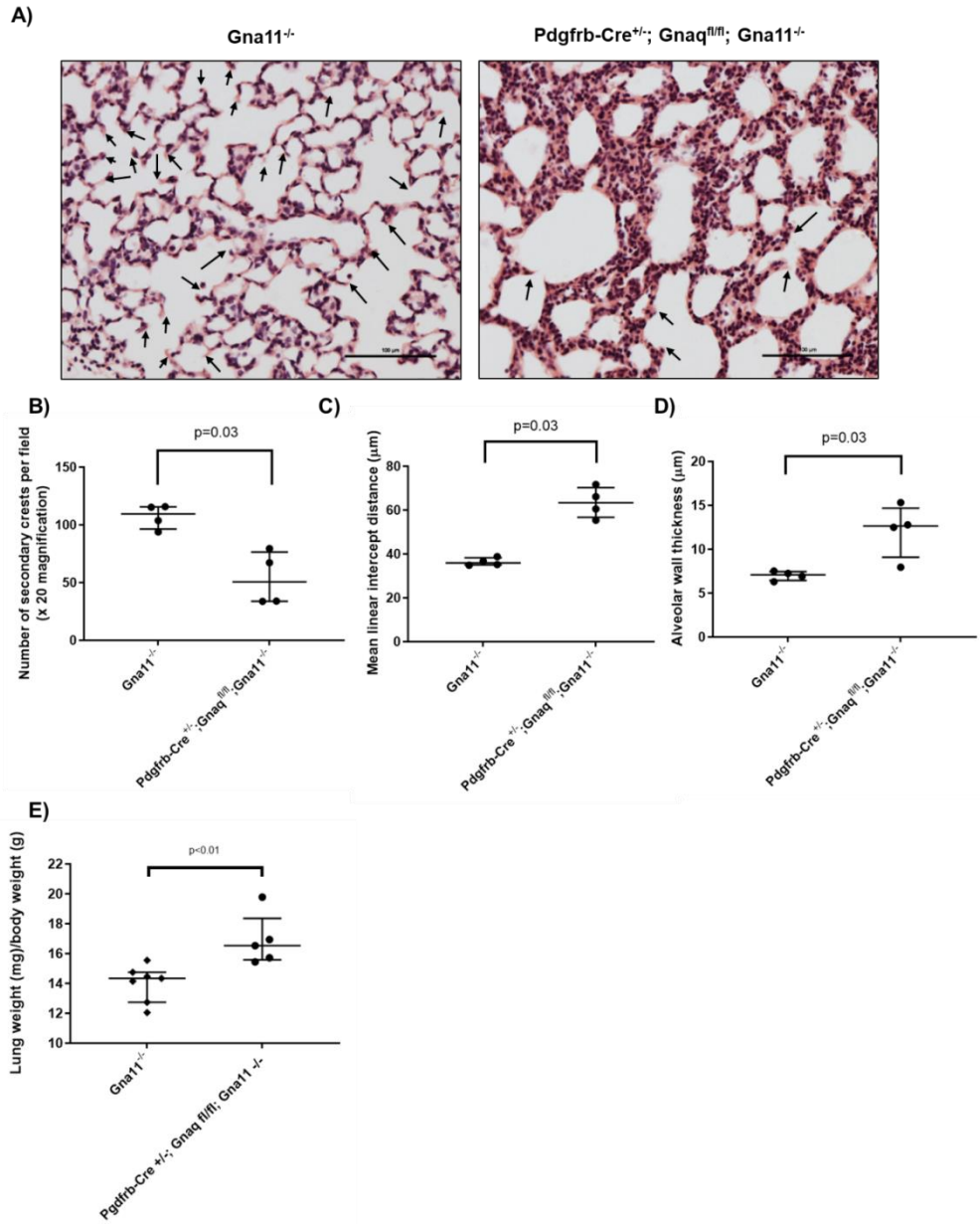

Figure 4-6: Mice lacking mesenchymal $G_{\alpha q/11}$ have disturbed alveolarisation

A) H&E staining of lung tissue from a *Pdgfrb-Cre*$^{+/-}$*;Gnaq*$^{fl/fl}$*;Gna11*$^{-/-}$ (*Gna11*$^{-/-}$, control) mouse (left) and a *Pdgfrb-Cre*$^{+/-}$*;Gnaq*$^{fl/fl}$*;Gna11*$^{-/-}$ mouse (right). Arrows indicate secondary crests. Representative histology images from four mice per group.

B-D) Quantification of the number of secondary crests (B), mean linear intercept distance (C), and alveolar wall thickness (D) from lung H&E staining (n=4 per group).

E) Lung weights relative to total body weight (n=5-7 per group) of 2 week old *Pdgfrb-Cre*$^{+/-}$*;Gnaq*$^{fl/fl}$*;Gna11*$^{-/-}$ and *Gna11*$^{-/-}$ control pups.

Comparisons made between *Pdgfrb-Cre*$^{+/-}$*;Gnaq*$^{fl/fl}$*;Gna11*$^{-/-}$ and control *Pdgfrb-Cre*$^{-/-}$*;Gnaq*$^{fl/fl}$*Gna11*$^{-/-}$ (*Gna11*$^{-/-}$) mice. Data shown as median ± interquartile range. Statistical analyses performed using two-tailed Mann Whitney Tests.

The abnormal histological appearances and morphometric analyses of *Pdgfrb-Cre*$^{+/-}$*;Gnaq*$^{fl/fl}$*Gna11*$^{-/-}$ lungs suggested a defect in alveolarisation in mice lacking mesenchymal $G_{\alpha q/11}$. As cellular proliferation is a key driver of normal alveolar development (86), immunohistochemical staining for Ki67, a proliferative marker, was performed. *Pdgfrb-Cre*$^{+/-}$*;Gnaq*$^{fl/fl}$*Gna11*$^{-/-}$ mouse lungs exhibited less Ki67 staining than *Gna11*$^{-/-}$ control lungs (median proportion of Ki67 positive cells 16.08% vs 21.14%, p=0.03, Figure 4-7A-C). These data suggest reduced cellular proliferation in mesenchymal $G_{\alpha q/11}$ knockout lungs.

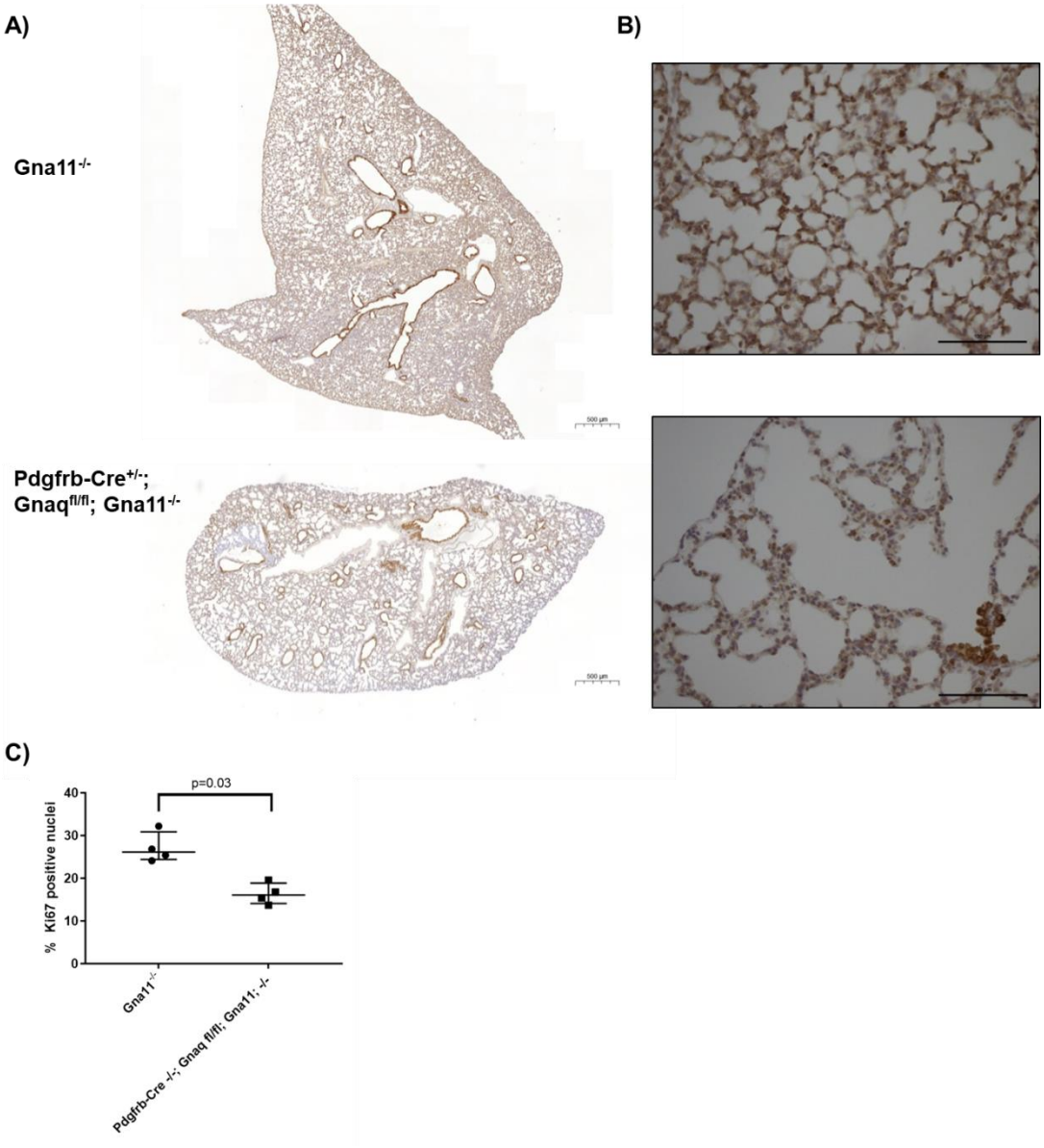

Figure 4-7: Mice lacking mesenchymal $G_{\alpha q/11}$ have reduced cellular proliferation in the lungs

A,B) Ki67 immunohistochemistry of *Gna11*$^{-/-}$ control (top) and *Pdgfrb-Cre*$^{+/-}$*;Gnaq*$^{fl/fl}$*;Gna11*$^{-/-}$ (bottom) mouse lungs at low (A) and high (B) magnification. Representative histology images from four animals per group.

C) Quantification of Ki67 positive cells in *Gna11*$^{-/-}$ and *Pdgfrb-Cre*$^{+/-}$*;Gnaq*$^{fl/fl}$*;Gna11*$^{-/-}$ mouse lungs. Data shown as median ± interquartile range. Statistical analysis performed using two-tailed Mann Whitney Test.

Overall, these data indicate that mice lacking mesenchymal $G_{\alpha q/11}$ have defective alveolarisation.

4.4.3 Myofibroblast differentiation and function are altered in mesenchymal $G_{\alpha q/11}$ knockout lungs

Myofibroblasts play essential roles in alveolar development through the deposition of extracellular matrix scaffolds and the formation of secondary crests (9, 25, 47). Therefore staining was undertaken to assess myofibroblast differentiation and function in *Pdgfrb-Cre*$^{+/-}$*;Gnaq*$^{fl/fl}$*;Gna11*$^{-/-}$ lungs.

Immunohistochemical staining of the myofibroblast marker αSMA, demonstrated fewer myofibroblasts in the lungs of 2 week old *Pdgfrb-Cre*$^{+/-}$*;Gnaq*$^{fl/fl}$*;Gna11*$^{-/-}$ mice compared with *Gna11*$^{-/-}$ controls (Figure 4-8A,B). Quantification of αSMA-positive secondary crests in the lungs demonstrated a small, but not statistically significant, reduction in the proportion of αSMA positive secondary crests in *Pdgfrb-Cre*$^{+/-}$*;Gnaq*$^{fl/fl}$*;Gna11*$^{-/-}$ compared with *Gna11*$^{-/-}$ lungs (0.69 vs 0.84 in controls, p =0.2, Figure 4-8C).

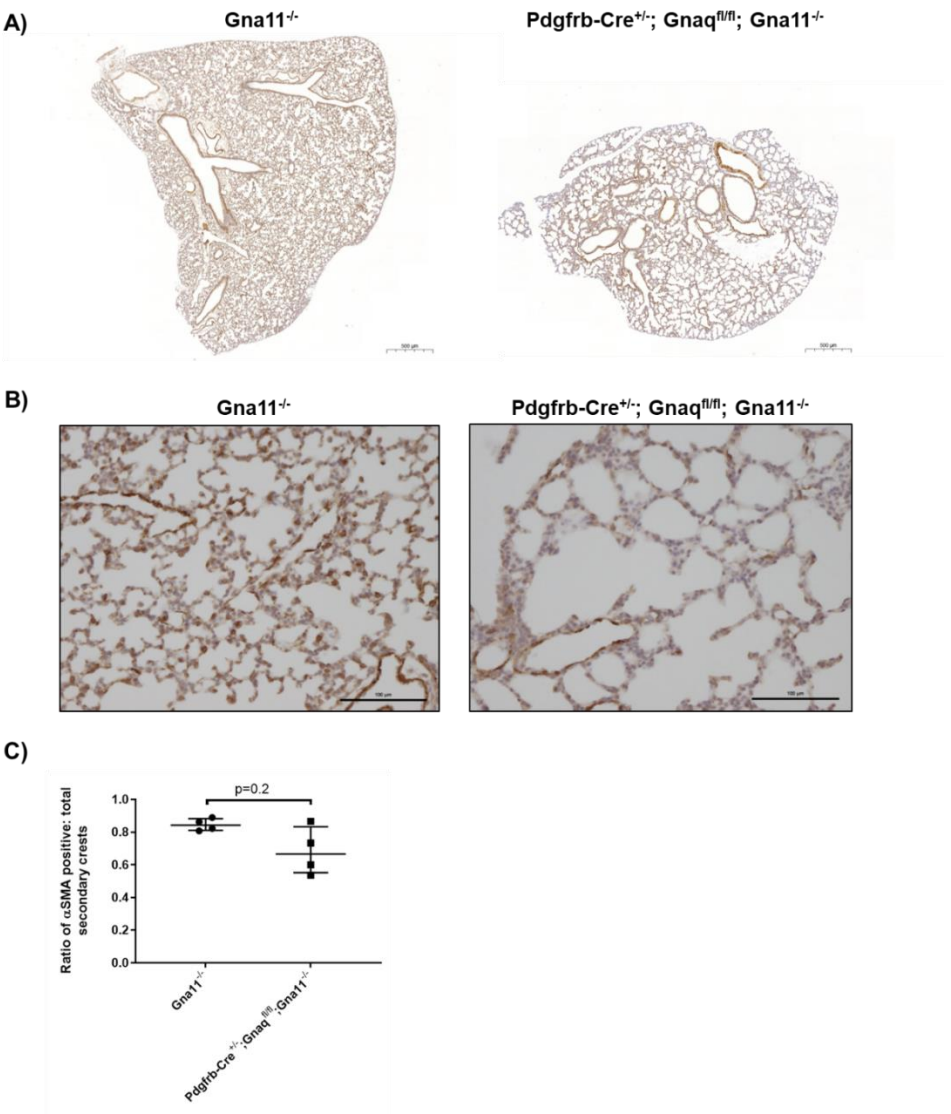

Figure 4-8: Mesenchymal $G_{\alpha q/11}$ knockout lungs contain fewer myofibroblasts

A,B) Low-magnification (A) and high-magnification (B) images of lungs stained for αSMA from representative *Gna11*$^{-/-}$ (left) and *Pdgfrb-Cre*$^{+/-}$*;Gnaq*$^{fl/fl}$*;Gna11*$^{-/-}$ (right) mice.

C) Quantification of the proportion of secondary crests that stained positively for αSMA in 2 week old *Gna11*$^{-/-}$ and *Pdgfrb-Cre*$^{+/-}$*;Gnaq*$^{fl/fl}$*;Gna11*$^{-/-}$ lungs. Data shown as median ± interquartile range. Statistical analysis performed using a two-tailed Mann Whitney Test.

To investigate whether $G_{\alpha q/11}$ deficiency influences myofibroblast differentiation from precursor cells, murine embryonic fibroblasts (MEFs) that were wild-type (WT), $G_{\alpha q/11}$ deficient (*Gnaq*$^{-/-}$;*Gna11*$^{-/-}$) or $G_{\alpha 12/13}$ deficient (*Gna12*$^{-/-}$;*Gna13*$^{-/-}$) were assessed for αSMA protein and mRNA (*Acta2*) expression. MEFs with a long-term deficiency in $G_{\alpha q/11}$ had lower *Acta2* mRNA (relative expression compared to WT MEFs 0.48, p=0.03, Figure 4-9A) than WT MEFs. Furthermore, *Gnaq*$^{-/-}$;*Gna11*$^{-/-}$ MEFs had lower αSMA protein expression compared with WT MEFs (relative densitometry value 0.4 arbitrary units (AU) in *Gnaq*$^{-/-}$;*Gna11*$^{-/-}$ MEFs compared with 0.8AU in WT MEFs, p=0.03, Figure 4-9B,C). This suggests that $G_{\alpha q/11}$ plays a role in the development of the myofibroblast phenotype.

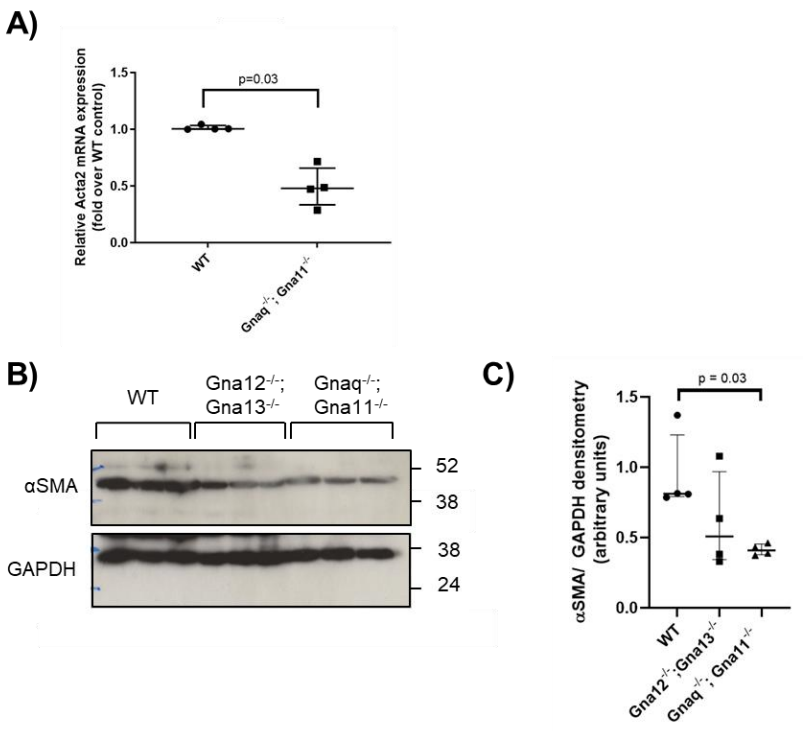

Figure 4-9: MEFs lacking $G_{\alpha q/11}$ have a less myofibroblast-like phenotype than wild-type cells.

A) *Acta2* mRNA expression in WT, *Gna12*$^{-/-}$*;Gna13*$^{-/-}$, and *Gnaq*$^{-/-}$*;Gna11*$^{-/-}$ MEFs assessed by qPCR.

B) Representative western blot showing αSMA expression in wild-type (WT), *Gna12*$^{-/-}$*;Gna13*$^{-/-}$, and *Gnaq*$^{-/-}$*;Gna11*$^{-/-}$ MEFs.

C) Densitometry of western blots of αSMA expression in wild-type (WT), *Gna12*$^{-/-}$*;Gna13*$^{-/-}$, and *Gnaq*$^{-/-}$*;Gna11*$^{-/-}$ MEFs.

Data shown as median ± interquartile range, n=4 per group. Statistical analyses performed using two-tailed Mann Whitney tests.

Having determined that mesenchymal $G_{\alpha q/11}$ deficiency reduces myofibroblast differentiation in the lungs, work was undertaken to assess the effect of this genetic alteration on the pulmonary ECM scaffold structure.

Staining for elastin revealed fewer elastin fibres (7.4 vs 24.9 fibres/ field, p=0.03) and fewer elastin-positive secondary crests (57.5% vs 84.8%, p=0.03) in 2 week old *Pdgfrb-Cre*$^{+/-}$*;Gnaq*$^{fl/fl}$*;Gna11*$^{-/-}$ mouse lungs compared with *Gna11*$^{-/-}$ controls (Figure 4-10A-C). In addition, *Gnaq*$^{-/-}$*;Gna11*$^{-/-}$ MEFs had lower elastin (*Eln*) mRNA expression than WT MEFs (relative *Eln* expression relative to WT MEFs 0.36, Figure 4-10D). Furthermore, picrosirius red staining revealed that 2 week old *Pdgfrb-Cre*$^{+/-}$*;Gnaq*$^{fl/fl}$*;Gna11*$^{-/-}$ mouse lungs contained less collagen than the lungs of *Gna11*$^{-/-}$ control mice (Figure 4-11A,B). This finding was supported by lower *Col1a1* and *Col3a1* mRNA expression in *Gnaq*$^{-/-}$*;Gna11*$^{-/-}$ MEFs than WT MEFs (*Col1a1* and *Col3a1* relative mRNA expression 0.63 and 0.74 compared with WT MEFs, respectively; Figure 4-11C,D).

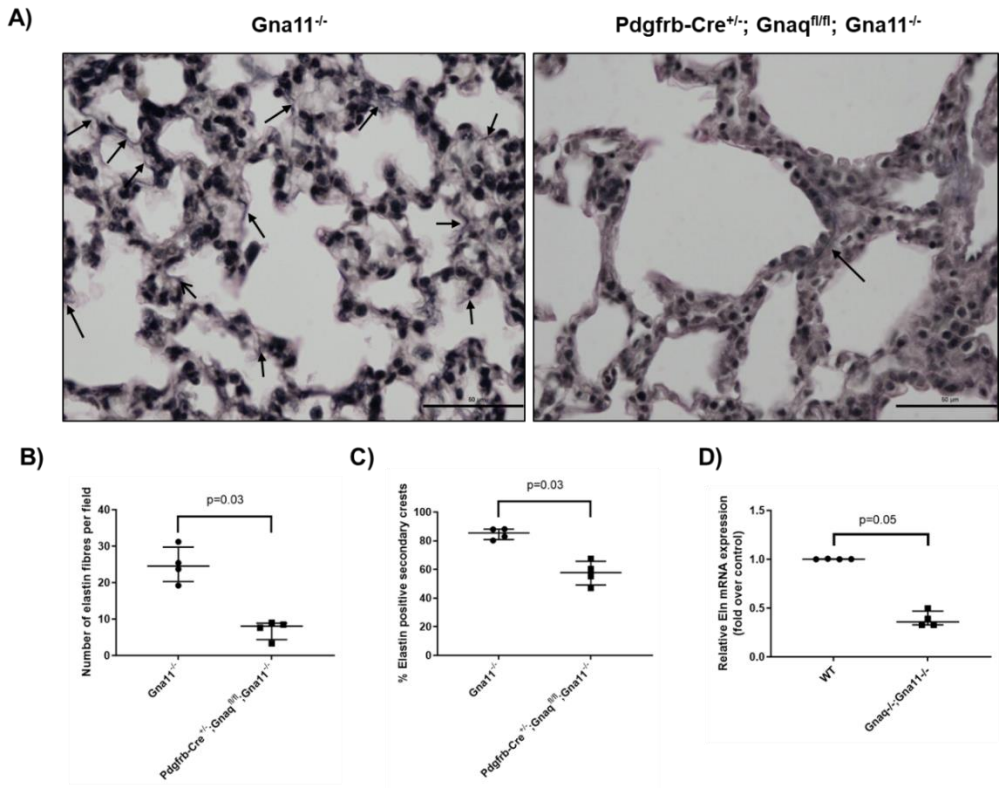

Figure 4-10: Mice lacking mesenchymal $G_{\alpha q/11}$ have abnormal elastin production and organisation

A) Representative images of Verhoeff van Gieson staining of 2 week old *Gna11*$^{-/-}$ and *Pdgfrb-Cre*$^{+/-}$*;Gnaq*$^{fl/fl}$*;Gna11*$^{-/-}$ mouse lungs. Nuclei and elastin shown by black staining. Yellow arrows indicate elastin fibres.

B, C) Quantification of elastin staining from 2 week old *Gna11*$^{-/-}$ and *Pdgfrb-Cre*$^{+/-}$*;Gnaq*$^{fl/fl}$*;Gna11*$^{-/-}$ mouse lungs. Data presented as the proportion of secondary crests that stained positively for elastin (B), and the number of elastin fibres per field (C).

D) Relative *Eln* mRNA expression in wild-type (WT) and *Gnaq*$^{-/-}$*;Gna11*$^{-/-}$ MEFs.

Data shown as median ± interquartile range. N=4 per group. Statistical analysis performed using a two-tailed Mann-Whitney test.

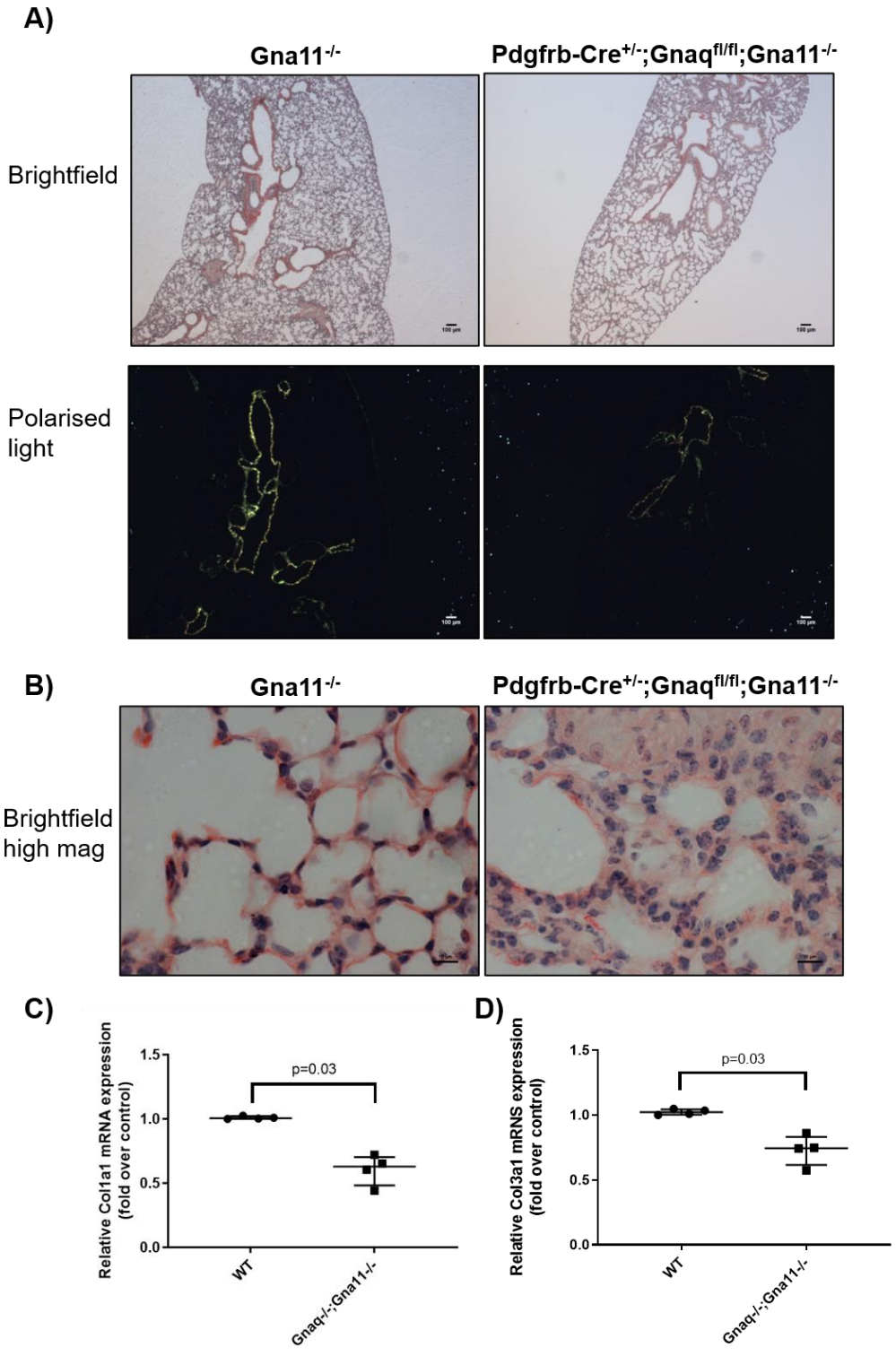

Figure 4-11: The lungs of mice lacking mesenchymal $G_{\alpha q/11}$ contain less collagen

A) Representative low magnification brightfield (top) and the

corresponding polarised light (bottom) images of picrosirius red staining of *Gna11*$^{-/-}$ (left) and *Pdgfrb-Cre*$^{+/-}$;*Gnaq*$^{fl/fl}$;*Gna11*$^{-/-}$ (right) mouse lungs. Collagen stains red, and shows as yellow/ green under polarised light.
B) Representative high magnification images of picrosirius red staining of *Gna11*$^{-/-}$ and *Pdgfrb-Cre*$^{+/-}$;*Gnaq*$^{fl/fl}$;*Gna11*$^{-/-}$ mouse lungs.
C,D) Relative *Col1a1* (C) and *Col3a1* (D) mRNA expression in wild-type (WT) and *Gnaq*$^{-/-}$;*Gna11*$^{-/-}$ MEFs.
Data shown as median ± interquartile range. N=4 per group. Statistical analysis performed using Mann-Whitney test.

Overall, these data suggest that there are defects in lung ECM protein production and organisation by mesenchymal cells deficient in $G_{\alpha q/11}$, and this may occur due to altered myofibroblast differentiation.

4.4.4 Lungs lacking mesenchymal $G_{\alpha q/11}$ contain abnormal blood vessels

In addition to the alveolar abnormalities described above, abnormal peripheral pulmonary vessels were observed in the lungs of *Pdgfrb-Cre*$^{+/-}$;*Gnaq*$^{fl/fl}$;*Gna11*$^{-/-}$ mice (Figure 4-12A). The walls of these vessels were thickened compared with peripheral vessel walls of *Gna11*$^{-/-}$ controls in both the minimum (4.5 vs 7.3µm, p=0.03, Figure 4-12B) and maximum (16.4 vs 7.3µm, p=0.03, Figure 4-12C) dimensions.

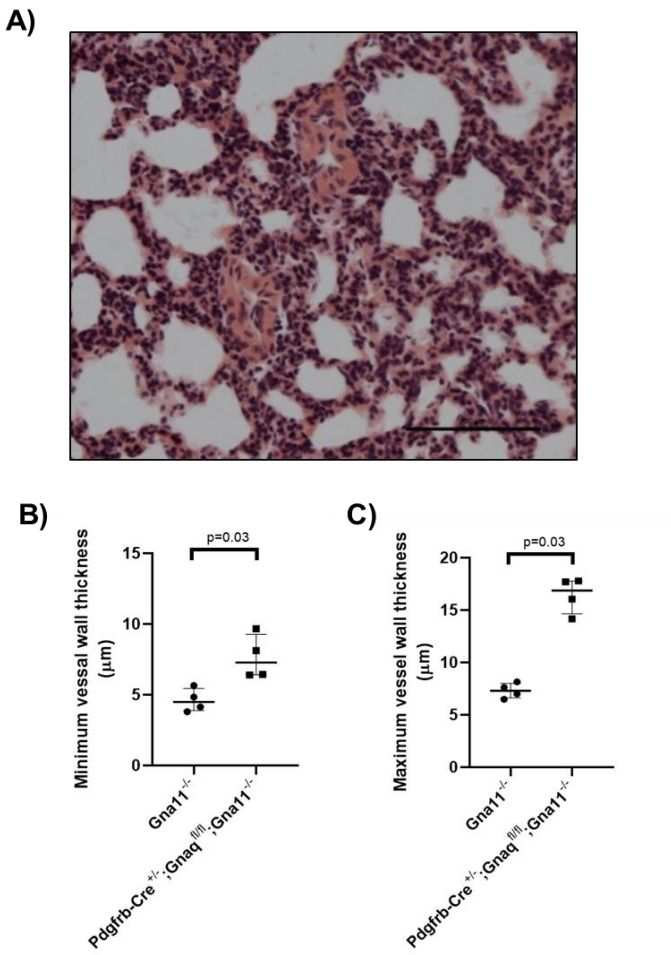

Figure 4-12: Mice lacking mesenchymal $G_{\alpha q/11}$ have thickened peripheral pulmonary vessels

A) Representative H&E stained lung section from a *Pdgfrb-Cre*$^{+/-}$*;Gnaq*$^{fl/fl}$*;Gna11*$^{-/-}$ mouse lung demonstrating abnormal blood vessels. Scale bar shows 100µm.

B,C) Peripheral vessel wall thickness in minimum (B) and maximum (C) dimensions in *Pdgfrb-Cre*$^{+/-}$*;Gnaq*$^{fl/fl}$*;Gna11*$^{-/-}$ and *Gna11*$^{-/-}$ mouse lungs. Data shown as median ± interquartile range, n=4 per group. Statistical analyses performed using a two-tailed Mann Whitney test.

Further staining was performed to characterise the abnormal *Pdgfrb-Cre*$^{+/-}$*;Gnaq*$^{fl/fl}$*;Gna11*$^{-/-}$ pulmonary vessels. The vessel walls did not contain significant elastin or collagen layers (Figure 4-13A,B), indicating that the increased vessel wall thickness was not due to excessive ECM deposition. The thickened vessel walls consisted of a thin endothelial layer (CD31^{+}, Figure 4-13C) surrounded by a thickened vascular smooth muscle layer (αSMA^{+}, Figure 4-13D), without a high degree of proliferation, determined using Ki67 staining (Figure 4-13E). This suggests that the vascular smooth muscle layer was hypertrophic rather than hyperplastic. Overall, the appearances were reminiscent of that seen in pulmonary arterial hypertension (PAH) (250).

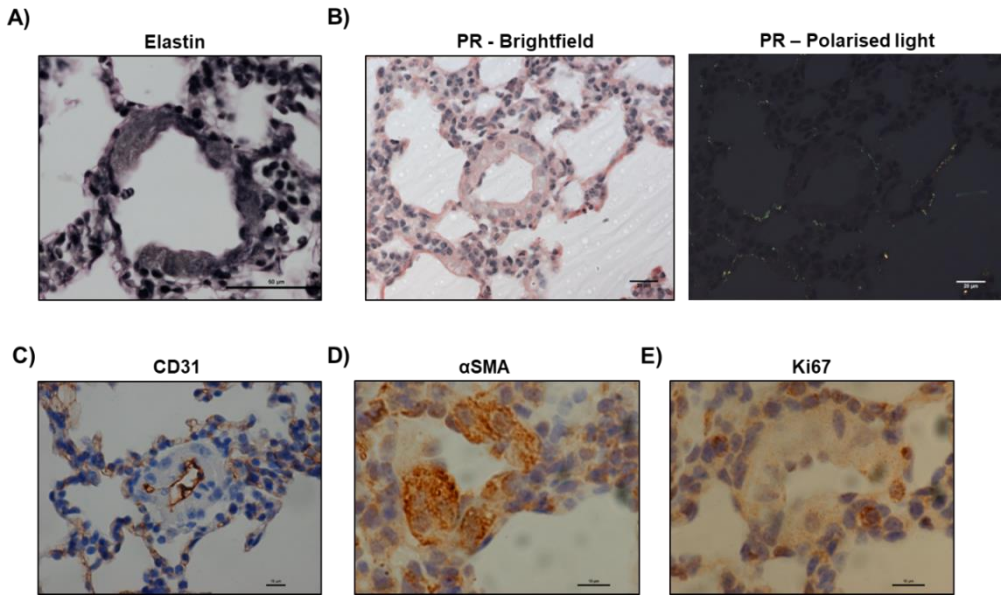

Figure 4-13: Pulmonary vessels in mesenchymal $G_{\alpha q/11}$ knockout lungs have appearances consistent with PAH

Lung sections from 2 week old *Pdgfrb-Cre*$^{+/-}$;*Gnaq*$^{fl/fl}$;*Gna11*$^{-/-}$ mice were stained using various techniques.

A) Verhoeff van Gieson stain for elastin. Elastin and nuclei stain black. Scale bar = 50µm.

B) Picrosirius red (PR) staining of same tissue section viewed under brightfield (left) or polarised light. Collagen fibres stain red and appear yellow/ green under polarised light. Scale bar = 10µm.

C-D) Immunohistochemistry for CD31 (C), αSMA (D), and Ki67 (E). Scale bars = 10µm.

Representative images from four mice shown.

To assess for the cardiac complications associated with PAH, the hearts of *Pdgfrb-Cre*$^{+/-}$;*Gnaq*$^{fl/fl}$;*Gna11*$^{-/-}$ mice were examined for evidence of right ventricular hypertrophy (Figure 4-14). There was no difference in the right: left ventricular wall thickness ratio between *Pdgfrb-Cre*$^{+/-}$;*Gnaq*$^{fl/fl}$;*Gna11*$^{-/-}$ mice and *Gna11*$^{-/-}$ controls (right: left ventricular wall thickness ratio 0.66 in both *Pdgfrb-Cre*$^{+/-}$;*Gnaq*$^{fl/fl}$;*Gna11*$^{-/-}$ mice and

Gna11$^{-/-}$ controls; Figure 4-14B). This suggests that *Pdgfrb-Cre*$^{+/-}$*;Gnaq*$^{fl/fl}$*;Gna11*$^{-/-}$ mice had no gross cardiac abnormality that would be consistent with PAH.

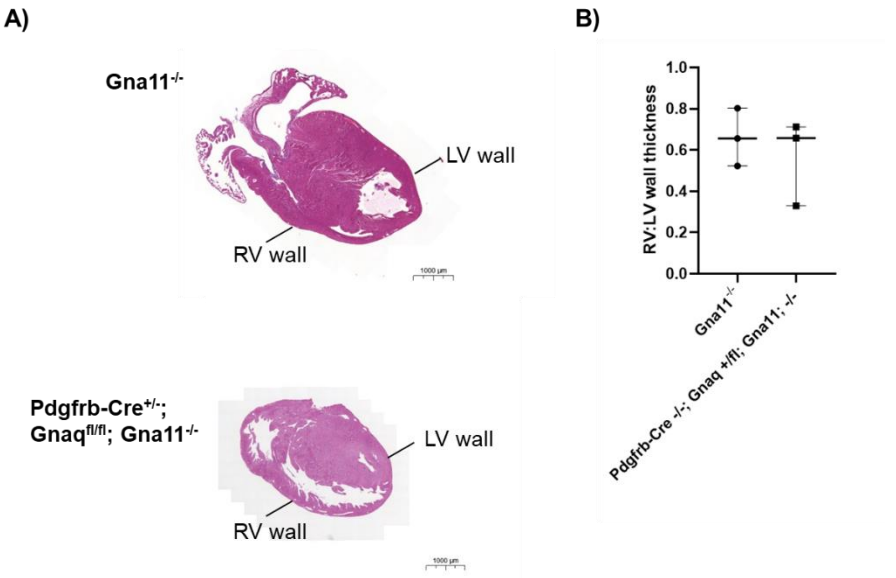

Figure 4-14: Mice lacking mesenchymal $G_{\alpha q/11}$ do not have evidence of cardiac complications of PAH.

A) Representative images of H&E stained hearts from a *Gna11*$^{-/-}$ (top) and *Pdgfrb-Cre*$^{+/-}$*;Gnaq*$^{fl/fl}$*;Gna11*$^{-/-}$ (bottom) mouse. Scale bars = 1000µm.
B) Right: left ventricular wall thickness ratio in *Gna11*$^{-/-}$ and *Pdgfrb-Cre*$^{+/-}$*;Gnaq*$^{fl/fl}$*;Gna11*$^{-/-}$ *mice*. Data shown as median ± interquartile range, n=3.

4.4.5 Mesenchymal $G_{\alpha q/11}$ knockout mice show evidence of altered lung epithelial differentiation

Tight control of mesenchymal-epithelial cell crosstalk is essential for organogenesis, and AECII-to-AECI differentiation is an essential component of normal lung development (195). Therefore, the lungs of 2

week old *Pdgfrb-Cre*$^{+/-}$*;Gnaq*$^{fl/fl}$*;Gna11*$^{-/-}$ mice were assessed for the AECII marker pro-surfactant protein C (pro-SPC).

Pdgfrb-Cre$^{+/-}$*;Gnaq*$^{fl/fl}$*;Gna11*$^{-/-}$ lungs contained fewer pro-SPC-positive cells than *Gna11*$^{-/-}$ control lungs (8.9% pro-SPC positive cells in Pdgfrb-Cre$^{+/-}$;Gnaq$^{fl/fl}$;Gna11$^{-/-}$ lungs, compared with 12.8% in *Gna11*$^{-/-}$ lungs, p=0.03, Figure 4-15A,B). This finding suggests that *Pdgfrb-Cre*$^{+/-}$*;Gnaq*$^{fl/fl}$*;Gna11*$^{-/-}$ lungs have a reduced AECII pool to act as progenitor cells for AECIs, which may be detrimental to normal lung development and repair.

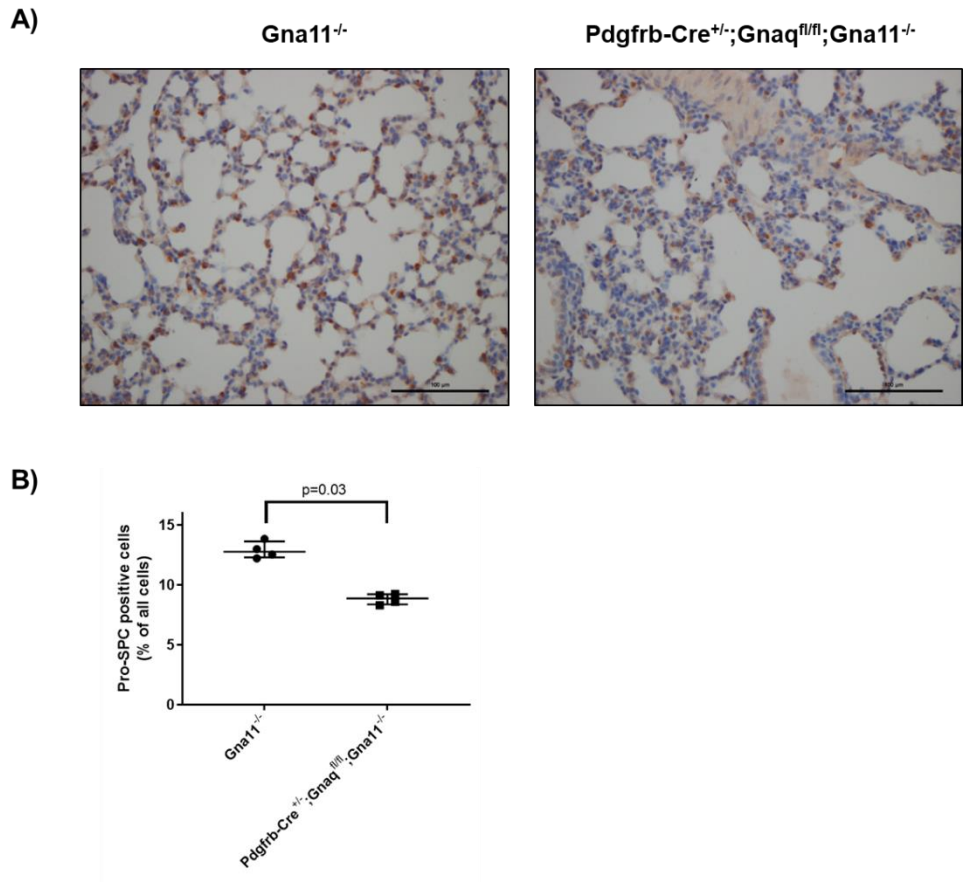

Figure 4-15: The lungs of mice lacking mesenchymal $G_{\alpha q/11}$ contain fewer type II alveolar epithelial cells

A) Representative pro-surfactant protein C (pro-SPC) immunohistochemistry of lung sections from 2 week old *Gna11*$^{-/-}$ (left) and *Pdgfrb-Cre*$^{+/-}$*;Gnaq*$^{fl/fl}$*;Gna11*$^{-/-}$ (right) mouse lungs.

B) Quantification of pro-SPC staining, shown as the percentage of cells staining positively for pro-SPC per image.

Data shown as median ± interquartile range, n=4 per group. Statistical analysis performed using a two-tailed Mann-Whitney test.

4.4.6 Mice lacking mesenchymal $G_{\alpha q/11}$ have abnormal kidneys

At necropsy, it was noted that the kidneys of *Pdgfrb-Cre*$^{+/-}$*;Gnaq*$^{fl/fl}$*;Gna11*$^{-/-}$ mice were smaller and paler than those of their *Gna11*$^{-/-}$ littermates (Figure 4-16A). As kidneys undergo branching

morphogenesis in a similar manner to the lungs (251), and renal failure could explain the poor condition and failure to thrive of *Pdgfrb-Cre*$^{+/-}$ *;Gnaq*$^{fl/fl}$*;Gna11*$^{-/-}$ mice, further work was carried out to investigate for kidney abnormalities.

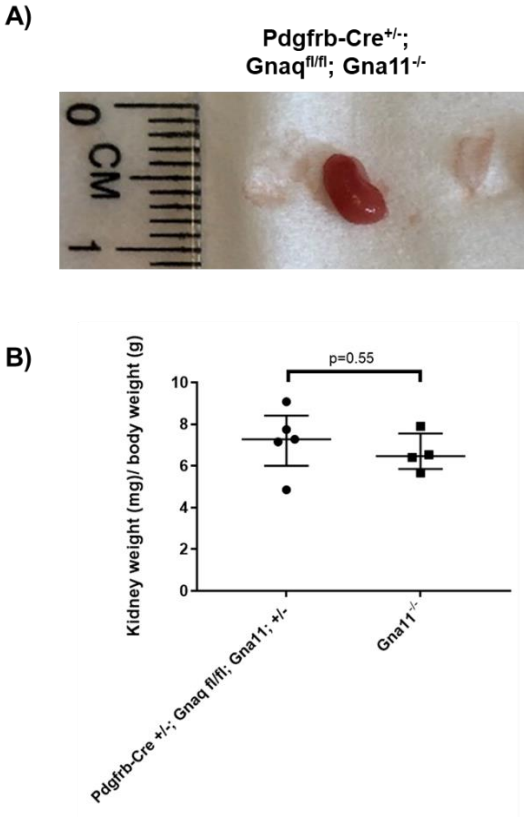

Figure 4-16: The kidneys of mice lacking mesenchymal $G_{\alpha q/11}$ have an abnormal macroscopic appearance

A) Photograph of representative kidneys from a *Pdgfrb-Cre*$^{+/-}$ *;Gnaq*$^{fl/fl}$*;Gna11*$^{-/-}$ mouse and a *Gna11*$^{-/-}$ littermate.

B) Relative kidney: total body weight ratios of *Pdgfrb-Cre*$^{+/-}$ *;Gnaq*$^{fl/fl}$*;Gna11*$^{-/-}$ and *Gna11*$^{-/-}$ mice. Data shown as median ± interquartile range, n=4-5 per group. Data analysed using a two-tailed Mann Whitney test.

On closer examination, the relative kidney weights of *Pdgfrb-Cre*$^{+/-}$*;Gnaq*$^{fl/fl}$*;Gna11*$^{-/-}$ mice were similar to those of *Gna11*$^{-/-}$ mice (median kidney: total body weight ratio 7.3 in *Pdgfrb-Cre*$^{+/-}$*;Gnaq*$^{fl/fl}$*;Gna11*$^{-/-}$ mice and 6.5 in *Gna11*$^{-/-}$ controls, p=0.55; Figure 4-16B), arguing against the possibility of chronic renal impairment. However, on histological staining *Pdgfrb-Cre*$^{+/-}$*;Gnaq*$^{fl/fl}$*;Gna11*$^{-/-}$ kidneys had neoplasm-like hyperproliferation of the medullary tubular epithelium (Figure 4-17A-E). This resulted in loss of the normal space within the Bowman's capsule (Figure 4-17A), and the appearance of crowding in the medulla (Figure 4-17B,C). There was also evidence of abnormal mitoses (Figure 4-17C), and greater Ki67 staining in the medulla suggested increased proliferation (Figure 4-17E). The overall appearance was consistent with a neoplastic process within the kidneys.

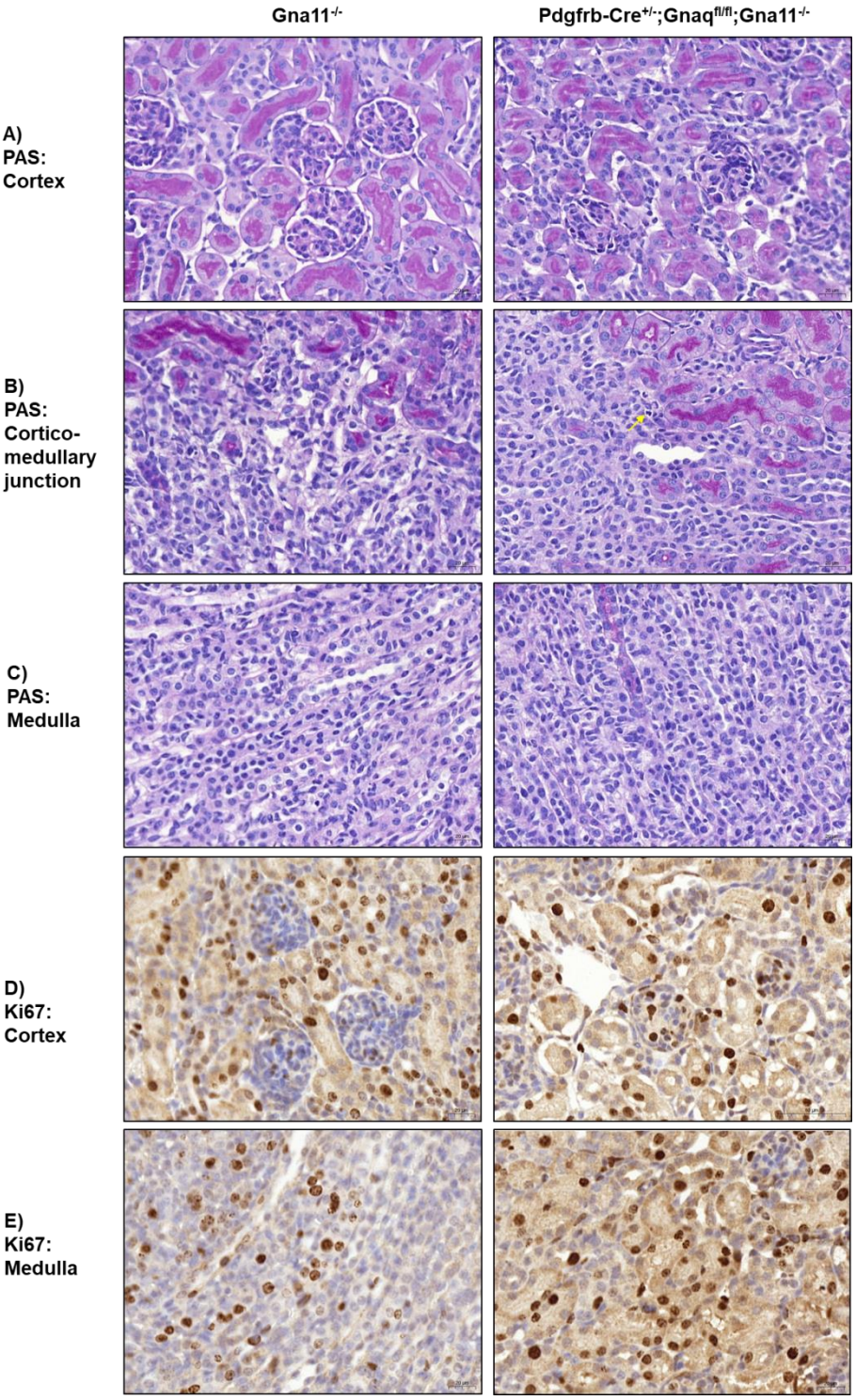

Figure 4-17: The kidneys of mice lacking mesenchymal $G_{\alpha q/11}$ have abnormal medullary tubular epithelial proliferation

A-C) PAS stained kidney sections at the cortex (A), corticomedullary junction (B), and medulla (C) of representative 2 week old *Gna11*$^{-/-}$ (left) and *Pdgfrb-Cre*$^{+/-}$*;Gnaq*$^{fl/fl}$*;Gna11*$^{-/-}$ (right) mice. Yellow arrow

shows an example of ongoing mitosis.
D,E) Ki67 staining at the cortex (D) and medulla (E) of *Gna11*$^{-/-}$ (left) and *Pdgfrb-Cre*$^{+/-}$;*Gnaq*$^{fl/fl}$;*Gna11*$^{-/-}$ mice (right)
Representative images from four mice per group.
With thanks to Professor Katalin Susztak and Dr Matthew Palmer, University of Pennsylvania, for assistance with the interpretation of the renal histology.

Overall, these data imply a role for mesenchymal $G_{\alpha q/11}$ signalling in the control of epithelial proliferation in the kidney, and suggests that mesenchymal $G_{\alpha q/11}$ signalling is important for tumour suppression.

4.4.7 Mice lacking mesenchymal $G_{\alpha q/11}$ have a normal liver appearance

As the lung and kidney histology suggested a multisystem phenotype in *Pdgfrb-Cre*$^{+/-}$;*Gnaq*$^{fl/fl}$;*Gna11*$^{-/-}$ mice, the livers of these animals were also examined histologically.

H&E, picrosirius red, and PAS staining did not reveal any abnormality in *Pdgfrb-Cre*$^{+/-}$;*Gnaq*$^{fl/fl}$;*Gna11*$^{-/-}$ mice (with thanks to Dr Tim Kendall, University of Edinburgh for interpretation of the liver histology; Figure 4-18). These data suggest that mesenchymal $G_{\alpha q/11}$ signalling is not required for normal liver development or homeostasis in the first 2 weeks of life.

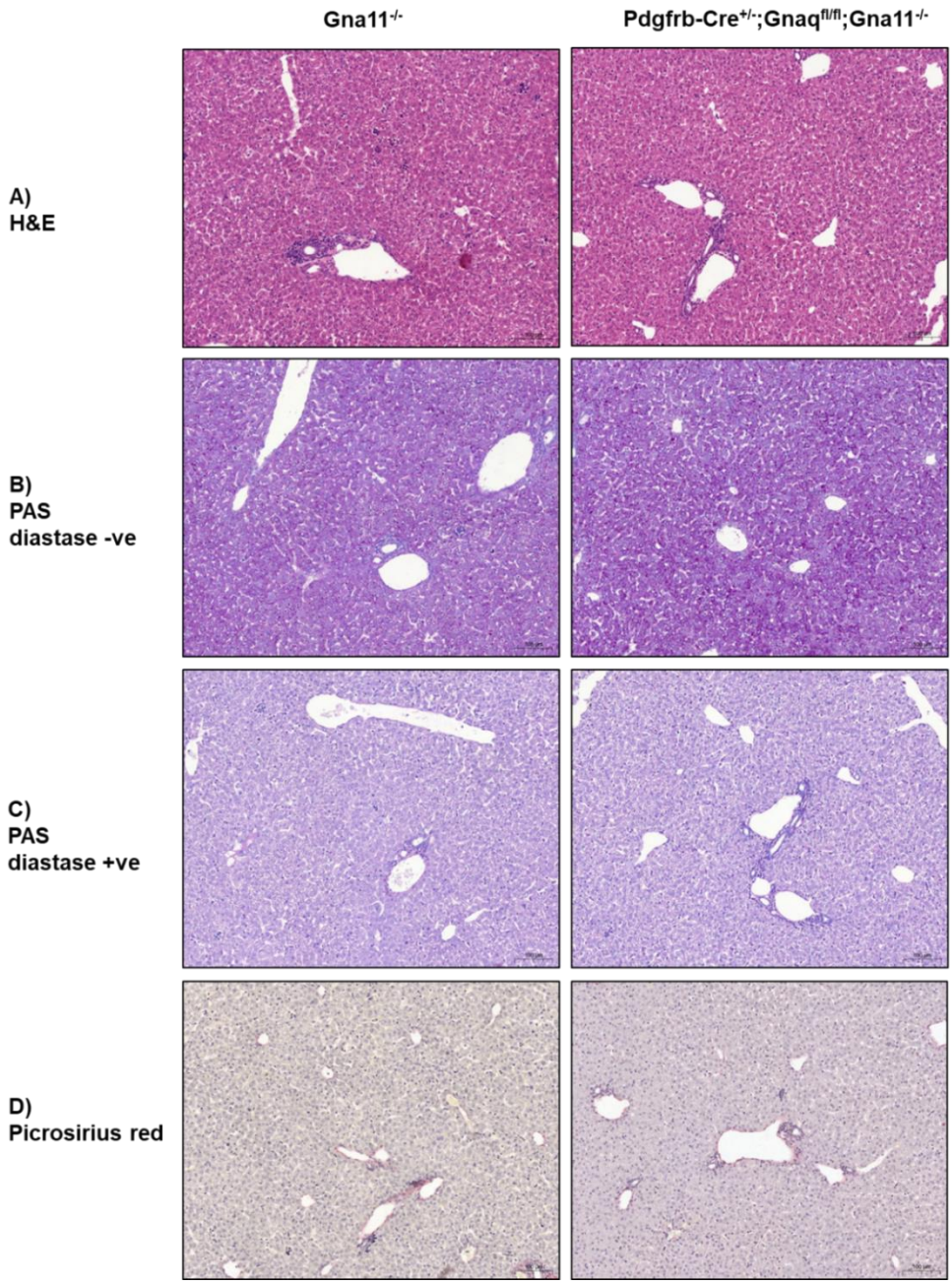

Figure 4-18: Mice lacking mesenchymal $G_{\alpha q/11}$ have normal liver appearances

Livers from 2 week old *Gna11*$^{-/-}$ control (left) and *Pdgfrb-Cre*$^{+/-}$*;Gnaq*$^{fl/fl}$*;Gna11*$^{-/-}$ mice were stained histologically.

A) H&E staining.

B) Periodic acid Schiff (PAS) stain with no diastase digestion.

C) Periodic acid Schiff (PAS) stain with diastase digestion.

D) Picrosirius red stain.
Representative images from four mice per genotype shown.

4.4.8 Mice with mesenchymal $G_{\alpha 12/13}$ deficiency are born at a lower frequency than expected

To generate mice lacking mesenchymal $G_{\alpha 12/13}$, a similar breeding strategy was used to that described for *Pdgfrb-Cre*$^{+/-}$;*Gnaq*$^{fl/fl}$;*Gna11*$^{-/-}$ mice, but involving *Pdgfrb-Cre*$^{+/-}$ and *Gna12*$^{-/-}$;*Gna13*$^{fl/fl}$ mice. Just one mesenchymal $G_{\alpha 12/13}$ knockout mouse (*Pdgfrb-Cre*$^{+/-}$;*Gna12*$^{-/-}$;*Gna13*$^{fl/fl}$) reached genotyping age, despite a total of 110 animals being born and an expected Mendelian ratio of 8.3% per genotype (expected absolute number of mice = 9 per genotype) (Figure 4-19A). These data imply that mice with a mesenchymal deletion of $G_{\alpha 12/13}$ are more likely to die *in utero* or in early life than a mouse with at least one intact mesenchymal *Gna12* or *Gna13* allele.

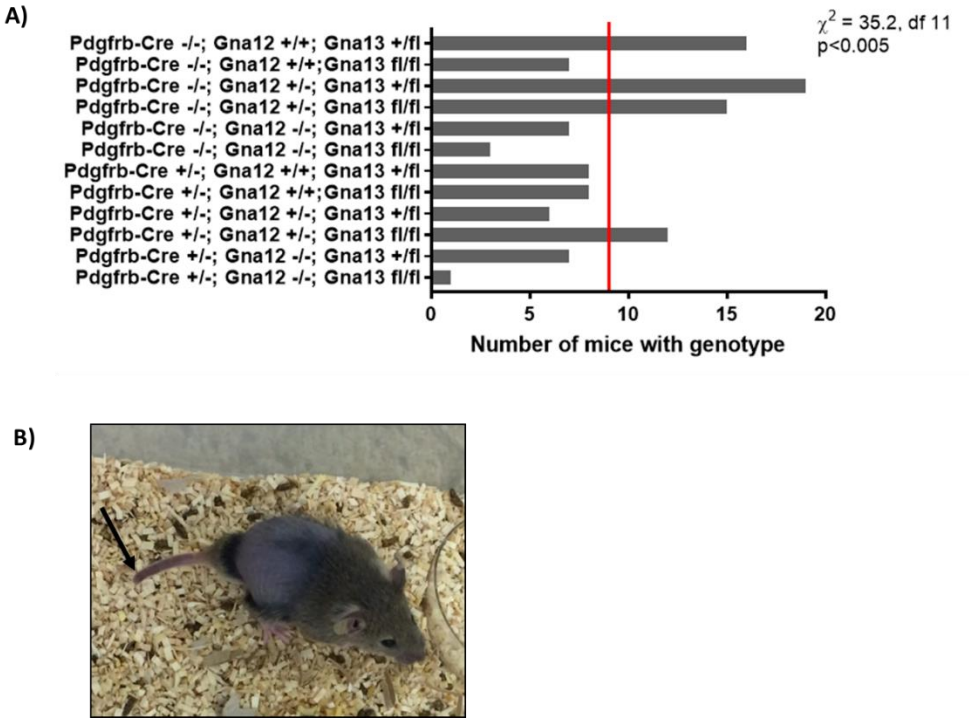

Figure 4-19: Mice lacking mesenchymal $G_{\alpha 12/13}$ are born at a lower than expected frequency

A) Mouse genotype frequencies from *Pdgfrb-Cre*$^{+/-}$ x *Gna12*$^{-/-}$;*Gna13*$^{fl/fl}$ mouse crosses. Red line indicates the expected absolute number of mice according to the expected Mendelian frequency of 8.3% per genotype (expected n=9). Total number of mice 110, 18 litters, mean litter size 6.1. Chi squared value = 35.2, degrees of freedom 11, p<0.005.

B) *Pdgfrb-Cre*$^{+/-}$;*Gna12*$^{-/-}$;*Gna13*$^{fl/fl}$ mouse had a tail deformity (arrow). Photograph shows mouse at 8 weeks old.

The single surviving mouse with a mesenchymal cell specific deletion of $G_{\alpha 12/13}$ had a shortened tail (Figure 4-19B). It was not clear whether this tail abnormality represented a congenital defect related to the genotype or occurred secondary to an injury that occurred shortly after birth. This mouse had a similar growth rate to littermates with at least one intact

Gna12 or *Gna13* allele, and normal lung and kidney histology. These findings suggest that animals lacking mesenchymal $G_{\alpha 12/13}$ that survive the perinatal period can develop normally, however the exact role of mesenchymal $G_{\alpha 12/13}$ in development is unclear.

4.5 Discussion

The results of this study demonstrate essential roles for mesenchymal cell $G_{\alpha q/11}$ and $G_{\alpha 12/13}$ in development. While the specific developmental roles of mesenchymal $G_{\alpha 12/13}$ cannot be concluded from this work, this study has identified essential roles for mesenchymal $G_{\alpha q/11}$ in normal alveolar development as well as tumour suppression in the kidneys.

The role of $G_{\alpha q/11}$ in alveolar development has not previously been investigated, primarily because the *Gnaq*$^{-/-}$;*Gna11*$^{-/-}$ is embryonically lethal (107, 143) and murine alveolarisation occurs entirely postnatally (14). Studies of cell type-specific *Gnaq* and *Gna11* deletion in a number of tissues have identified manifestations ranging from no phenotype to profound cardiac abnormalities associated with perinatal death (Table 4-1). However, abnormalities of lung development have not been described in germline or conditional $G_{\alpha q/11}$ knockout mice, implying a unique role for mesenchymal $G_{\alpha q/11}$ in alveolar development.

Table 4-1: Studies of Conditional $G_{\alpha q/11}$ Knockout Mice

Study	Cre	Target tissue	Phenotype
Babwah et al (252)	GnRH-Cre	GnRH positive neurones	Subfertility (male), Infertility (female), delayed puberty
Broicher et al (253) **Wettschureck et al (254)** **Coulon et al (255)**	Camkcre4	Forebrain	Lack of maternal behaviour, reduced seizure threshold
Dettlaff-Swiercz et al (256)	P0-Cre	Neural Crest	Craniofacial defects
Gangadharan et al (257)	SNS-Cre	Sensory neurones	Attenuated LPI-induced pain sensitisation
Hoyer et al (258)	MLC2a-Cre	Cardiomyocytes	Resistance to diebtees-induced cardiac hypertrophy
John et al (219)	SPC-Cre	Type 2 alveolar epithelial cells	Emphysema (age-related)
Kero et al (259)	Tg-Cre	Thyrocytes	Hypothyroidism (age-related)
Li et al (260)	Sim-1-Cre	Periventricular nucleus of hypothalamus	Hyperphagia, obesity, inactivation of hypothalamic-pituitary-adrenal axis
Ogata et al (261)	Col1a1-Cre	Osteoblasts	Increased bone volume and turnover in response to PTH

Reiken et al (262)	cd-19-cre	B cells	No phenotype
Sassmann et al (263)	Rip-Cre	B cells	Impaired glucose tolerance
Tappe-Theodor et al (264)	SNS-Cre	Sensory neurones	Reduced nociception. Viable, normal development.
Wettschureck et al (244)	MCL-2a-Cre	cardiomyocytes	75% perinatal death, myocardial hypoplasia
Wettschureck et al (265)	Nestin-Cre	Sensory neuronal and glial cell precursors	Failure to establish normal breathing at birth, perinatal death, normal lung appearance
Wettschureck et al (266)	PTH-Cre	Parathyroid cells	Growth retardation, early postnatal death, hypercalcaemia, skeletal abnormalities
LPI = Lysophosphatidylinositol; PTH = parathyroid hormone; GnRH = gonadotrophin releasing hormone; SPC = surfactant protein C			

The evidence presented here suggests that the key mechanisms underlying the failure of normal alveologenesis in *Pdgfrb-Cre*$^{+/-}$*;Gnaq*$^{fl/fl}$*;Gna11*$^{-/-}$ mice are abnormalities in pericyte-to-myofibroblast differentiation and loss of myofibroblast synthetic function. This was evidenced by the existence of fewer lung parenchymal myofibroblasts in *Pdgfrb-Cre*$^{+/-}$*;Gnaq*$^{fl/fl}$*;Gna11*$^{-/-}$ lungs, which differentiate from pericytes and migrate away from the perivascular area (247, 267, 268). Furthermore, *Pdgfrb-Cre*$^{+/-}$*;Gnaq*$^{fl/fl}$*;Gna11*$^{-/-}$ lungs contained reduced

amounts of collagen and elastin compared with controls, and mesenchymal cells lacking $G_{\alpha q/11}$ express less *Col1a1*, *Col3a1*, and *Eln* mRNA than cells with intact $G_{\alpha q/11}$ signalling. As myofibroblasts induce secondary septation by depositing ECM proteins at the tips of developing secondary septa (269), these data suggest that mesenchymal $G_{\alpha q/11}$-induced myofibroblast differentiation and ECM production are required for normal alveolar development.

In addition to reduced myofibroblast differentiation and activity, *Pdgfrb-Cre*$^{+/-}$*;Gnaq*$^{fl/fl}$*;Gna11*$^{-/-}$ mice showed evidence of altered epithelial cell differentiation. *Pdgfrb-Cre*$^{+/-}$*;Gnaq*$^{fl/fl}$*;Gna11*$^{-/-}$ mouse lungs contained fewer pro-SPC-positive AECII cells. AECII cells are widely accepted to be epithelial progenitor cells in the lung which differentiate into the AECI cells that form the gas exchange surface of the alveoli (270, 271). AECII cells are essential for both normal developmental and repair processes in the lung, and the defect in their differentiation in *Pdgfrb-Cre*$^{+/-}$*;Gnaq*$^{fl/fl}$*;Gna11*$^{-/-}$ mice implies that mesenchymal $G_{\alpha q/11}$ signalling helps to drive epithelial cell activity in the lungs. The mechanisms underlying the lower numbers of AECII cells in this study are not certain, however a previous study found that a *Pdgfra*$^{+}$ mesenchymal cell population supported the growth and differentiation of ATII cells (270). While the current study does not prove a mechanistic link, these data support a role for *Pdgfrb*$^{+}$ cells in supporting AECII cell growth.

Furthermore, the epithelial abnormalities were not restricted to the lungs of *Pdgfrb-Cre*$^{+/-}$*;Gnaq*$^{fl/fl}$*;Gna11*$^{-/-}$ mice, as animals with mesenchymal

$G_{\alpha q/11}$ knockout also exhibited neoplasm-like renal tubular epithelial proliferation. This, along with the pulmonary findings, suggests that mesenchymal $G_{\alpha q/11}$ signalling plays tissue-specific roles in the regulation of epithelial differentiation and growth. Further study of the mechanisms underlying this mesenchymal-epithelial crosstalk could have implications for the study of both developmental and malignant diseases.

A key process in alveolarisation is secondary septation, where primitive sacculi are divided by myofibroblast-driven outgrowths, which eventually form the alveoli. Secondary septation is a complex process involving interactions between AECI, AECII, endothelial, and mesenchymal cells, and is a period of high cellular proliferation (272). Mesenchymal $G_{\alpha q/11}$ knockout mice exhibited lower degrees of staining for Ki67, a proliferative marker, in the lungs compared with control mice. While these data do not indicate which cell types have an altered proliferative rate with mesenchymal $G_{\alpha q/11}$ deletion, the overall reduction in proliferation in mesenchymal $G_{\alpha q/11}$ knockout lungs suggests that this may be a driving factor for the abnormal lung appearances.

In addition to failed myofibroblast differentiation from precursor cells, *Pdgfrb-Cre*$^{+/-}$*;Gnaq*$^{fl/fl}$*;Gna11*$^{-/-}$ mouse lungs showed evidence of altered pericyte migration. *Pdgfrb-Cre*$^{+/-}$*;Gnaq*$^{fl/fl}$*;Gna11*$^{-/-}$ lungs contained abnormal peripheral pulmonary vessels characterised by a hypertrophic vascular smooth muscle layer. This suggests that pericyte $G_{\alpha q/11}$ deletion may prevent pericytes from migrating away from the perivascular region

to the alveolar parenchyma, and could result in dysregulated vascular smooth muscle growth. However, pericytes are also known to signal to the endothelium and can influence endothelial activity and vasculogenesis (273), indicating that altered mesenchymal-endothelial crosstalk could also have contributed to the abnormal vascular appearances observed in *Pdgfrb-Cre*$^{+/-}$*;Gnaq*$^{fl/fl}$*;Gna11*$^{-/-}$ lungs. Further study is required to confirm the cell types and signalling pathways involved in generating the abnormal peripheral pulmonary vascular appearances in *Pdgfrb-Cre*$^{+/-}$*;Gnaq*$^{fl/fl}$*;Gna11*$^{-/-}$ mice.

Furthermore, as the abnormal pulmonary vessels observed in *Pdgfrb-Cre*$^{+/-}$*;Gnaq*$^{fl/fl}$*;Gna11*$^{-/-}$ mice were similar to those seen in PAH (250), and disturbed GPCR signalling can increase hypoxia-induced pulmonary vascular remodelling (274), *Pdgfrb-Cre*$^{+/-}$*;Gnaq*$^{fl/fl}$*;Gna11*$^{-/-}$ mice could have had PAH secondary to hypoxia caused by the abnormal alveolar architecture. *Pdgfrb-Cre*$^{+/-}$*;Gnaq*$^{fl/fl}$*;Gna11*$^{-/-}$ mice did not exhibit signs of respiratory distress at 2 weeks of age, and cardiac histology did not show evidence of right ventricular hypertrophy. This supports the former hypothesis of altered pericyte crosstalk with endothelial and smooth muscle cells. However, firm conclusions on the cause of the abnormal peripheral pulmonary vessels in *Pdgfrb-Cre*$^{+/-}$*;Gnaq*$^{fl/fl}$*;Gna11*$^{-/-}$ mice cannot be drawn from this study, and this hypothesis requires further investigation.

Pdgfrb-expressing cells include pericytes, fibroblasts, myofibroblasts, and vascular smooth muscle cells (48), therefore the conditional $G_{\alpha q/11}$

knockout in this model will have affected a wide range of cell types. It is not possible to dissect the precise roles for each cell type in the phenotype observed in *Pdgfrb-Cre*$^{+/-}$*;Gnaq*$^{fl/fl}$*;Gna11*$^{-/-}$ mice. However, as pericytes are a major mesenchymal precursor cells for fibroblasts, myofibroblasts and smooth muscle-like cells in the lung (267), it is reasonable to hypothesise that pericyte $G_{\alpha q/11}$ knockout may be the primary cause for the abnormalities seen in *Pdgfrb-Cre*$^{+/-}$*;Gnaq*$^{fl/fl}$*;Gna11*$^{-/-}$ mice.

The role of PDGFRα-expressing mesenchymal cell precursors in the development of the secondary crest myofibroblasts that drive alveolarisation has been established by previous work (275). However, a role for PDGFRβ-expressing cells in alveolar development has not been described prior to this study. It is possible that secondary crest myofibroblasts derived from a PDGFRβ-expressing precursor, possibly losing the expression of this receptor, however it was not possible to perform lineage tracing studies as part of this project. Further work is required to better characterise the role of PDGFRβ-expressing precursor cells in alveolar development, and the cell lineages involved.

The underlying mechanism by which mesenchymal $G_{\alpha q/11}$ signalling controls the activities of numerous cell types in addition to pericytes and myofibroblasts is likely to be related to TGFβ signalling. $G_{\alpha q/11}$ signalling induces TGFβ activation in epithelial cells (74, 219), and TGFβ regulates cellular proliferation, differentiation, and ECM generation, all of which are essential for normal lung development (54, 59). All three TGFβ isoforms

are expressed at high levels during development with distinct spatial and temporal expression patterns (82). The importance of tightly regulated TGFβ signalling in alveolar development is well established, with both over- and under-activity being implicated in disturbances to alveologenesis (87-97). However, the role of mesenchymal cell $G_{\alpha q/11}$-mediated TGFβ activation in lung development has not been investigated previously.

There are several mechanisms by which $G_{\alpha q/11}$ could induce TGFβ activation in alveolar development. Mechanical stretch of the lungs induces TGFβ activation via $G_{\alpha q/11}$ signalling in the epithelium (219), and pericyte YAP/TAZ, another mechanosensitive signalling pathway, has been found to be important in alveolarisation (272). However, the role of mesenchymal cell stretch in TGFβ activation is unknown. Additionally, several $G_{\alpha q/11}$-coupled GPCRs are known to induce TGFβ signalling, and mice with a global knockout of LPA receptor 1, which induces $G_{\alpha q/11}$ signalling, have abnormal alveolarisation similar to the appearance of *Pdgfrb-Cre*$^{+/-}$*;Gnaq*$^{fl/fl}$*;Gna11*$^{-/-}$ mouse lungs described here (142). The roles of G proteins in interpreting these stimuli in mesenchymal TGFβ signalling will be explored in subsequent chapters of this thesis.

While mesenchymal $G_{\alpha q/11}$ knockout was clearly detrimental, *Pdgfrb* expression, and thus pericytes, are found in many tissues, therefore the exact cause of the demise of *Pdgfrb-Cre*$^{+/-}$*;Gnaq*$^{fl/fl}$*;Gna11*$^{-/-}$ mice is not certain. *Pdgfrb-Cre*$^{+/-}$*;Gnaq*$^{fl/fl}$*;Gna11*$^{-/-}$ mice did not have overt signs of respiratory distress, thus it is unlikely that the pulmonary abnormalities

were the only cause of death. The profound renal abnormalities may have been sufficient to cause renal failure, which could have been the primary cause of deterioration of the *Pdgfrb-Cre*$^{+/-}$*;Gnaq*$^{fl/fl}$*;Gna11*$^{-/-}$ mice at around 3 weeks old. Renal mesangial cells are specialised pericytes that form an essential part of the glomerular functional unit in the kidneys, providing structural support and growth factors essential for endothelial cell and podocyte function (276). The failure to thrive of *Pdgfrb-Cre*$^{+/-}$*;Gnaq*$^{-/-}$*;Gna11*$^{fl/fl}$ mice could be consistent with renal dysfunction, culminating in electrolyte imbalance and/ or uraemia as the final cause of death. Further study is required to determine the precise biochemical consequences of mesenchymal $G_{\alpha q/11}$ deletion *in vivo*, specifically the effect of this genotype on renal function.

An alternative explanation for the failure to thrive of *Pdgfrb-Cre*$^{+/-}$*;Gnaq*$^{-/-}$*;Gna11*$^{fl/fl}$ mice could be nutrient malabsorption secondary to gut dysfunction. PDGFRβ is expressed in the gut (268), and defective gut-related blood vessel formation could reduce the efficiency of nutrient absorption from the gut. This hypothesis is supported by the accelerated deterioration of *Pdgfrb-Cre*$^{+/-}$*;Gnaq*$^{-/-}$*;Gna11*$^{fl/fl}$ animals at around 3 weeks of age, when pups have usually weaned from their mother's milk and start taking a normal diet consisting of more complex nutrients. While the gut appearances of *Pdgfrb-Cre*$^{+/-}$*;Gnaq*$^{-/-}$*;Gna11*$^{fl/fl}$ mice were macroscopically normal at necropsy, histological analyses of the bowel were not performed, thus the contribution of gut defects to the *Pdgfrb-*

Cre$^{+/-}$*;Gnaq*$^{-/-}$*;Gna11*$^{fl/fl}$ mouse phenotype cannot be determine by this study.

While it could be argued that the severe phenotype observed in *Pdgfrb-Cre*$^{+/-}$*:Gnaq*$^{fl/fl}$*;Gna11*$^{-/-}$ mice should have been anticipated prior to breeding, the *Pdgfrb-Cre*$^{+/-}$ mouse has been used for several studies of fibrosis, malignancy and tissue repair without seriously detrimental phenotypes from gene knockout in *Pdgfrb*-expressing cells (48, 49, 57, 277). Similarly, cell type-specific $G_{\alpha q/11}$ knockout mice have been generated in a number of cell types without severe developmental phenotypes (Table 4-1). It is likely that the combination of Cre recombinase expression in pericytes, key cells for normal development, alongside the knockdown of a central signalling mediator, $G_{\alpha q/11}$, in this study explains the severe phenotype seen in *Pdgfrb-Cre*$^{+/-}$*:Gnaq*$^{fl/fl}$*;Gna11*$^{-/-}$ mice.

The abnormalities in *Pdgfrb-Cre*$^{+/-}$*;Gnaq*$^{fl/fl}$*;Gna11*$^{-/-}$ mice were sufficiently significant to cause the animals with this genotype to be unviable beyond 3 weeks of age. Additionally, the lower numbers of *Pdgfrb-Cre*$^{+/-}$*;Gnaq*$^{fl/fl}$*;Gna11*$^{-/-}$ mice reaching genotyping age (2 weeks) suggests that these mice were also more likely to die *in utero* or in early life compared with mice with at least one intact mesenchymal *Gnaq* or *Gna11* allele. Similarly, mice lacking mesenchymal $G_{\alpha 12/13}$ were born at much lower than the expected frequency, suggesting either death *in utero* or in early life. There are fewer published studies of cell type-specific $G_{\alpha 12/13}$ knockout mice (Table 4-2). From the data presented here,

it is unclear what precise effects mesenchymal $G_{\alpha 12/13}$ deletion has on normal development.

Table 4-2: Studies of Conditional $G_{\alpha 12/13}$ Knockout Mice

Study	Cre	Target tissue	Phenotype
Dettlaff-Swiercz et al (256)	P0-Cre	Neural Crest	Cardiac malformations, embryonic lethal
Herroeder et al (278)	Lck-cre	T cells	Lymphadenopathy, increased weight and cellularity of thymus
Moers et al (279)	Nestin-Cre	Neurons	Death between P10-P40 Abnormal development of cerebrum and cerebellum
Reiken et al (262, 280)	CD-19-Cre	B cells	Fewer splenic marginal zone B cells, reduced antibody production
P = postnatal day			

A single *Pdgfrb-Cre*$^{+/-}$*;Gna12*$^{-/-}$*;Gna13*$^{fl/fl}$ mouse reached genotyping age, and besides a tail deformity this animal behaved normally and grew in a comparable manner to its littermates. It is unclear whether this tail abnormality occurred secondary to an injury, or whether this reflects a role for $G_{\alpha 12/13}$ in normal tail development. *Gna12*$^{-/-}$ mice have no visible

phenotype, but *Gna13*$^{-/-}$ embryos die *in utero* at embryonic day 10 due to defective vasculogenesis (144). No reports of abnormal tail formation in *Gna13*$^{-/-}$ mice were reported in the studies that characterised these germline mutant animals, but as the tail bud normally appears at around embryonic day 10 (281), it is possible that these animals died before any tail abnormality could be detected. Given that fibroblast-like cells from *Gna13*$^{-/-}$ mouse embryos have impaired migratory responses (144), it is possible that *Pdgfrb-Cre*$^{+/-}$*;Gna12*$^{-/-}$*;Gna13*$^{fl/fl}$ mice have defective tail development because of a key role of $G_{\alpha 12/13}$ in tail elongation. However, firm conclusions cannot be drawn from the single *Pdgfrb-Cre*$^{+/-}$*;Gna12*$^{-/-}$*;Gna13*$^{fl/fl}$ mouse observed in this study. As there were limited organ samples to pursue any mechanistic studies to further define any abnormalities, these experiments were not pursued. While the effects of mesenchymal $G_{\alpha 12/13}$ deletion on development cannot be concluded from this study, these data clearly demonstrate that the breeding of *Pdgfrb-Cre*$^{+/-}$*;Gna12*$^{-/-}$*;Gna13*$^{fl/fl}$ mice for a bleomycin model of pulmonary fibrosis would not be feasible.

The presumption that most *Pdgfrb-Cre*$^{+/-}$*;Gna12*$^{-/-}$*;Gna13*$^{fl/fl}$ animals die *in utero* is seemingly contradicted by the lack of detrimental phenotype in the surviving *Pdgfrb-Cre*$^{+/-}$*;Gna12*$^{-/-}$*;Gna13*$^{fl/fl}$ mouse. However, in previous work using a surfactant protein C (SPC)-Cre model with the same *Gna12*$^{-/-}$*;Gna13*$^{fl/fl}$ mice used in this study found that *Spc-Cre*$^{+/-}$*; Gna12*$^{-/-}$*; Gna13*$^{fl/fl}$ animals were born at approximately half the expected Mendelian frequency, but did not show any detrimental phenotype (219).

This suggests that other factors may influence whether *Pdgfrb-Cre*$^{+/-}$*;Gna12*$^{-/-}$*;Gna13*$^{fl/fl}$ mice can overcome any detrimental phenotype.

The hypothesis underlying the work presented here was that interrupting mesenchymal $G_{\alpha q/11}$ or $G_{\alpha 12/13}$ signalling would be protective against pulmonary fibrosis. The phenotypes of *Pdgfrb-Cre*$^{+/-}$*;Gnaq*$^{fl/fl}$*;Gna11*$^{-/-}$ and *Pdgfrb-Cre*$^{+/-}$*;Gna12*$^{-/-}$*;Gna13*$^{fl/fl}$ mice were sufficiently detrimental to preclude the use of these animals in the bleomycin model of pulmonary fibrosis. This is because mice lacking mesenchymal $G_{\alpha q/11}$ would not be fit enough to withstand bleomycin administration, and mice lacking mesenchymal $G_{\alpha 12/13}$ could not be bred in sufficient numbers for a well-powered study. Therefore, it is not currently possible to conclude whether mesenchymal $G_{\alpha q/11}$ or $G_{\alpha 12/13}$ blockade is protective against pulmonary fibrosis *in vivo*. The abnormalities observed in *Pdgfrb-Cre*$^{+/-}$*;Gnaq*$^{fl/fl}$*;Gna11*$^{-/-}$ and *Pdgfrb-Cre*$^{+/-}$*;Gna12*$^{-/-}$*;Gna13*$^{fl/fl}$ mice are thought to be due to disturbances in developmental processes, and the exaggerated wound healing responses seen in IPF are often driven by the same pathways that drive normal lung development (282). Therefore, an inducible Cre expression model may allow us to test the original study hypothesis. This approach will be evaluated later in this thesis.

4.6 Limitations

The main limitation of this work is the single timepoint at which *Pdgfrb-Cre*$^{+/-}$*;Gnaq*$^{fl/fl}$*;Gna11*$^{-/-}$ mouse tissue was assessed (2 weeks old). Analysis of lung histology at several timepoints would have pinpointed the time point at which alveolarisation began to fail in the lungs, and when

the renal abnormalities began to appear. These assessments would also rule out destructive processes leading to the normal lung appearance in *Pdgfrb-Cre*$^{+/-}$*;Gnaq*$^{fl/fl}$*;Gna11*$^{-/-}$ mice, as pericytes have been implicated in the immune response to lung injury (283). Furthermore, assessment of neonatal lung and renal tissue would have ascertained whether the abnormalities were present at birth or developed postnatally. Unfortunately, it was not feasible to obtain tissue from *Pdgfrb-Cre*$^{+/-}$*;Gnaq*$^{fl/fl}$*;Gna11*$^{-/-}$ mice at multiple timepoints because of the low numbers of mice born with this genotype and the ethical considerations of breeding large numbers of animals with such a severe phenotype. In addition, the primary aim of this study was not to perform detailed phenotyping, but to assess whether these animals developed normally enough to undergo experimental pulmonary fibrosis studies. On discovery of the detrimental phenotype, assessments were performed to describe the abnormalities as well as possible to avoid these animals being bred again for ethical reasons, but in-depth developmental studies were beyond the scope of this project.

Due to technical issues, it was not possible to confirm the $G_{\alpha q}$ knockout in *Pdgfrb*-expressing cells in *Pdgfrb-Cre*$^{+/-}$*;Gnaq*$^{fl/fl}$*;Gna11*$^{-/-}$ mice. Other studies have shown that *Pdgfrb-Cre*$^{+/-}$ mice do not undergo Cre-mediated DNA recombination in lung epithelial and endothelial cells (272). However, Cre recombinase efficiency can vary according to the characteristics of the floxed gene, such as DNA tertiary structure (224), and it is therefore possible that Cre-mediated recombination occurred in

cells other than pericytes, myofibroblasts, fibroblasts, and smooth muscle cells, which hasn't been reported previously.

In this study histology was used to phenotype *Pdgfrb-Cre*$^{+/-}$*;Gnaq*$^{fl/fl}$*;Gna11*$^{-/-}$ mice, however it could be argued that this approach is not sufficient. The Wellcome Sanger Institute uses multiple assessments when phenotyping a new transgenic mouse line, including body weight, hair morphology, grip strength, indirect calorimetry, glucose tolerance, auditory brainstem response, radiological imaging, and slit lamp examination and ophthalmoscopy for eye morphology (284). However, all of these examinations other than body weight occur at 4 weeks old or later, which would not have been possible for the *Pdgfrb-Cre*$^{+/-}$*;Gnaq*$^{fl/fl}$*;Gna11*$^{-/-}$ mice, which did not survive beyond 3 weeks of age. Hence, while it is possible that some abnormalities have been missed by the approach taken in this study, many of the aforementioned phenotyping tests would not have been feasible in *Pdgfrb-Cre*$^{+/-}$*;Gnaq*$^{fl/fl}$*;Gna11*$^{-/-}$ mice.

4.7 Conclusion

This is the first study to generate mesenchymal $G_{\alpha q/11}$ and $G_{\alpha 12/13}$ knockout mice, and this work has demonstrated important roles for these G proteins in normal development. Specifically, mesenchymal $G_{\alpha q/11}$ signalling is essential for normal alveolar development and tumour suppression in the kidney. Animals with germline deletion of $G_{\alpha q/11}$ or $G_{\alpha 12/13}$ in mesenchymal cells are not suitable for use in the bleomycin

model of pulmonary fibrosis, and alternative investigations should be performed to ascertain the role of these G proteins in fibrogenesis.

5 The Role of $G_{\alpha q/11}$ and $G_{\alpha 12/13}$ in Driving Myofibroblast Activity

5.1 Introduction

The data presented in Chapter 4 demonstrated that deficiency of $G_{\alpha q/11}$ or $G_{\alpha 12/13}$ signalling in *Pdgfrb*-expressing cells results in severe developmental phenotypes, including abnormal alveolarisation in mesenchymal $G_{\alpha q/11}$ knockout mice. These phenotypes may have occurred due to altered TGFβ signalling and myofibroblast activities, which could make mesenchymal $G_{\alpha q/11}$ or $G_{\alpha 12/13}$ deficiency protective against pulmonary fibrosis. In addition, many of the signalling pathways that drive normal lung development are reactivated during fibrogenesis, and TGFβ signalling is essential for both processes, suggesting that mesenchymal $G_{\alpha q/11}$-deficient lungs may be resistant to developing pulmonary fibrosis. However, mice deficient in mesenchymal $G_{\alpha q/11}$ and $G_{\alpha 12/13}$ were not suitable for us in *in vivo* experimental pulmonary fibrosis models, and the exact roles of mesenchymal $G_{\alpha q/11}$ and $G_{\alpha 12/13}$ in myofibroblast function and TGFβ signalling remain unclear. *In vitro* methods to assess the role of mesenchymal cell $G_{\alpha q/11}$ and $G_{\alpha 12/13}$ in TGFβ signalling and myofibroblast function could reveal important mechanisms of both normal lung development and fibrosis.

Myofibroblasts are key cells in both fibrogenesis and normal lung development. These cells differentiate from fibroblasts in response to a range of stimuli, including TGFβ signalling and increased stiffness of the surrounding extracellular matrix (ECM) (164-166). In turn, myofibroblasts organise and generate increasingly stiff ECM, and activate latent TGFβ from the ECM through cellular contraction (161). In normal wound

healing or development, myofibroblast activity is tightly controlled, however in fibrosis myofibroblast activity is exaggerated, resulting in a positive feedback loop of fibrogenesis (9). Investigations of the mechanisms that induce mesenchymal cell TGFβ signalling and myofibroblast differentiation in response to matrix stiffness are key to understanding how pulmonary fibrosis progresses. However, the roles of $G_{\alpha q/11}$ and $G_{\alpha 12/13}$ in these processes have not been investigated prior to the current study.

To model the effects of mesenchymal $G_{\alpha q/11}$ and $G_{\alpha 12/13}$ knockout in lung development and pulmonary fibrosis, an *in vitro* G protein coupled receptor (GPCR) agonist-induced TGFβ activation system relevant to both conditions is required. The bioactive phospholipid LPA is a GPCR agonist that activates TGFβ in epithelial cells (74) and is found at elevated levels in the lungs of patients with IPF (127). Furthermore, mice with impaired LPA signalling due to LPA receptor 1 (*Lpa1*) knockout exhibit abnormal alveolarisation (142). Therefore, LPA-induced TGFβ signalling experiments are ideal to model the influence of mesenchymal $G_{\alpha q/11}$ and $G_{\alpha 12/13}$ signalling on myofibroblast activities.

5.2 Aims and Hypothesis

The aims of this work were to:

1) Establish an *in vitro* model of GPCR agonist (LPA)-induced TGFβ signalling in mesenchymal cells.

2) Understand the roles of $G_{\alpha q/11}$ and $G_{\alpha 12/13}$ in LPA-induced TGFβ signalling.
3) Understand how mesenchymal cell $G_{\alpha q/11}$ and $G_{\alpha 12/13}$ are involved in the detection of matrix stiffness and how this affects the myofibroblast phenotype.

The hypotheses underlying this work were:

$G_{\alpha q/11}$ and $G_{\alpha 12/13}$ mediate TGFβ signalling in response to the GPCR agonist LPA via Rho-ROCK signalling in mesenchymal cells.

$G_{\alpha q/11}$ and $G_{\alpha 12/13}$ are important for the detection of matrix stiffness by mesenchymal cells.

5.3 Methods

5.3.1 LPA stimulations of MEFs

WT, *Gnaq*$^{-/-}$*;Gna11*$^{-/-}$, and *Gna12*$^{-/-}$*;Gna13*$^{-/-}$ MEFs were seeded at 2 x 10^5 cells per well of a six well plate in full media, allowed to adhere overnight, then growth arrested in 0% FCS DMEM for 24 hours. Cells were stimulated with 50µM LPA in 0% FCS DMEM for 4 hours, then lysed for protein analysis.

To assess the role of ROCK signalling in this system, cells were treated with 10µM of the ROCK1/2 inhibitor Y27632 for 1 hour prior to and throughout a 4 hour 50µM LPA stimulation.

5.3.2 LPA stimulation of HLFs with and without $G_{\alpha q/11}$ or $G_{\alpha 12/13}$ knockdown

HLFs were seeded at 1.5 x 10^5 cells per well of a six well plate in antibiotic-free full media and allowed to adhere overnight.

15nM per siRNA of *GNAQ* and *GNA11* siRNA, or *GNA12* and *GNA13* siRNA, were applied with 4µl/ml DharmaFECT 1 transfection reagent in 0% FCS DMEM. A non-targeting control siRNA was applied to control cells at 25nM, as per the manufacturer's protocol. After 24 hours, the transfection media was replaced with antibiotic-free full media, then 24 hours later this was replaced with 0% FCS DMEM to growth arrest the cells. Cells were stimulated with 50µM LPA for 4 hours, and cell lysates collected for protein analysis.

5.3.3 Matrix stiffness experiments

5.3.3.1 Generation of soft tissue culture substrates

5.3.3.1.1 Principle

Cellular activity can be influenced by the mechanical properties of the environment, therefore work to generate tissue culture substrates with modifying elastic moduli has increased over recent years. In the method used in this thesis, silicone-based propriety polymers were mixed in pre-defined ratios, resulting in a reaction that generates a polymer of a known elastic modulus.

5.3.3.1.2 Method

Silicone cell culture substrates were generated using a proprietary method in the laboratory of Dr Boris Hinz (University of Toronto, Canada). Substrates were generated by mixing “Polymer A” and “Polymer B” at pre-defined ratios to achieve substrate with the desired elastic modulus (Table 5-1: Components of soft tissue culture gels. Each batch of the proprietary polymers was validated as producing the correct polymer stiffness in house.

Table 5-1: Components of soft tissue culture gels

Stiffness (kPa)	**5**	**36**	**100**
Polymer A: Polymer B ratio	1.8: 1	1.2: 1	0.67: 1

An appropriate volume of Polymer B was mixed with a polymerisation retardant (proprietary, University of Toronto, 0.3-0.6% of the final total volume of Polymers A and B), on a THINKY centrifugal mixer for 3 minutes at 1600rpm. Polymer A was added to the Polymer B/ retardant mixture, and mixed for 3 minutes at 1600rpm. A syringe pump was used to dispense 600µl Polymer A/ Polymer B mixture into the centre of 35mm dishes, or 100µl onto the centre of each well of a 24 well plate, and the polymer mixture allowed to spread evenly on a flat surface overnight. Substrate-coated plates were then baked at 60^{o}C for 4 days.

5.3.3.2 Functionalisation and protein coating of soft substrates

To overcome the hydrophobicity of the polymerised silicone, the substrates were plasma oxygen treated for 25 seconds using a Plasma Etch system (Plasma Etch, USA). Plasma oxygen treatment results in the formation of a hydrophilic layer on the surface of the polymer due to the formation of high energy surface groups produced by the reactions between the surface of the polymer and reactive plasma species (285). As the hydrophilization of the polymer surface is unstable, the polymer was immediately covered with 10µg/ml gelatin in PBS, and incubated overnight at 37^{o}C. The gelatin solution was aspirated just before cells were seeded for experiments.

5.3.3.3 Cell culture on soft substrates

Cells were seeded on gelatin-coated tissue culture plastic or soft silicone substrates of 5kPa, 36kPa, and 100kPa stiffness, at 1 x 10^3 cells per 35mm dish in full media. Cells were allowed to grow for 6 days, then lysed for protein analysis.

5.3.3.4 LPA stimulations on soft substrates

Cells were seeded on gelatin-coated tissue culture plastic, or soft silicone substrates of 5, 36, and 100kPa stiffness, at a density of 2 x 10^4 cells per well of a 24 well plate, and allowed to adhere overnight. Cells were growth arrested in 0% FCS DMEM for 24 hours before stimulation with 50µM LPA for 4 hours. Cells were lysed for protein analysis.

5.3.4 Online data repository searches

LungMAP (286) and IPF Cell Atlas (287, 288) are online repositories of single cell RNA sequencing (scRNASeq) and proteonomic data from developing and adult lungs, respectively. These repositories were searched for *PDGFRB* and LPA receptor (*LPA1, LPA2, LPA3, LPA4, LPA5,* and *LPA6*) gene expression in developing and adult lung mesenchymal cells in mice and humans.

The GPCRdb website (289, 290) was used to identify the G_{α} subunit family couplings to mammalian LPA receptors.

5.4 Results

5.4.1 Murine embryonic fibroblasts (MEFs) and human lung fibroblasts (HLFs) express *PDGFRB*

To establish which cell type would be most appropriate to model the mesenchymal $G_{\alpha q/11}$ and $G_{\alpha 12/13}$ knockout in the *Pdgfrb-Cre* murine models reported in Chapter 4, IPF Cell Atlas and LungMAP were used to identify cells that express *PDGFRB* in humans and mice.

RNASeq data from LungMAP showed that mesenchymal cells in mouse lung consistently express higher levels of *Pdgfrb* than epithelial, endothelial, and immune cells (Figure 5-1A). This mesenchymal *Pdgfrb* expression peaks on postnatal day 7 (P07), a time when alveolarisation is underway (14), thus supporting the role of *Pdgfrb*-expressing mesenchymal cells in alveologenesis. While pericytes have the highest *Pdgfrb* expression, lung fibroblasts also express *Pdgfrb* (Figure 5-1B).

This evidence suggests that mouse fibroblasts are appropriate tools for *in vitro* models of molecular signalling in *Pdgfrb*-expressing cells. Murine embryonic fibroblasts (MEFs) were chosen for these *in vitro* models, as they are an immature cell that would be present during developmental processes. Furthermore, MEFs with stable *Gnaq* and *Gna11* (*Gnaq*$^{-/-}$*;Gna11*$^{-/-}$) , and *Gna12* and *Gna13*, knockdown (*Gna12*$^{-/-}$*;Gna13*$^{-/-}$ MEFs) are available, allowing the investigations of the role of mesenchymal $G_{\alpha q/11}$ and $G_{\alpha 12/13}$ in developmental and fibrotic pathways *in vitro*.

A)

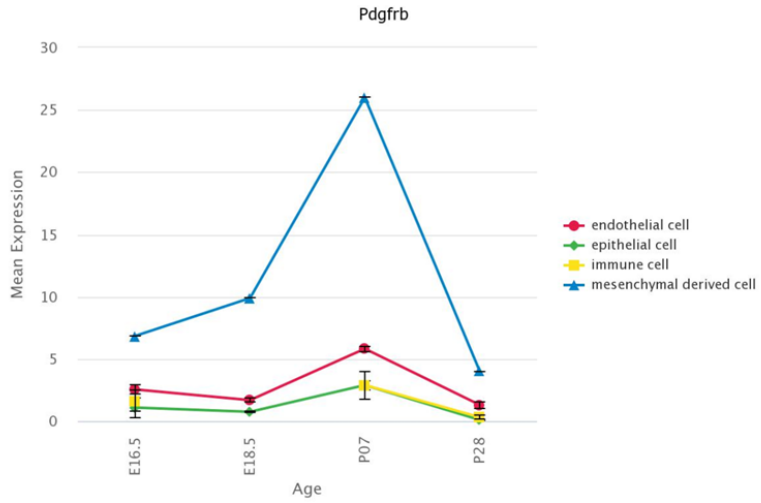

B)

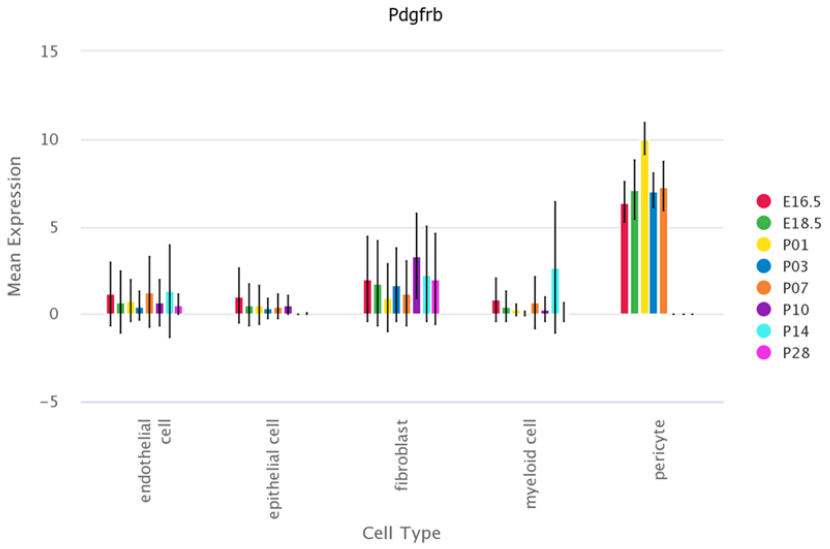

Figure 5-1: *Pdgfrb* gene expression is highest in mesenchymal cells during lung development.

A) *Pdgfrb* expression in mouse lung cells during development. Data generated from RNA Seq analysis of sorted cells. Data shown is mean gene expression value from 16-24 C57BL6 mice per age group. Data and graph from LungMAP (286).

B) Single cell RNA Seq data showing mean *Pdgfrb* expression in mouse lung cells during development in different cell types. Data shown as mean ± standard error of the mean. Data and graphs from LungMAP

(286).
E = embryonic day; P= postnatal day

To increase the translatability of any *in vitro* models used in this study to human lung development and disease, the LungMAP and IPF Cell Atlas data repositories were searched for *PDGFRB* expression in developing and mature human lung cells. In a similar pattern to developing mouse lungs, human lung mesenchymal cells consistently expressed the highest levels of PDGFRβ protein (Figure 5-2A) and *PDGFRB* mRNA (Figure 5-2B) compared with other cell types during development.

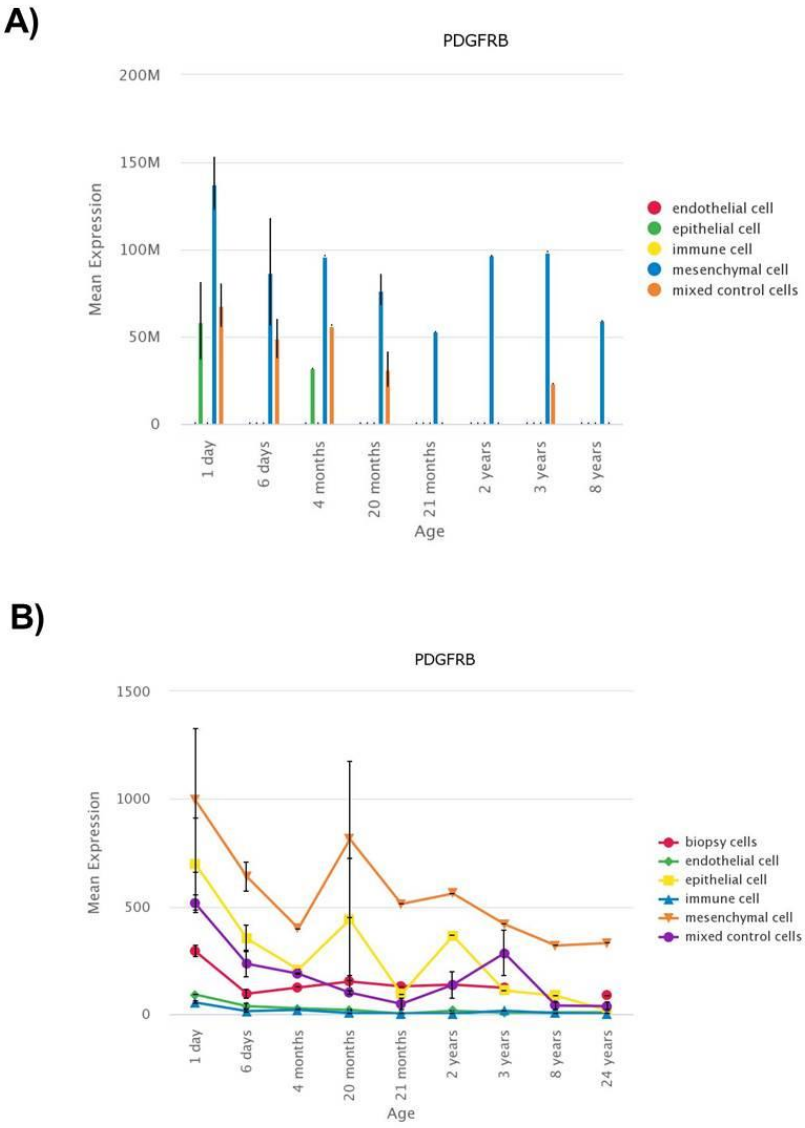

Figure 5-2: *PDGFRB* is expressed at high levels in mesenchymal cells in the developing human lung

A) Proteonomic data from sorted cells showing PDGFRβ protein expression in different lung types at different developmental stages in the human lung. Data shown as mean ± standard error of the mean, n=2 for 1 day, 6 day, and 20 months old, n=1 for other ages (286).

B) RNA-Seq data from sorted human lung cells at different stages of development. Data shown as mean ± standard error of the mean. Data from lungs from 2 subjects at 1 day, 6 day, and 20-month-old data points. Data for other timepoints from 1 donor each. Data and graphs from LungMAP (286).

Furthermore, in adult human lungs affected and unaffected by pulmonary fibrosis mesenchymal cells continued to be the only cell types with significant *PDGFRB* expression (Figure 5-3A-C). Pericytes, fibroblasts, myofibroblasts, and smooth muscle cells had the highest *PDGFRB* expression levels (Figure 5-3D). These data confirm that HLFs are ideal for use for *in vitro* experiments that investigate the functions of $G_{\alpha q/11}$ and $G_{\alpha 12/13}$ signalling in *PDGFR*-expressing cells in development and disease.

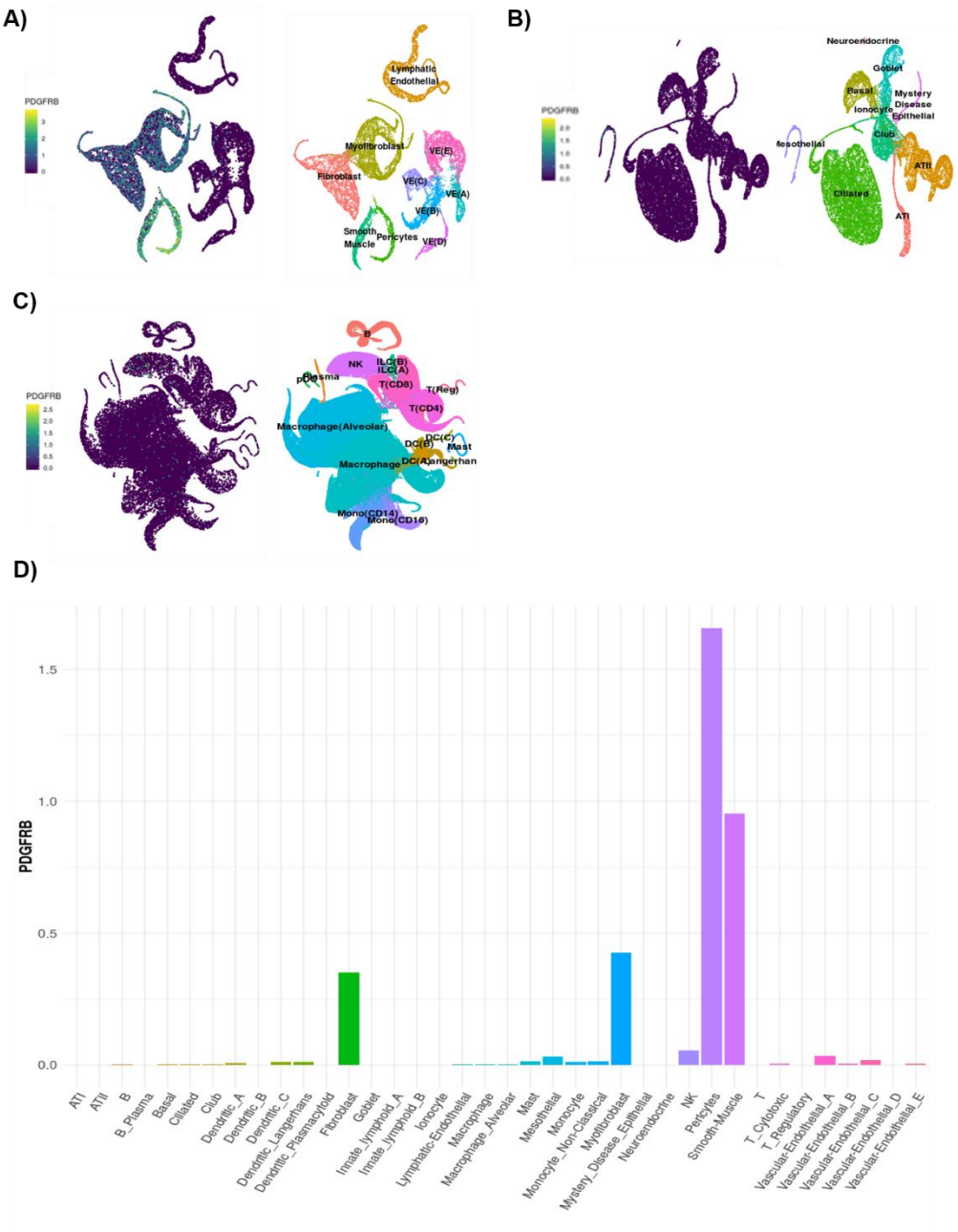

Figure 5-3: *PDGFRB* expression in different cell types in the adult lung

A-C) Uniform Manifold Approximation and Projection (UMAP) images showing *PDGFRB* expression in A) stromal cells, B) immune cells, and C) epithelial cells. Gene expression on left side and key of cell types on the right of each image. Yellow colour indicates higher gene expression, indigo indicates low gene expression. 312,928 cells from 32 IPF, 18 COPD, and 28 control donor lungs. Each dot represents a

single cell.
D) Single cell RNASeq data of *PDGFRB* expression in adult lung cells. Single cell RNASeq data and graphs from IPF Cell Atlas (287, 288).

VE = vascular endothelial cell; VE(A) = venous; VE(B) = capillary A; VE(C)= arterial; VE(D) = Capillary B; VE(E) = peribronchial; DC=dendritic cell; mono= monocyte; ILC = innate lymphatic cell; AT1 = alveolar type 1 epithelial cell; ATII = alveolar type II epithelial cell.

5.4.2 *Gnaq*$^{-/-}$;*Gna11*$^{-/-}$ and *Gna12*$^{-/-}$;*Gna13*$^{-/-}$ MEFs are appropriate for models of mesenchymal $G_{\alpha q/11}$ and $G_{\alpha 12/13}$ signalling *in vitro*.

To confirm the suitability of *Gnaq*$^{-/-}$;*Gna11*$^{-/-}$ and *Gna12*$^{-/-}$;*Gna13*$^{-/-}$ MEFs for the mechanistic experiments that were used in this chapter, the $G_{\alpha q/11}$ and $G_{\alpha 12/13}$ expression status of *Gnaq*$^{-/-}$;*Gna11*$^{-/-}$ and *Gna12*$^{-/-}$;*Gna13*$^{-/-}$ MEFs was validated. *Gnaq*$^{-/-}$; *Gna11*$^{-/-}$ MEFs were confirmed to have significantly reduced *Gnaq* and *Gna11* mRNA expression (Figure 5-4A,B) and complete $G_{\alpha q}$ and $G_{\alpha 11}$ protein knockout (Figure 5-4C,D). *Gna12*$^{-/-}$;*Gna13*$^{-/-}$ MEFs did not have reduced $G_{\alpha q}$ and $G_{\alpha 11}$ protein expression compared with WT MEFs (Figure 5-4C-D).

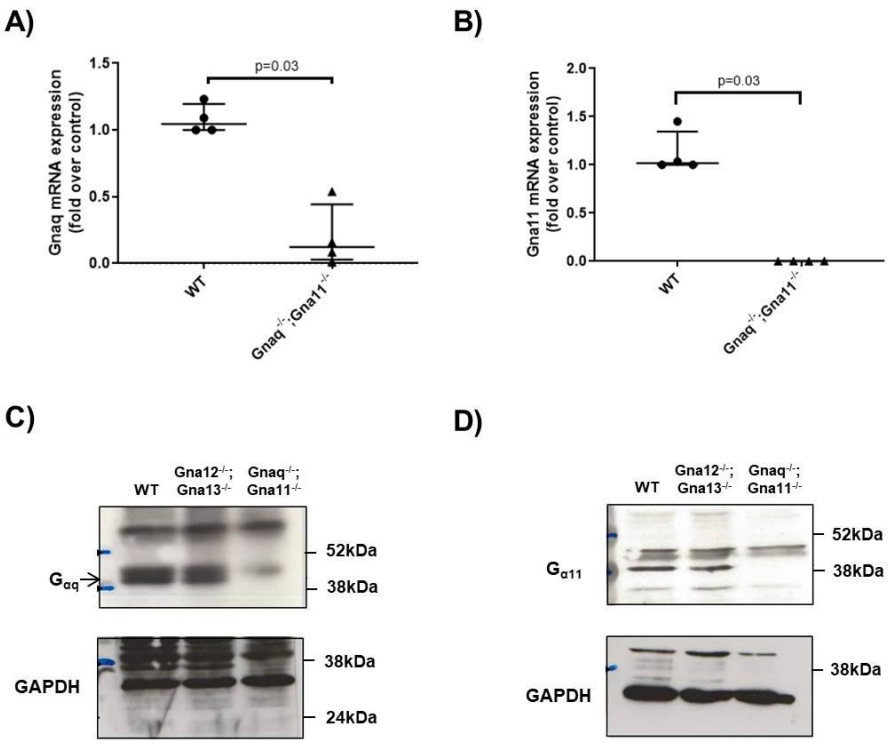

Figure 5-4: $G_{\alpha q/11}$ knockdown is confirmed in *Gnaq*$^{-/-}$;*Gna11*$^{-/-}$ MEFs

A-B) *Gnaq* (A) and *Gna11* (B) mRNA expression as assessed by qPCR. Data shown as median ± interquartile range of 4 independent experiments. Statistical analysis performed using a two-tailed Mann Whitney Test.

C-D) $G_{\alpha q}$ and $G_{\alpha 11}$ protein expression in wild-type (WT) Gna12$^{-/-}$;Gna13$^{-/-}$, and Gnaq$^{-/-}$;Gna11$^{-/-}$ MEFs. Western blots are representative of three independent experiments.

Similarly, *Gna12* and *Gna13* mRNA expression were significantly reduced in *Gna12*$^{-/-}$; *Gna13*$^{-/-}$ MEFs compared with WT MEFs (Figure 5-5A,B), and complete $G_{\alpha 12}$ and $G_{\alpha 13}$ protein knockdown was confirmed in *Gna12*$^{-/-}$; *Gna13*$^{-/-}$ MEFs (Figure 5-5C,D). *Gnaq*$^{-/-}$;*Gna11*$^{-/-}$ MEFs expressed equivalent levels of the $G_{\alpha 12}$ and $G_{\alpha 13}$ proteins to WT MEFs (Figure 5-5C-D).

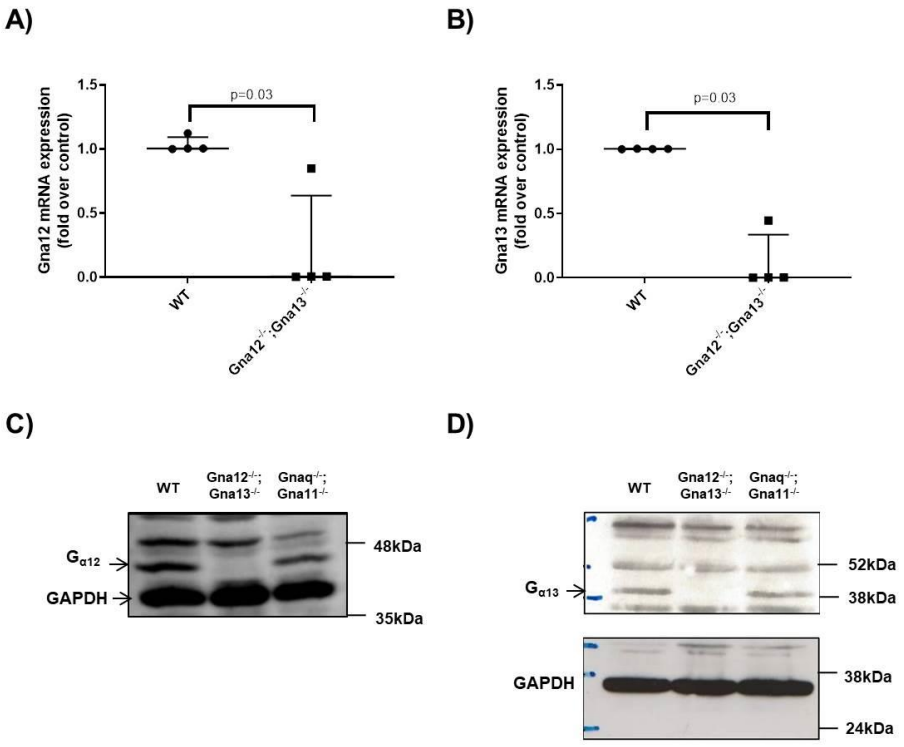

Figure 5-5: $G_{\alpha 12/13}$ knockdown is confirmed in *Gna12$^{-/-}$;Gna13$^{-/-}$* MEFs

A-B) *Gna12* (A) and *Gna13* (B) mRNA expression as assessed by qPCR. Data shown as median ± interquartile range of 4 independent experiments. Statistical analysis performed using a two-tailed Mann Whitney Test.

C-D) $G_{\alpha 12}$ and $G_{\alpha 13}$ protein expression in wild-type (WT) *Gna12$^{-/-}$;Gna13$^{-/-}$*, and *Gnaq$^{-/-}$;Gna11$^{-/-}$* MEFs. Western blots are representative of three independent experiments.

These data confirm that the *Gnaq$^{-/-}$;Gna11$^{-/-}$* and *Gna12$^{-/-}$;Gna13$^{-/-}$* MEFs were appropriate tools to investigate the role of mesenchymal $G_{\alpha q/11}$ and $G_{\alpha 12/13}$ in TGFβ signalling and myofibroblast function.

5.4.3 LPA receptors are expressed by mesenchymal cells in developing and adult lungs

To confirm whether *in vitro* studies based on LPA stimulations were an appropriate model to assess the role of mesenchymal cell G protein signalling in development and disease, the LungMAP and IPF Cell Atlas repositories were searched for LPA receptor gene expression in developing mouse and adult human lungs, respectively.

In the developing mouse lung, expression of all 6 mammalian LPA receptor genes was detected in mesenchymal cells, and *Lpa1, Lpa4, Lpa5,* and *Lpa6* were all elevated relative to earlier timepoints at P07 (Figure 5-6A-F), a key time point in alveologenesis. As the overall expression of *Lpa1* was the highest of all of the LPA receptor genes (Figure 5-6), LPA1 may be the most relevant of the LPA receptors in alveolarisation. These data confirm that murine mesenchymal cells can respond to LPA stimulation in a manner relevant to alveolarisation, and that MEFs are appropriate for use in LPA-induced TGFβ signalling experiments.

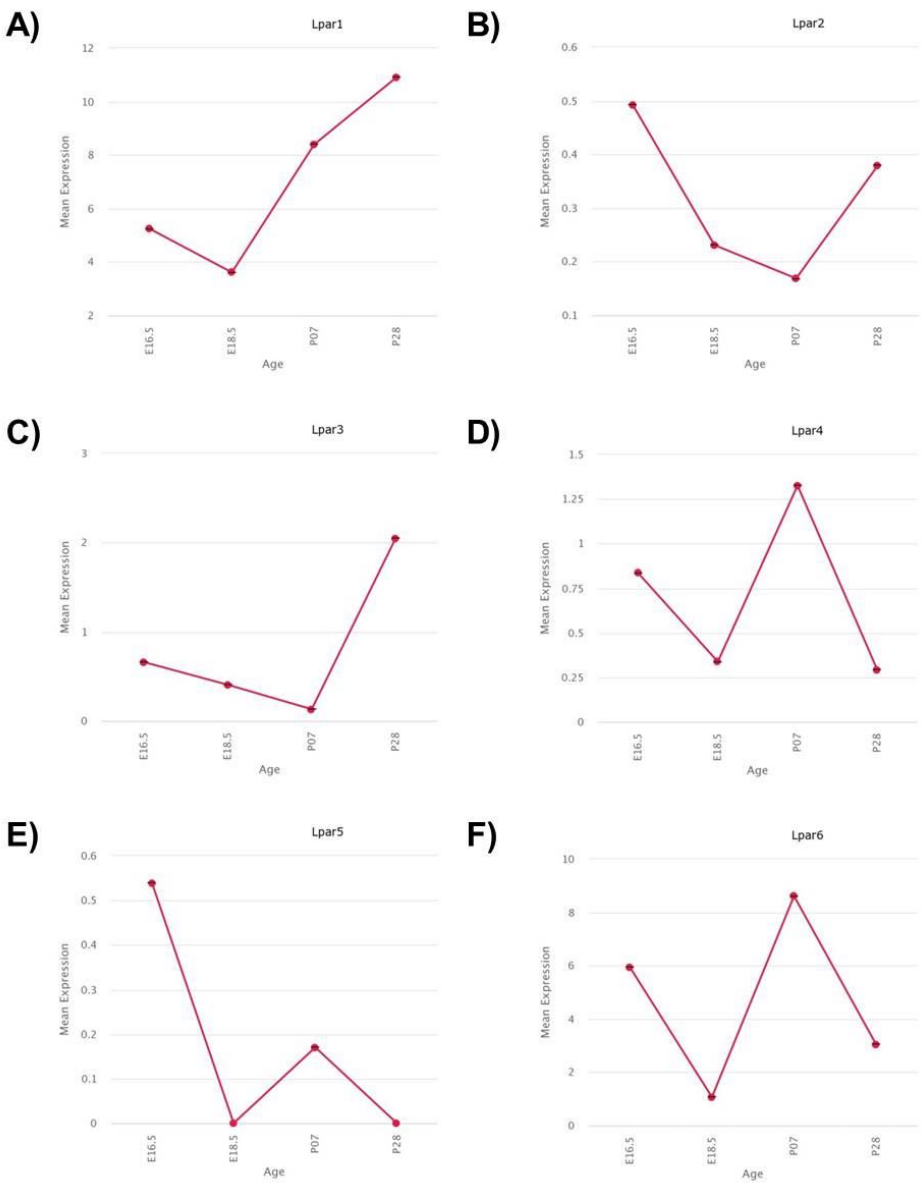

Figure 5-6: The expression of the LPA receptor genes in mouse lung mesenchymal cells during development

LPA receptor gene expression in mouse lung mesenchymal cells at embryonic days 16 and 18 (E16, E18), and postnatal days 7 and 28 (P07, P28).

A) *Lpa1*, B) *Lpa2*, C) *Lpa3,* D) *Lpa4*, E) *Lpa5*, F) *Lpa6*

Data generated from RNA Seq analysis of sorted cells. Data shown is mean gene expression value from 16-24 C57BL6 mice per age group. Data and graph from LungMAP (286).

To confirm the relevance of an LPA-induced TGFβ signalling model to adult mesenchymal cell activity and fibrogenesis, the IPF Cell Atlas data repository was searched for LPA receptor gene expression in human lung. In a similar pattern to that seen in murine cells, *LPA1* gene expression was the highest of all of the LPA receptors in fibroblasts, myofibroblasts, and pericytes in adult human lung (Figure 5-7A). Furthermore, *LPA1* was expressed more frequently in IPF compared with non-IPF myofibroblasts and pericytes (Figure 5-7B), confirming the relevance of this receptor to pulmonary fibrosis.

Unlike the genes for LPA1-5, *LPA6* expression was found in endothelial cells (Figure 5-7A). However, endothelial cells did not have high *Pdgfrb* gene expression (Figure 5-3), and thus were unlikely to be relevant to the *Pdgfrb-Cre* mice being modelled here.

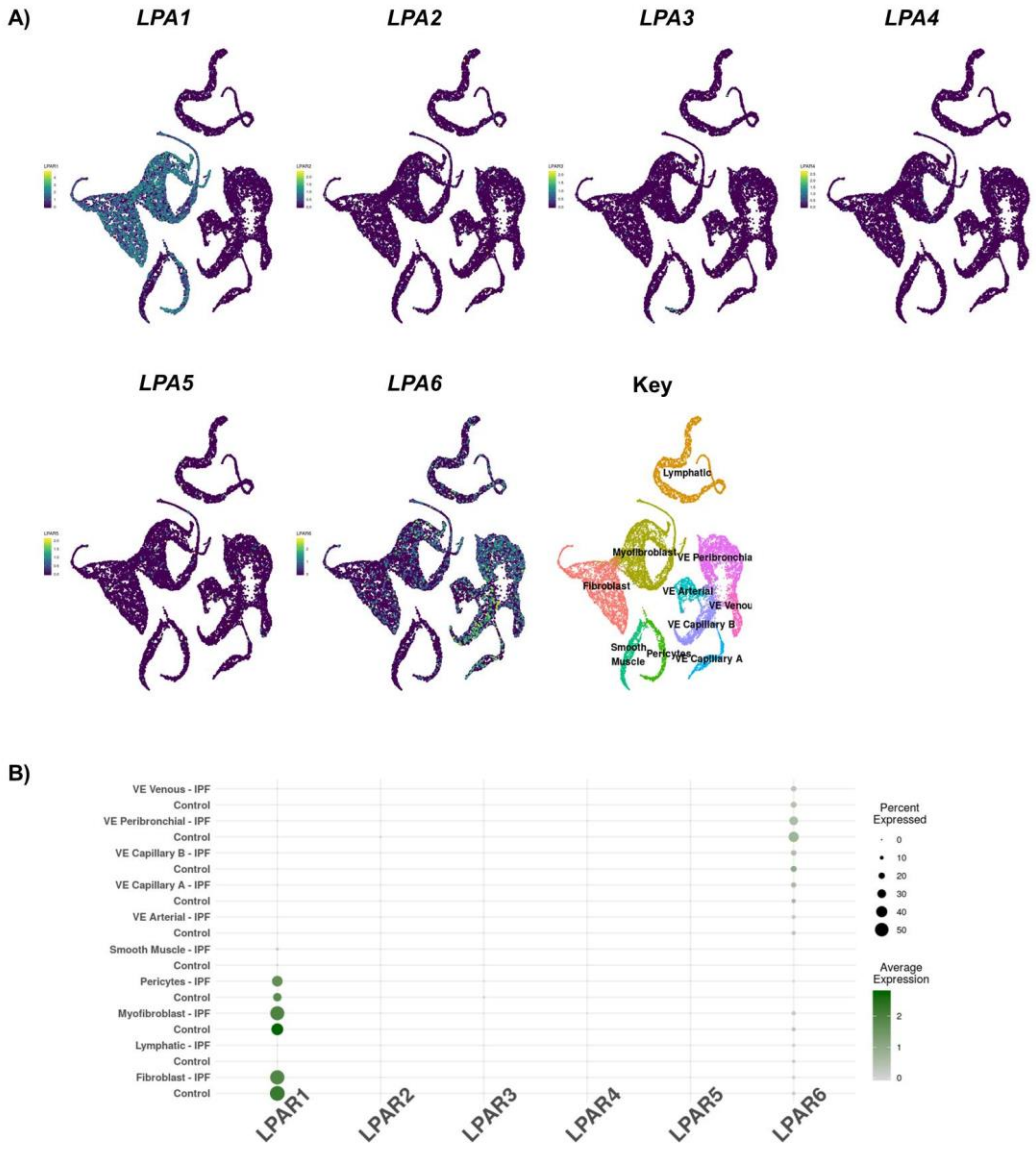

Figure 5-7: LPA receptor 1 has the highest expression of the LPA receptors in mesenchymal cells

A) Uniform Manifold Approximation and Projection (UMAP) images showing expression of LPA receptor genes (*LPA1, LPA2, LPA3, LPA4, LPA5*, and *LPA6*) in mesenchymal cells of the adult human lung. Each dot represents a single cell. Yellow indicates the highest gene expression levels.

B) LPA receptor gene expression in mesenchymal cells from donors with and without IPF. Dot size indicates the percentage of cells

expressing the gene. Darker green colour indicates higher gene expression.

Single cell RNASeq data and graphs from IPF Cell Atlas (287, 288). VE = vascular endothelial cell; VE(A) = venous; VE(B) = capillary A; VE(C)= arterial; VE(D) = Capillary B; VE(E) = peribronchial.

Finally, to confirm that the most relevant LPA receptor to lung development and pulmonary fibrosis, LPA1, couples to G protein α subunits relevant to these studies, the GPCRdb database was searched for GPCR-G protein coupling data. LPA receptors 1,2,4, and 5 all couple to both $G_{\alpha q/11}$ and $G_{\alpha 12/13}$ (Figure 5-8). LPA3 couples to $G_{\alpha q/11}$ but not $G_{\alpha 12/13}$, and LPA6 couples to $G_{\alpha 12/13}$ but not $G_{\alpha q/11}$ (Figure 5-8B).

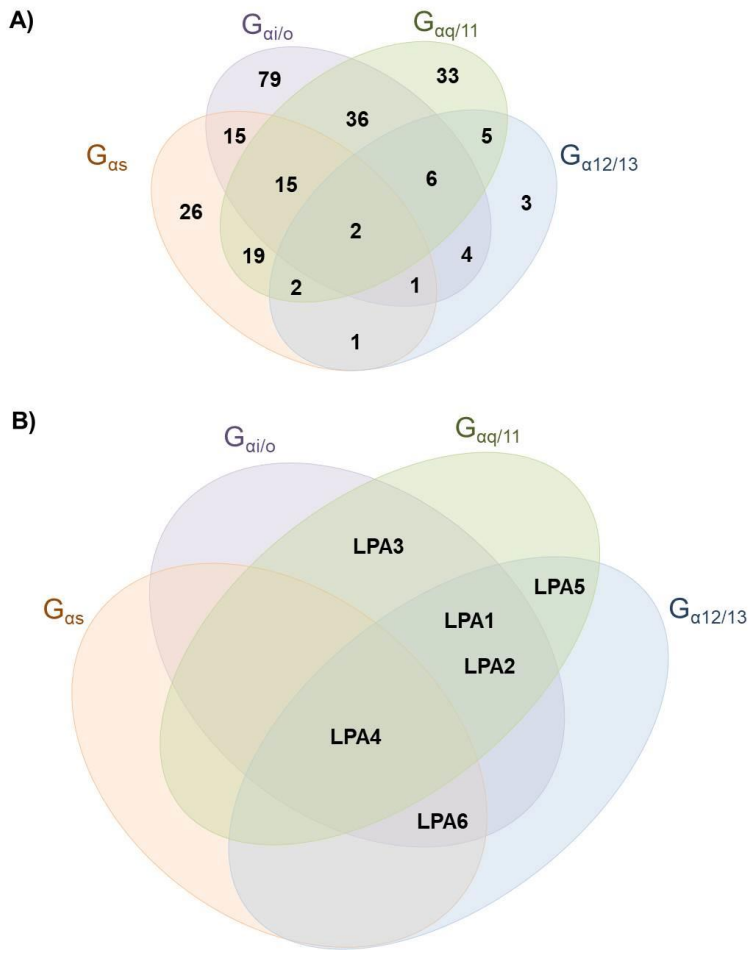

Figure 5-8: Mammalian LPA receptors couple to $G_{\alpha q/11}$ and $G_{\alpha 12/13}$
A) A Venn diagram of GPCR-G protein α subunit family coupling data. Numbers are the number of mammalian G proteins that couple to the G protein α subunit families shown. Figure adapted from GPCRdb (289, 290)
B) GPCR-G protein α subunit family coupling data for the mammalian LPA receptors. Data from GPCRdb (289, 290).

Overall, these data indicate that an *in vitro* LPA-induced TGFβ signalling model in MEFs and HLFs would be relevant to both lung development and the pathogenesis of pulmonary fibrosis. As LPA1 couples to both $G_{\alpha q/11}$ and $G_{\alpha 12/13}$, the LPA-induced TGFβ signalling model was an

appropriate model to assess the role of mesenchymal $G_{\alpha q/11}$ and $G_{\alpha 12/13}$ in processes relevant to alveolarisation and fibrogenesis.

5.4.4 $G_{\alpha q/11}$ and $G_{\alpha 12/13}$ mediate LPA-induced TGFβ signalling

To assess the role of $G_{\alpha q/11}$ and $G_{\alpha 12/13}$ in LPA-induced TGFβ signalling, WT, *Gna12*$^{-/-}$;*Gna13*$^{-/-}$, and *Gnaq*$^{-/-}$;*Gna11*$^{-/-}$ MEFs were stimulated with 50μM LPA for four hours, and TGFβ signalling assessed by measuring Smad2 phosphorylation (pSmad2) on western blots. The *Gnaq*$^{-/-}$;*Gna11*$^{-/-}$ MEFs failed to significantly increase Smad2 phosphorylation in response to LPA (pSmad2 relative to Smad2 densitometry values of 0.0AU in unstimulated *Gnaq*$^{-/-}$;*Gna11*$^{-/-}$ MEFs, compared with 0.56 in stimulated cells, p=0.2; Figure 5-9A,B) . Additionally, *Gna12*$^{-/-}$;*Gna13*$^{-/-}$ MEFs also had an abrogated LPA-induced TGFβ signalling response (pSmad2 relative to Smad2 densitometry values of 1.0AU and 1.2AU in unstimulated and stimulated *Gna12*$^{-/-}$;*Gna13*$^{-/-}$ MEFs, respectively. p=0.99; Figure 5-9A,B). Conversely, WT MEFs demonstrated significantly increased pSmad2 expression after LPA stimulation (pSmad2 relative to Smad2 densitometry value of 0.46AU in unstimulated cells and 3.8AU in LPA-stimulated cells, p=0.03; Figure 5-9A,B). These data suggest that $G_{\alpha q/11}$ and $G_{\alpha 12/13}$ are both essential components of the LPA-induced TGFβ signalling pathway in MEFs.

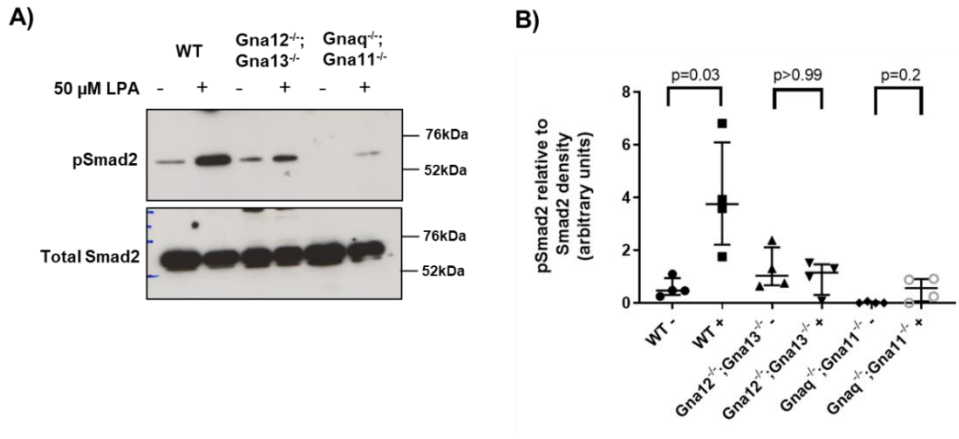

Figure 5-9: Knockout of $G_{\alpha q/11}$ or $G_{\alpha 12/13}$ reduces LPA-induced TGFβ signalling in MEFs

A) Representative western blot showing pSmad2 expression in wild-type (WT), *Gnaq*$^{-/-}$*;Gna11*$^{-/-}$, and *Gna12*$^{-/-}$*;Gna13*$^{-/-}$ MEFs stimulated with 50µM LPA for 4 hours.

B) Relative expression of pSmad2 to Smad2 from densitometry of western blots. Data shown as median ± interquartile range from 4 independent experiments. Statistical analysis performed using two-tailed Mann Whitney Tests.

- = 0µM LPA; + = 50µM LPA

To assess whether $G_{\alpha q/11}$ and $G_{\alpha 12/13}$ are also important in LPA-induced TGFβ signalling in human mesenchymal cells, siRNA was used to induce *GNAQ* and *GNA11*, or *GNA12* and *GNA13*, knockdown in HLFs. With *GNAQ* and *GNA11* knockdown, LPA-induced Smad2 phosphorylation was significantly reduced compared with cells treated with non-targeting siRNA (relative pSmad2 to Smad2 densitometry value of 3.8AU with control siRNA compared with 0.3AU with *GNAQ* and *GNA11* siRNA; Figure 5-10A,B). Similarly, siRNA-induced *GNA12* and *GNA13* knockdown reduced LPA-induced Smad2 phosphorylation from a relative pSmad2 to Smad2 densitometry value of 3.1AU with control

siRNA to 1.6AU, although this was not the complete knockdown seen with *GNAQ* and *GNA11* siRNA (Figure 5-11A,B).

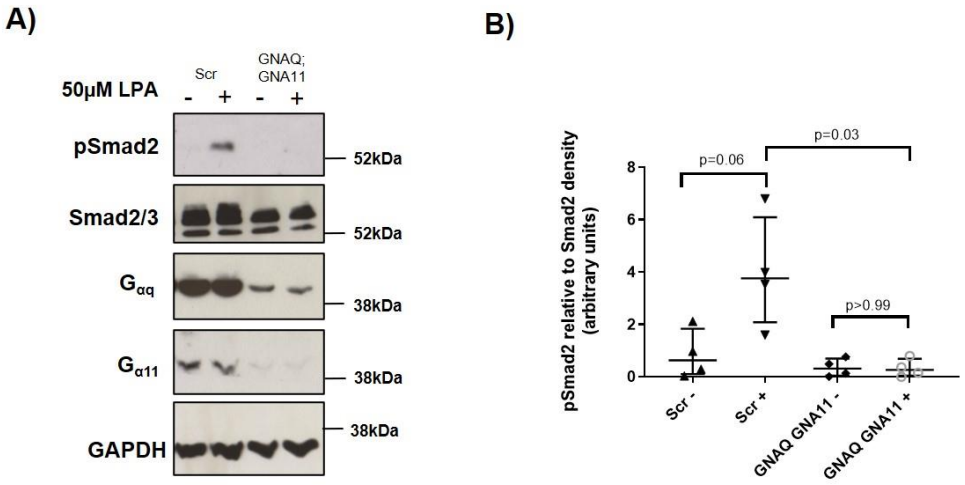

Figure 5-10: $G_{\alpha q/11}$ knockdown reduces LPA-induced TGFβ signalling in HLFs

A) Representative pSmad2 and Smad2 western blots from human lung fibroblasts treated with non-targeting (Scr) or *GNAQ* and *GNA11* siRNA and stimulated with 50μM LPA for 4 hours. SiRNA-induced *GNAQ* and *GNA11* knockdown was confirmed by western blot.

B) Relative expression of pSmad2 to Smad2 from densitometry of western blots. Data shown as median ± interquartile range, 4 independent experiments on cells from different donors. Statistical analyses performed using two-tailed Mann Whitney Tests.

- = 0μM LPA; + = 50μM LPA

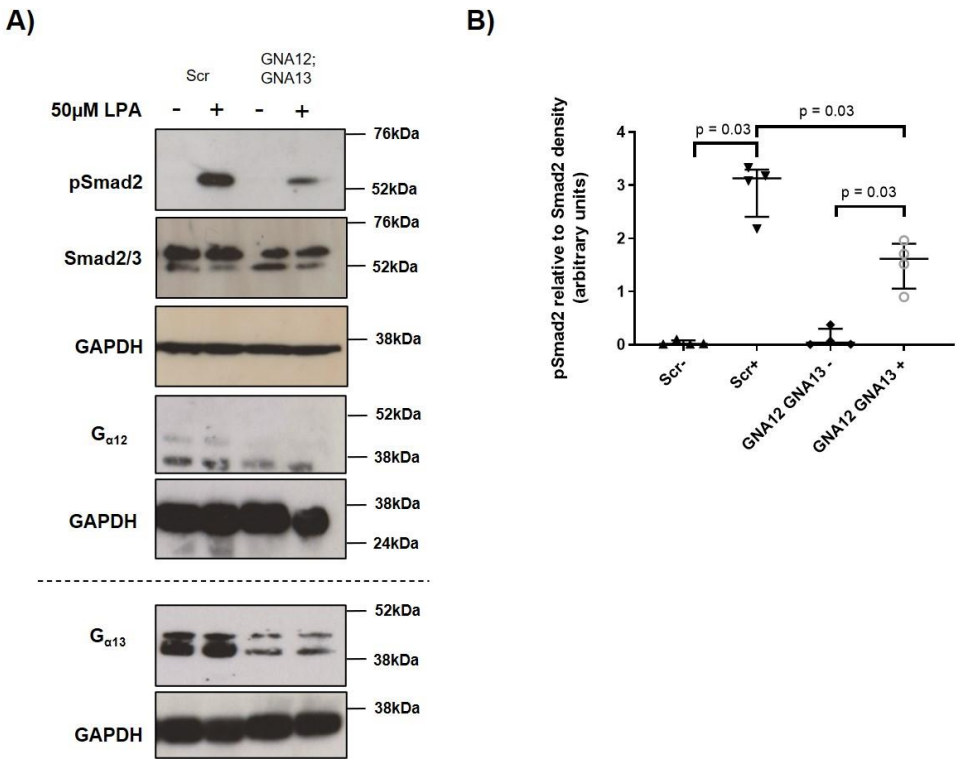

Figure 5-11: $G_{\alpha 12/13}$ knockdown reduces LPA-induced TGFβ signalling in HLFs

A) Representative pSmad2 and Smad2 western blots from HLFs treated with non-targeting (Scr) or *GNA12* and *GNA13* siRNA and stimulated with 50μM LPA for 4 hours. Dotted line indicates that a separate western blot was performed on the same samples to assess $G_{\alpha 12}$ and $G_{\alpha 13}$ protein expression.

B) Relative expression of pSmad2 to Smad2 from densitometry of western blots. Data shown as median ± interquartile range from 4 independent experiments on cells from different donors. Statistical analysis performed using two-tailed Mann Whitney tests.

- = 0μM LPA; + = 50μM LPA

These findings demonstrate that $G_{\alpha q/11}$ and $G_{\alpha 12/13}$ both act as key components of the LPA-induced TGFβ signalling pathway in mouse and human mesenchymal cells.

5.4.5 ROCK-dependent and ROCK-independent mechanisms are involved in LPA-induced TGFβ signalling

Upon GPCR activation, both $G_{\alpha q/11}$ and $G_{\alpha 12/13}$ activate signalling via the Rho-ROCK cascade. Therefore, the role of ROCK in G protein-mediated TGFβ signalling in mesenchymal cells was assessed using the ROCK1/2 inhibitor Y27632 in the LPA-induced TGFβ activation model.

ROCK inhibition reduced both baseline Smad2 phosphorylation, and partially inhibited LPA-induced Smad2 phosphorylation in WT MEFs, although this did not reach statistical significance (relative pSmad2 to Smad2 densitometry value reduced from 0.68AU to 0.46AU with ROCK inhibition at baseline, p=0.1, and 2.4AU to 1.5AU with LPA stimulation, p=0.4; Figure 5-12A-C). A similar pattern of reduced Smad2 phosphorylation was seen in *Gna12*$^{-/-}$*;Gna13*$^{-/-}$ and *Gnaq*$^{-/-}$*;Gna11*$^{-/-}$ MEFs with ROCK inhibition (Figure 5-12D,E), but the differences between LPA simulated and unstimulated cells were less clear due to the blunted LPA-induced TGFβ signalling response in these cells.

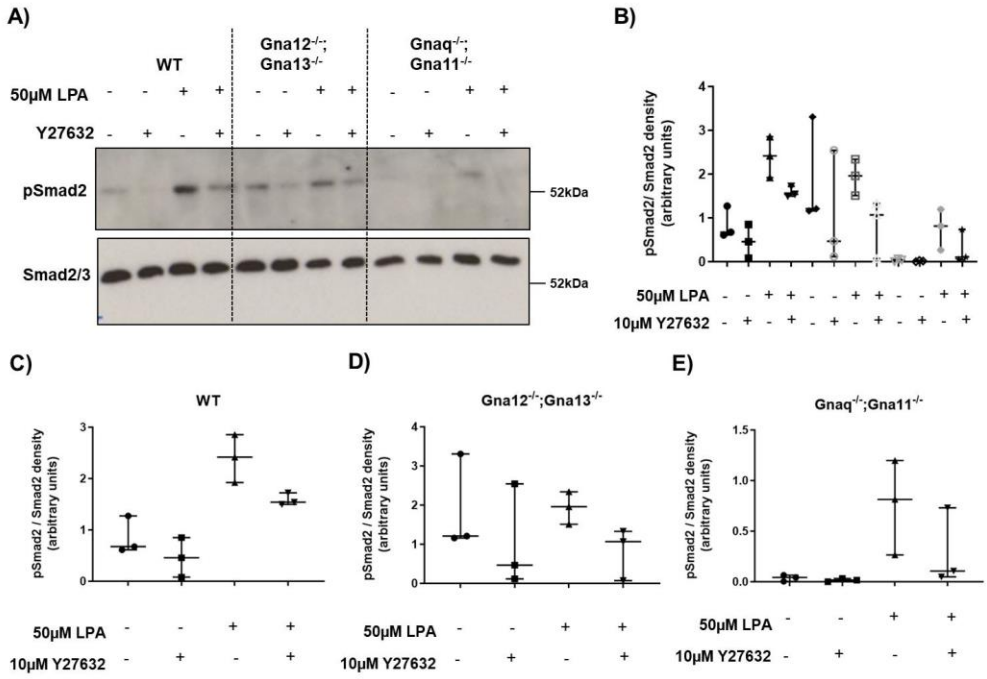

Figure 5-12: ROCK inhibition partially reduces LPA-induced TGFβ signalling in MEFs

A) Representative pSmad2 and Smad2 western blot from wild-type (WT), *Gnaq*$^{-/-}$*;Gna11*$^{-/-}$ and *Gna12*$^{-/-}$*;Gna13*$^{-/-}$ MEFs stimulated with 50μM LPA for 4 hours with and without the ROCK inhibitor Y27632 (10μM).

B-D) Relative pSmad2 to Smad2 densitometry in all cell types (B), WT (C) , *Gna12*$^{-/-}$*;Gna13*$^{-/-}$ (D), and *Gnaq*$^{-/-}$*;Gna11*$^{-/-}$ (E) MEFs. Data shown as median ± interquartile range, n=3.

These data suggest that LPA-induced TGFβ signalling occurs at least in part via the Rho ROCK cascade. However, the incomplete inhibition of LPA-induced TGFβ signalling with ROCK inhibition suggests that other LPA-induced signalling pathways may also be present.

5.4.6 $G_{\alpha q/11}$ signalling influences the myofibroblast phenotype in response to matrix stiffness, but this is not due to altered LPA-induced TGFβ signalling

As detection of surrounding matrix stiffness is a key characteristic of myofibroblasts, and this mechanosensitivity is a key aspect of both fibrogenesis and development, further experiments were performed to assess the role of $G_{\alpha q/11}$ and $G_{\alpha 12/13}$ in detecting matrix stiffness. The expression of αSMA was used as a measure of the myofibroblast phenotype, as αSMA is a myofibroblast marker that is known to be expressed at increased levels by fibroblasts grown in stiff tissue culture environments (53).

When MEFs were transferred from tissue culture plastic (TCP; ~2GPa) to soft tissue culture substrates designed to mimic normal (5kPa), earlier fibrotic (36kPa), and late fibrotic (100kPa) lung, only *Gnaq*$^{-/-}$;*Gna11*$^{-/-}$ MEFs exhibited significantly reduced αSMA expression after 6 days of culture on softer substrates (αSMA to GAPDH relative densitometry values of 0.2AU and 0.4AU on the 100kPa and 36kPa substrates, respectively, compared with 1.0AU on TCP, $p<0.05$; Figure 5-13A-D). While *Gnaq*$^{-/-}$;*Gna11*$^{-/-}$ MEFs transferred to the 5kPa soft substrates exhibited reduced αSMA expression (median αSMA to GAPDH relative densitometry value of 0.4AU compared with 1.0 on TCP), this did not reach statistical significance ($p=0.2$, Figure 5-13D). Conversely, WT and *Gna12*$^{-/-}$;*Gna13*$^{-/-}$ MEFs did not show any trend towards reduced αSMA expression on transfer from TCP to soft culture substrates (Figure

5-13B,C). Overall, these data imply that $G_{\alpha q/11}$, but not $G_{\alpha 12/13}$, is required to maintain the myofibroblast phenotype in response to the mechanical environment, and that further loss of mechanical stimulus by transfer to a softer environment tips cells towards a less myofibroblast-like phenotype. Furthermore, $G_{\alpha q/11}$ may also drive myofibroblast mechanical memory.

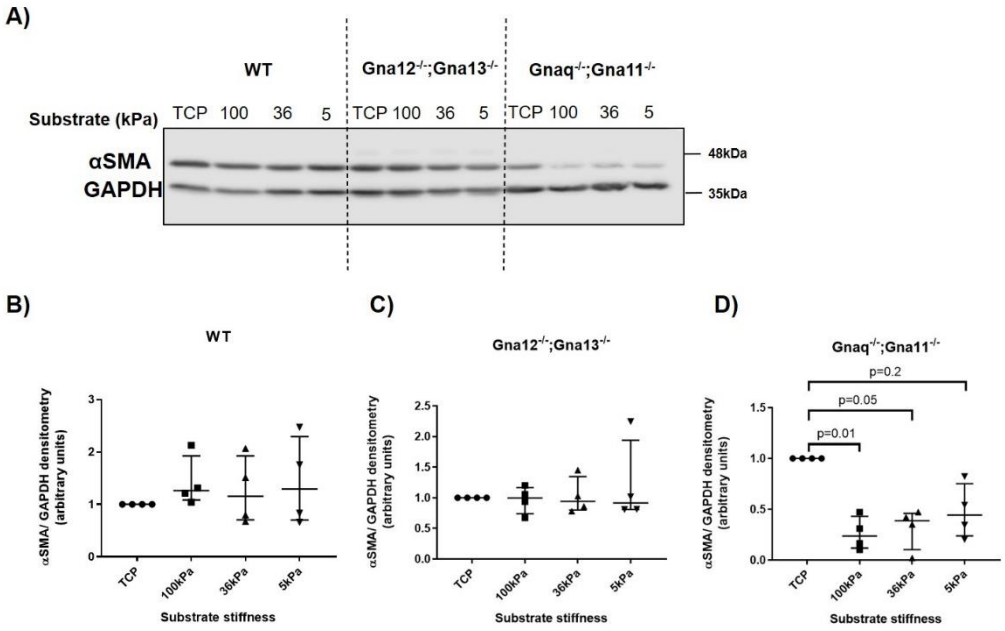

Figure 5-13: $G_{\alpha q/11}$ is important for detecting matrix stiffness
A) Representative αSMA and GAPDH western blot of wild-type (WT), *Gna12*$^{-/-}$*;Gna13*$^{-/-}$, and *Gnaq*$^{-/-}$*;Gna11*$^{-/-}$ MEFs grown on tissue culture plastic (TCP) or silicone gels of 100kPa, 36kPa, or 5kPa.
B) αSMA relative to GAPDH densitometry for MEFs grown on tissue culture plastic or soft silicone substrates. Data shown as median ± interquartile range, n=4. Statistical analysis performed using a Kruskal Wallis test with Dunn's multiple comparisons test.

To assess whether the reduction of αSMA expression in *Gnaq*$^{-/-}$*;Gna11*$^{-/-}$ MEFs in softer environments was due to further reduction in the ability

of these cells to activate TGFβ, LPA-induced TGFβ signalling experiments were performed in WT, *Gna12*$^{-/-}$*;Gna13*$^{-/-}$, and *Gnaq*$^{-/-}$*;Gna11*$^{-/-}$ MEFs on soft tissue culture substrates.

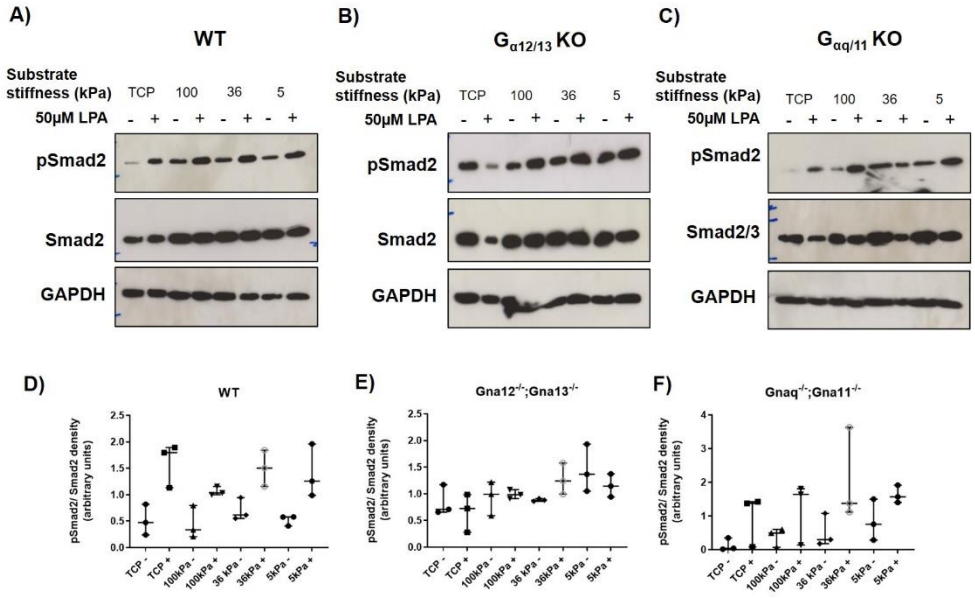

Figure 5-14: LPA-induced TGFβ signalling in MEFs is not affected by the mechanical properties of the surroundings

A-C) Representative western blots of wild-type (WT, A), *Gna12*$^{-/-}$*;Gna13*$^{-/-}$, and *Gnaq*$^{-/-}$*;Gna11*$^{-/-}$ MEFs grown on tissue culture plastic (TCP) or silicone gels of 100kPa, 36kPa, or 5kPa stiffness, and stimulated with 50μM LPA for 4 hours.

D-E) Relative pSmad2 to Smad2 densitometry of western blots. Data shown as median ± interquartile range, n=3.

Short-term (36-48 hour) culture of MEFs on soft tissue culture substrates did not reduce LPA-induced Smad2 phosphorylation in WT, *Gna12*$^{-/-}$*;Gna13*$^{-/-}$, or *Gnaq*$^{-/-}$*;Gna11*$^{-/-}$ MEFs (Figure 5-14). These data suggest that a mechanism unrelated to TGFβ signalling causes the soft substrate-induced reduction of αSMA expression in cells lacking $G_{\alpha q/11}$.

5.5 Discussion

The work presented here has identified *in vitro* systems to model the role of $G_{\alpha q/11}$ and $G_{\alpha 12/13}$ in myofibroblast functions in mesenchymal cells that could not be fully explored in *Pdgfrb-Cre*$^{+/-}$*:Gnaq*$^{fl/fl}$*;Gna11*$^{-/-}$ and *Pdgfrb-Cre*$^{+/-}$*;Gna12*$^{-/-}$*;Gna13*$^{fl/fl}$ mice (Chapter 4). Specifically, this is the first work to dissect the mechanisms of LPA-induced TGFβ signalling in mesenchymal cells, and it is also the first to find a role for G proteins in detecting matrix stiffness. These findings have implications for the understanding of both normal alveologenesis and the pathogenesis of pulmonary fibrosis.

Online data repositories were initially used to establish which cells would be appropriate for use in the *in vitro* models. Data from the LungMAP and IPF Cell Atlas data repositories confirmed that both murine and human lung fibroblasts express *PDGFRB*, and so would have had Cre-induced *Gnaq* or *Gna13* knockout in the *in vivo* model described in Chapter 4. Although fibroblasts and myofibroblasts are different to pericytes, which were the primary *Pdgfrb*-expressing targets of the *in vivo* models, they differentiate from pericytes and perform fibrosis-driving functions (291, 292). MEFs and HLFs were therefore chosen for *in vitro* studies of the role of mesenchymal $G_{\alpha q/11}$ and $G_{\alpha 12/13}$ in profibrotic signalling.

LPA is found at elevated levels in the lungs of patients with IPF (127), as well as in other fibrotic tissues (293, 294), and drives many of the exaggerated repair processes characteristic of fibrosis. LPA influences the activities of several different cell types, such as by inducing vascular

leak, fibroblast recruitment, epithelial cell apoptosis, and fibroblast survival (127, 129). LPA is also known to induce TGFβ activation in epithelial cells via $G_{\alpha q/11}$ and RhoA/ ROCK signalling (74), however the effect of LPA on TGFβ signalling in mesenchymal cells, and the signalling pathways involved, have not been reported previously.

The LPA receptors LPA1, LPA2, and LPA3 are thought to be the predominant LPA receptors in pulmonary fibrosis (74, 127, 129, 140, 295), with both *Lpa1*$^{-/-}$ and *Lpa2*$^{-/-}$ mice being protected against pulmonary fibrosis (74, 127, 129, 140, 295). LPA1 is also essential for normal alveolarisation (142), indicating an overlap between LPA-induced developmental and fibrogenic signalling. However, the LPA receptor that drives these pathways in mesenchymal cells specifically is less clear. Both murine and human lung mesenchymal cells express mRNA for all 6 LPA receptors (286, 287). Of all of the LPA receptor genes, *LPA1* expression was the highest in both human and mouse lung mesenchymal cells. As LPA1 couples to both $G_{\alpha q/11}$ and $G_{\alpha 12/13}$ (289), LPA stimulations of MEFs and HLFs was a model relevant to fibrogenesis, alveolarisation, and the *in vivo* models described in Chapter 4.

LPA consistently increased TGFβ signalling, as indicated by Smad2 phosphorylation, in both MEFs and HLFs. However, either $G_{\alpha q/11}$ or $G_{\alpha 12/13}$ genetic inhibition significantly suppressed this response, indicating that both G protein families are important for LPA-induced TGFβ activation in mesenchymal cells. The similar findings between

murine and human, and immature and mature, mesenchymal cells demonstrates the generalisability of LPA-induced TGFβ signalling across species and suggests that this pathway may be involved in normal lung development and fibrogenesis.

The results of this study are in keeping with previous work, which found that LPA stimulation of epithelial cells results in TGFβ activation via $G_{\alpha q/11}$ in both lung and kidney (74) (296). However, the current study is the first to investigate LPA-induced TGFβ signalling in mesenchymal cells. Furthermore, while $G_{\alpha 12/13}$ signalling is known to drive cardiac fibrosis (216, 297), there was little previous evidence of a role for $G_{\alpha 12/13}$ in pulmonary fibrosis prior to this study. This work demonstrates that $G_{\alpha 12/13}$ signalling is important in LPA-induced TGFβ signalling, and may therefore mediate a key process in pulmonary fibrosis.

The different LPA receptors signal via various combinations of G_{α} subunit families, so it is likely that there is some crossover in the G proteins involved in LPA-induced TGFβ signalling. For example, siRNA-induced $G_{\alpha 12/13}$ knockdown incompletely reduced LPA-induced TGFβ signalling in HLFs, which could reflect partial compensation by $G_{\alpha q/11}$ signalling. However, this contrasts with the complete knockdown of LPA-induced TGFβ signalling observed in $G_{\alpha q/11}$-deficient MEFs. While it was not the aim of this study to investigate the role of specific LPA receptors in mesenchymal LPA-induced TGFβ signalling, future studies may focus on defining LPA receptor-specific responses in lung development and fibrogenesis.

$G_{\alpha q/11}$ and $G_{\alpha 12/13}$ can both activate the Rho/ ROCK cascade, and LPA is known to induce cytoskeletal reorganisation via ROCK activity, resulting in traction-induced liberation of latent TGFβ from the ECM (74, 121, 296). In the current study, ROCK inhibition incompletely abrogated LPA-induced TGFβ signalling in MEFs, implying that other signalling mechanisms, such as PLC-, PI3K-, or Src-related pathways, may also be activated downstream of $G_{\alpha q/11}$ and $G_{\alpha 12/13}$ (111). LPA also induces signalling by a number of other pathways, including MAPK and PKC signalling (298), and can activate a number of transcription factors, e.g. NF-κB, AP-1, C/EBPβ, all of which could modify TGFβ signalling. How $G_{\alpha q/11}$ and $G_{\alpha 12/13}$ interact with these other signalling pathways in TGFβ activation in health and disease should be a topic for future studies.

Previous studies of LPA-induced $G_{\alpha q/11}$ and subsequent ROCK-induced TGFβ signalling both found the αvβ6 integrin to be key to this process (74, 296). However, the αvβ6 integrin is found only in epithelial cells and therefore cannot be involved in the LPA-induced TGFβ signalling in mesenchymal cells described here. The αvβ1, αvβ3, and αvβ5 integrins are all expressed by fibroblasts and are known to be involved in TGFβ activation (9), and the αvβ5 integrin is involved in contraction-related LPA-induced TGFβ signalling in airway smooth muscle cells (137). However, evidence for the integrin involved in LPA-induced TGFβ signalling in fibroblasts or myofibroblasts is currently lacking.

As Rho/ ROCK signalling is a mechanosensitive pathway (119, 120, 299, 300), and responses to matrix stiffness are characteristic of

myofibroblasts, the roles of $G_{\alpha q/11}$ and $G_{\alpha 12/13}$ in matrix stiffness-induced myofibroblast differentiation were investigated. When MEFs were transferred from tissue culture plastic, which has an unphysiologically high elastic modulus of around 2 GPa, to silicone substrates of stiffness relevant to normal lung (5kPa), moderate pulmonary fibrosis (36kPa), or advanced (100kPa) pulmonary fibrosis (162), only MEFs lacking $G_{\alpha q/11}$ reduced αSMA expression. This result indicates that $G_{\alpha q/11}$-deficient MEFs become less myofibroblast-like when transferred to a softer environment, and suggests that $G_{\alpha q/11}$ may be involved in detecting stiffer surroundings.

Alternatively, $G_{\alpha q/11}$ signalling could be involved in inducing the "mechanical memory" of myofibroblasts, where a myofibroblast grown in a stiff environment retains elevated αSMA expression even when transferred to softer environments (53, 301). Conversely, $G_{\alpha 12/13}$-deficient MEFs maintained a steady level of αSMA expression when transferred to softer substrates. While there was no difference in αSMA expression between cells grown on the 5kPa, 36kPa, and 100kPa substrates, overall these data indicate a role for $G_{\alpha q/11}$ in modulating the myofibroblast phenotype in response to the mechanical environment, specific to this G protein family. There are a number of cell surface mechanosensors, including integrins (302, 303), glycoproteins (304), receptors (305), and mechanosensitive ion channels (305), but this is the first study to find a role for G proteins in detecting tissue stiffness.

In pulmonary fibrosis, the lungs become stiff as ECM deposition, crosslinking, and remodelling increases (306). As a result, TGFβ activation increases in these stiffer environments, as greater traction forces are possible if a cell contracts against a more rigid and organised ECM (168, 170). Mechanical properties are also key for directing normal lung development (307), a process to which TGFβ signalling is also essential. A potential mechanism for the reduction in αSMA expression in $G_{\alpha q/11}$-deficient MEFs on transfer to softer culture environments is that MEFs lacking $G_{\alpha q/11}$ activate less TGFβ, leading to reduced myofibroblast differentiation. However, this study found no change in Smad2 phosphorylation, either at baseline or with LPA stimulation, in WT, *Gnaq*$^{-/-}$*;Gna11*$^{-/-}$, or *Gna12*$^{-/-}$*;Gna13*$^{-/-}$ MEFs when transferred to soft tissue culture environments. These data suggest that a mechanism unrelated to TGFβ signalling regulates the loss of αSMA expression when cells lacking $G_{\alpha q/11}$ are grown on soft substrates. While it is impossible to rule out alterations to the production of second messengers that may influence αSMA expression in $G_{\alpha q/11}$-deficient MEFs, the relatively short period of culture of the cells on soft culture substrates in these experiments supports the hypothesis that $G_{\alpha q/11}$ is itself mechanosensitive. Future work should focus on the role of $G_{\alpha q/11}$ in detecting other matrix characteristics that are altered in pulmonary fibrosis, such as the composition and organisation of ECM proteins (306), and in driving stiffness-induced responses to tissue stiffness, such as fibroblast proliferation, migration, and ECM production (162) (158, 308-310).

A number of studies have found that LPA receptor inhibition reduces experimental pulmonary (141, 295, 311, 312) and non-pulmonary fibrosis (313-315) *in vivo*. Furthermore, inhibition of autotaxin, an enzyme involved in LPA production, is being investigated as a potential therapeutic strategy in IPF (316, 317). Unfortunately, development of the LPA1 inhibitor BMS968020 was stopped because of cholecystitis in clinical trial participants, although this drug did reduce forced vital capacity (FVC) decline in IPF (150). Cholecystitis was thought to be an off-target effect unrelated to LPA1 antagonism, therefore alternative ways of inhibiting LPA signalling may still be beneficial in fibrosis. Given that numerous GPCRs are implicated in the pathogenesis of IPF, and that different GPCR-driven processes may predominate in individuals patients with IPF (5), G_{α} subunits may be beneficial targets in IPF.

5.6 Limitations

This study used LPA to assess the roles of $G_{\alpha q/11}$ and $G_{\alpha 12/13}$ in GPCR agonist induced TGFβ signalling. Although this pathway is relevant to fibrosis, other GPCR agonists induce TGFβ signalling in pulmonary fibrosis, and they may do so via different pathways. While non-LPA GPCR agonists may induce similar $G_{\alpha q/11}$- and $G_{\alpha 12/13}$-mediated effects to that observed with LPA, it is possible that other GPCR agonists may induce other signalling pathways to different degrees. Therefore, the results of this study should not be generalised to other GPCR agonists. However, LPA is a GPCR agonist that can activate $G_{\alpha q/11}$ and $G_{\alpha 12/13}$

signalling, and thus the LPA models used in this study were appropriate to meet the aims of this study.

Furthermore, while $G_{\alpha q/11}$ and $G_{\alpha 12/13}$ were the only G protein families investigated in this study, LPA1 is also known to signal via the $G_{\alpha i/o}$ family of G proteins (289), and recent work has implicated LPA1-induced $G_{\alpha i/o}$ signalling in profibrotic pathways (318). Future work should assess the relative contributions and crossover between $G_{\alpha i/o}$, $G_{\alpha 12/13}$, and $G_{\alpha q/11}$ downstream of LPA1 in fibrosis and lung development, however it was beyond the scope of this study to assess the role of $G_{\alpha i/o}$ in LPA-induced TGFβ signalling.

For the matrix stiffness experiments, the cells used had undergone long-term culture on tissue culture plastic. This supraphysiological degree of stiffness is known to alter cellular phenotypes which persist even when cells are transferred back to softer environments (53), therefore it is possible that a role for $G_{\alpha 12/13}$ in detecting matrix stiffness could have been missed by this study. The culture of primary cells directly onto soft culture substrates would have avoided stiffness-related changes in cellular phenotype. However, only $G_{\alpha q/11}$- and $G_{\alpha 12/13}$-deficient MEFs that had been cultured on tissue culture plastic were available for use in this study. The effects of tissue culture plastic on cellular phenotype should be considered when designing future studies investigating responses to tissue stiffness.

5.7 Conclusion

Mesenchymal cell $G_{\alpha q/11}$ and $G_{\alpha 12/13}$ are both mediators of LPA-induced TGFβ signalling, which occurs in a partially ROCK-dependent manner. Myofibroblast differentiation in response to matrix stiffness is driven by $G_{\alpha q/11}$, but not $G_{\alpha 12/13}$ signalling, and this does not relate to reduced ability to activate TGFβ signalling in cells lacking $G_{\alpha q/11}$. These data indicate important but unique roles for $G_{\alpha q/11}$ and $G_{\alpha 12/13}$ in key myofibroblast functions that are important to lung development and fibrogenesis.

6 The Roles of $G_{\alpha q/11}$ and $G_{\alpha 12/13}$ in Fibroblast Contraction

6.1 Introduction

Cellular contraction is essential for wound healing, a process that is exaggerated in pulmonary fibrosis. The data presented in Chapter 5 demonstrated that the GPCR agonist LPA induces TGFβ signalling at least in part via Rho/ROCK signalling. The Rho/ ROCK cascade stimulates reorganisation of the actin cytoskeleton, which is essential for cellular contraction. Prior work has found that LPA stimulation of epithelial and airway smooth muscle cells results in TGFβ signalling, via integrin-mediated traction forces on the latent TGFβ complex (74, 137).

Human lung fibroblasts from patients with IPF are more contractile than non-fibrotic fibroblasts (167, 319, 320). In fibrosis, fibroblasts differentiate into myofibroblasts, a transition characterised by the acquisition of the smooth muscle-like characteristics αSMA expression and increased contractility (321). This contractility is a key phenotypic feature of myofibroblasts (321), which are essential scar-forming cells in pulmonary fibrosis. Myofibroblast contractility is essential for the ECM organisation, increased matrix stiffness, and TGFβ signalling that further drive fibrosis (161, 168, 322-324). However, the mechanisms underlying enhanced fibroblast contractility in IPF are unclear. Furthermore, while LPA has been identified as a key driver in IPF, the role of LPA on human lung fibroblast contraction has not been investigated previously.

Although there is no published research investigating the role of GPCRs in fibroblast contraction, much work has been done on the role of GPCR signalling in smooth muscle cells. Both $G_{\alpha q/11}$ and $G_{\alpha 12/13}$ have been

implicated in vascular and bladder smooth muscle contraction, playing keys roles in several physiological processes (211, 325-328). As LPA is a GPCR agonist that signals via $G_{\alpha q/11}$ and $G_{\alpha 12/13}$, and that can induce smooth muscle cell contraction (137), it is possible that LPA-induced fibroblast contractility is a pathophysiological mechanism in IPF.

6.2 Aims and Hypothesis

The aims of this study were to:

- Assess how lung fibroblast contraction is altered in IPF.
- Understand the role of $G_{\alpha q/11}$ and $G_{\alpha 12/13}$ in LPA-induced lung fibroblast contraction.

The hypothesis underlying this work was:

> *"LPA induces lung fibroblast contraction via $G_{\alpha q/11}$ and $G_{\alpha 12/13}$ signalling, and this is an important disease mechanism in IPF"*

6.3 Methods

6.3.1 Wrinkling assay

6.3.1.1 Principle

This assay depends on the principle that cells will create wrinkles on the surface of a soft deformable polymer that they are adhered to when they contract. Substrate wrinkling can be viewed using light microscopy, and wrinkling can be visualised in response to contractile agonists and time-lapse images obtained by taking a series of images at the same position at several timepoints.

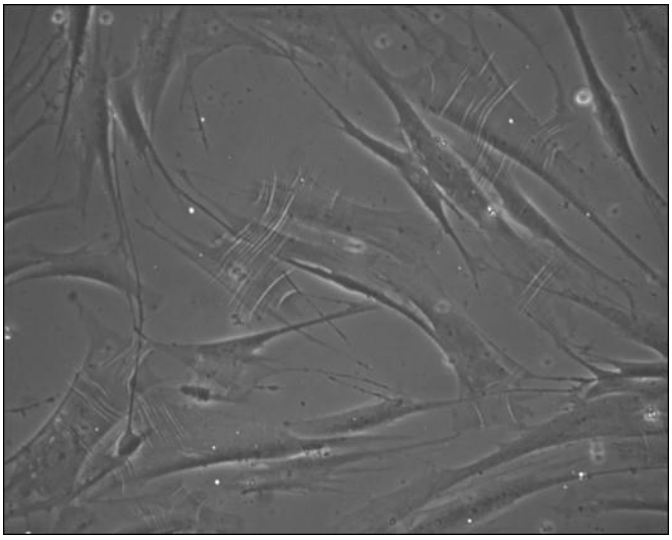

Figure 6-1: The wrinkling assay
A representative image of human lung fibroblasts grown on wrinkling substrates. When cells contract on the deformable silicone substrates, wrinkles are created that can be visualised by light microscopy (bright lines).

6.3.1.2 Method

6.3.1.2.1 Generation of wrinkling substrates

2kPa thin silicone substrates were made using a proprietary method in the laboratory of Dr Boris Hinz (University of Toronto). Briefly, Polymers A and B were mixed at a 2:1 ratio with a polymerisation retardant using a THINKY mixer at 1600rpm for 3 minutes. 125µl of polymer mixture was dispensed onto the centre of 35mm dishes using a syringe pump. Substrates were spin casted at 1500rpm, with an acceleration of 1500rpm/s^2, for 3.2 seconds. The spin casting process was repeated if the polymer mixture had not reached the edges of the dish. Substrates were left to settle on a flat surface overnight, then baked at 60^{o}C for 4 days.

6.3.1.3 Functionalisation and protein coating of wrinkling substrates

To functionalise the hydrophobic silicone substrates so that cells would adhere, substrates were plasma oxygen treated for 2 seconds using a Plasma Etch machine. Surfaces were then coated with 2µg/cm^2 gelatin in PBS overnight at 37ºC. The gelatin solution was aspirated and cells seeded for experiments without a rinsing step.

6.3.1.4 GPCR agonist-induced contraction experiments

HLFs from either non-diseased or IPF donors, and wild-type, *Gna12*$^{-/-}$*;Gna13*$^{-/-}$, and *Gnaq*$^{-/-}$*;Gna11*$^{-/-}$ MEFs were used for contraction experiments. Cells were seeded at a density of 7.5 x 10^4 cells per 35mm dish in full media, and allowed to attach for 6 hours, when the culture media was changed to 0% FCS in DMEM. The wrinkling assay was performed the following day.

6.3.1.5 Image acquisition

Low magnification images were obtained using a 4x objective on a Zeiss Axioplan microscope and Zen 2.5 software. High magnification images were obtained using a 10x objective and 1.6x magnifier on a Zeiss Axiovert 135 inverted phase-contrast microscope and Micromanager version 1.4 software. In both microscope systems, cells were maintained in a live cell imaging chamber at 37ºC and 5% CO_2. The microscope software and a motorised stage were used to program the coordinates of each position to allow images to be taken at the same location at each timepoint. Baseline images were obtained prior to stimulation with 30µM

LPA in 0% FCS DMEM, and every 5 minutes at the same positions following GPCR agonist stimulation for 30 minutes. Control (0µM LPA) wells were treated with an equal volume of 0% FCS DMEM to the volume of LPA added to the 30µM LPA wells.

Five images per well were taken for low magnification images, and 10 images per well were taken for the higher magnification images. Two wells per condition were used per cell line for each experiment. Each experiment was repeated 4 times for experiments on MEFs, and in at least 4 non-diseased and 4 IPF HLF cell lines.

6.3.1.6 *GNA12* and *GNA13* siRNA

Pooled siRNAs for human *GNA12* and GNA13 were used to knock down $G_{\alpha 12/13}$ expression in HLFs. A non-targeting siRNA pool was used as a control.

HLFs were seeded onto gelatin-coated silicone substrates at 7.5 x 10^4 cells per 35mm dish in antibiotic-free full media and allowed to adhere overnight. *GNA12* and *GNA13* siRNAs were applied together to HLFs at a final concentration of 10nM per siRNA. Control siRNA was applied at a final concentration of 25nM, as per the manufacturer's instruction. DharmaFECT 1 transfection reagent was used at a final concentration of 2µl/ml. Both non-targeting siRNA and transfection media only experiments were used as controls. Knockdown of *GNA12* and *GNA13* was confirmed by western blot. Transfection mixtures were removed

from cells after 24 hours. The wrinkling assay was performed at 72 hours after siRNA application.

6.3.2 Wrinkling assay quantification

6.3.2.1 Wrinkle counts

Images were opened in ImageJ, and the “count” tool used to count each wrinkle in the silicone substrate. A wrinkle was defined as a single bright line that was distinct from the cell edge or any defects in the silicone substrates, and wrinkles usually ran perpendicular to the cell edges (Figure 6-2). If it was unclear whether a line was a wrinkle or a cell edge, it was not counted.

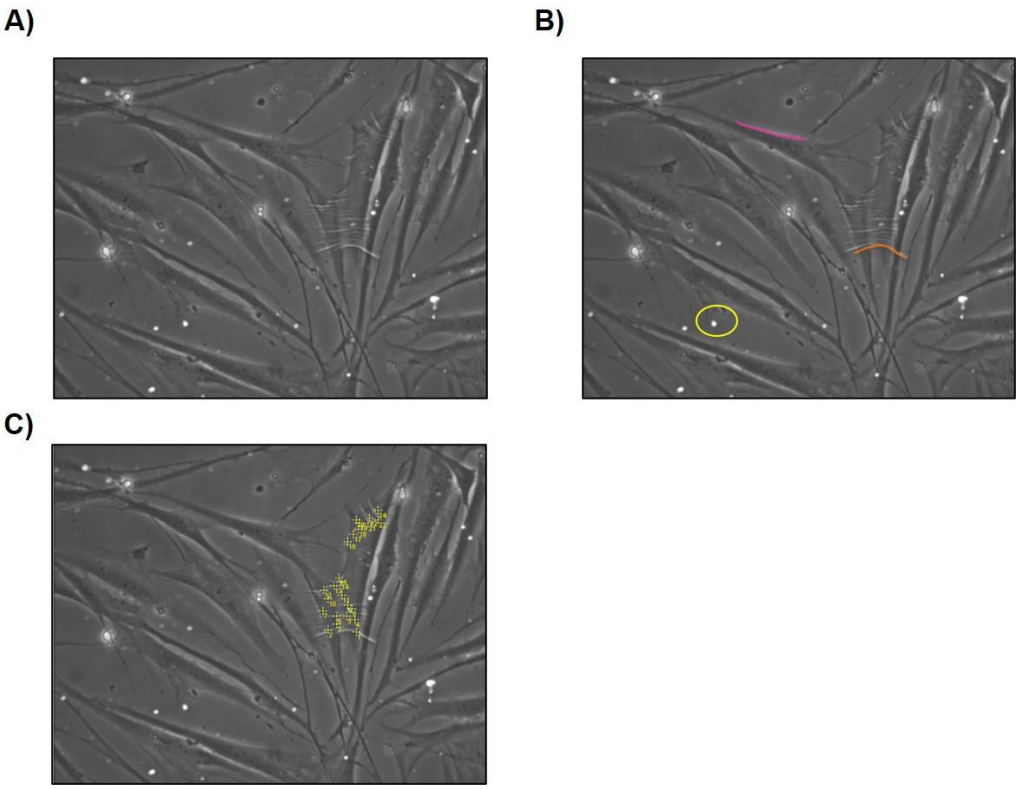

Figure 6-2: Quantification of the wrinkling assay

A) Unmarked image of human lung fibroblasts grown on a thin wrinkling substrate. Wrinkles appear bright and tend to run perpendicular to the cell edge.

B) The same image as shown in (A) marked to show an example of a wrinkle (highlighted in orange), a cell edge (highlighted in pink), and a defect in the underlying substrate (yellow circle).

C) The same image following the wrinkle counting process using the "count" tool in Image J. Each wrinkle identified is clicked, and a number left on the image in this position. The total number of wrinkles is then recorded for each image.

For both low and high magnification images, wrinkles were counted before the addition of the GPCR agonist, and on a subsequent image taken at the same position after 30 minutes of GPCR agonist stimulation.

6.3.3 Immunofluorescence

Indirect immunofluorescence was performed to detect cellular antigens. This method uses a similar principle to that described for IHC in the General Methods section, but with fluorescent secondary antibodies. Immunofluorescence staining was performed either immediately following the winkling assay or on cells grown at seeded on 35mm plastic dishes at low confluency (1 x 10^4 cells per well). Cells were fixed in 3% paraformaldehyde in PBS at room temperature for 10 minutes. Cells were then permeabilised with 0.2 Triton X-100 (TX-100) in PBS for 5 minutes, then washed once in PBS before staining. Samples were incubated in primary antibody in PBS/ 0.02% TX-100 for 60 minutes at room temperature, followed by three 10-minute washes with PBS/0.02% TX-100. Secondary antibodies were applied in PBS/0.02% TX-100 for 60 minutes at room temperature, and 4′,6-diamidino-2-phenylindole (DAPI) (1:50) was added with the secondary antibody. This was followed by three 15-minute washing steps in PBS/0.02% TX-100. Coverslips were mounted using polyvinyl acetate (PVA) following a brief wash with distilled water and left to dry overnight.

The following antibodies were used: mouse IgG2a anti αSMA (1:100), anti-phalloidin Alexa Fluor 488 (1:100), anti-mouse IgG2a-TRITC (1:200).

Imaging was performed using a Nikon 90i microscope and NIS Elements software.

6.3.4 Cell viability tests

The viability of cells following the wrinkling assay and *GNA12* and *GNA13* siRNA treatment was assessed using two methods: the MTT assay and trypan blue exclusion.

6.3.4.1 MTT assay

6.3.4.1.1 Principle

The assay depends on the principle that living cells with active mitochondrial respiration will convert 3-[4,5-dimethylthiazole-2-yl]-2,5-diphenyltetrazolium bromide (MTT) to MTT-formazan. MTT formazan is purple in colour, and can be detected using a plate reader. The degree of colour change acts as an indicator of cell viability.

6.3.4.1.2 Method

500µg/ml MTT was prepared in 0% FCS DMEM. The culture supernatant was aspirated and 1ml of MTT solution added to each 35mm dish. After incubating in the dark at 37^{o}C for 4 hours, the MTT solution was removed and 1ml DMSO added to each well.

Absorbance at 596nm was measured for each sample. Each cellular sample was assessed in triplicate, with 200µl of each sample transferred to a well of a 96 well plate. “blank” water only samples were also run in triplicate, and the absorbance from these wells used to generate blank-corrected data for the calculation of cell viability.

6.3.4.2 Trypan blue exclusion

6.3.4.2.1 Principle

This method uses the principle that the dark dye trypan blue will not be taken up by cells with living cells, which have intact cell membranes. Dead cells will stain blue in this method, thus allowing them to be distinguished from living cells microscopically.

6.3.4.2.2 Method

0.4% trypan blue was mixed in 1:1 ratio with a cell suspension in normal media. The cell suspension was then loaded onto a haemocytometer, and the number of stained and unstained cells counted. The proportion of viable cells was calculated using the following equation:

Viable cell proportion = Unstained cells / Total number of cells

6.4 Results

6.4.1 Human lung fibroblasts from IPF donors have enhanced contractility

To understand how fibroblast contractility is altered in IPF, HLFs from donors with and without IPF were grown on wrinkling substrates and imaged without stimulation. IPF HLFs generated more substrate wrinkling than non-fibrotic HLFs, with a median number of wrinkles per lowered-powered field of 42 in non-diseased HLFs and 91 in IPF HLFs ($p=0.02$, Figure 6-3A-B). These data demonstrate that IPF HLFs are more contractile than non-IPF cells at baseline, and that the wrinkling

assay can be used to assess IPF-associated alterations in lung fibroblast contractility.

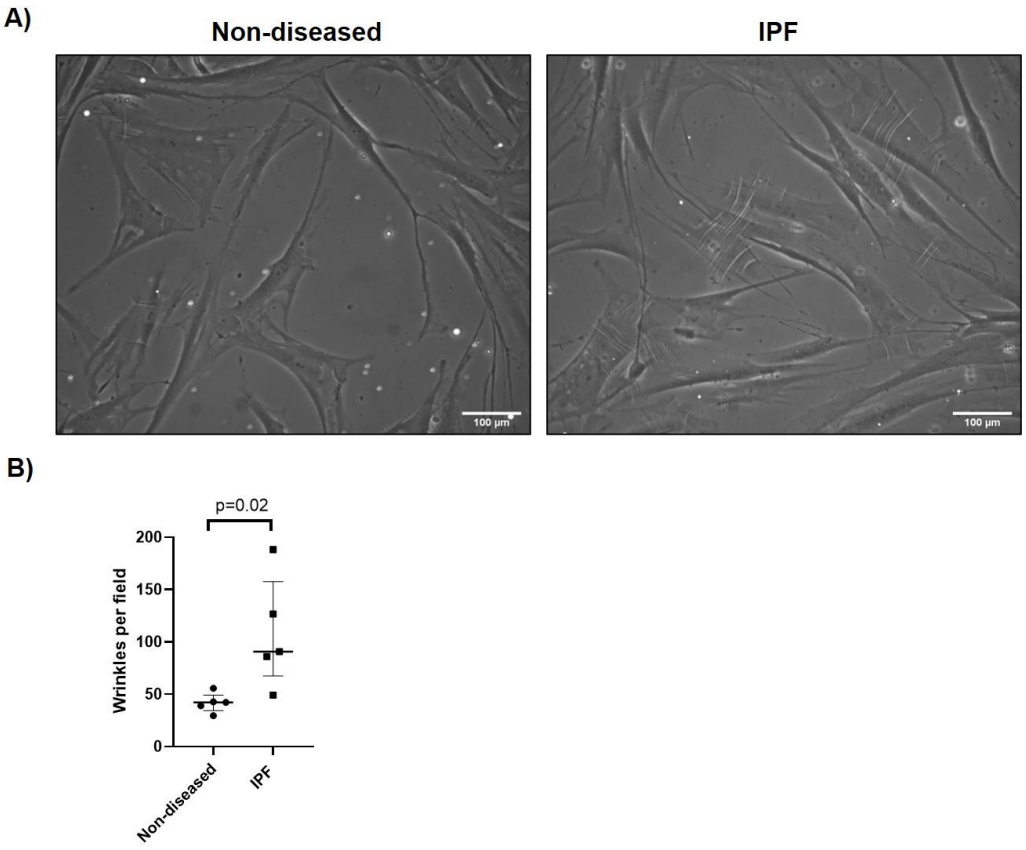

Figure 6-3: Lung fibroblasts from donors with IPF have enhanced contractility

A) Representative high-powered images of HLFs from non-diseased (left) and IPF (right) donors.

B) Quantification of substrate wrinkling shown as the number of wrinkles per low powered field generated by non-diseased and IPF HLFs. Data shown as median ± interquartile range, 5 donors per group. Statistical analysis performed using a two-tailed Mann Whitney test.

6.4.2 GPCR agonists induce contraction in HLFs

To identify the optimal timepoint for the assessment of LPA-induced fibroblast contraction, a timecourse experiment of LPA stimulation was performed on WT MEFs. Substrate wrinkling increased steadily beginning 5 minutes after LPA stimulation, and reached a steady level at around 30 minutes (Figure 6-4A,B). This was maintained for 4 hours before reducing at 6 hours (Figure 6-4B). Based on this pilot experiment, wrinkling was quantified at 30 minutes of LPA stimulation in all subsequent experiments.

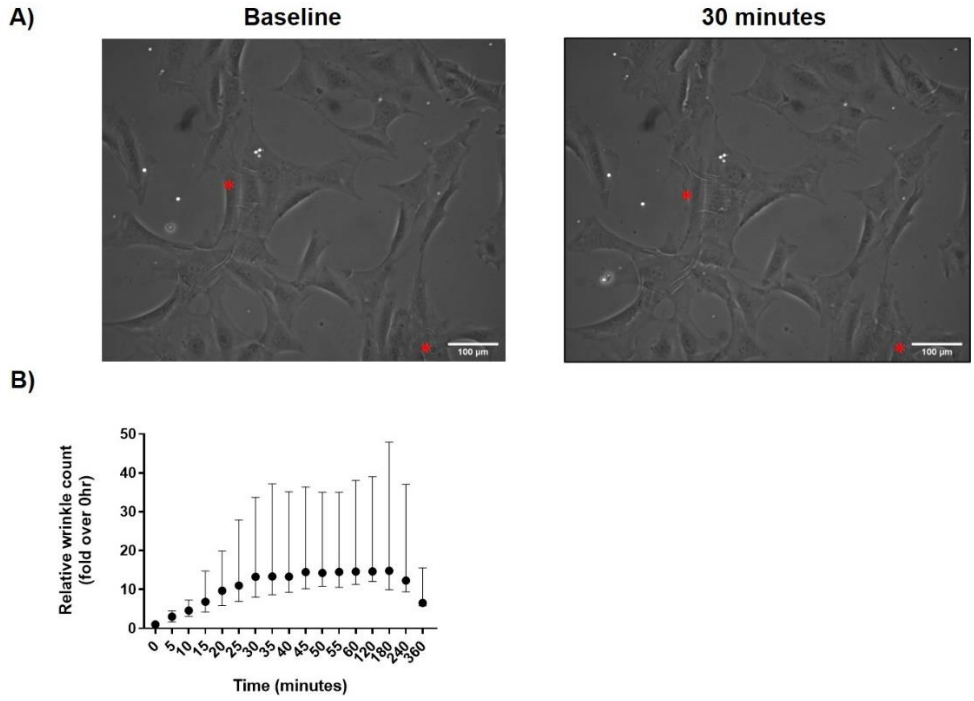

Figure 6-4: LPA induces WT MEF contraction

A) Representative images of WT MEFs stimulated with 30µM LPA at baseline (left) and 30 minutes (right). Red stars mark areas where substrate wrinkling increased with LPA stimulation.

B) Wrinkling relative to baseline at 5-360 minutes in WT MEFs stimulated with 30µM LPA. Wrinkles counted on 10 low magnification images taken across two separate wells. Data shown as median ± interquartile range.

To determine whether LPA-induced fibroblast contraction is exaggerated in IPF, non-diseased and IPF HLFs were subject to LPA stimulation in the wrinkling assay. Both non-diseased and IPF HLFs exhibited an LPA-induced increase in substrate wrinkling, with a median increase of 30.5 and 59.8 wrinkles per low-powered field in non-diseased and IPF HLFs, respectively (p=0.03, Figure 6-5B,C). Although the absolute wrinkle counts were higher pre- and post-LPA stimulation in IPF HLFs compared

with non-diseased cells, the median fold increase in substrate wrinkling with LPA was not significantly different between fibroblasts from non-diseased and IPF donors (median fold increase of 1.9 for both groups, p>0.99, Figure 6-5D). Overall, these data show that IPF fibroblasts are more contractile than non-diseased HLFs.

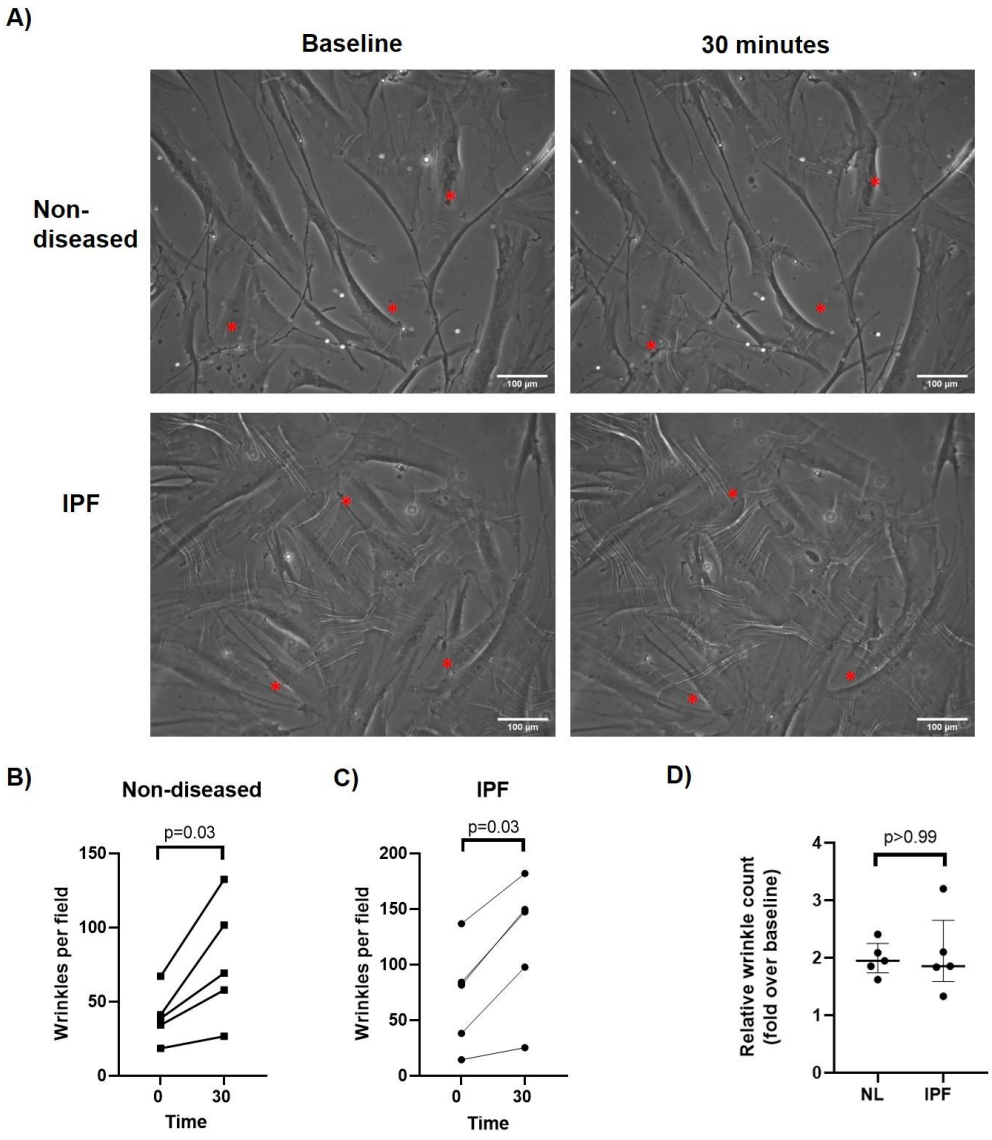

Figure 6-5: LPA induces an equivalent degree of contraction in lung fibroblasts from non-diseased and IPF donors

A) Representative images of HLFs from non-diseased (top) and IPF (right) donors before (left) and after (right) 30 minutes of 30μM LPA stimulation. Red stars indicate areas where wrinkling increased with LPA stimulation.

B and C) The number of wrinkles per low-powered field at 0 and 30 mins 30μM LPA stimulation in non-diseased (B) and IPF (C) HLFs. Data points are mean of 10 images per cell line. Statistical anlsyis performed using a one tailed Wilcoxon signed rank test.
D) LPA-induced substrate wrinkling in non-diseased and IPF HLFs expressed as fold icnrease over baseline. Statistical anlsyis performed using a two-tailed Mann Whitney test.
5 non-diseased and 5 IPF donor cell lines were used for these experiments.

6.4.3 Fibroblasts lacking $G_{\alpha 12/13}$ have reduced baseline contractility

To evaluate the role of $G_{\alpha q/11}$ and $G_{\alpha 12/13}$ in fibroblast contractility, WT, *Gnaq*$^{-/-}$;*Gna11*$^{-/-}$ and *Gna12*$^{-/-}$;*Gna13*$^{-/-}$ MEFs were grown on wrinkling substrates and imaged (Figure 6-6A-C). *Gna12*$^{-/-}$;*Gna13*$^{-/-}$ MEFs induced fewer substrate wrinkles than WT MEFs, with a median of 2.4 and 7.6 wrinkles per field, respectively ($p<0.01$, Figure 6-6D). Conversely, baseline wrinkling in *Gnaq*$^{-/-}$;*Gna11*$^{-/-}$ MEFs was not significantly different to that seen in WT MEFs, at a median of 4.5 wrinkles per image (Figure 6-6D). This implies that $G_{\alpha 12/13}$, but not $G_{\alpha q/11}$, plays a key role in baseline MEF contractility.

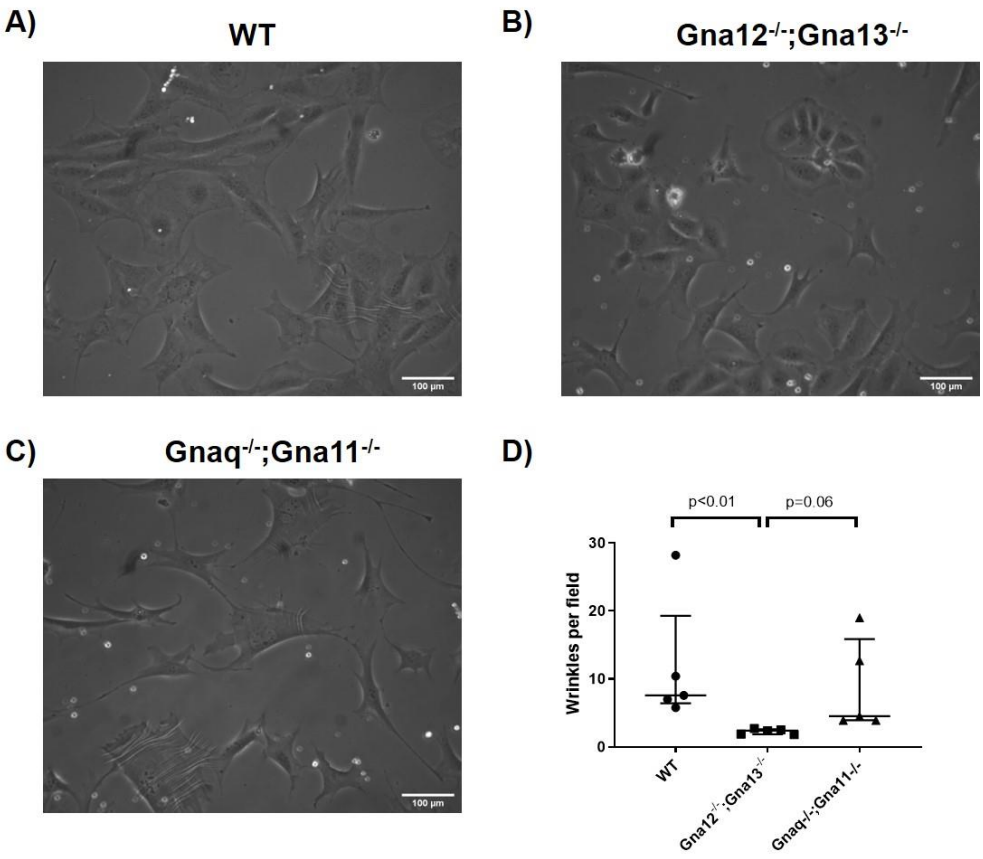

Figure 6-6: $G_{\alpha 12/13}$ is important for baseline contractility in MEFs
A-C) Representative images of WT (A), *Gna12*$^{-/-}$;*Gna13*$^{-/-}$ (B), and *Gnaq*$^{-/-}$;*Gna11*$^{-/-}$ (C) MEFs on wrinkling substrates.
D) The number of wrinkles per low-powered field generated by WT, *Gna12*$^{-/-}$;*Gna13*$^{-/-}$, and *Gnaq*$^{-/-}$;*Gna13*$^{-/-}$ MEFs. Data shown as median ± interquartile range of 4 independent experiments. Statistical analysis performed using a Kruskall Wallis test with Dunn's multiple comparisons test.

To confirm the translation of this finding to human cells, HLFs were subject to siRNA-induced knockdown of *GNA12* and *GNA13* and imaged (Figure 6-7A). HLFs from non-diseased donors had significantly reduced substrate wrinkling when treated with *GNA12* and *GNA13* siRNA compared with cells treated with non-targeting siRNA (24.6 vs 7.4 wrinkles per image with control and *GNA12*; *GNA13* siRNA, respectively,

$p<0.01$, Figure 6-7B). Importantly, this occurred without significant degrees of cell death induced by the siRNA protocol (Figure 6-7D,E), suggesting that the differences in cellular contractility were due to *GNA12* and *GNA13* knockdown.

While the reduction in substrate wrinkling with *GNA12* and *GNA13* siRNA did not reach statistical significance in HLFs from IPF donors (30.9 vs 7 wrinkles per image with control and *GNA12*; *GNA13* siRNA, respectively, $p=0.09$), four of the five IPF cell lines subject to siRNA-induced $G_{\alpha 12/13}$ knockdown had comparable degrees of wrinkling to siRNA-treated non-diseased HLFs (Figure 6-7C). These data confirmed that fibroblast $G_{\alpha 12/13}$ is important in GPCR agonist-induced fibroblast contraction. Furthermore, inhibition of $G_{\alpha 12/13}$ signalling could reduce HLF contractility to non-diseased levels in IPF.

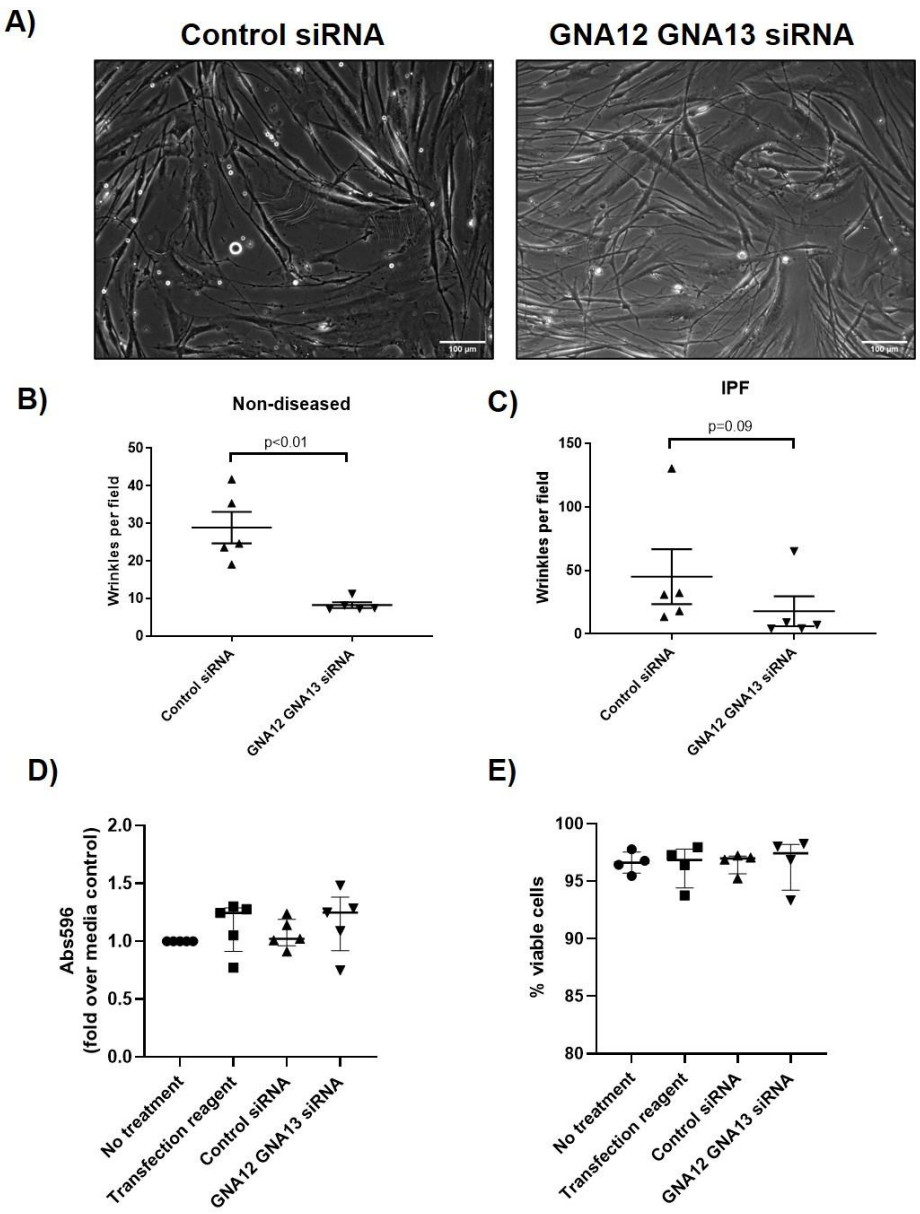

Figure 6-7: *GNA12* and *GNA13* knockdown reduces HLF contractility without cell death

A) Representative images of non-diseased HLFs treated with non-targetting (control, left) or *GNA12* and *GNA13* siRNA (right). Note fewer wrinkles in the *GNA12* and *GNA13* siRNA treated cells.

B, C) The number of wrinkles per low powered field in non-diseased (B) and IPF (C) HLFs, treated with control or *GNA12* and *GNA13* siRNA. HLFs from 5 non-diseased and 5 IPF donors used. Data shown as median ± interquartile range. Statistical analyses performed using a

two-tailed Mann Whitney test.
D) MTT assay of HLFs subject to the siRNA protocol used in the wrinkling assay.
E) Trypan blue staining of HLFs subject to the siRNA protocol used in the wrinkling assay. Data for MTT and Trpyan blue experiments from 5 independent experiments on cells from different donors. Data shown as median ± interquartile range.

6.4.4 Fibroblasts lacking $G_{\alpha 12/13}$ have reduced GPCR agonist-induced contractility

In order to assess the role of $G_{\alpha q/11}$ and $G_{\alpha 12/13}$ in GPCR agonist-induced fibroblast contraction, WT, *Gnaq*$^{-/-}$;*Gna11*$^{-/-}$ and *Gna12*$^{-/-}$;*Gna13*$^{-/-}$ MEFs were stimulated with LPA and substrate wrinkling assessed. WT and *Gnaq*$^{-/-}$;*Gna11*$^{-/-}$ MEFs generated 1.5 and 2.2 fold increases in substrate wrinkling with LPA stimulation, respectively (p=0.03, Figure 6-8B). Conversely, *Gna12*$^{-/-}$;*Gna13*$^{-/-}$ MEFs exhibited significantly lower LPA-induced wrinkling than WT MEFs (1.1-fold increase in $G_{\alpha 12/13}$-deficient MEFs, compared with 1.5-fold increase in WT MEFs, Figure 6-8C).

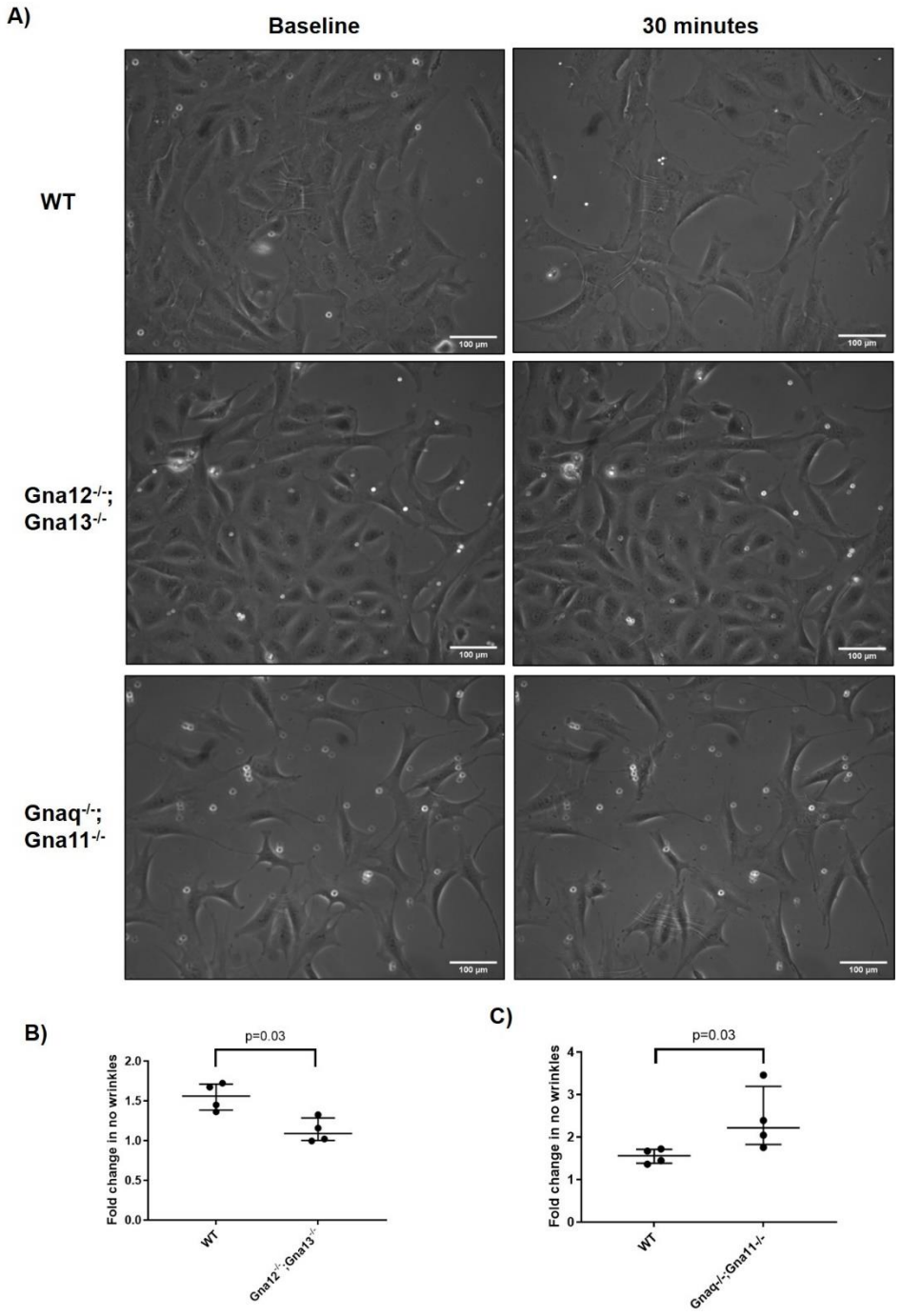

Figure 6-8: MEFs lacking $G_{\alpha 12/13}$ have reduced LPA-induced wrinkling

A) Representative images of WT (top panel), *Gna12*$^{-/-}$*;Gna13*$^{-/-}$ (middle panel), and *Gnaq*$^{-/-}$*;Gna11*$^{-/-}$ (bottom panel) MEFs before (left) and after (right) 30 minutes of LPA stimulation.

B, C) Wrinkling quantification of *Gna12*$^{-/-}$*;Gna13*$^{-/-}$ (B) and *Gnaq*$^{-/-}$

;Gna11$^{-/-}$ (C) MEFs compared with WT MEFs. Data shown as fold increase over baseline. Data from 4 independent experiments, shown as median ± interquartile range. Statistical analyses performed using two-tailed Mann Whitney tests.

To validate this finding in HLFs, *GNA12* and *GNA13* siRNA was used to knock down $G_{\alpha 12/13}$ expression, and the LPA-induced wrinkling assay performed. HLFs with siRNA-induced $G_{\alpha 12/13}$ inhibition had a lower LPA-induced wrinkling response compared with HLFs treated with control siRNA (Figure 6-9A). This finding was seen in HLFs from non-diseased and IPF donors, which had LPA-induced substrate wrinkling of 2.6- and 3.6-fold over baseline, respectively, with control siRNA. This reduced to 1.1- and 1.2-fold with *GNA12* and *GNA13* siRNA ($p<0.03$, Figure 6-9B, C)). These data suggest that $G_{\alpha 12/13}$ is essential for LPA-induced fibroblast contraction.

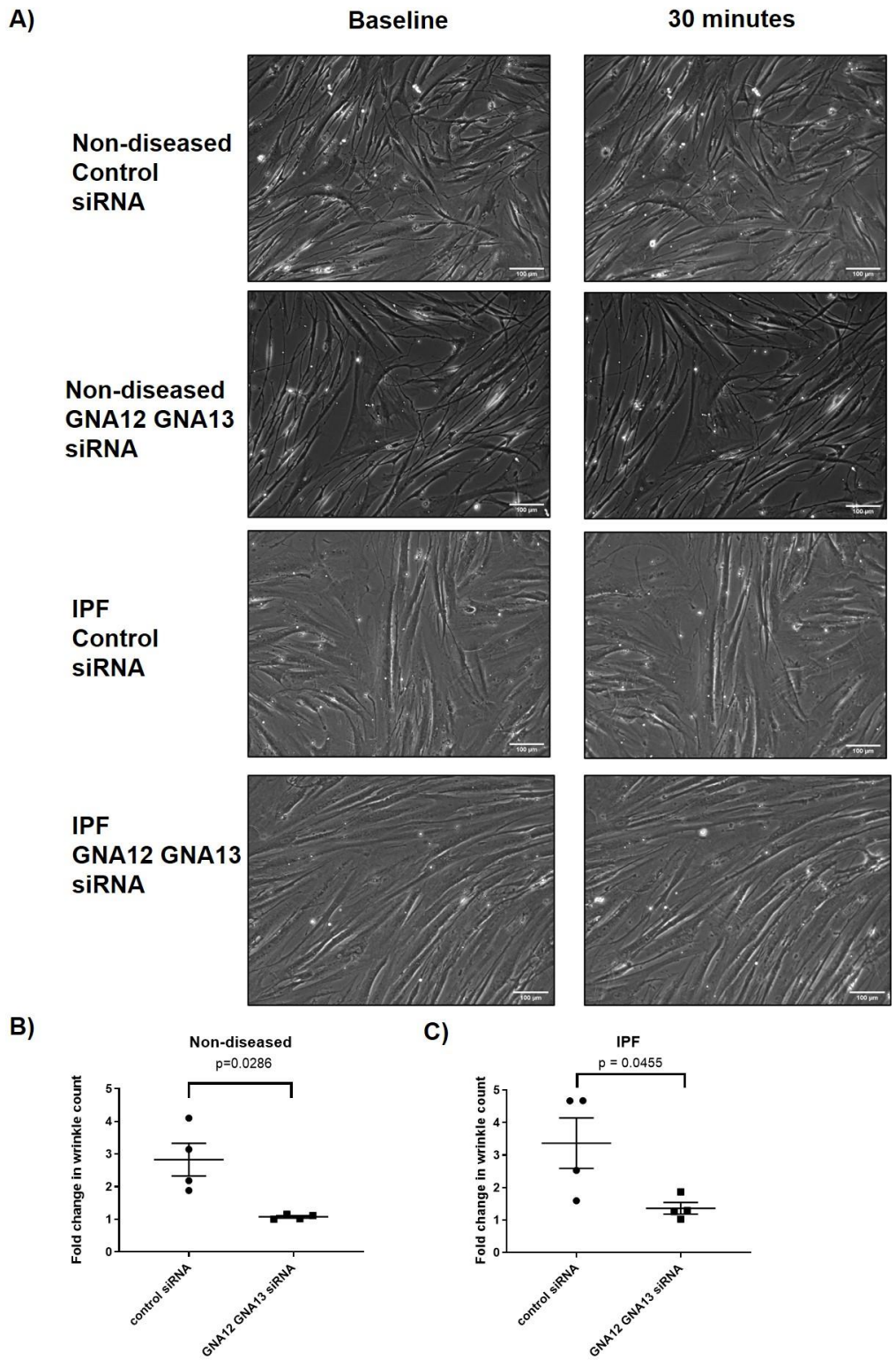

Figure 6-9: Knockdown of *GNA12* and *GNA13* inhibits LPA-induced wrinkling in HLFs

A) Representative images of non-diseased and IPF HLFs subject to

control (rows 1 and 3) or *GNA12* and *GNA13* (rows 2 and 4) siRNA, before (left) and after (right) 30μM LPA stimulation.
B) Quantification of wrinkling in non-diseased (B) and IPF (C) HLFs subject to control or *GNA12* and *GNA13* siRNA and stimulated with LPA. Data shown as fold increase in wrinkle counts over baseline. HLFs from 4 non-diseased and 4 IPF donors used. Data shown as median ± interquartile range. Statistical analyses performed using two tailed Mann Whitney tests.

6.4.5 Chronic $G_{\alpha 12/13}$ deficiency is associated with an altered cytoskeletal appearance

The actin cytoskeleton plays an important role in cellular contraction. When immunofluorescence was performed on HLFs that had been grown on wrinkling substrates, substrate wrinkles were observed perpendicular to F-actin and αSMA stress fibres (Phalloidin staining, Figure 6-10). This observation confirms that the cytoskeleton is important in driving the wrinkling response observed in the experiments in this chapter.

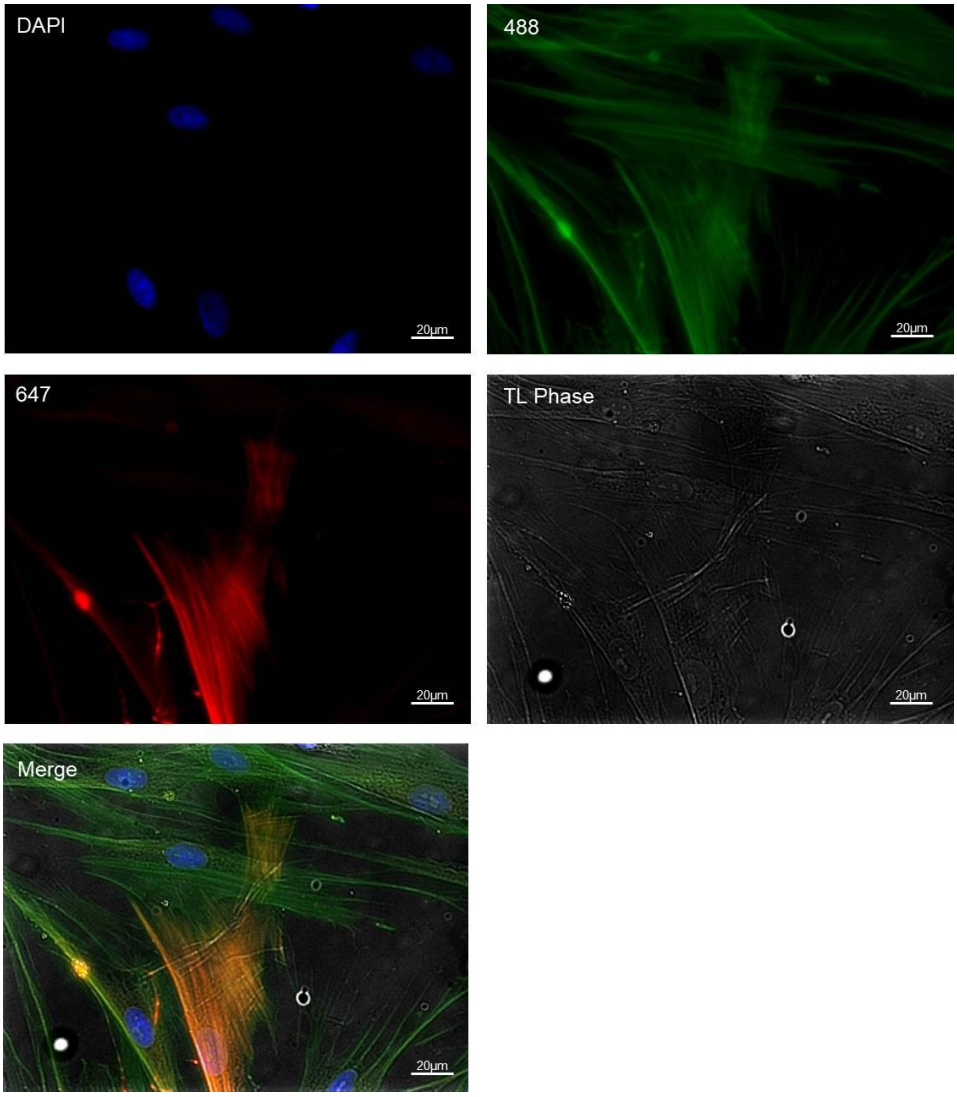

Figure 6-10: Substrate wrinkling occurs perpendicular to the actin cytoskeleton and αSMA stress fibres

Example immunofluorescence images of a human lung fibroblast contracting on a wrinkling silicone substrate. Substrate wrinkles can be seen on TL Phase image as bright lines perpendicular to the actin fibres.

Blue = DAPI; Green (488) = Phalloidin (F-actin); Red (647) = αSMA; TL Phase = trasmitted light, phase 2 image; Merge= DAPI, Phalloidin, αSMA, and TL Phase images merged.

To assess the effect of $G_{\alpha 12/13}$ knockdown on the cytoskeleton, immunofluorescence was performed on WT, *Gna12*$^{-/-}$;*Gna13*$^{-/-}$, and

Gnaq$^{-/-}$;*Gna11*$^{-/-}$ MEFs. Phalloidin immunofluorescence revealed an epithelial-like F-actin structure in *Gna12*$^{-/-}$;*Gna13*$^{-/-}$ MEFs, which was clearly different to the more fibroblast-like F-actin appearance seen in WT and *Gnaq*$^{-/-}$;*Gna11*$^{-/-}$ MEFs (Figure 6-11).

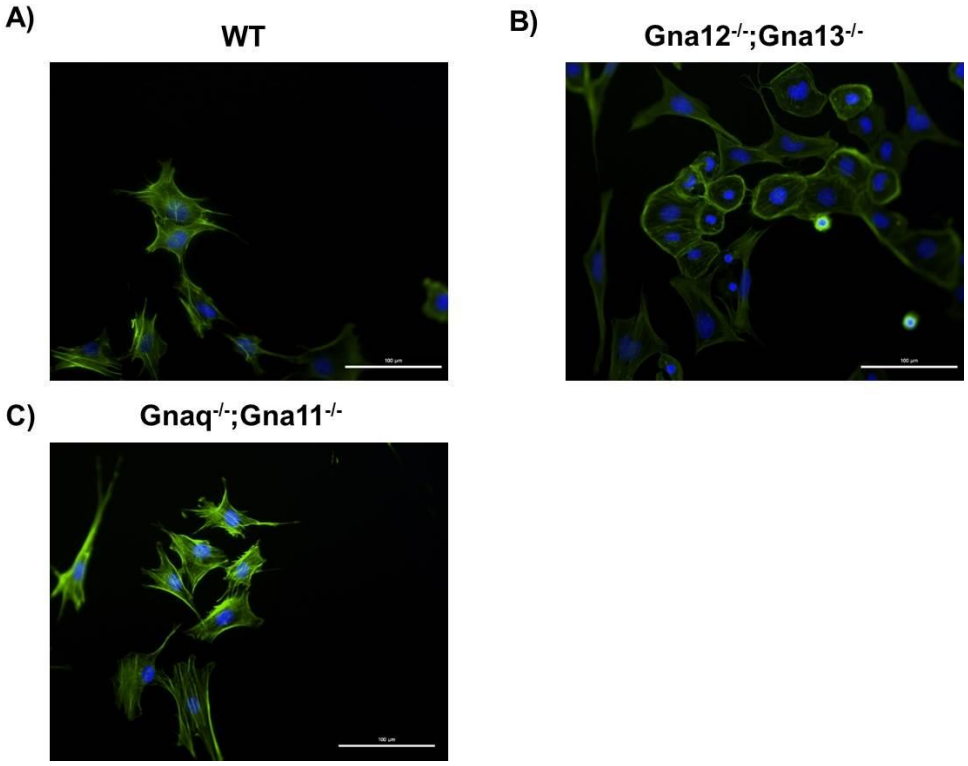

Figure 6-11: Long-term $G_{\alpha12/13}$ deficiency is associated with an abnormal cytoskeletal appearance
Representative immunoflurescence images of wild-type (A), *Gna12*$^{-/-}$;*Gna13*$^{-/-}$ (B), and *Gnaq*$^{-/-}$;*Gna11*$^{-/-}$ (C) MEFs.
Blue = DAPI; Green = Phalloidin (F-actin).

These results imply that chronic $G_{\alpha12/13}$ deficiency is associated with altered cytoskeletal arrangement, and that this may be the reason for the reduced contractility observed in $G_{\alpha12/13}$-deficient cells.

6.5 Discussion

The results presented here confirm previous reports of increased contractility in lung fibroblasts from donors with IPF compared with fibroblasts from non-diseased individuals (167, 319, 320). This consistency with previous work demonstrates that the wrinkling assay is a suitable method for the investigation of IPF-related differences in fibroblast contractility.

Fibroblast and myofibroblast contraction are important for several profibrotic processes including TGFβ activation, and enhanced organisation and stiffness of the ECM (161, 168, 322-324). The exact mechanisms that drive increased fibroblast contractility in IPF are not certain, however increased matrix stiffness and TGFβ signalling in IPF lungs are known to increase fibroblast-to-myofibroblast differentiation, and myofibroblasts are highly contractile cells (321). This is the first work to identify a role for $G_{\alpha 12/13}$ in fibroblast contractility, and importantly siRNA-induced $G_{\alpha 12/13}$ knockdown reduced baseline fibroblast contractility to near non-diseased levels in most IPF lung fibroblast lines tested. This finding suggests that fibroblast $G_{\alpha 12/13}$ may be a good therapeutic target that could prevent further ECM remodelling in fibrosis.

Much of the literature on G proteins in cellular contractility has focussed on vascular smooth muscle cells (VSMCs). Several GPCRs have been implicated in the myogenic response of VSMCs, which is essential for inducing vasoconstriction in response to increased blood flow (325). While this is secondary to GPCR agonist release in some cases (326), it

can also occur independently of GPCR-ligand binding (212), suggesting intrinsic mechanosensitivity of the receptors. As G_{α} subunits signal downstream of GPCRs, these signalling mediators could also be considered potentially mechanosensitive mediators of cellular contractility.

The roles of G_{α} subunits in VSMC contraction is an ongoing area of research. Both $G_{\alpha q/11}$ and $G_{\alpha 12/13}$ have been shown to have roles in VSMC contraction via PLC-β and calcium signalling, and Rho/ROCK signalling, respectively (329-331). Deficiency of either $G_{\alpha q/11}$ or $G_{\alpha 12/13}$ in smooth muscle normalises age-related hypertension in mice, a condition associated with vascular tone and vasoconstriction (328). However, mice lacking $G_{\alpha 12/13}$ in the vascular smooth muscle of small arteries have a complete loss of myogenic vasoconstriction (325), where animals lacking VSMC $G_{\alpha q/11}$ have a response comparable to wild-type mice (325).

While evidence for the role of $G_{\alpha q/11}$ in vascular smooth muscle contraction appears inconsistent, $G_{\alpha q/11}$ has been found to have a role in cellular contractility in other tissues. $G_{\alpha q/11}$ mediates NK2-induced bladder smooth muscle contraction via RhoA (327). Furthermore, $G_{\alpha q/11}$ can activate the contraction-associated Rho/ROCK signalling (74, 219, 327). There is also evidence for G protein-mediate cellular contraction in respiratory disease. Expression of both $G_{\alpha 12}$ and $G_{\alpha 13}$ are increased in the bronchial smooth muscle of airway hyper-responsive rats (332). Furthermore, deficiency of $G_{\alpha 13}$ inhibits methacholine-induced bronchial contraction in mice (333), and $G_{\alpha 12}$ plays a crucial role in human airway

smooth muscle cell contraction (334). However, the role of $G_{\alpha q/11}$ and $G_{\alpha 12/13}$ in fibroblast contractility, and how this influences the pathogenesis of IPF, was unknown prior to this study.

This study found that MEFs and HLFs lacking $G_{\alpha 12/13}$ had reduced baseline and LPA-induced contractility. Conversely, MEFs lacking $G_{\alpha q/11}$ had comparable baseline levels of contraction to WT cells. Furthermore, $G_{\alpha q/11}$ deficient MEFs exhibited increased LPA-induced contraction compared with WT MEFs. This finding may have been driven by a particularly high LPA-induced wrinkling response in one experimental repeat that contributed to these data, however it is notable that three of the four experiments showed LPA-induced wrinkling to be higher in *Gnaq*$^{-/-}$;*Gna11*$^{-/-}$ than WT MEFs. While this phenomenon has not been described in the smooth muscle cell literature, LPA-induced neurite retraction has been shown to be reduced in primary neurones from brains lacking $G_{\alpha 12/13}$, but paradoxically enhanced in $G_{\alpha q/11}$-deficient neurones (335). This may indicate that there is compensation by $G_{\alpha 12/13}$-related pathways in $G_{\alpha q/11}$-deficient cells, or that signalling pathways driven by $G_{\alpha q/11}$ usually antagonise $G_{\alpha 12/13}$-driven effects. This finding emphasises the possibility G_{α} subunit inhibition resulting in unintended adverse effects caused by over-compensation by other G_{α} subunits.

The reduction in baseline and LPA-induced contraction in MEFs and HLFs lacking $G_{\alpha 12/13}$ suggests that the $G_{\alpha 12/13}$-mediated LPA-induced TGFβ signalling described in Chapter 5 probably occurs secondary to cellular contraction, with resulting traction forces on the latent TGFβ

complex, and is in keeping with previous work on LPA-induced TGFβ signalling (137). Conversely, MEFs lacking $G_{\alpha q/11}$ did not exhibit reductions in cellular contraction, suggesting that contraction-independent pathways may be involved in $G_{\alpha q/11}$-mediated LPA-induced TGFβ signalling. The normal cytoskeletal appearance of $G_{\alpha q/11}$-deficient MEFs suggests that the actin machinery is intact in these cells. However other factors, such as altered cell surface molecule expression or integrin-large latent TGFβ complex interactions, have not been assessed in $G_{\alpha q/11}$-deficient cells and cannot be ruled out as playing a role in this observation.

Previous work on LPA-induced VSMC contraction has suggested that this occurs via a $G_{\alpha i}$-dependent signalling pathway downstream of LPA1, and autocrine or paracrine signalling secondary to the release of thromboxane A2 (336). It was beyond the scope of the current study to assess the role of second messenger release in response to LPA, but it is possible that LPA induces the production of another mediator that itself induces contraction via $G_{\alpha 12/13}$ signalling. Alternatively, the production of this second mediator could be dependent on $G_{\alpha 12/13}$. This should be assessed in future studies investigating the pathways linking LPA and contraction in fibroblasts.

The actin cytoskeleton is essential for cellular contractility. Actin exists in two forms, with globular G actin monomers polymerising to form filamentous F-actin (104). The extent of actin polymerisation, and thus actin cytoskeletal structure, is controlled by actin binding proteins in

response to a variety of stimuli (104). Cytoskeletal proteins such as calmodulin, cAMP signalling, and RhoA have all been reported to act as links between GPCRs and the actin cytoskeleton (104).

The signalling pathways required to form or maintain the actin cytoskeleton structure are mediated by members of the Rho family of small GTPases (122). Rho/ROCK signalling also regulates myofibroblast contraction (337, 338), and is the classical signalling pathway downstream of $G_{\alpha 12/13}$. As $G_{\alpha 12/13}$ deficiency has been associated with reduced Rho activity and reduced wound-healing associated cellular migration (339), it is unsurprising that cells with longstanding $G_{\alpha 12/13}$ knockdown had an altered actin cytoskeletal structure.

Previous work demonstrated that $G_{\alpha 12/13}$-deficient MEFs do not form orientated, stable microtubules during wound healing in response to LPA (339), and this may explain the reduced LPA-induced contraction response in these cells. The previous report described only moderate differences between the F-actin structure of WT and $G_{\alpha 12/13}$-deficient MEFs, although phalloidin staining was reported to be reduced in $G_{\alpha 12/13}$-deficient MEFs (339). However the images of $G_{\alpha 12/13}$-deficient MEFs from the current study show a dramatic difference between the two cell types, with an almost epithelial cell-like actin appearance in *Gna12*$^{-/-}$;*Gna13*$^{-/-}$ MEFs. It is difficult to compare the images from the work presented here and the previous study, and it should be noted that the immunofluorescence images from this research were obtained from unstimulated cells, whereas the previous study presented images of cells

after wounding. Additionally, the present work did not include staining for all of the cytoskeletal components assessed by Goulimari et al (339). The exact reason for the altered actin appearance in MEFs lacking $G_{\alpha 12/13}$ is presently unclear, but as contractile stimuli are known to induce the formation of F-actin (340), the loss of ability to detect such stimuli via $G_{\alpha 12/13}$ may be an important factor.

Actin stress fibre formation is governed by signals generated by the physical and chemical characteristics of the ECM, and TGFβ signalling (122). The data in this study are in keeping with work that showed that $G_{\alpha q/11}$-deficient fibroblasts form stress fibres normally in response to LPA receptor activation, but that LPA-mediated stress fibre formation is dependent on $G_{\alpha 13}$ (341), as LPA-induced contraction and the actin cytoskeleton were altered only in $G_{\alpha 12/13}$-deficient cells. The role that $G_{\alpha 12/13}$ plays in detecting the physical surroundings, with resulting influence on the cytoskeletal structure, is less clear, because culture on soft substrates did not affect LPA-induced TGFβ signalling in MEFs lacking $G_{\alpha 12/13}$ (Chapter 5). Furthermore, *Gna12*$^{-/-}$*;Gna13*$^{-/-}$ MEFs did not respond to a transfer from tissue culture plastic to soft substrates in terms of altered αSMA expression (Chapter 5). These data, although limited, suggest that the altered cytoskeletal appearance in $G_{\alpha 12/13}$-deficient MEFs is not related to altered detection of matrix stiffness.

Therapeutic targeting of fibroblast contractility has the potential to be beneficial in pulmonary fibrosis, and this has been the topic of previous investigation. While the exact antifibrotic mechanisms of pirfenidone, one

of the two drugs license for IPF, are unclear, this drug has been shown to inhibit lung fibroblast contraction *in vitro* (342). In addition, relaxin showed promise as an antifibrotic drug, and is thought to act by inhibiting cellular contraction (343). Unfortunately, subsequent relaxin trials did not replicate the benefits seen in earlier studies in terms of skin thickening and stabilisation of lung function in systemic sclerosis (344, 345). The results in this and earlier chapters of this thesis indicate that the inhibition of mesenchymal $G_{\alpha 12/13}$ signalling may inhibit important pathophysiological processes in IPF. However, the loss of $G_{\alpha 12/13}$-mediated contraction in myofibroblasts could be anticipated to significantly impact ECM organisation and TGFβ signalling, which could have serious implications for wound healing and other physiological processes. Therefore, an *in vivo* model of mesenchymal cell $G_{\alpha 12/13}$ inhibition is required to properly assess the antifibrotic effects of mesenchymal $G_{\alpha 12/13}$ inhibition, as well as to understand any undesired consequences of this approach.

In addition to playing a key role in fibrogenesis, cellular contraction is important for lung development, in particular by the secondary crest myofibroblasts that generate and organise the ECM proteins to form secondary crests during alveolarisation (21, 346). Although the effect of mesenchymal $G_{\alpha 12/13}$ in lung development was not determined in Chapter 4 because of insufficient numbers of mesenchymal $G_{\alpha 12/13}$ knockout mice, it is likely that a loss of myofibroblast contraction is not the underlying mechanism for the defective alveolarisation seen in *Pdgfrb*-

Cre$^{+/-}$;*Gnaq*$^{fl/fl}$;*Gna11*$^{-/-}$ mice. This is because MEFs lacking $G_{\alpha q/11}$ could contract with and without LPA stimulation, and therefore this mechanism should have been intact in *Pdgfrb-Cre*$^{+/-}$;*Gnaq*$^{fl/fl}$;*Gna11*$^{-/-}$ mice. The working hypothesis of this study is that the altered ECM characteristics seen in *Pdgfrb-Cre*$^{+/-}$;*Gnaq*$^{fl/fl}$;*Gna11*$^{-/-}$ mice may be related to altered ECM production and remodelling by enzymes rather than cellular contraction. However, this must be confirmed with further mechanistic work.

6.6 Limitations

The wrinkling assay used in this project has not been widely used to assess cellular contractility. However, this method is based the relationship between cellular contraction and the deformation of a soft substrate, similar to the more well-established methods such as traction force microscopy (TFM). Additionally, the wrinkling assay has been found to be a comparable method to TFM in investigations by the founding laboratory (347) , although TFM may be more sensitive to low degrees of cellular contraction that are insufficient to generate substrate wrinkles. While TFM may have detected some low-level contractility that was not seen in this study, the overall finding of reduced contractility in $G_{\alpha 12/13}$-deficient cells is unlikely to have changed.

There is a risk that the quantification method used for the wrinkling assay, manually counting wrinkles on images, could have created bias by the observer. While the wrinkles were counted by an observer blinded to cell type the $G_{\alpha 12/13}$-deficient MEFs could be identified on appearance alone

due to their morphological differences to WT cells, which may have influenced the baseline contractility wrinkle counts. However, independent observers agreed that $G_{\alpha12/13}$-deficient MEFs appeared to generate fewer substrate wrinkles. Furthermore, the observer that counted the wrinkles was blinded to timepoint and LPA treatment status, therefore observer bias could not explain the reduction in LPA-induced substrate wrinkling in $G_{\alpha12/13}$-deficient cells.

While automated image analysis may be used to reduce the risk of observer bias, this was not possible for the images generated by this study. An automated wrinkle quantification process was trialled on the images from the wrinkling assay, however this required significant manual image clean-up as the software was unable to distinguish cell edges from substrate wrinkles. As this clean-up process itself could generate significant bias, the wrinkle counting method, which required no modification of the original images, was used.

This study established a role for $G_{\alpha12/13}$ in fibroblast contraction, however the individual roles of $G_{\alpha12}$ and $G_{\alpha13}$ were not assessed. Previous work has found that LPA-mediated stress fibre formation is dependent on $G_{\alpha13}$, whilst endothelin-A (ET_A) signalling induces stress fibre formation via $G_{\alpha12}$ (341). Furthermore, deficiency of $G_{\alpha13}$, but not $G_{\alpha12}$, reduces methacholine-induced bronchoconstriction (333), suggesting that different receptors induce Rho activation via different G_{α} subunits even within G protein families. Future work should analyse the individual roles of $G_{\alpha12}$ and $G_{\alpha13}$ in fibroblast contractility in fibrosis, as a more targeted

approach towards one of these G proteins may have similar antifibrotic effects but with fewer adverse effects if applied *in vivo*.

This study evaluated only cellular contraction as a function of the actin cytoskeleton. However, the actin cytoskeleton is essential for many other myofibroblast functions such as focal adhesion assembly, ECM organisation, wound contraction, tail retraction during cellular migration, and transcriptional regulation (122). It is possible that these processes are also altered in $G_{\alpha 12/13}$-deficient cells, and conversely that $G_{\alpha q/11}$-deficient cells have functional abnormalities of the actin cytoskeleton not identified by this work. This should be evaluated in future studies.

This chapter includes data from murine and human fibroblasts, however cellular contractility is typically thought to be a function of myofibroblasts. While fibroblasts can contract, it is likely that the cells used in this study had differentiated into myofibroblasts secondary to long term culture on tissue culture plastic (348). While similar experiments on freshly isolated lung fibroblasts that have not been exposed to stiff culture environments would be more relevant to the *in vivo* environment, the data presented in this chapter has still established an important role for $G_{\alpha 12/13}$ in fibroblast contraction.

Finally, this study evaluated the role of G proteins in cellular contraction induced by just one GPCR agonist, LPA. Other GPCR agonists, such as thrombin and the protease activated receptor agonists SFLLRN and TFLLRN induced similar patterns of $G_{\alpha 12/13}$-induced cellular contraction

(data not presented), although the analysis of these datasets is incomplete. LPA is a good example of a GPCR agonist that is relevant to both pulmonary fibrosis and lung development, and thus was appropriate to use in the model presented here.

6.7 Conclusion

$G_{\alpha 12/13}$ signalling plays a vital role in mediating both baseline and LPA-induced fibroblast contraction. Cellular contractility is exaggerated in lung fibroblasts from donors with IPF, but this can be reduced to normal levels by inhibiting $G_{\alpha 12/13}$ signalling. $G_{\alpha 12/13}$ may therefore be a useful therapeutic target that can normalise fibroblast activity in IPF.

7 The Molecular Mechanisms of Cyclical Mechanical Stretch-Induced TGFβ Signalling in Fibroblasts

7.1 Introduction

The data presented in Chapter 5 demonstrated that $G_{\alpha q/11}$ mediates LPA-induced TGFβ signalling in fibroblasts, therefore $G_{\alpha q/11}$ inhibition may protect against pulmonary fibrosis. However, mesenchymal $G_{\alpha q/11}$ deletion *in vivo* resulted in disturbed lung alveolarisation (Chapter 4). Tight regulation of TGFβ signalling is essential for normal lung development (64, 89-91, 101, 102), and many developmental signalling pathways are reactivated to drive the abnormal wound healing response characteristic of IPF (22). Therefore, mesenchymal cell-driven $G_{\alpha q/11}$-mediated TGFβ activation may be a key driver of both fibrosis and normal lung development.

Mechanical stimuli can activate TGFβ, and stretch has been shown to induce TGFβ signalling in numerous systems (113, 219, 349-354). Cyclical mechanical stretch (CMS) in the lungs increases dramatically after birth with the commencement of normal respiration. As alveolarisation occurs entirely postnatally in mice (14), breathing-related CMS-induced TGFβ signalling may be an important pathway in normal lung development. Furthermore, ventilator-related stretch-induced TGFβ signalling is reduced in mouse lungs lacking $G_{\alpha q/11}$ in type II alveolar epithelial cells (219), suggesting that $G_{\alpha q/11}$ may have a role in stretch-induced TGFβ signalling. In epithelial cells, $G_{\alpha q/11}$ mediates LPA-induced TGFβ signalling via ROCK and the αvβ6 integrin (74), and ROCK and integrin signalling have been implicated in stretch-induced TGFβ signalling (113). However, the role of $G_{\alpha q/11}$ in CMS-induced TGFβ

signalling in fibroblasts, and the molecular pathways involved, are unknown.

7.2 Aims and Hypothesis

This worked aimed to:

- Understand the role of breathing-related CMS in TGFβ signalling in embryonic and adult fibroblasts.
- Dissect the molecular pathway from CMS to TGFβ signalling in fibroblasts.
- Assess the contribution of breathing-related CMS to the pathogenesis of IPF.

The hypothesis underlying this work was:

> *Breathing-related CMS induces TGFβ signalling in fibroblasts via $G_{\alpha q/11}$, ROCK, and integrin signalling, and is an important driver of IPF*

7.3 Methods

7.3.1 Cyclical mechanical stretch (CMS) experiments

MEFs or HLFs were seeded at a density of 2 x 10^5 cells per well on collagen I-coated Bioflex® six well culture plates in full media and allowed to attach to the plate for 24 hours. The media was changed to 1% FCS DMEM for 24 hours prior to stretching.

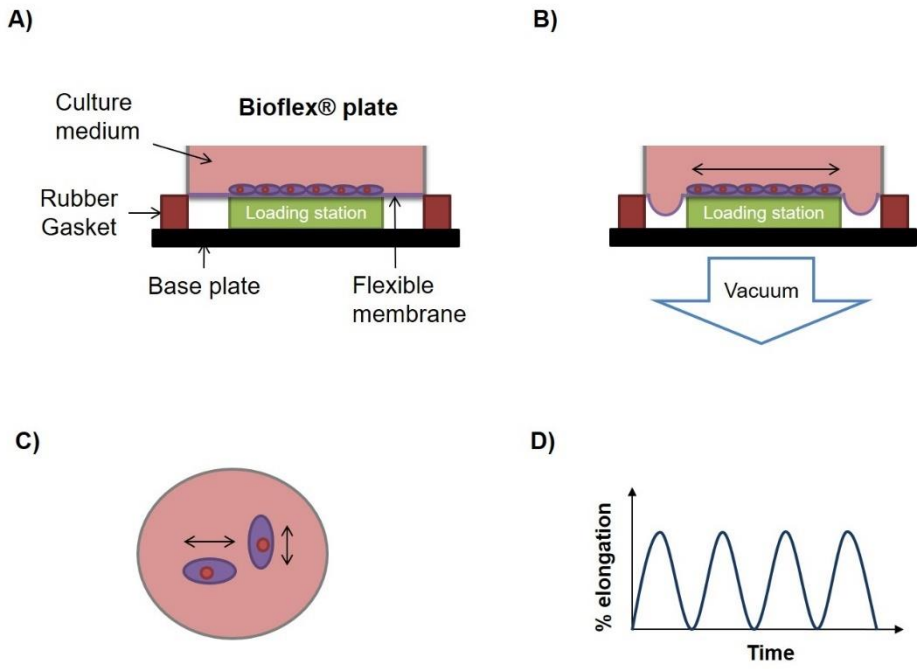

Figure 7-1: The Flexcell® cell stretching system

A) Cells are grown on Bioflex® plates, which have flexible bottoms. These are loaded onto the Flexcell apparatus, which consists of loading posts that are aligned with the centre of the cell culture well, and a loading station. Cross-section of a well from an example Bioflex® plate shown

B) When a vacuum is applied, the flexible bottom of the Bioflex® plate is pulled downwards, stretching the attached cells.

C) View of a Bioflex® plate from above when stretch is applied. Cells are subject to equibiaxial stretch, indicating that cells are stretched equally in all directions.

D) A schematic showing a stretch regimen using a sine waveform designed to mimic normal breathing.

Equibiaxial CMS was applied to cells *in vitro* using a Flexcell® system (FX-5000T, Flexcell International Corporation), which applies a vacuum beneath the flexible-bottomed Bioflex® cell culture plates (Figure 7-1). CMS regimens were designed to mimic normal tidal breathing in the

relevant organism, i.e. 1Hz (60 stretch cycles/ minute) in mouse cells, and 0.3Hz (18 stretch cycles/ minute) in human cells.

TGFβ signalling was measured using pSmad2 western blot and a TMLC luciferase reporter assay. Fibrosis-related gene expression (*PAI-1, TGFB1, ACTA2*, and *CTGF*) was measured using qPCR. TGFβ1, TGFβ2 and αSMA protein expression were assessed by western blot.

7.3.2 CMS regimens

For CMS time course experiments, WT MEFs were stretched for 4, 24 and 48 hours at 1Hz and 15% elongation. For CMS dose-response experiments, WT MEFs were stretched at a frequency of 1Hz at 5%, 10%, 15%, and 20% elongation. For comparisons between WT, *Gnaq*$^{-/-}$*;Gna11*$^{-/-}$, and *Gna12*$^{-/-}$*;Gna13*$^{-/-}$ MEFs, cells were subject to CMS at 15% elongation and a frequency of 1Hz. All HLF CMS experiments were performed at a frequency of 0.3Hz and 15% elongation for 48 hours, unless otherwise stated. A sine waveform was used for all experiments.

Unstretched control cells were cultured on Bioflex® plates under identical conditions to stretched cells alongside the Flexcell® apparatus. TGFβ stimulated positive control wells were treated with 2ng/ml TGFβ (R&D Systems) for 1 hour prior to cell lysis.

7.3.3 Chemical inhibitors used in CMS system

When used, chemical inhibitors were applied in 1% FCS in DMEM 30-60 minutes prior to the commencement of the CMS regimen, and remained throughout the CMS regimen. 50μM SB-525334, an activin receptor-like

kinase (ALK5)/ type I TGFβ-receptor kinase inhibitor, was used as a positive control for TGFβ inhibition. Inhibitors of phospholipase C (U73122), $G_{\alpha q/11}$ (YM254890), ROCK (Y27632), αv integrins (CWHM-12), β1 integrins (NOTT19955), matrix metalloproteinases (GM-6001), and serine proteases (4-(2-Aminoethylbenzenesulfonyl fluoride hydrochloride (AEBSF)) were used at varying concentrations. 48 hours of CMS was used for all inhibitor protocols, except for the U73122 experiments. 24 hours of CMS was applied for the U73122 experiments because of excessive cell death observed at the longer timepoint.

7.3.4 *GNAQ* and *GNA11* siRNA

Pooled siRNAs for human *GNAQ* and *GNA11* were used to knock down $G_{\alpha q/11}$ in human cells. A non-targeting siRNA pool was used under the same conditions as a control.

Cells were seeded at 1.5 x 10^5 cells per well of a six well Bioflex® plate in antibiotic-free full media. After 24 hours, *GNAQ* and *GNA11* siRNA was applied at a concentration of 15nM each with 4µl/ml DharmaFECT 1 transfection reagent, as per the manufacturer's instructions. 24 hours later, the transfection media was replaced with antibiotic-free full media. At 48 hours after transfection, cells were growth arrested in 1% FCS DMEM, and a 24 hour CMS regimen commenced 72 hours after the transfection protocol began. Cell lysates were collected for protein analysis at 96 hours post-transfection. The optimal conditions for $G_{\alpha q/11}$ knockdown were confirmed by western blot and qPCR in preliminary experiments.

7.3.5 TMLC stretch co-culture assay

7.3.5.1 Principle of assay

TMLCs are cells that have been permanently transfected and express the enzyme luciferase under the control of the promoter for the *PAI-1* gene (229). As TGFβ is known to induce *PAI-1* gene expression, luciferase activity in these cells can be used to measure the amount of active TGFβ stimulating the cells. Luciferase activity is determined by incubating TMLC lysates with luciferase substrate, resulting in the emission of light that can be measured by a plate reader. The concentration of active TGFβ is used by comparing the luciferase activity from experimental samples with that of a TGFβ standard curve.

7.3.5.2 Method

HLFs were seeded on Bioflex® plates at 2 x 10^5 cells per well in full media, allowed to adhere overnight, then growth arrested in 1% FCS DMEM for 24 hours. TMLCs were seeded over the HLFs at 4 x 10^5 cells per well in 1% FCS, and allowed to adhere for 2 hours. A 24 hour CMS regimen was applied, then cells were lysed in Reporter Lysis Buffer, and the plate stored at -80^{o}C for at least 4 hours. Lysates were transferred to a white luminometer plate, and luciferase activity determined using the following protocol: 100µl luciferase assay reagent injected per well, 2 second measurement delay, 10 second measurement read time. Luminescence readings were performed using an automated plate reader with luciferase injection capabilities, and analysis was performed with Omega software (BMG Labtech). A TGFβ standard curve was

applied for 24 hours to TMLCs seeded in normal tissue culture plastic six well plates, to validate the TGFβ activation response in these cells. As controls, TMLCs were seeded on Bioflex® plates, and the effects of stretch on TMLCs alone on luciferase activity subtracted from the HLF/TMLC co-culture stretch luciferase activity.

7.4 Results

7.4.1 CMS of wild-type MEFs induces TGFβ activation

To identify the optimal conditions for the assessment of CMS-induced TGFβ signalling *in vitro*, preliminary experiments were performed on WT MEFs. When WT MEFs were subject to CMS at 1Hz and 15% elongation, increased Smad2 phosphorylation was seen at 48 hours of CMS (Figure 7-2A,B; unstretched vs stretched p=0.05). A similar magnitude of pSmad2 expression was observed with 4 and 24 hours of CMS, but this was less consistent than that observed at 48 hours (Figure 7-2A,B). Therefore, 48 hours was chosen as the optimal duration for further CMS experiments unless other experimental requirements precluded this.

The optimal degree of stretch for use in CMS-induced TGFβ signalling experiments was investigated by applying 1Hz CMS to WT MEFs with increasing degrees of elongation, within the range possible in normal tidal breathing. CMS at 5%, 10% and 15% elongation increased pSmad2 expression compared with unstretched controls to a similar magnitude, but this became inconsistent at 20% elongation (Figure 7-2, C,D; p=0.05 stretched vs unstretched).

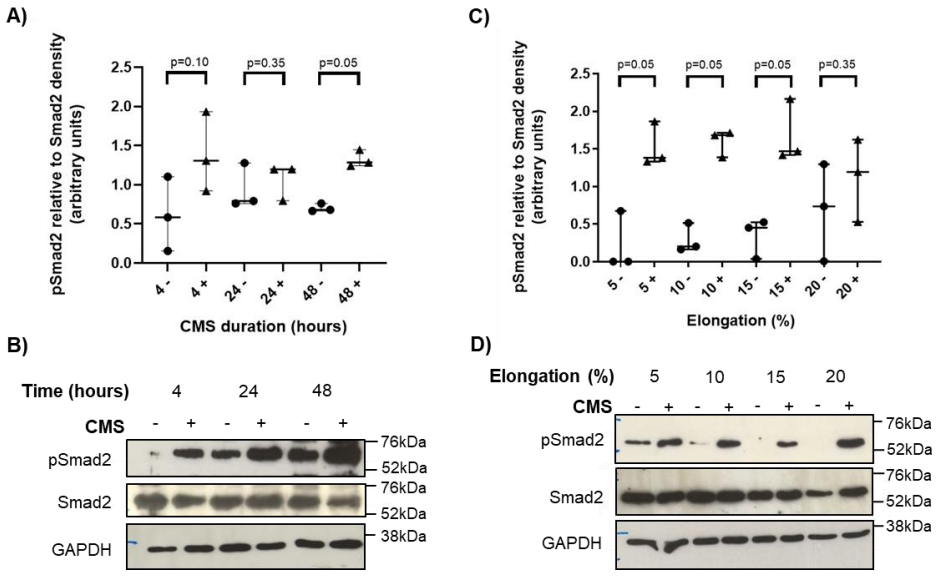

Figure 7-2: CMS induces TGFβ signalling in WT MEFs

WT MEFs were subject to 15% CMS at 1Hz for 4, 24 and 48 hours (A,B), or 48 hours of 1Hz CMS at 5%, 10%, 15%, or 20% elongation (C,D).

A) Relative pSmad2/Smad2 densitometry from 3 independent CMS time course experiments.

B) Representative pSmad2, Smad2 and GAPDH western blot from CMS time course experiments.

C) Relative pSmad2/Smad2 densitometry from 3 independent dose-response CMS experiments.

D) Representative pSmad2, Smad2 and GAPDH western blot from CMS dose-response experiments

Graphs show median ± interquartile range from 3 independent experiments. Statistical analyses performed using one-tailed Mann-Whitney Test comparing each stretch condition with the corresponding unstretched control. (-) = unstretched cells, (+) = stretched cells. Western blots representative of 3 independent experiments.

These data indicate that a CMS regimen of 15% elongation, at a frequency of 1Hz, for 48 hours induces TGFβ signalling in WT MEFs. As 15% elongation was estimated to represent a degree of stretch relevant to breathing, and any alteration to the percentage elongation did not alter the pSmad2 signal, this was deemed to be the optimal degree of stretch for further CMS experiments.

7.4.2 CMS increases TGFβ activation in IPF lung fibroblasts to a greater extent than non-IPF lung fibroblasts

Having found that breathing-related CMS induces TGFβ signalling in murine embryonic cells, experiments were carried out to assess the role of CMS-induced TGFβ signalling in adult human lung fibroblasts.

Similar to WT MEFs, breathing-related CMS increased pSmad2 expression in HLFs from donors with IPF and non-diseased controls at 48 hours (Figure 7-3A,B; $p<0.01$). Non-fibrotic HLFs exhibited an increase in median pSmad2/Smad2 expression of 0.01 (unstretched) to 1.24 Arbitrary Units (AU) (stretched) (Figure 7-3A,B, $p<0.01$). IPF HLFs also increased the median pSmad2/Smad2 expression with cyclical stretch from 0.06 to 2.97 AU ($p<0.01$), and this stretch-induced pSmad2 expression was greater than that observed in non-fibrotic HLFs (Figure 7-3; 1.24 vs 2.97U, $p<0.01$). A TMLC-HLF co-culture CMS system confirmed a greater CMS-induced TGFβ signalling response in IPF HLFs compared with HLFs from non-diseased donors (Figure 7-3C, 5 non-fibrotic vs 5 IPF HLF lines, $p=0.04$). While CMS-induced TGFβ signalling was consistent in HLFs, this was less than that induced by 2ng/ml TGFβ for 1 hour (Figure 7-3D) and, in most cases, 500pg/ml TGFβ signalling (Figure 7-3E). These data indicate that breathing-related CMS induces TGFβ signalling in HLFs, and IPF cells generate a greater degree of TGFβ signalling in response to CMS. However, the degree of TGFβ signalling induced by CMS was often less than that observed with 500pg/ml TGFβ stimulation.

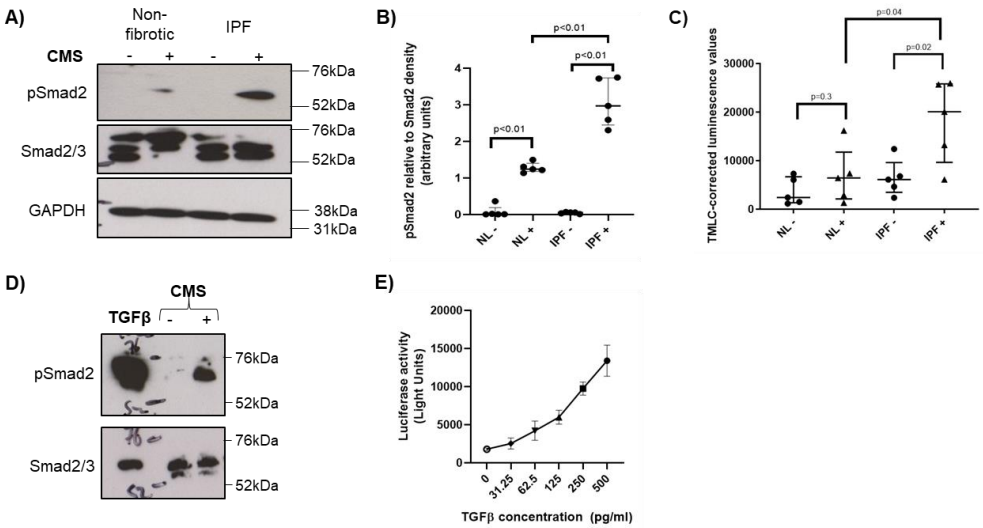

Figure 7-3: Breathing-related CMS induces a greater TGFβ signalling response in IPF lung fibroblasts compared with non-diseased cells

CMS was applied to HLFs from 5 non-fibrotic and 5 IPF donors at 15% elongation and 0.3Hz for 48 hours.

A) Representative pSmad, Smad2/3 and GAPDH western blot of non-fibrotic and IPF HLF cell lines subject to CMS.

B) Relative pSmad2/ total Smad2 densitometry from western blots of 5 non-fibrotic and 5 IPF HLF cell lines subject to CMS.

C) Luminescence from TMLC-HLF stretch co-culture assay using 5 non-fibrotic and 5 IPF HLF cell lines in independent experiments.

D) Representative pSmad2 and Smad2/3 western blot of HLFs subject to CMS, alongside cells treated with 2ng/ml TGFβ for 16 hour.

E) Luminescence values from TMLCs treated with 31.25-500pg/ml TGFβ for 24 hours. Data shown as mean ± SEM from 4 independent TMLC standard curves.

Densitometry data shown as median ± interquartile range. Statistical analyses performed using two-tailed Mann Whitney test. NL = normal (non-diseased), (-) unstretched, (+) stretched.

To further assess the effect of CMS on profibrotic signalling, TGFβ-related gene expression was assessed in HLFs subject to CMS using qPCR. 48 hours of CMS induced a significant increase in *TGFB1* and *PAI-1* mRNA expression in non-fibrotic HLFs (median fold increase with stretch 2.6 and 1.8 respectively, $p<0.01$; Figure 7-4A,C). A trend towards increased *TGFβ1* and *PAI-1* mRNA was also seen in IPF HLFs subject to CMS (median fold increase with stretch 1.3 and 1.6 respectively) but this did not reach statistical significance (Figure 7-4B,D).

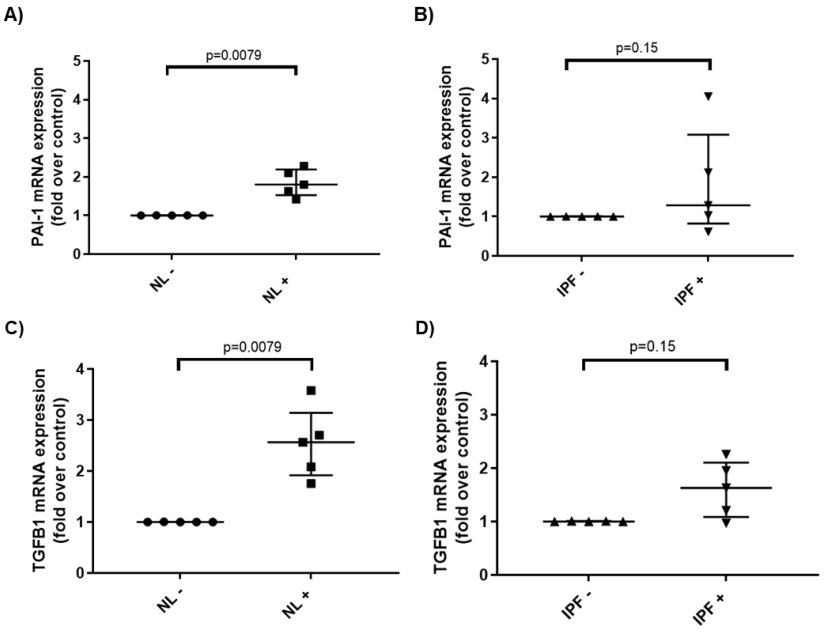

Figure 7-4: CMS induces *PAI-1* and *TGFB1* mRNA expression in human lung fibroblasts

HLFs from non-diseased (NL) and IPF (IPF) donors were subject to 48 hours CMS at 1Hz and 15% elongation.

A, B) PAI-1 mRNA expression in non-diseased (A) and IPF (B) HLFs subject to CMS
C, D) TGFB1 mRNA expression in non-diseased (C) and IPF (D) HLFs subject to CMS
Data shown as median ± interquartile range. Statistical analyses performed using two-tailed Mann Whitney test. (-) unstretched, (+) stretched.

Overall, these data demonstrate that breathing-related CMS induces TGFβ signalling and TGFβ-related gene expression in HLFs. CMS-induced TGFβ signalling is greater in fibrotic HLFs than in non-diseased cells, but this may not translate to greater increases in TGFβ-related mRNA expression.

7.4.3 CMS has no effect on total αSMA protein expression in MEFs or human lung fibroblasts

TGFβ is an established stimulus of fibroblast to myofibroblast differentiation, a key process in the pathogenesis of IPF (69). As earlier data demonstrated that CMS induces TGFβ signalling, the effect of CMS on the expression of αSMA, a myofibroblast marker, was assessed.

CMS did not increase total αSMA protein expression in WT MEFs stretched between 5%-20% elongation at 1Hz for 48 hours (Figure 7-5A). Similarly, neither IPF nor non-diseased HLFs increased total αSMA protein expression in response to 48 hours of breathing-related CMS (Figure 7-5B). Furthermore, mRNA analysis of HLFs subject to CMS demonstrated a small decrease in *ACTA2* mRNA expression with CMS in IPF HLFs (median fold change in *ACTA2* mRNA expression 0.68, IQR 0.52-0.91, p=0.03). However, this failed to reach statistical significance in non-diseased cells (median fold change in *ACTA2* mRNA expression 0.76, IQR 0.67-1.06; p=0.69) (Figure 7-5D). These data suggest that 48 hours of CMS does not significantly alter the myofibroblast phenotype.

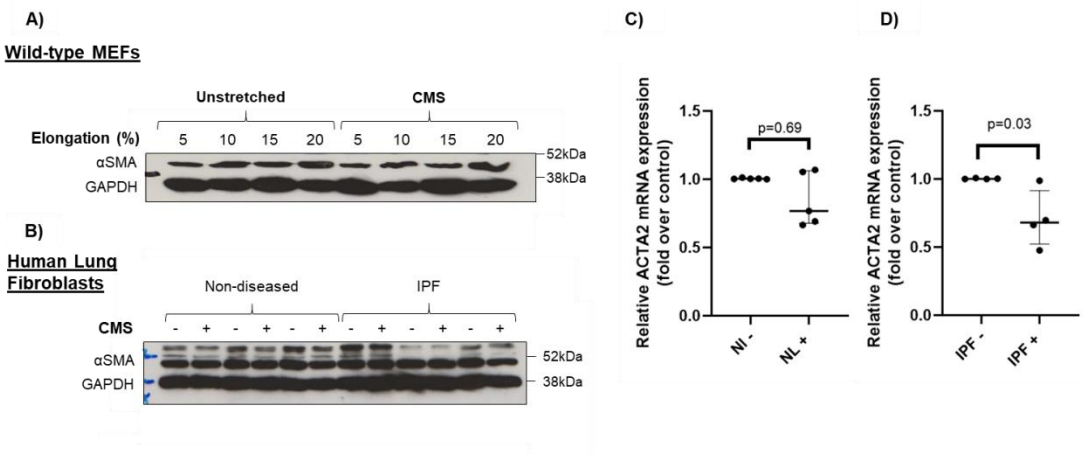

Figure 7-5: CMS does not affect αSMA protein expression in murine embryonic or adult human lung fibroblasts

WT MEFs and HLFs were subject to 48 hours of breathing-related CMS.

A) Representative αSMA and GAPDH western blot from WT MEFs subject to CMS at 1Hz and increasing degrees of elongation.

B) αSMA and GAPDH western blot from 3 non-fibrotic and 3 IPF HLF lines subject to CMS at 0.3Hz and 15% elongation. This result was validated in a further 3 non-fibrotic and 3 IPF HLF lines.

C, D) *ACTA2* mRNA expression in non-diseased (C) and IPF HLFs subject to CMS at 0.3Hz and 15% elongation.

Data shown as median ± interquartile range. Statistical analyses performed using two-tailed Mann Whitney test. NL = normal (non-diseased), (-) unstretched, (+) stretched.

7.4.4 Genetic knockdown of $G_{\alpha q/11}$ inhibits CMS-induced TGFβ activation in MEFs and HLFs

Subsequent experiments were performed to identify the molecular mechanisms underlying CMS-induced TGFβ signalling. The expression

of pSmad2 in response to 48 hours of CMS in *Gnaq*$^{-/-}$;*Gna11*$^{-/-}$ MEFs was compared with that of WT MEFs. WT MEFs increased pSmad2 expression with CMS, with a median pSmad2/Smad2 expression increase from 0.65 AU to 1.67 AU (p=0.03) with CMS (Figure 7-6A,B). However, pSmad2 expression in *Gnaq*$^{-/-}$;*Gna11*$^{-/-}$ MEFs subject to CMS was lower than that observed in WT MEFs (1.67AU vs 0.29AU; p=0.03) (Figure 7-6A,B). *Gna12*$^{-/-}$;*Gna13*$^{-/-}$ MEFs had a similar CMS-induced increase in pSmad2 expression to WT MEFs (Figure 7-6A). These data indicate that $G_{\alpha q/11}$ is a key mediator of CMS-induced TGFβ signalling in embryonic fibroblasts, and that this is specific to the $G_{\alpha q/11}$ family of G_{α} subunits.

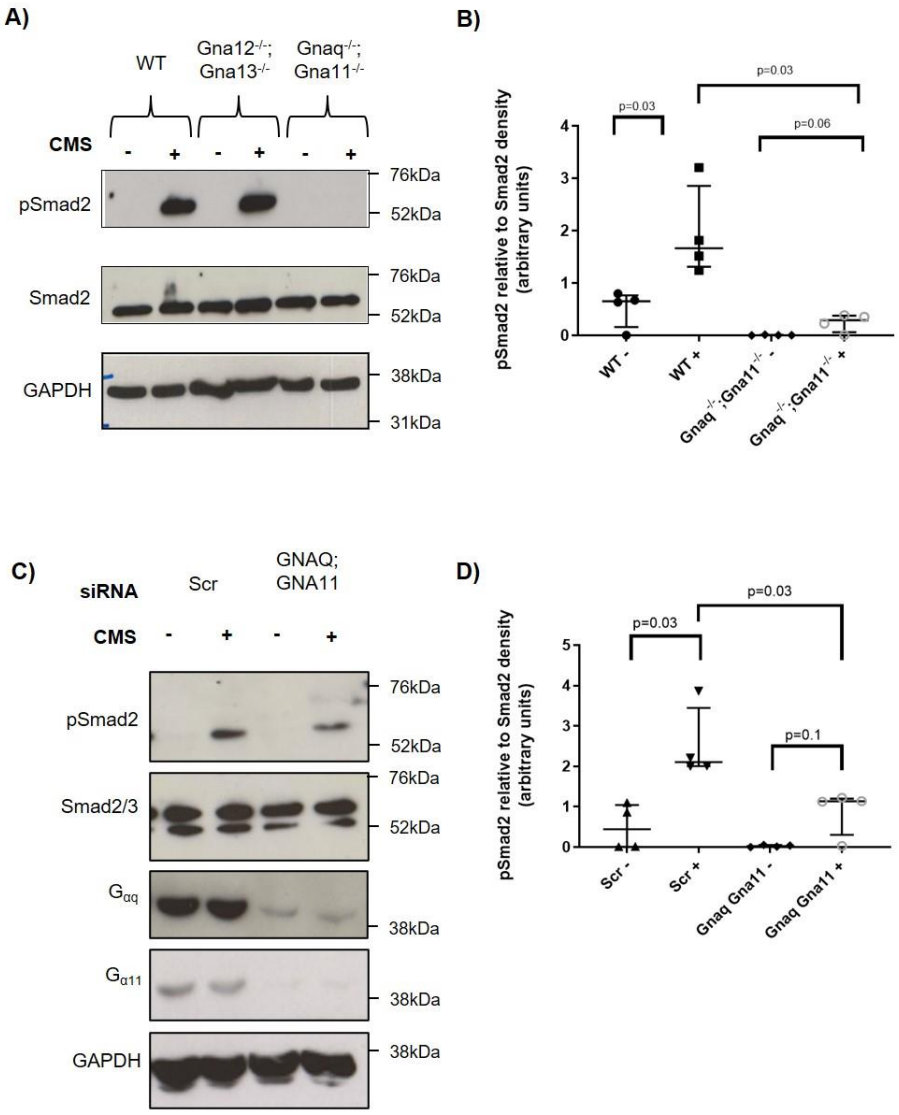

Figure 7-6: $G_{\alpha q/11}$ mediates CMS-induced TGFβ signalling in MEFs and HLFs

MEFs (A,B) and HLFs (C,D) with either intact $G_{\alpha q/11}$ signalling or genetic $G_{\alpha q/11}$ knockdown were subject to breathing-related CMS, and TGFβ signalling assessed by pSmad2 western blot

A) Representative pSmad2, Smad2, and GAPDH western blot from wild-type (WT), *Gna12*$^{-/-}$*;Gna13*$^{-/-}$, and *Gnaq*$^{-/-}$*Gna11*$^{-/-}$ MEFs subject to CMS.

B) Relative pSmad2/Smad2 densitometry in WT, *Gna12*$^{-/-}$*;Gna13*$^{-/-}$, and *Gnaq*$^{-/-}$*Gna11*$^{-/-}$ MEFs subject to CMS

C) Representative pSmad2, Smad2/3, GAPDH, $G_{\alpha q}$, and $G_{\alpha 11}$ western

blot in HLFs subject to siRNA-induced *GNAQ* and *GNA11* knockdown and CMS.
D) Relative pSmad2/Smad2 densitometry from western blots of HLFs with siRNA-induced *GNAQ* and *GNA11* knockdown subject to CMS
Data shown as median ± interquartile range, n=4. Statistical analyses performed using two-tailed Mann Whitney Tests. (+) CMS; (-) unstretched

To validate this finding in adult lung fibroblasts, non-diseased HLFs were subject to $G_{\alpha q/11}$ knockdown using *GNAQ* and *GNA11* siRNA. In these experiments, 24 hours of cyclical stretch was used rather than the 48 hours used in other experiments, to ensure that the CMS regimens occurred during the period of siRNA-induced *GNAQ* and *GNA11* knockdown (72-96 hours after siRNA transfection). HLFs with siRNA-induced $G_{\alpha q/11}$ knockdown had a blunted TGFβ signalling response to 24 hours of CMS compared to HLFs treated with non-targeting siRNA (relative pSmad2 to Smad2 densitometry values of 2.1 AU with control siRNA compared with 1.1 AU with *GNAQ* and *GNA11* siRNA, p=0.03; Figure 7-6C,D).

Converse to the above data, a chemical inhibitor of $G_{\alpha q/11}$, YM-254890, did not inhibit CMS-induced TGFβ signalling in HLFs at concentrations at the typically used concentration of 1μM (Figure 7-7).

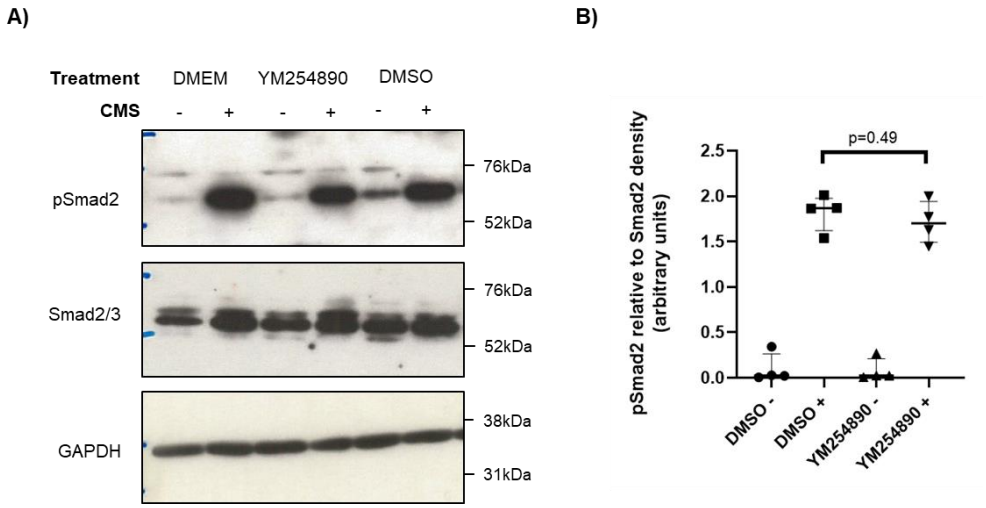

Figure 7-7: Chemical inhibition of $G_{\alpha q/11}$ does not inhibit CMS-induced TGFβ signalling

HLFs were subject to 48 hours of breathing-related CMS in the presence of 1µM YM254890.

A) Representative pSmad2, Smad2/3, and GAPDH western blot

B) Relative pSmad2/Smad2 densitometry from 4 western blots.

Data shown as median ± interquartile range, n=4. Statistical analyses performed using two-tailed Mann Whitney Tests. (+) CMS; (-) unstretched

Overall, these findings suggest that $G_{\alpha q/11}$ is a key component of CMS-induced TGFβ activity in both embryonic and adult fibroblasts. However, genetic knockdown of $G_{\alpha q/11}$ rather than chemical inhibition is required to reduce CMS-induced TGFβ signalling.

7.4.5 CMS induces TGFβ signalling via a ROCK- and integrin-independent pathway

As Rho-ROCK signalling occurs downstream of $G_{\alpha q/11}$ (74) and has been implicated in stretch-mediated TGFβ activation (113), the ROCK1/2 inhibitor Y-27632 was used in the breathing-related CMS system to assess the role of ROCK in CMS-induced TGFβ signalling in fibroblasts.

ROCK1/2 inhibition did not reduce stretch-induced TGFβ signalling in MEFs or HLFs (Figure 7-8), even at concentrations far exceeding the IC_{50} of Y27632 (K_i=140nM (355)). This suggests that ROCK is not an essential component of the stretch-mediated TGFβ activation pathway in fibroblasts.

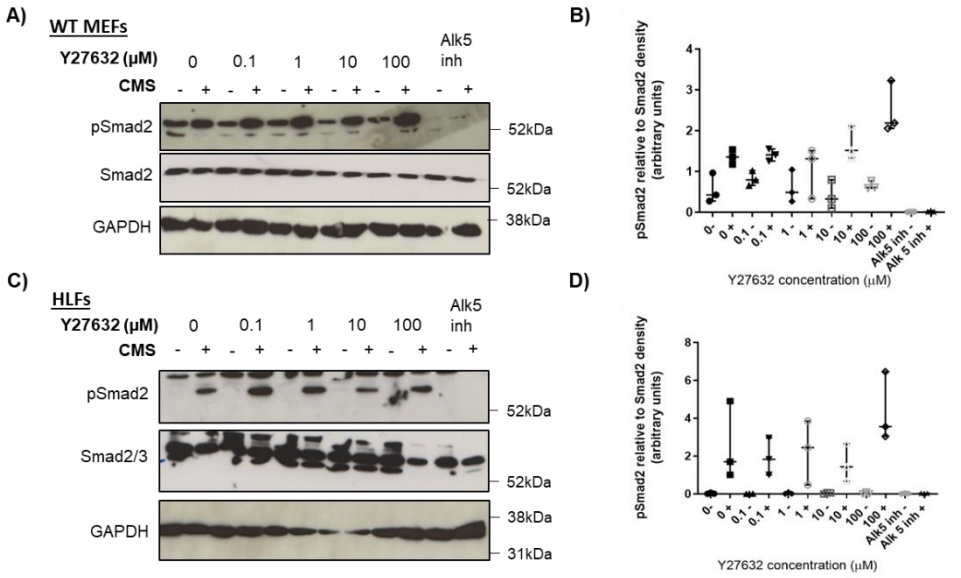

Figure 7-8: CMS-induced TGFβ signalling is a ROCK-independent process

WT MEFs (A,B) and non-diseased HLFs (C,D) were treated with 10μM of the ROCK1/2 inhibitor Y27632 then subject to breathing-related CMS for 48 hours.

A) Representative pSmad2, Smad2, and GAPDH western blot of wild type MEFs treated with Y27632 then subject to 48 hours of CMS.

B) Relative pSmad2/ Smad2 densitometry from western blots of wild-type MEFs treated with Y27632 then subject to CMS.

C) Representative pSmad2, Smad2/3, and GAPDH western blot of HLFs treated with Y27632 then subject to 48 hours of CMS.

D) Relative pSmad2 to Smad2 densitometry from western blots of HLFs treated with Y27632 then subject to CMS.

Data shown as median ± interquartile range, n=3 for each experiment. (+) stretched; (-) unstretched. Alk5 inh = 50μM Alk5 inhibitor (SB525334).

As cell surface integrins play key roles in the activation of TGFβ, and several integrins are expressed by fibroblasts and drive TGFβ activation (356, 357), the effects of integrin inhibition on CMS-induced TGFβ signalling in fibroblasts was assessed. The pan-αv integrin inhibitor CWHM-12 (a gift from Dr David Griggs, St Louis University) did not reduce cyclical stretch-induced TGFβ signalling in HLFs (Figure 7-9A,B). Furthermore, β1 integrin inhibition with NOTT199SS had no effect on CMS-induced TGFβ signalling in human lung fibroblasts (Figure 7-9C,D). Together, these results imply that CMS-induced TGFβ signalling in fibroblasts is integrin-independent.

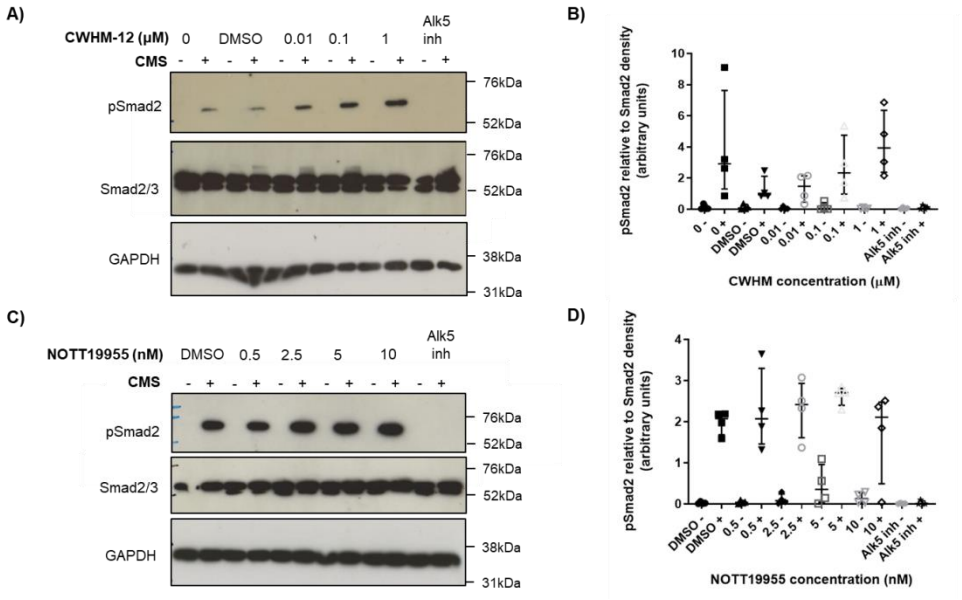

Figure 7-9: αv and β1 integrins are not required for CMS-induced TGFβ signalling in human lung fibroblasts

Non-diseased HLFs were subject to 48 hours of breathing-related CMS in the presence of inhibitors of αv integrins (A,B) or β1 integrins (C,D).

A) Representative pSmad2, Smad2/3, and GAPDH western blot of HLFs subject to CMS in the presence of increasing concentrations of CWHM-12.

B) pSmad2/Smad2 densitometry of HLFs subject to CMS in the presence of CWHM-12.

C) Representative pSmad2, Smad2/3, and GAPDH western blot of HLFs subject to CMS in the presence of NOTT199SS.

D) pSmad2/ Smad2 densitometry of HLFs subject to CMS in the presence of NOTT199SS.

Data shown as median ± interquartile range, n=4. Statistical analysis performed using two-tailed Mann Whitney Tests. (+) stretched; (-) unstretched. Alk5 inh = 50μM Alk5 inhibitor (SB525334).

Overall, these findings indicate that breathing-related CMS-induced TGFβ signalling occurs via a ROCK- and integrin-independent pathway in fibroblasts.

7.4.6 CMS-induced TGFβ signalling requires the activity of serine proteases, but not matrix metalloproteinases

Protease activity can induce TGFβ activation independently of integrins (68), therefore the effect of serine protease and matrix metalloproteinase (MMP) activity on CMS-induced TGFβ signalling in fibroblasts was assessed.

The MMP inhibitor GM6001 did not inhibit CMS-induced TGFβ signalling at any of the concentrations tested (Figure 7-10A,B). Conversely, the serine protease inhibitor AEBSF inhibited CMS-induced TGFβ signalling at 10μM and 100μM when compared with cells not treated with AEBSF (CMS-induced pSmad2/Smad2 density values 0.20 and 1.10AU for 10μM and 100μM, respectively, vs 4.93 AU on untreated cells; p=0.03) (Figure 7-10C,D). These data indicate that CMS-induced TGFβ signalling requires serine protease activity.

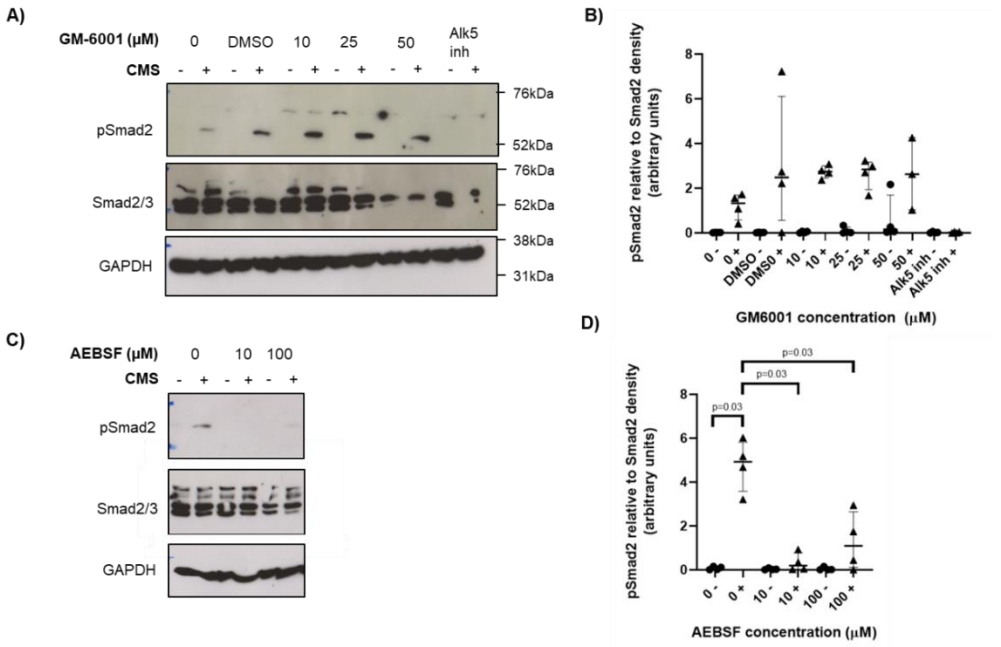

Figure 7-10: CMS-induced TGFβ signalling requires serine proteases but not matrix metalloproteinases

HLFs were subject to 48 hours of breathing-related CMS in the presence of increasing concentrations of an MMP inhibitor (GM6001) (A,B) or a serine protease inhibitor (AEBSF).

A) Representative pSmad2, Smad2/3, and GAPDH western blot from HLFs subject to CMS in the presence of GM6001.

B) Relative pSmad2/ Smad2 densitometry from HLFs subject to CMS in the presence of GM6001.

C) Representative pSmad2, Smad2/3, and GAPDH western blot from HLFs subject to CMS in the presence of AEBSF.

D) Relative pSmad2/ Smad2 densitometry from HLFs subject to CMS in the presence of AEBSF.

Data shown as median ± interquartile range, n=4. Statistical analyses performed using two-tailed Mann Whitney tests. (+) stretched; (-) unstretched. Alk5 inh = 50μM Alk5 inhibitor (SB525334).

7.4.7 $G_{\alpha q/11}$-deficient cells generate less TGFβ2

Proteases can activate all three TGFβ isoforms, however TGFβ1 and TGFβ3 are preferentially activated by integrins (66, 68). Therefore, the expression of TGFβ2 in response to CMS and $G_{\alpha q/11}$ knockdown was assessed in fibroblasts.

HLFs subject to siRNA-induced $G_{\alpha q/11}$ knockdown expressed less TGFβ2 protein than cells treated with non-targeting siRNA, with a median pSmad2/Smad2 densitometry reduction from 1.41AU with non-targeting siRNA to 0.50 AU with *GNAQ* and *GNA11* siRNA (p=0.03; Figure 7-11A,B). This observation was specific to TGFβ2, as TGFβ1 levels were not altered by $G_{\alpha q/11}$ knockdown (median pSmad2/Smad2 densitometry 0.95AU with control siRNA and 1.05AU with *GNAQ* and *GNA11* siRNA, p=0.34; Figure 7-11C,D). 24 hours of CMS did not alter TGFβ1 or TGFβ2 protein expression (Figure 7-11A,C). Overall, these data suggest that $G_{\alpha q/11}$ signalling contributes to TGFβ2 production, which may then subsequently be deposited in the ECM and amenable to protease-induced activation.

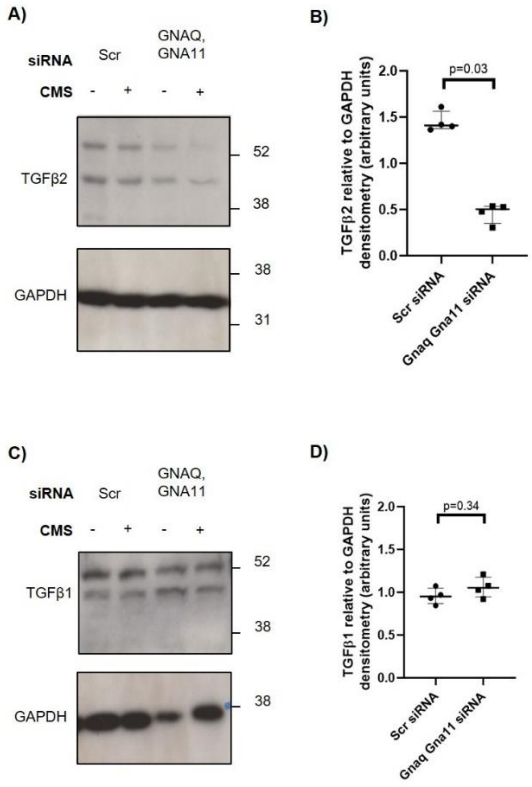

Figure 7-11: TGFβ2 protein expression is reduced by $G_{\alpha q/11}$ knockdown, but not affected by CMS

Non-fibrotic HLFs were subject to siRNA-induced $G_{\alpha q/11}$ knockdown then 24 hours of cyclical stretch.

A) Representative TGFβ2 western blot of HLFs subject to non-targeting (Scr) or *GNAQ* and *GNA11* siRNA, then CMS.

B) Relative TGFβ2/ GAPDH densitometry from HLFs with $G_{\alpha q/11}$ knockdown then subject to CMS.

C) Representative TGFβ1 western blot of HLFs subject to non-targeting (Scr) or *GNAQ* and *GNA11* siRNA, then CMS.

B) Relative TGFβ1/ GAPDH densitometry from HLFs with $G_{\alpha q/11}$ knockdown then subject to CMS.

Data shown as median ± interquartile range, n=4. Statistical analyses performed using two-tailed Mann Whitney tests. (+) stretched; (-) unstretched.

7.4.8 Mesenchymal $G_{\alpha q/11}$ knockout mouse lungs contain reduced amounts of TGFβ2

As the above data suggest that mesenchymal $G_{\alpha q/11}$ deficiency results in impaired TGFβ2 production, and TGFβ signalling is essential for normal lung development, TGFβ2 expression in *Pdgfrb-Cre*$^{+/-}$;*Gnaq*$^{fl/fl}$;*Gna11*$^{-/-}$ lungs was assessed using immunohistochemistry.

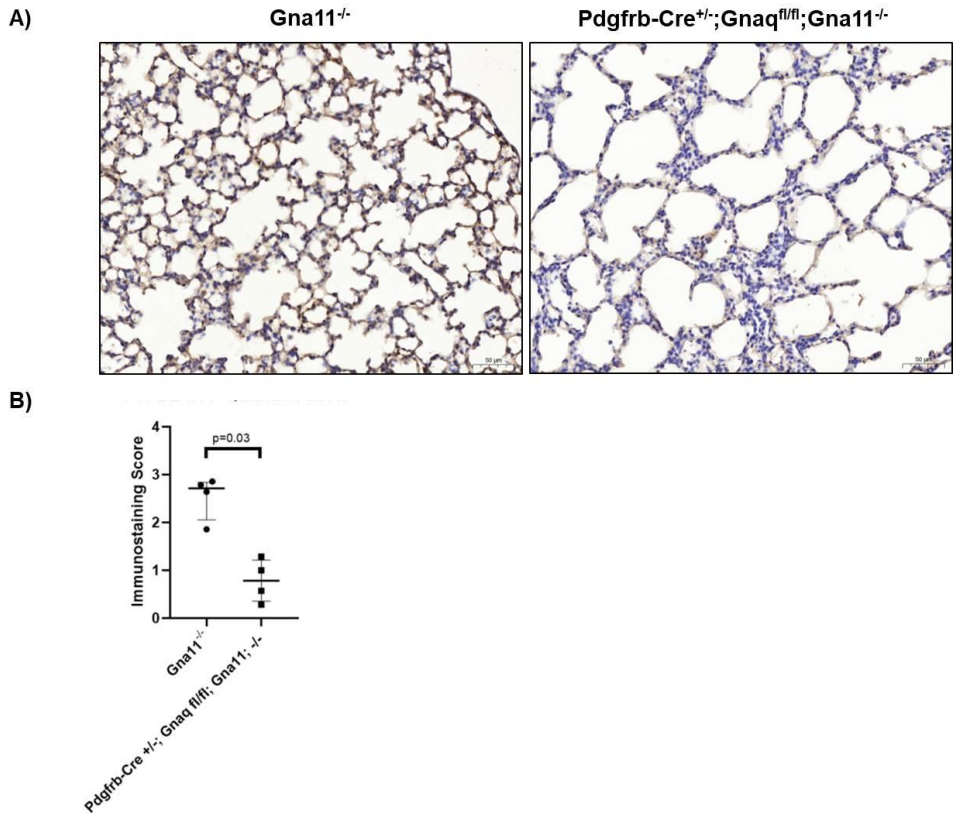

Figure 7-12: The lungs of mice lacking mesenchymal $G_{\alpha q/11}$ contain less TGFβ2

A) Representative TGFβ2 immunohistochemistry images from 2 week old *Gna11*$^{-/-}$ (left) and *Pdgfrb-Cre*$^{+/-}$;*Gnaq*$^{fl/fl}$;*Gna11*$^{-/-}$ (right) mouse lungs. Staining performed by Chitra Joseph, Division of Respiratory Medicine, University of Nottingham.

B) TGFβ2 immunostaining score of 2 week old *Gna11*$^{-/-}$ and *Pdgfrb-Cre*$^{+/-}$;*Gnaq*$^{fl/fl}$;*Gna11*$^{-/-}$ mouse lungs. 4 mice per group, 7 images analysed per mouse. Data shown as median ± interquartile range. Statistical analysis performed using a two-tailed Mann Whitney test.

Pdgfrb-Cre$^{+/-}$;*Gnaq*$^{fl/fl}$;*Gna11*$^{-/-}$ mouse lungs contained significantly less TGFβ2 than *Gna11*$^{-/-}$ controls (Figure 7-12), suggesting that mesenchymal cell $G_{\alpha q/11}$ may be involved in TGFβ2 production. This finding implies that the abnormal alveolarisation seen in *Pdgfrb-Cre*$^{+/-}$

;Gnaq$^{fl/fl}$*;Gna11*$^{-/-}$ mouse lungs may occur due to TGFβ deficiency, and implies a potential isoform-specific role for TGFβ2 in alveolarisation.

7.5 Discussion

TGFβ signalling is a key factor in the pathogenesis of IPF and in normal lung development. Mechanical stretch has been shown to induce TGFβ signalling in several disease models (113, 180, 181, 183-186, 188, 219, 349-354). Breathing-related CMS is a ubiquitous stimulus in the lungs, however the role of breathing-related CMS on TGFβ signalling in lung fibroblasts has not been previously investigated.

This work demonstrated that breathing-related CMS induces TGFβ signalling in both embryonic and adult fibroblasts, and that this occurs via a previously undescribed ROCK- and integrin-independent pathway that requires serine protease activity. The findings of this study also suggest that $G_{\alpha q/11}$ signalling drives the production of TGFβ2, and the working hypothesis from these data is that this may lead to increased TGFβ2 deposition in the ECM which is then susceptible to protease-mediated activation (Figure 7-13). One or several of these pathway components may be dysregulated in IPF, leading to the excessive CMS-induced TGFβ signalling in IPF lung fibroblasts observed in this study. A greater understanding of these pathways may identify novel therapeutic targets for use in the management and prevention of pulmonary fibrosis, as well as developmental lung diseases such as BPD.

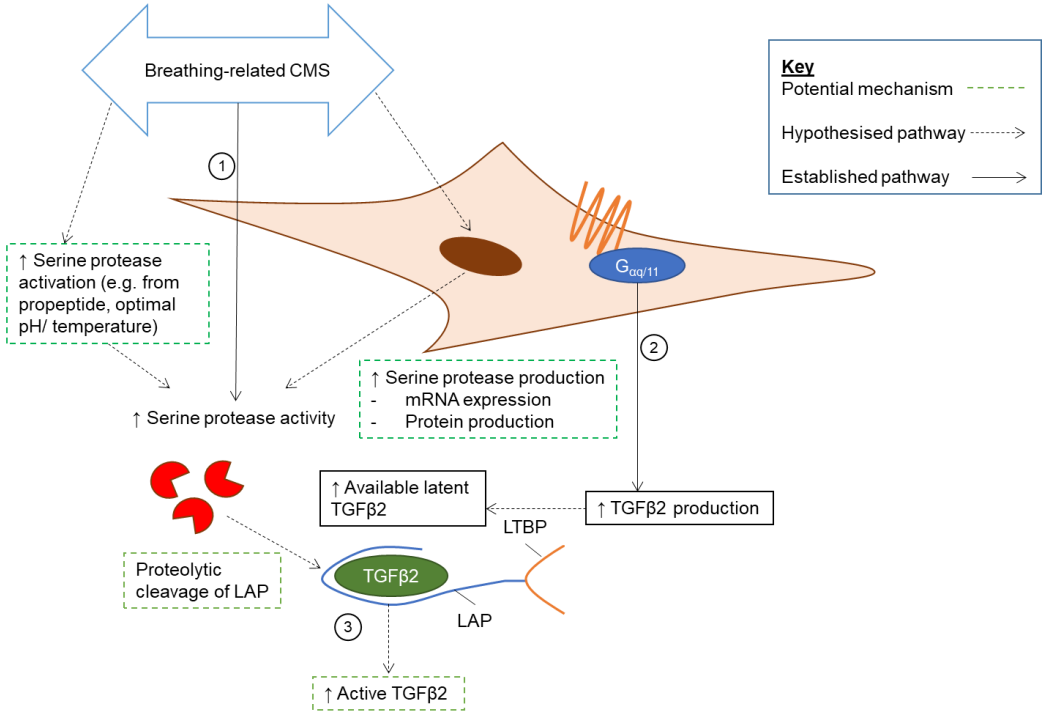

Figure 7-13: The mechanisms of CMS-induced TGFβ signalling in lung fibroblasts

Breathing-related CMS increases serine protease activity, potentially via increased activity of existing proteases or increased serine protease production (1). $G_{\alpha q/11}$ signalling increases TGFβ2 protein production (2), leading to greater availability of latent TGFβ2 in the ECM available for protease-mediated activation (3).

LAP = latency associated peptide; LTBP = latent TGFβ binding protein**.**

Solid boxes arrows show mechanisms demonstrated by this study.

Dashed arrows show hypothesised pathways.

Initial experiments focussed on identifying the optimal CMS protocol, in terms of duration and degree of elongation, for assessing CMS-induced TGFβ signalling. CMS at a physiologically-relevant rate (1Hz in murine cells) consistently induced pSmad2 expression in WT MEFs at 48 hours. This time point was therefore used for most subsequent CMS experiments, unless experiment-specific issues precluded this. CMS

experiments involving siRNA-induced $G_{\alpha q/11}$ knockdown were performed for 24 hours to ensure that CMS was applied while $G_{\alpha q/11}$ expression was reduced. Experiments involving the PLC inhibitor U73122 were also performed using 24 hours of CMS, due to cell death observed at 48 hours.

In this work, no relationship between the degree of CMS elongation and TGFβ signalling was found in WT MEFs. Conversely, Froese et al reported a dose-response relationship between the force applied to fibrotic rat lung strips and TGFβ activation (113). The results of the present study are not comparable to this earlier work for several reasons. Lung tissue slices consist of multiple different cell types and connective tissue structures, unlike the fibroblast monolayers used in this study. Additionally, Froese et al used a CMS frequency twice that used here (2Hz vs 1Hz on animal samples), and TGFβ signalling was assessed at an earlier time point (15 minutes vs 48 hours). Therefore, direct comparisons in terms of a dose-response relationship between CMS and TGFβ signalling, cannot be made between the two studies.

An alternative explanation for the lack of CMS-induced TGFβ signalling dose-response relationship observed in this study is that there is a stretch threshold above which the degree of TGFβ activation does not increase further. If this threshold is lower than the lowest degree of stretch investigated in this study (5% elongation), then no CMS-TGFβ signalling dose-response relationship could be observed using this model. However, as CMS with 5% elongation is at the lower end of the

degree of stretch induced by physiological breathing (358), it is unlikely that such a threshold of TGFβ activation would have been reached in these experiments.

Following the initial dose-response experiments, 15% elongation was used for further CMS regimens. This decision was based on the consistent CMS-induced TGFβ signalling response to 15% elongation in MEFs, and the published literature. Given the heterogeneous distribution of mechanical forces in the lung (172), and the fact that cells adjacent to fibrotic areas may be subject to increased stretch forces (113, 359), it is difficult to estimate the degree of stretch a typical lung fibroblast is subject to *in vivo* in health and disease. A study of *ex vivo* rat lung ventilation reported that a 20% increase in epithelial basement membrane surface area occurs with breathing at 40-90% of total lung capacity (358). The 15% elongation used in the present study lies within this range, although unlike epithelial cells lung fibroblasts do not “pleat” at low lung volumes, and therefore fibroblast stretch may have a different relationship to lung inflation. In addition, several studies of lung disease have used 15% elongation using the Flexcell® and other systems (113, 182, 190, 191, 198, 207, 360). Finally, in the present work 5% and 10% elongation induced the same degree of TGFβ signalling as 15% elongation, therefore it is unlikely that the data would have changed even if 15% is an overestimate of breathing-related CMS. 20% elongation gave inconsistent TGFβ signalling in the Flexcell® model, possibly because of cell detachment, therefore was not used for further experiments.

While the degree to which lung fibroblasts are stretched by breathing is unclear, normal respiration was mimicked as closely as possible in this study by using physiologically-relevant respiratory rates (60 or 18 stretch cycles per minute in mouse and human cells, respectively). This is the first study to investigate the effect of physiological breathing on TGFβ signalling in lung fibroblasts.

The initial optimisation experiments investigating CMS-induced TGFβ signalling were carried out in MEFs, however previous work suggests that embryonic cells have different TGFβ signalling responses to stretch compared with adult differentiated cells (361). 48 hours of breathing-related CMS consistently induced TGFβ signalling in HLFs, validating the applicability of this Flexcell® CMS-induced TGFβ signalling to both developmental and adult disease models. Therefore, MEFs and HLFs were used for the subsequent mechanistic experiments.

In this study, phosphorylation of Smad2, which occurs directly downstream of TGFβ activating its receptor (7), was used as a measure of TGFβ activation. Previous studies of CMS-induced TGFβ activity measured TGFβ production, by assessing *TGFB1* mRNA (180-184, 187, 190, 216, 362, 363) or protein expression by enzyme-linked immunosorbent assay (ELISA) (181, 184, 186, 364, 365). Alternatively, some groups performed TGFβ-induced luciferase activity assays on stretch-conditioned media, which often requires heat or acid-mediated activation of TGFβ within the samples (189, 366). However, these methods do not indicate TGFβ activation by the experimental conditions,

nor do they confirm the induction of signalling downstream of TGFβ. While it could be argued that CMS could increase pSmad2 expression via a non-TGFβ-induced signalling pathway, for example via MAPK signalling (367), a TGFβ receptor inhibitor (SB-525334) completely inhibited CMS-induced pSmad2 expression in all of the chemical inhibitor experiments in this study. Additionally, TMLC-HLF co-culture experiments and TGFβ-related mRNA expression assays confirmed that breathing-related CMS induces TGFβ signalling under the same conditions. Therefore, Smad2 phosphorylation was used as the primary measure of TGFβ signalling in this study.

It is likely that CMS induces low level TGFβ signalling in fibroblasts, based on the lower pSmad2 expression in CMS-stimulated samples compared with 2ng/ml TGFβ stimulated controls (Figure 7-3). This relatively low TGFβ signalling compared with that seen in whole lung slice models likely reflects the lower number of cells present in monolayer culture (113). Additionally, lung slices contain epithelial cells, which express a different integrin repertoire and therefore have different TGFβ-activating capabilities to fibroblasts (74, 126, 357, 368). It is impossible to extrapolate the active TGFβ concentration induced by CMS from the western blots in this study, however previous publications have suggested that CMS may induce active TGFβ concentrations as low as 75-100pg/ml (186). It could therefore be argued that the degree of CMS-induced TGFβ activation is too low to have any relevant effect. Conversely, this study found that HLFs from IPF donors had elevated

CMS-induced TGFβ signalling compared with non-fibrotic HLFs using two independent assays, suggesting that this is a disease-relevant process. As breathing-related CMS is a continuous stimulus in all human lungs, even low-level increases in TGFβ signalling could facilitate fibrogenesis over time. Therefore, breathing-related CMS of fibroblasts may contribute to the pathogenesis of IPF.

The distribution of CMS forces is altered in the fibrotic lung, due to alveolar collapse in fibrotic areas and corresponding over distension of surrounding alveoli (176, 177). Mechanical forces are further disturbed by surfactant abnormalities in IPF, which result in increased alveolar surface tension and greater strain (178, 369-372). The fibroblast monolayers used in this study would not have formed the mature lung structure or established the architectural distortion of the surroundings typical of IPF, yet were still more sensitive to CMS in terms of TGFβ activation. This novel finding supports the hypothesis that IPF fibroblasts have inherent differences that increase their sensitivity to CMS, and challenges the concept that fibroblasts merely respond to profibrotic stimuli during fibrogenesis. Alternatively, IPF cells may produce ECM with properties that facilitate CMS-induced TGFβ signalling, e.g. by having greater stiffness (168, 373) or TGFβ content. This study demonstrates that fibroblast CMS-induced TGFβ signalling is an important driver of IPF, and may contribute to the progressive nature of pulmonary fibrosis.

The data from this study have several clinical implications. Patients with IPF are prone to developing acute exacerbations when mechanically ventilated (173-175), and a better understanding of the mechanisms involved in stretch-induced TGFβ activation could identify targets for novel therapeutics to prevent ventilator-associated acute exacerbations in those at risk. Similar to IPF, genetic variants have been linked to greater susceptibility to developing BPD if a baby is born prematurely (43). It is possible that lung fibroblasts from BPD patients may behave differently to healthy lung fibroblasts in response to CMS, and this could explain inter-patient differences in the susceptibility to BPD. While this is a speculative hypothesis, the response of BPD lung fibroblasts to CMS warrants further investigation.

TGFβ signalling is known to promote fibroblast to myofibroblast differentiation (69), however this study found that αSMA protein expression was not affected by CMS in MEFs or HLFs. While this seems counterintuitive, this finding is consistent with previous work on stretch of fibroblasts and myofibroblasts (190, 374, 375). It is possible that, while the overall expression of αSMA is unchanged, CMS alters the incorporation of αSMA into intracellular stress fibres, leading to a more myofibroblast-like phenotype. Alternatively, the 48 hours of CMS used in this study could be too early to see an increase in αSMA protein expression. Additionally, CMS may activate TGFβ concentrations too low to significantly increase αSMA expression. Conversely, previous work has suggested that CMS reduces TGFβ-induced αSMA expression at a

supraphysiological TGFβ (10ng/ml) concentration in lung fibroblasts (190), and this was consistent with the mRNA data from this study. Overall, the data from the present and previous studies suggest that CMS itself does not enhance myofibroblast differentiation.

Having identified that CMS enhanced fibroblast TGFβ signalling in a disease-relevant manner, further experiments focussed on the molecular mechanisms of CMS-induced TGFβ signalling. MEFs and HLFs lacking $G_{\alpha q/11}$ exhibited reduced CMS-induced TGFβ signalling, suggesting that $G_{\alpha q/11}$ is a key mediator of this pathway. This was specific to the $G_{\alpha q/11}$ G protein, as *Gna12*$^{-/-}$*;Gna13*$^{-/-}$ MEFs exhibited CMS-induced TGFβ signalling in a comparable fashion to WT MEFs. These data are consistent with earlier work showing that type II alveolar epithelial cell $G_{\alpha q/11}$ is essential for stretch-mediated TGFβ activation in a ventilator-induced lung injury model (219), but this is the first study to identify a role for $G_{\alpha q/11}$ in fibroblast CMS-induced TGFβ signalling.

It should be noted that $G_{\alpha q/11}$-deficient MEFs and HLFs had lower pSmad2 expression in unstretched control samples than cells with intact $G_{\alpha q/11}$ signalling. This may reflect a lower baseline TGFβ activation in response to growth factors in the media or signals from the surrounding extracellular matrix, both of which may signal via $G_{\alpha q/11}$. Despite the lower baseline pSmad2 expression in $G_{\alpha q/11}$-deficient cells, the abrogated CMS-induced pSmad2 expression in cells lacking $G_{\alpha q/11}$ is clear, and the data support a role for $G_{\alpha q/11}$ in CMS-induced TGFβ signalling.

CMS-induced TGFβ signalling was abrogated to a lesser degree in $G_{\alpha q/11}$-deficient HLFs compared with *Gnaq*$^{-/-}$;*Gna11*$^{-/-}$ MEFs. This less prominent signal may be due to the short duration of siRNA-induced $G_{\alpha q/11}$ knockdown in the HLF model, which typically lasted for 24-48 hours, compared with the stable knockdown in the $G_{\alpha q/11}^{-/-}$ MEFs. Furthermore, siRNA incompletely knocked down $G_{\alpha q/11}$ expression in HLFs, as opposed to the complete knockdown in the $G_{\alpha q/11}^{-/-}$ MEFs. Moreover, this longstanding $G_{\alpha q/11}$ knockout could allow for significant alterations to the mechanical and chemical properties of the deposited ECM, or compensation by other signalling pathways that alter CMS-induced TGFβ signalling. While the exact reasons for the differences in CMS-induced TGFβ signalling in $G_{\alpha q/11}$-deficient MEFs and HLFs are uncertain, this study clearly demonstrates an important role for fibroblast $G_{\alpha q/11}$ in CMS-induced TGFβ signalling in both embryonic and mature differentiated fibroblasts.

Although genetic knockdown of $G_{\alpha q/11}$ expression inhibited CMS-induced TGFβ signalling, the chemical inhibitor of $G_{\alpha q/11}$ YM254890 did not. These data suggest that chemical and genetic inhibition of $G_{\alpha q/11}$ may have different effects on cells in culture. One potential explanation is that genetic $G_{\alpha q/11}$ knockdown leads to alterations in gene expression of other genes involved in CMS-induced TGFβ signalling, either by compensatory up- or downregulation, or through off target effects of the gene knockdown strategy. Alternatively, the short half-life of YM-254890 (around 4 hours, information from discussion at American Thoracic

Society Meeting 2018) could have prevented its effects being seen after 48 hours of CMS. Conversely, genetic $G_{\alpha q/11}$ knockdown approaches may have longer lasting effects than chemical inhibition. Alternatively, no assays were performed to confirm that the YM254890 had engaged with its target, and it is therefore possible that the inhibitor was not working correctly in this study.

Additionally, it was not possible to establish the role of phospholipase C (PLC), which signals directly downstream of $G_{\alpha q/11}$, in CMS-induced TGFβ signalling, as concentrations of the PLC inhibitor U73122 above 5μM (half maximal inhibitory concentration (IC_{50}) 1-7μM (376-378)) resulted in cell detachment over the 24-48 hour timeframe required for a CMS experiment. Despite these technical problems with chemical inhibition of the $G_{\alpha q/11}$ pathway, the data from genetic $G_{\alpha q/11}$ knockdown gives strong evidence of an important role for $G_{\alpha q/11}$ in CMS-induced TGFβ signalling.

Previous work found that CMS-induced TGFβ signalling occurs via Rho-ROCK signalling and αv integrins, but not protease activity, in fibrotic lung slices (113). Additionally, CMS of human airway smooth muscle cells induced *TGFβ1* mRNA expression via RhoA and ROCK signalling in work using a similar Flexcell® CMS regimen (12%, 0.3Hz) (379). Furthermore, LPA-induced TGFβ signalling, another $G_{\alpha q/11}$-dependent pathway, occurs via RhoA and αvβ6 integrin in epithelial cells (74). In contrast, the present study showed that CMS of fibroblasts occurs independently of ROCK and αv integrins, but requires serine proteases.

This discrepancy may be explained by a distinct CMS-induced TGFβ signalling pathway in fibroblasts compared to other cell types found in the lung. It is likely that epithelial stretch-induced TGFβ signalling predominates in lung slices, because αvβ6, an epithelial-specific integrin, is a major driver of TGFβ signalling (74, 126, 223, 368, 380), and could mask serine protease-dependent pathways triggered by fibroblast stretch. Overall, these data suggest that regulation of TGFβ activation may be cell type specific.

While the finding that CMS-induced TGFβ signalling is ROCK-independent in fibroblasts was unexpected, this is in keeping with data presented elsewhere in this thesis. MEFs with longstanding $G_{\alpha 12/13}$ knockdown have an atypical cytoskeletal appearance, yet $G_{\alpha q/11}^{-/-}$ MEFs have a similar cytoskeletal appearance to WT MEFs (Chapter 6). The unaltered CMS-induced TGFβ signalling in $G_{\alpha 12/13}^{-/-}$ MEFs despite an atypical cytoskeletal appearance suggests that the cytoskeleton, and thus ROCK signalling, is not involved in CMS-induced TGFβ signalling fibroblasts.

Several cell surface integrins can bind to and activate latent TGFβ, including αvβ1, αvβ3, αvβ5, αvβ6, αvβ8, and α8β1 (357). In this study, inhibitors of both αv and β1 integrins did not affect CMS-induced TGFβ signalling in HLFs. While contrary to previous work in lung slices (113), the independent experiments using both integrin inhibitors strongly support the existence of a novel integrin-independent pathway of CMS-induced TGFβ signalling.

Proteases are a diverse group of enzymes categorised according to their structure and enzymatic activity (381), and several proteases including MMPs, plasmin, urokinase-type and tissue-type plasminogen activators, thrombin, elastase, and cathepsin, can activate TGFβ by proteolytic release of TGFβ from the large latent complex (357). As CMS-induced TGFβ signalling was integrin-independent, the role of proteases in CMS-induced TGFβ signalling was assessed. An MMP inhibitor, GM6001, did not affect CMS-induced TGFβ signalling, ruling out a role for MMPs in this pathway. Conversely, the pan-serine protease inhibitor AEBSF reduced CMS-induced TGFβ signalling in HLFs. Serine proteases that activate TGFβ include plasmin, thrombin, neutrophil elastase, chymase, and tryptase (68), and CMS could enhance the activity of one or more of these proteases by increasing production or activation, or by enhancing substrate availability (160). Overall, these data imply that CMS induces serine protease activity, resulting in subsequent TGFβ activation, but the exact mechanisms of stretch-induced protease activity in this model are yet to be determined.

Protease activity is required for both normal alveolarisation during development and lung homeostasis in the adult. The excessive ECM accumulation seen in IPF is contributed to by an imbalance between protease and antiprotease activity (381). In addition, the dysregulation of several serine proteases has been implicated in the pathogenesis of pulmonary fibrosis, including the coagulation proteases (thrombin, factor Xa, activated protein C) (126, 128, 382-386), neutrophil elastase (387),

and tryptase (388). Furthermore, coagulation proteases are known to contribute to TGFβ signalling via PARs (126, 381), GPCRs that can signal via $G_{\alpha q/11}$. Tight regulation of protease activity is required to maintain lung homeostasis, and selective inhibition of just one protease may further disturb lung homeostasis. In addition, broad protease inhibition could alter other signalling pathways and ECM dynamics such that fibrosis is worsened. Further work is therefore required to define the role of CMS-induced protease activity in IPF before this can be manipulated with therapeutic intent.

In addition to the potential role of CMS in the pathogenesis of IPF, CMS also plays a key role in lung growth and development. CMS is known to induce lung growth post-pneumonectomy (197). Furthermore, in oligohydramnios, an abnormally low volume of amniotic fluid available for inhalation results in lung hypoplasia (389). In addition, tight spatiotemporal regulation of TGFβ signalling is essential for normal alveolarisation (102). Therefore, it is possible that disturbances to CMS-induced TGFβ signalling caused the abnormal lung development observed in the mice lacking mesenchymal $G_{\alpha q/11}$ described in Chapter 4.

Protease activity is important in alveologenesis, and altered responses to CMS-related protease activity may link the data presented in this chapter to the abnormal lung appearance of mice lacking mesenchymal $G_{\alpha q/11}$ (Chapter 4). Remodelling of the ECM is an important process in secondary septation, and several proteases have been shown to be

important lung development (390-393). Furthermore, protease activity can be influenced by mechanical forces (394, 395). For example, elastase inhibition in the vascular endothelium reduces mechanical ventilation-induced TGFβ signalling in neonatal mouse lungs, demonstrating a link between CMS and protease-mediated TGFβ signalling (396). Furthermore, thrombin is produced by vascular smooth muscle cells in response to stretch (397), and may increase susceptibility ventilation-induced lung injury by increasing epithelial cell stiffness (398). Mechanical stretch of the lungs has also been shown to increase the release of tryptase from mast cells, with associated increases in TGFβ activation (388), and enhances elastase activity alongside the availability of binding sites on elastin (395). Further work is required to determine the exact mechanisms by which fibroblast CMS influences protease activity, and how this affects the healthy and diseased lung.

Having ascertained that CMS-induced TGFβ signalling is integrin-independent and serine protease-dependent in fibroblasts, further work focussed on the TGFβ isoform involved. Of the three TGFβ isoforms, activation of TGFβ2 is integrin-independent due to an absence of the RGD motif in the LAP, but this isoform is activated by protease activity (68). $G_{\alpha q/11}$-deficient fibroblasts expressed less TGFβ2 protein, but had unchanged levels of TGFβ1, compared with cells with intact $G_{\alpha q/11}$. This finding implies that $G_{\alpha q/11}$ signalling is important for TGFβ2 production in fibroblasts, and that mesenchymal $G_{\alpha q/11}$ deficiency may result in less TGFβ2 deposited in the ECM for protease-mediated activation.

There is evidence for an important role of TGFβ2 in fibrotic disease and responses to mechanical signalling. In systemic sclerosis, epigenetic upregulation of TGFβ2 gene expression has been described, and this leads to a profibrotic synthetic state in fibroblasts (399). Additionally, CMS of mitral valvular interstitial cells results in increased *TGFβ2* mRNA expression (400). Furthermore, in glaucoma, an ophthalmic condition characterised by increased intraocular pressure, TGFβ2 is found at elevated concentrations in the aqueous humour (401). While suggestive, the role of CMS on TGFβ2 activation specifically is not conclusive from the present study or the existing literature. Further work is required to confirm the role of $G_{\alpha q/11}$ in the production and activation of TGFβ2, and the specificity of activation of specific TGFβ isoforms by cyclical stretch of fibroblasts.

This is the first study to propose an isoform-specific role for TGFβ2 in mammalian alveolar development. TGFβ2 was dramatically reduced in mesenchymal $G_{\alpha q/11}$ knockout lungs, suggesting a previously undescribed role for TGFβ2 in alveolar development. *Tgfb2*$^{-/-}$ mice die shortly after birth from a range of developmental defects that do not overlap with those seen in *Tgfb1*$^{-/-}$ or *Tgfb3*$^{-/-}$ mice (61, 63, 64). *Tgfb2*$^{-/-}$ mice have no gross lung morphological abnormalities in late intrauterine gestation, however collapsed conducting airways are found postnatally (63). While the *Pdgfrb-Cre*$^{+/-}$*;Gnaq*$^{fl/fl}$*;Gna11*$^{-/-}$ mice generated in the present study did not exhibit any of the developmental defects characteristic of *Tgfb2*$^{-/-}$ mice, it is possible that TGFβ2 production by

non-mesenchymal cells types is sufficient to allow normal prenatal development. Additionally, as alveolarisation occurs entirely postnatally in mice, it is possible that TGFβ2 plays a role in alveolar development that could not be observed in *Tgfb2*$^{-/-}$ mice due to perinatal death.

An alternative explanation to an isoform-specific role for TGFβ2 in alveolar development is that the abnormal alveolar appearances observed in *Pdgfrb-Cre*$^{+/-}$*;Gnaq*$^{fl/fl}$*;Gna11*$^{-/-}$ mice occurs due to a reduction in overall TGFβ signalling. For example, *Tgfb2* deletion can reverse abnormalities in prenatal lung development associated with excessive TGFβ signalling (65). However, the non-overlapping phenotypes observed in *Tgfb1*$^{-/-}$, *Tgfb2*$^{-/-}$, and *Tgfb3*$^{-/-}$ mice, and the spatial- and temporal-specific expression patterns of each isoform in the developing lung (82, 83, 402), suggest that there may be isoform-specific roles for TGFβ in lung development. What is clear is that loss of mesenchymal $G_{\alpha q/11}$ dysregulates the precise control of TGFβ signalling in the lungs, resulting in abnormal alveologenesis.

7.6 Limitations and Suggested Future work

Several limitations must be considered when interpreting the work presented in this chapter.

This study used *in vitro* cultures of a single cell type, fibroblasts, to model breathing-related CMS. This is not truly reflective of any physiological state, as no single cell type is subject to mechanical forces in isolation *in vivo*. It could therefore be argued that work using lung slices, 3D cell

culture, or in vivo models may be more appropriate. However, these models limit the study of the contribution of individual cell types, and the aim of the present study was to specifically understand the role of fibroblast signalling in response to CMS.

In this project, the serine protease inhibitor AEBSF was used to establish a role for serine proteases in CMS-induced TGFβ signalling, rather than using protease activity assays. Potential off-target effects of AEBSF resulting in reduced CMS-induced TGFβ signalling can therefore not be ruled out. For example, AEBSF is known to inhibit Nicotinamide adenine dinucleotide phosphate (NADPH) oxidase (NOX), an enzyme complex that contributes to the generation of reactive oxygen species and can induce TGFβ activation (403-405). CMS has been shown to induce NOX activity in type II alveolar epithelial cells (406), but previous work reported that NOX activity is induced by CMS at around 10 minutes (404). The optimisation experiments used in this work found that the earliest time point assessed, 4 hours of CMS, inconsistently increased TGFβ signalling in fibroblasts. It is therefore unlikely that NAPDH oxidase activation is the predominant source pf TGFβ signalling in this model, although alternative methods of assessing serine protease activity, such as protease activity assays, chemical inhibitors of specific serine proteases, and measurements of protease production are required to support this assumption.

Finally, the data presented here suggest that $G_{\alpha q/11}$ is essential for TGFβ2 production, which would subsequently be available for CMS-

induced protease-mediated activation. However, this study did not directly assess the effect of CMS on TGFβ2 signalling, and the use of a TGFβ2 inhibitor in this system is required to confirm this hypothesis.

7.7 Conclusion

CMS-induced TGFβ signalling in fibroblasts is an important profibrotic stimulus which is exaggerated in IPF. This is the first study to assess the role of breathing-related CMS of TGFβ signalling in fibroblasts, and identified a novel CMS-induced TGFβ signalling pathway in these cells. This work is also the first to show enhanced TGFβ activation in response to CMS in HLFs from patients with IPF, suggesting that this pathway may be important in the pathogenesis of IPF. This study has also identified a potential role for CMS-induced TGFβ2 activation, which can be modified by $G_{\alpha q/11}$ knockdown. These data have implications for lung development, which is also influenced by mechanical forces and TGFβ signalling. Further dissection of the novel pathway described here may identify therapeutic targets that could be exploited for the prevention and treatment of developmental and fibrotic lung diseases.

8 The Effects of Mesenchymal $G_{\alpha q/11}$ and $G_{\alpha 12/13}$ Knockdown In Adult Mice

8.1 Introduction

The data presented in Chapters 4-7 demonstrated important and distinct roles for fibroblast $G_{\alpha q/11}$ and $G_{\alpha 12/13}$ in fibrosis-related processes, including stretch-mediated TGFβ signalling, ligand-induced TGFβ signalling, detection of matrix stiffness, and fibroblast contraction. However, it was not possible to test the role of mesenchymal $G_{\alpha q/11}$ and $G_{\alpha 12/13}$ signalling in an experimental pulmonary fibrosis model *in vivo* using mice with germline mesenchymal $G_{\alpha q/11}$ and $G_{\alpha 12/13}$ deletion because of the significant developmental abnormalities in these animals (Chapter 4).

The Cre-lox system for cell-specific gene knockout can be further modified to allow the temporal control of gene expression and the avoidance of any developmental defects that occur with genetic mutations, as gene knockdown can be induced in adulthood when developmental processes are complete (224). The tamoxifen-inducible Cre recombinase expression model is a widely used method for spatiotemporal control of gene expression and depends on the metabolism of tamoxifen in the liver into more potent metabolites 4-hydroxytamoxifen (4-OH-TAM), and endoxifen (END) (407). In this model Cre^{ERT2}, a recombinant fusion protein comprised of Cre recombinase and a mutant ligand binding domain of the human oestrogen receptor, is expressed under the control of a cell-type specific gene (407). Cre^{ERT2} is sequestered in the cytoplasm unless bound to a synthetic oestrogen antagonist such as tamoxifen or its metabolites (407), when it

translocates to the nucleus and induces the recombination of floxed alleles (224) (Figure 8-1).

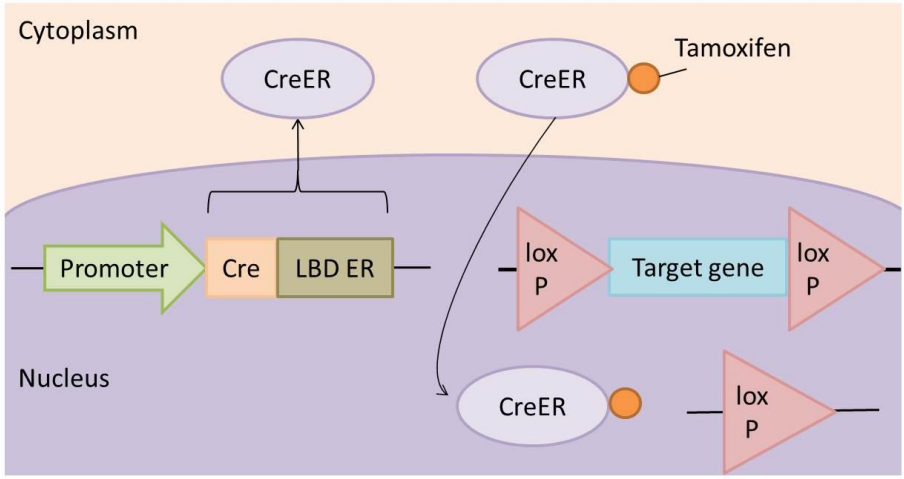

Figure 8-1: The mechanism of Cre^{ERT2}-induced gene knockdown

Cre recombinase is fused to a mutant ligand binding domain of the oestrogen receptor (LBD ER) to form Cre^{ERT2}. In the absence of tamoxifen, Cre^{ERT2} is trapped in the cytoplasm. Cre^{ERT2} translocates to the nucleus when bound to an oestrogen receptor antagonist, such as tamoxifen or its metabolites, and catalyses the recombination of DNA sequences flanked by loxP (floxed) genes. Image adapted from Kohan 2008 (224).

Transgenic mice with tamoxifen-inducible expression of Cre recombinase in *Pdgfrb*-expressing cells (*Pdgfrb-Cre/ERT2*$^{+/-}$) have been used in models of induced knockdown of floxed genes in *Pdgfrb*-expressing cells, including pericytes (408-410), and are commercially available. While studies involving *Pdgfrb-Cre/ERT2*$^{+/-}$ mice could provide valuable insight into the roles of mesenchymal cells in pulmonary fibrosis, they have never been used to assess the functions of G protein signalling *in vivo* or for fibrosis models.

8.2 Aims and Hypothesis

The aims of this work were to:

- Establish the breeding of mice with tamoxifen-inducible knockdown of mesenchymal $G_{\alpha q/11}$ and $G_{\alpha 12/13}$.
- Understand the impact of tamoxifen-induced mesenchymal $G_{\alpha q/11}$ and $G_{\alpha 12/13}$ knockdown on the lungs in adult mice.
- Assess the feasibility of tamoxifen-inducible mesenchymal $G_{\alpha q/11}$ and $G_{\alpha 12/13}$ knockout mice for use in the bleomycin model of pulmonary fibrosis.

The hypothesis underlying this work was:

> *The abnormalities observed in germline mesenchymal $G_{\alpha q/11}$ and $G_{\alpha 12/13}$ knockout mice occurred due to disturbances to normal developmental processes, and tamoxifen-induced $G_{\alpha q/11}$ and $G_{\alpha 12/13}$ knockdown will not cause abnormalities that preclude pulmonary fibrosis models.*

8.3 Methods

8.3.1 Animals

8.3.1.1 Husbandry

Pdgfrb-Cre/ERT2$^{+/-}$ mice were purchase from Jackson Laboratories, and the generation of these animals has been described previously (409). Mice were kept under standard conditions as described in the General Methods, with food and water available *ad libitum*. Standard rodent chow

was used outside of tamoxifen-induced Cre recombinase expression studies.

8.3.1.2 Breeding strategy

To generate mice with a tamoxifen-inducible knockout of $G_{\alpha q/11}$ or $G_{\alpha 12/13}$ in mesenchymal cells, a similar breeding strategy was used to that described in Chapter 4, with the following modifications: *Pdgfrb-Cre/ERT2*$^{+/-}$ mice were used instead of *Pdgfrb-Cre*$^{+/-}$ mice, and F1 mice were bred back onto *Gna12*$^{-/-}$*;Gna13*$^{fl/fl}$ mice, rather than *Gna12*$^{+/-}$*;Gna13*$^{fl/fl}$ mice, in the $G_{\alpha 12/13}$ mouse colony breeding.

8.3.2 Tamoxifen-inducible Cre recombinase expression studies

F2 mice from the *Gnaq*$^{fl/fl}$*;Gna11*$^{-/-}$ x *Pdgfrb-Cre/ERT2*$^{+/-}$ colony were kept under standard conditions until aged 7 weeks. Food was then changed to tamoxifen-containing rodent chow (400mg/kg tamoxifen citrate) for 3 weeks for mice of all genotypes. Mice were monitored daily with weight and health score measurements. Mice were humanely killed after 3 weeks of tamoxifen, or if humane endpoints were reached, and organs collected for histology (Figure 8-2).

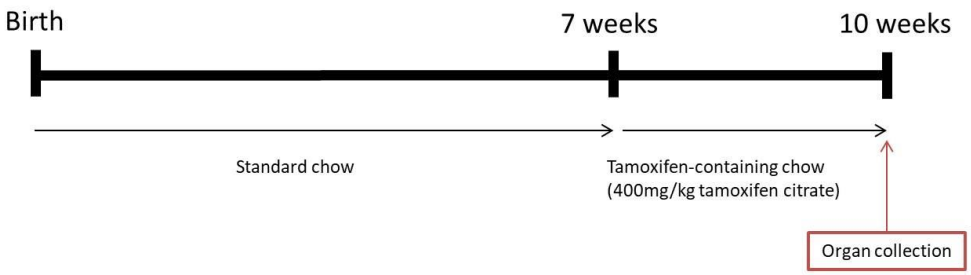

Figure 8-2: Tamoxifen-inducible Cre recombinase expression study protocol

Mice were kept under standard conditions until 7 weeks of age, when rodent chow was changed to 400mg/kg tamoxifen citrate. After 3 weeks of tamoxifen-containing chow, mice were humanely killed and organs collected.

8.3.3 Histology

Lung and kidney tissue staining using haematoxylin and eosin (H&E) and periodic acid Schiff (PAS) were performed as described in the General Methods (Chapter 3). Mean liner intercept measurements, to assess airspace size, were performed as described in the General Methods (Chapter 3).

8.4 Results

8.4.1 The genotype that confers tamoxifen-inducible mesenchymal $G_{\alpha q/11}$ deletion does not cause a developmental phenotype, and mesenchymal $G_{\alpha q/11}$ knockdown is tolerated by adult mice

To establish whether the having the genotype that gives tamoxifen-inducible mesenchymal $G_{\alpha q/11}$ knockout (*Pdgfrb-Cre/ERT2*$^{+/-}$*;Gnaq*$^{fl/fl}$*;Gna11*$^{-/-}$) causes any developmental defect, the frequencies of each genotype in F2 mice from the *Pdgfrb-Cre/ERT2*$^{+/-}$ x *Gnaq*$^{fl/fl}$*;Gna11*$^{-}$

$^{/-}$ breeding were analysed. The supplier of the *Pdgfrb-Cre/ERT2*$^{+/-}$ mice reported an expected *Pdgfrb-Cre/ERT2*$^{+/-}$ rate of 20% in offspring from breeding of the Cre-expressing hemizygous mice with wild type mice (237), rather than the 50% Cre positive rate observed in the germline *Pdgfrb-Cre*$^{+/-}$ mouse colony. Therefore, this breeding strategy is expected to result in 5% of F2 mice having any of the Cre-expressing (*Pdgfrb-Cre/ERT2*$^{+/-}$*)* genotypes, and 20% of F2 mice having any of the non-Cre expressing (*Pdgfrb-Cre/ERT2*$^{-/-}$) genotypes.

Pdgfrb-Cre/ERT2$^{+/-}$*;Gnaq*$^{fl/fl}$*;Gna11*$^{-/-}$ mice reached genotyping age at the expected frequency, and represented 6.4% of all F2 mice born compared with the expected 5% (total number of mice born 109; Figure 8-3). This indicates that having the *Pdgfrb-Cre/ERT2*$^{+/-}$*;Gnaq*$^{fl/fl}$*;Gna11*$^{-/-}$ genotype, without administration of tamoxifen, does not cause any gross developmental defects.

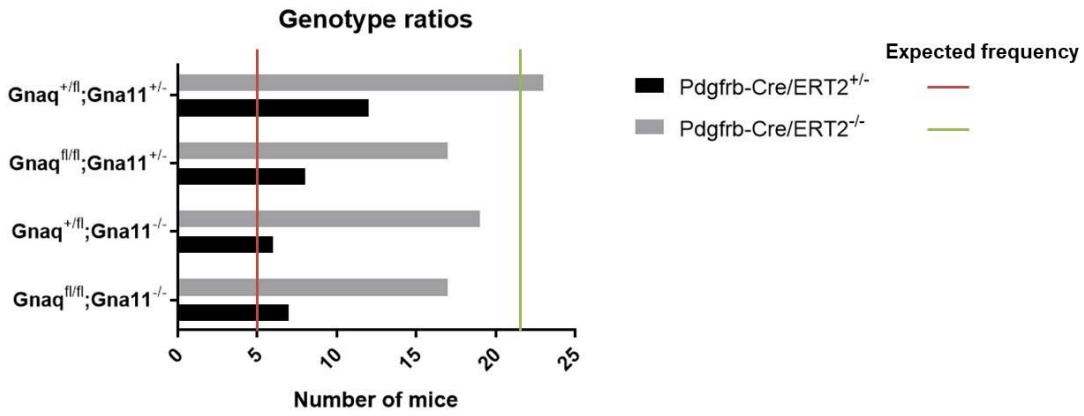

Figure 8-3: Mice bred to have tamoxifen-inducible $G_{\alpha q/11}$ knockout are born at the expected frequency

Genotype ratios from *Pdgfrb-Cre/ERT2*$^{+/-}$ x *Gnaq*$^{fl/fl}$*;Gna11*$^{-/-}$ breeding. Expected genotype frequencies of the *Pdgfrb-Cre/ERT2*$^{+/-}$ (red line) and *Pdgfrb-Cre/ERT2*$^{-/-}$ mice (green line) are shown. 109 mice born in total across 20 litters.

When a 3 week course of tamoxifen was administered to 7 weeks old *Pdgfrb-Cre/ERT2*$^{+/-}$*;Gnaq*$^{fl/fl}$*;Gna11*$^{-/-}$ mice (n=4, 1 female 3 male), no detrimental effect to health status was observed compared with littermate controls treated with tamoxifen. Furthermore, *Pdgfrb-Cre/ERT2*$^{+/-}$*;Gnaq*$^{fl/fl}$*;Gna11*$^{-/-}$ mice gained weight at the same rate as littermate controls with the other genotypes during the tamoxifen protocols (median weight on day 21 of tamoxifen 104.3% of day 1 vs 106.2% of day 1 in other genotypes, p=0.71; Figure 8-4). A small but statistically insignificant reduction in weight was observed in both mouse groups at around four days of tamoxifen administration, as was expected with a change in diet and in keeping with previous studies using tamoxifen-containing chow (411). This tamoxifen-related weight loss was independent of genotype and did not reach the 15% weight reduction humane endpoint that would

have required an animal to be humanely killed. These data suggest that short-term mesenchymal $G_{\alpha q/11}$ knockout is feasible and does not cause gross physiological disturbances *in vivo*.

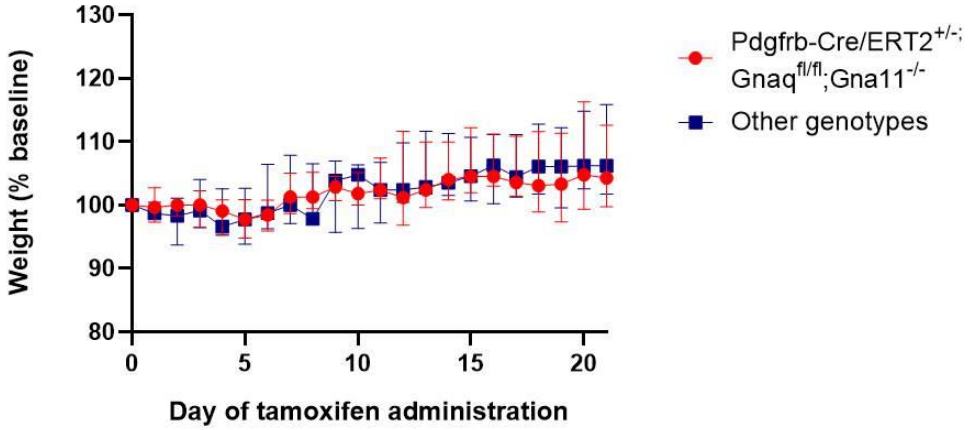

Figure 8-4: Tamoxifen administration does not affect weight gain of mice with tamoxifen-inducible mesenchymal $G_{\alpha q/11}$ knockdown. Weights of *Pdgfrb-Cre/ERT2$^{+/-}$;Gnaq$^{fl/fl}$;Gna11$^{-/-}$* (red) mice and littermates with all other genotypes (blue line) during 3 weeks of oral tamoxifen administration. Data shown as percentage of weight measured at baseline, median ± interquartile range.

8.4.2 Mice with tamoxifen-induced knockdown of mesenchymal $G_{\alpha q/11}$ have lung abnormalities

As bleomycin-induced pulmonary fibrosis causes histological lung abnormalities, the evaluation of which is important in assessing study outcomes and may be complicated by any abnormalities present at baseline, histological straining of lung tissue sections from tamoxifen-treated *Pdgfrb-Cre/ERT2$^{+/-}$;Gnaq$^{fl/fl}$;Gna11$^{-/-}$* mice was performed. The lungs of tamoxifen-treated *Pdgfrb-Cre/ERT2$^{+/-}$;Gnaq$^{fl/fl}$;Gna11$^{-/-}$* mice had an emphysema-like appearance, with a small but statistically significant

increase in airspace size in *Pdgfrb-Cre/ERT2$^{+/-}$;Gnaq$^{fl/fl}$;Gna11$^{-/-}$* mice after 3 weeks of oral tamoxifen (mean linear intercept distance 52.5µm in *Pdgfrb-Cre/ERT2$^{+/-}$;Gnaq$^{fl/fl}$;Gna11$^{-/-}$* mice compared with 39.3µm in *Gna11$^{-/-}$* controls, p=0.03, Figure 8-5A,B).

Furthermore, 3 out of 4 of the *Pdgfrb-Cre/ERT2$^{+/-}$;Gnaq$^{fl/fl}$;Gna11$^{-/-}$* mice subject to 3 weeks of tamoxifen exhibited abnormal cellular aggregates in the lungs, which predominated at the pleural surfaces and had an appearance similar to collections of mononuclear cells (Figure 8-6). Similar cellular aggregates were not seen in the lungs of littermate control mice.

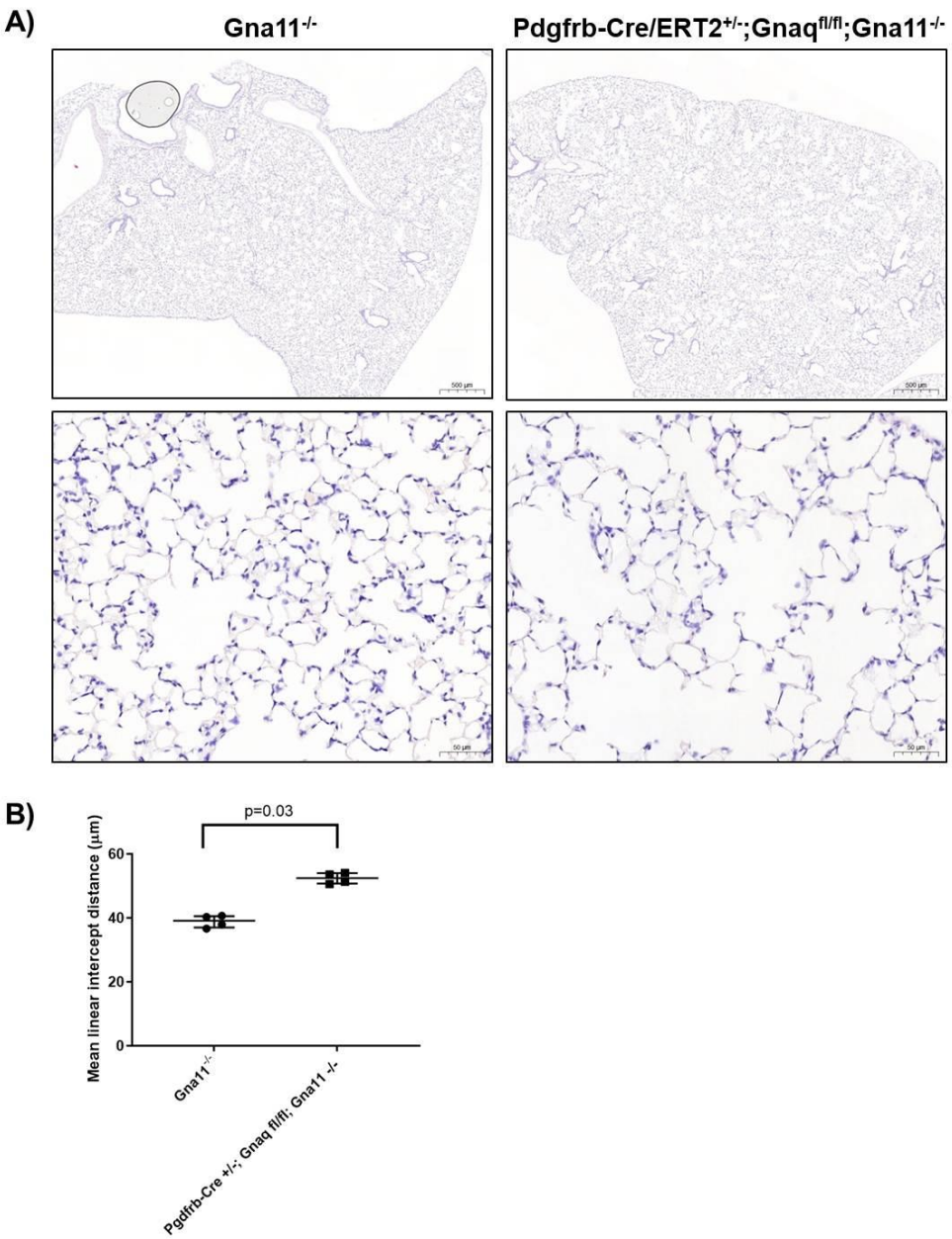

Figure 8-5: Tamoxifen-induced mesenchymal $G_{\alpha q/11}$ knockdown causes an emphysema-like appearance

A) H&E staining of representative *Gna11*$^{-/-}$ (left) and *Pdgfrb-Cre/ERT2*$^{+/-}$*;Gnaq*$^{fl/fl}$*;Gna11*$^{-/-}$ (right) mice subject to 3 weeks oral tamoxifen, at low (top) and high (bottom) magnification.

B) Mean linear intercept measurements from *Gna11*$^{-/-}$ and *Pdgfrb-Cre/ERT2*$^{+/-}$*;Gnaq*$^{fl/fl}$*;Gna11*$^{-/-}$ mice subject to 3 weeks of oral tamoxifen. Data shown as median ± interquartile range, n=4 per group.

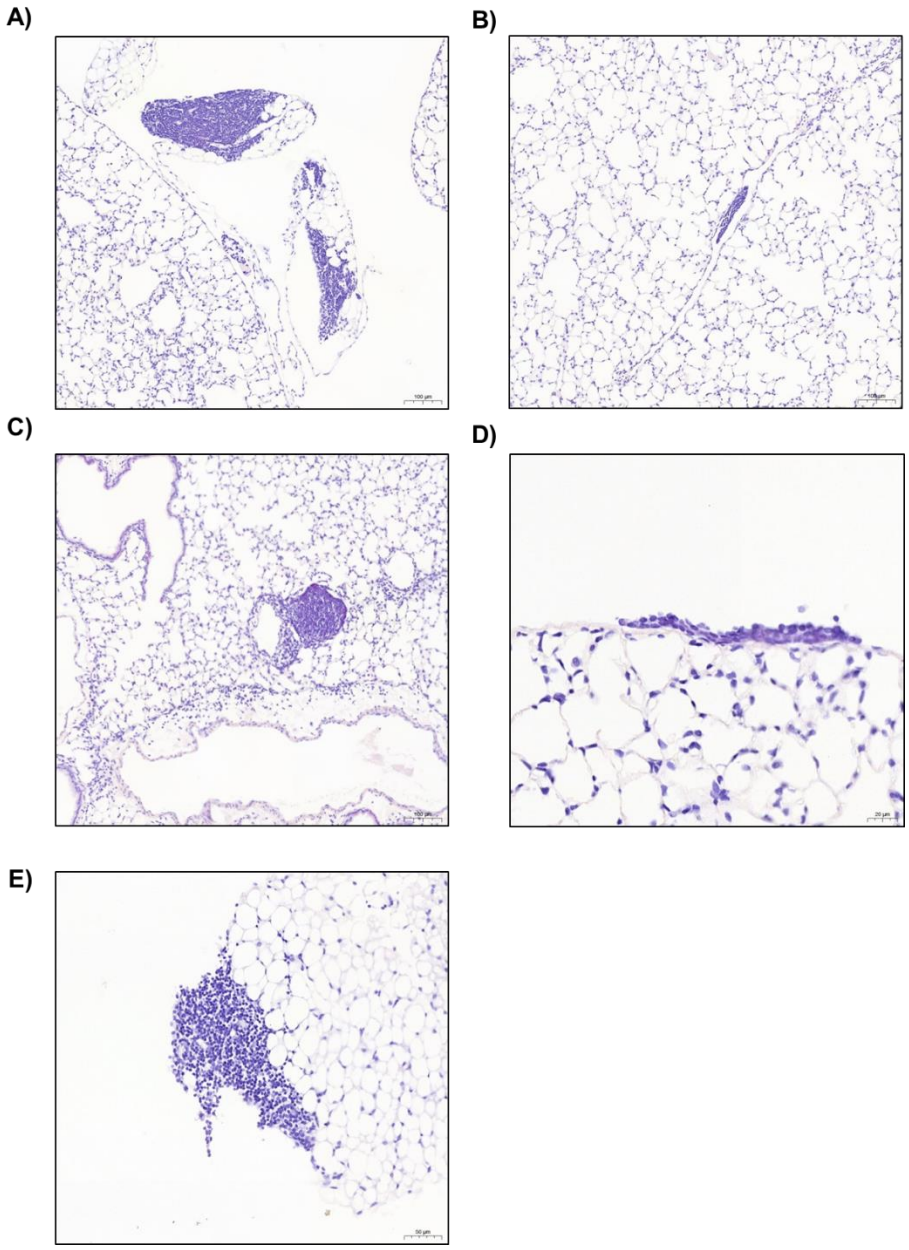

Figure 8-6: Mice with tamoxifen-induced mesenchymal $G_{\alpha q/11}$ knockdown have abnormal cellular aggregates in the lungs

Example images of H&E stained lung tissue sections from *Pdgfrb-Cre/ERT2*$^{+/-}$;*Gnaq*$^{fl/fl}$;*Gna11*$^{-/-}$ mice after 3 weeks of oral tamoxifen.

A-C) low magnification H&E stained lung sections

D-E) high magnification H&E stained lung sections

Example images from three mice.

Although *Pdgfrb-Cre/ERT2$^{+/-}$;Gnaq$^{fl/fl}$;Gna11$^{-/-}$* mice treated with tamoxifen showed no signs of respiratory distress on health screening, these data demonstrate that even short-term knockdown of mesenchymal $G_{\alpha q/11}$ signalling can disturb lung homeostasis sufficiently to cause structural lung abnormalities.

8.4.3 Adult mice subject to tamoxifen-induced knockdown of mesenchymal $G_{\alpha q/11}$ have normal kidneys

As mice with a germline mesenchymal $G_{\alpha q/11}$ knockout exhibited a significant renal abnormality that significantly impacted the health of these animals, renal histology was performed in *Pdgfrb-Cre/ERT2$^{+/-}$;Gnaq$^{fl/fl}$;Gna11$^{-/-}$* mice after 3 weeks of tamoxifen to assess for evidence of kidney disease.

PAS staining revealed no obvious structural renal abnormality in *Pdgfrb-Cre/ERT2$^{+/-}$;Gnaq$^{fl/fl}$;Gna11$^{-/-}$* mice subject to 3 weeks of oral tamoxifen (Figure 8-7). This indicates that short-term mesenchymal $G_{\alpha q/11}$ knockdown does not induce the same renal abnormalities in adult mice as those seen with germline mesenchymal $G_{\alpha q/11}$ knockdown, and that the abnormalities observed in the germline mesenchymal $G_{\alpha q/11}$ knockout animals may have been developmental in nature.

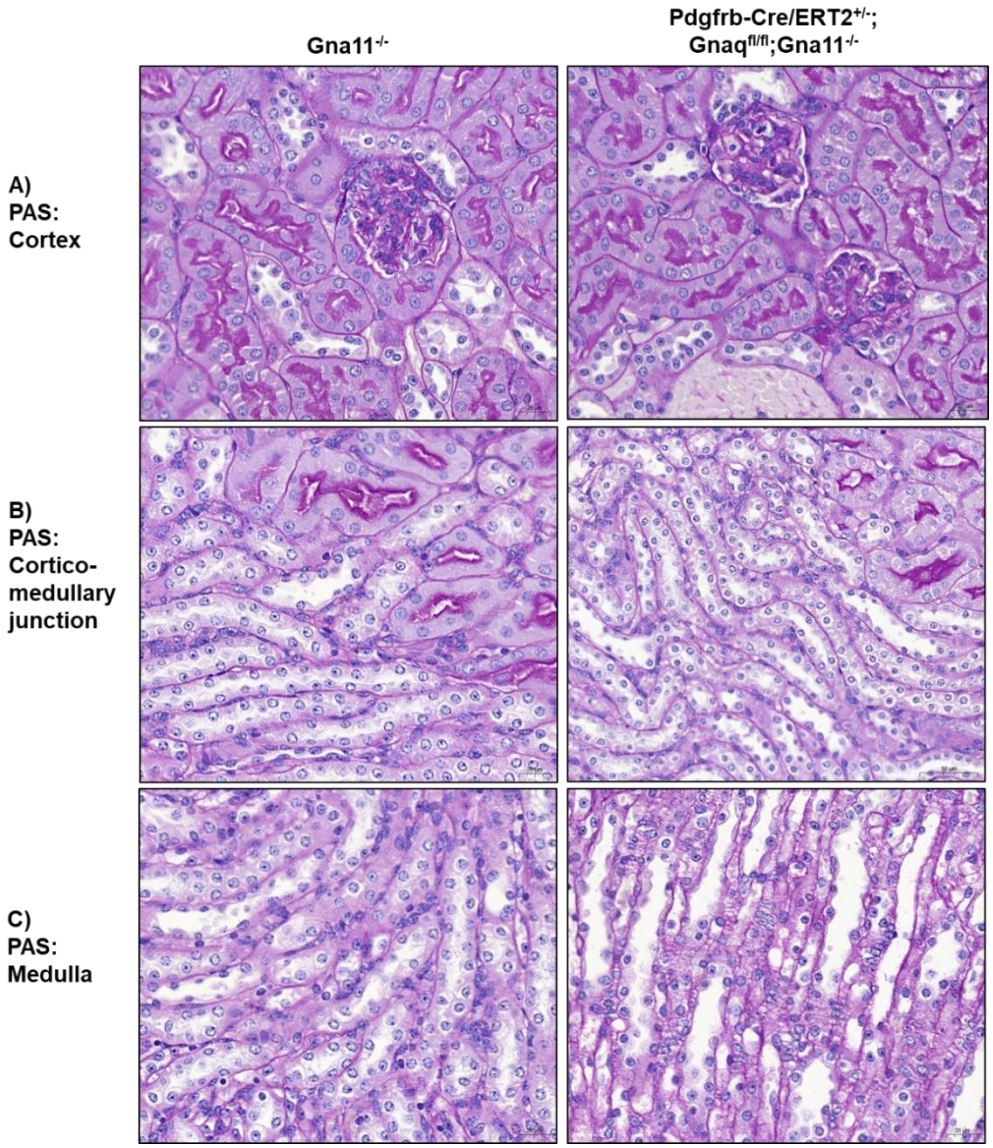

Figure 8-7: Mice with adult-onset mesenchymal $G_{\alpha q/11}$ knockdown have no kidney abnormalities

Kidney sections from *Gna11*$^{-/-}$ (left) and *Pdgfrb-Cre/ERT2*$^{+/-}$*;Gnaq*$^{fl/fl}$*;Gna11*$^{-/-}$ (right) mice were PAS stained.

Representative images from the renal cortex (A), corticomedullary junction (B), and renal medulla (C) shown.

Overall, these pilot studies of tamoxifen administration to *Pdgfrb-Cre/ERT2*$^{+/-}$*;Gnaq*$^{fl/fl}$*;Gna11*$^{-/-}$ mice suggest that these animals may be physically fit enough to undergo the bleomycin model of pulmonary fibrosis.

8.4.4 The genotype that confers tamoxifen-inducible mesenchymal $G_{\alpha 12/13}$ knockout does not cause a developmental phenotype

As germline mesenchymal $G_{\alpha 12/13}$ knockout mice were unsuitable for use in the bleomycin model of pulmonary fibrosis, *Pdgfrb-Cre/ERT2*$^{+/-}$ mice were bred with *Gna12*$^{-/-}$*; Gna13*$^{fl/fl}$ mice to generate *Pdgfrb-Cre/ERT2*$^{+/-}$*;Gna12*$^{-/-}$*;Gna13*$^{fl/fl}$ mice, which are expected to have mesenchymal $G_{\alpha 12/13}$ knockout with tamoxifen.

This breeding programme, which was expected to have a 5% yield for the *Pdgfrb-Cre/ERT2*$^{+/-}$*;Gna12*$^{-/-}$*;Gna13*$^{fl/fl}$ genotype, generated the expected number of *Pdgfrb-Cre/ERT2*$^{+/-}$ animals (5.7% *Pdgfrb-Cre/ERT2*$^{+/-}$*;Gna12*$^{-/-}$*;Gna13*$^{fl/fl}$ compared with 5% expected, Figure 8-8). No physical abnormalities were observed in any of the F2 mice resulting from the *Pdgfrb-Cre/ERT2*$^{+/-}$ x *Gna12*$^{-/-}$*;Gna13*$^{fl/fl}$ mouse breeding.

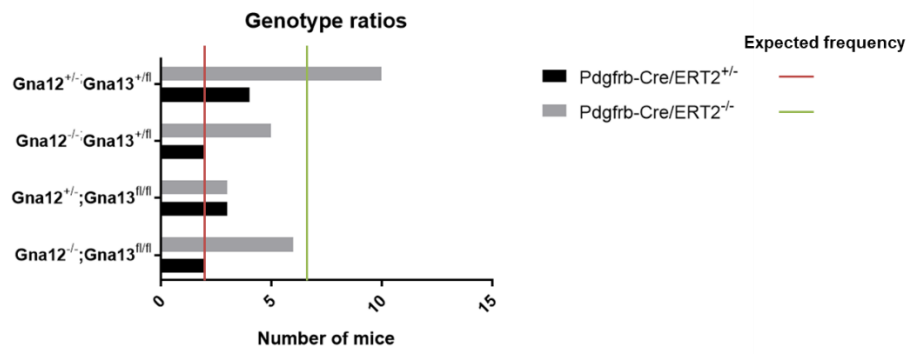

Figure 8-8: Mice bred to have tamoxifen-inducible $G_{\alpha 12/13}^{-/-}$ knockdown are born at the expected frequency
Genotype frequencies from *Pdgfrb-Cre/ERT2*$^{+/-}$ x *Gna12*$^{-/-}$;*Gna13*$^{fl/fl}$ mouse breeding. Red and green lines show the expected frequency of Cre-expressing (*Pdgfrb-Cre*$^{+/-}$, 5% for each genotype) and non-Cre-expressing (*Pdgfrb-Cre*$^{-/-}$, 20% for each genotype) mice, respectively. 35 mice born in total across 3 litters.

These data suggest that it is feasible to breed mice for tamoxifen-induced mesenchymal $G_{\alpha 12/13}$ knockdown.

8.5 Discussion

This work has shown that mice bred to have tamoxifen-inducible mesenchymal $G_{\alpha q/11}$ or $G_{\alpha 12/13}$ knockout (*Pdgfrb-Cre/ERT2*$^{+/-}$;*Gnaq*$^{fl/fl}$;*Gna11*$^{-/-}$ and *Pdgfrb-Cre/ERT2*$^{+/-}$;*Gna12*$^{-/-}$;*Gna13*$^{fl/fl}$, respectively) are born at the expected frequencies and show no gross physiological disturbance on health monitoring, indicating that major developmental abnormalities are unlikely with either genotype. To test the hypothesis that the abnormalities observed in germline mesenchymal $G_{\alpha q/11}$ and $G_{\alpha 12/13}$ knockout mice were purely developmental and would

not occur if gene knockout was induced in adulthood, tamoxifen administration studies were performed.

Pdgfrb-Cre/ERT2$^{+/-}$*;Gnaq*$^{fl/fl}$*;Gna11*$^{-/-}$ mice tolerated a 3 week course of oral tamoxifen, and did not show any abnormalities on health surveillance or weight monitoring compared with littermate controls. These preliminary data indicate that short-term mesenchymal $G_{\alpha q/11}$ deletion is feasible and does not cause life-threatening physiological disturbances that would preclude the use of disease models in these animals.

The lungs of *Pdgfrb-Cre/ERT2*$^{+/-}$*;Gnaq*$^{fl/fl}$*;Gna11*$^{-/-}$ showed early emphysematous change and inflammatory cell infiltrates, however these mice did not exhibit signs of respiratory distress. The bleomycin model of pulmonary fibrosis has been used in transgenic mice predisposed to emphysema previously (412), and it is possible that *Pdgfrb-Cre/ERT2*$^{+/-}$*;Gnaq*$^{fl/fl}$*;Gna11*$^{-/-}$ mice would also tolerate this disease model. However, the emphysematous changes in *Pdgfrb-Cre/ERT2*$^{+/-}$*;Gnaq*$^{fl/fl}$*;Gna11*$^{-/-}$ mice were present after a relatively short period of gene knockdown, and the effects of an additional 3 weeks of mesenchymal $G_{\alpha q/11}$ knockdown that would occur with a typical 21 day bleomycin protocol are unknown. Any progression in the emphysema could increase the loss of animals due to complications of bleomycin and complicate the analysis of fibrosis-related abnormalities on histology. It was not possible to progress to the bleomycin model in *Pdgfrb-Cre/ERT2*$^{+/-}$*;Gnaq*$^{fl/fl}$*;Gna11*$^{-/-}$ mice because of working restrictions associated with the COVID-19 pandemic, however modified bleomycin doses and controls for the degree of baseline lung

abnormalities in *Pdgfrb-Cre/ERT2$^{+/-}$;Gnaq$^{fl/fl}$;Gna11$^{-/-}$* mice should be considered for any future studies using these animals.

The emphysematous changes in *Pdgfrb-Cre/ERT2$^{+/-}$;Gnaq$^{fl/fl}$;Gna11$^{-/-}$* mouse lungs suggest that short-term mesenchymal $G_{\alpha q/11}$ knockdown can impair lung homeostasis sufficiently to cause structural lung abnormalities. While further characterisation of *Pdgfrb-Cre/ERT2$^{+/-}$;Gnaq$^{fl/fl}$;Gna11$^{-/-}$* mouse lungs was not performed, John et al found emphysema and abnormal lung inflammation characterised by M2 macrophage polarisation in mice lacking $G_{\alpha q/11}$ in type II alveolar epithelial cells, and this was related to reduced stretch-induced TGFβ signalling in the lungs (219). Furthermore, deficiencies in the TGFβ signalling pathway components Smad3 and TGFβ receptor type II (TGFBRII) result in emphysema (97, 412), and genetic polymorphisms in genes involved in TGFβ signalling have been associated with chronic obstructive pulmonary disease (COPD), a disease that includes emphysema (413, 414). Given the results in Chapters 5 and 7 demonstrating the roles of fibroblast $G_{\alpha q/11}$ in LPA- and stretch-induced TGFβ signalling, it is likely that *Pdgfrb-Cre/ERT2$^{+/-}$;Gnaq$^{fl/fl}$;Gna11$^{-/-}$* mice also have altered TGFβ signalling when administered tamoxifen.

Pdgfrb-Cre/ERT2$^{+/-}$;Gnaq$^{fl/fl}$;Gna11$^{-/-}$ lungs also contained abnormal subpleural cellular aggregates. While the cells within these aggregates had the appearance of mononuclear cells, further staining to clarify the cell types was not performed. It was assumed that these cellular aggregates reflected cellular recruitment due to disturbances to TGFβ

signalling, for example through an abnormal inflammatory process (415). However a malignant expansion of immune cells or a granulomatous condition, which are also associated with TGFβ dysregulation (416, 417), cannot be ruled out with the current data.

The kidneys of *Pdgfrb-Cre/ERT2*$^{+/-}$*;Gnaq*$^{fl/fl}$*;Gna11*$^{-/-}$ mice did not have any histological abnormalities, which was in stark contrast to the severe kidney abnormalities seen in mice with germline mesenchymal $G_{\alpha q/11}$ deletion (Chapter 4). It is possible that the kidney abnormalities in germline mesenchymal $G_{\alpha q/11}$ knockout animals occurred due to a developmental abnormality that was avoided in *Pdgfrb-Cre/ERT2*$^{+/-}$*;Gnaq*$^{fl/fl}$*;Gna11*$^{-/-}$ mice by inducing gene knockout during adulthood. Alternatively, *Pdgfrb-Cre/ERT2*$^{+/-}$*;Gnaq*$^{fl/fl}$*;Gna11*$^{-/-}$mice may develop renal abnormalities with a longer duration of gene knockdown than was induced in this study. Should the *Pdgfrb-Cre/ERT2*$^{+/-}$*;Gnaq*$^{fl/fl}$*;Gna11*$^{-/-}$ mice be taken forward for longer studies, close surveillance for renal abnormalities must be performed.

Due to delays to the *Pdgfrb-Cre/ERT2*$^{+/-}$ x *Gna12*$^{-/-}$*;Gna13*$^{fl/fl}$ breeding, only two *Pdgfrb-Cre/ERT2*$^{+/-}$;*Gna12*$^{-/-}$*;Gna13*$^{fl/fl}$ mice were born before breeding was stopped, despite *Pdgfrb-Cre/ERT2*$^{+/-}$;*Gna12*$^{-/-}$*;Gna13*$^{fl/fl}$ mice being born at the expected frequency. As no *Pdgfrb-Cre/ERT2*$^{+/-}$;*Gna12*$^{-/-}$*;Gna13*$^{fl/fl}$ mice underwent tamoxifen administration, it is not possible to conclude whether these mice would be suitable for disease models, as they were not assessed for physical abnormalities with short

term mesenchymal $G_{\alpha 12/13}$ knockout. The effect of mesenchymal $G_{\alpha 12/13}$ deletion in adult mice should be confirmed in future studies.

8.6 Limitations

The limitations of this work predominantly relate to the small number of animals available for study secondary to the nature of this breeding programme and the cessation of animal work because of the COVID-19 pandemic. The results presented here are therefore preliminary, and further optimisation of tamoxifen-induced mesenchymal $G_{\alpha q/11}$ and $G_{\alpha 12/13}$ knockdown must be performed prior to any disease models being performed.

A conclusion of this work is that the *Pdgfrb-Cre/ERT2*$^{+/-}$*;Gnaq*$^{fl/fl}$*;Gna11*$^{-/-}$ and *Pdgfrb-Cre/ERT2*$^{+/-}$*;Gna12*$^{-/-}$*;Gna13*$^{fl/fl}$ mice would be suitable for disease models following tamoxifen-induced mesenchymal $G_{\alpha q/11}$ and $G_{\alpha 12/13}$ knockdown. However, the very low frequencies of these genotypes (5% of each litter) means that the breeding programme would have to be scaled up significantly to obtain enough mice for a disease model experiment with sufficient power to detect relevant differences between genotypes. Furthermore, the variability in litter size, frequency, and genotype distribution means that several disease model experiments with different mouse cohorts at different times may be required, and the inclusion of both male and female mice, which is not typical for bleomycin studies (418), may also need to be considered. These factors indicate that disease model experiments with *Pdgfrb-Cre/ERT2*$^{+/-}$*;Gnaq*$^{fl/fl}$*;Gna11*$^{-/-}$ and *Pdgfrb-Cre/ERT2*$^{+/-}$*;Gna12*$^{-/-}$*;Gna13*$^{fl/fl}$

mice, while theoretically possible, are impractical due to cost, time, high variability between experiment cohorts, and the large numbers of animals required.

Due to technical issues with histological staining for $G_{\alpha q}$, the extent of $G_{\alpha q}$ knockdown in *Pdgfrb-Cre/ERT2*$^{+/-}$*;Gnaq*$^{fl/fl}$*;Gna11*$^{-/-}$ mice treated with tamoxifen was not confirmed. Previous work using *Pdgfrb-Cre/ERT2*$^{+/-}$ mice (410) and other Cre^{ERT2} lines found 3-4 weeks of tamoxifen delivered via rodent chow to be sufficient to induce gene recombination (411, 419-421). As *Pdgfrb-Cre/ERT2*$^{+/-}$*;Gnaq*$^{fl/fl}$*;Gna11*$^{-/-}$ animals were originally intended to continue oral tamoxifen during a 21 day bleomycin-induced pulmonary fibrosis protocol, a 3 week loading period of tamoxifen-containing chow was chosen for the initial induction of gene knockdown. However, the efficiency of gene inactivation in Cre^{ERT2}-loxP models depends on a number of experiment-specific factors (Table 8-1) (407, 422), therefore oral tamoxifen protocols from previous studies should not be extrapolated to the *Pdgfrb-Cre/ERT2*$^{+/-}$*;Gnaq*$^{fl/fl}$*;Gna11*$^{-/-}$ mice. However, the lung phenotype observed in *Pdgfrb-Cre/ERT2*$^{+/-}$*;Gnaq*$^{fl/fl}$*;Gna11*$^{-/-}$ mice that received tamoxifen suggests that some gene recombination occurred, even if complete mesenchymal *Gnaq* knockout was not achieved.

Table 8-1: Parameters that determine the specificity and efficiency of gene recombination in Cre^{ERT2}-loxP models (407)

Parameter	**Experiment-specific factors**
Tissue tamoxifen concentrations	**Tamoxifen protocol:** dose, duration, route of administration formulation **Animal metabolism:** Age, sex, strain
Level of Cre^{ERT2} expression	Specific to *Pdgfrb-Cre/ERT2*$^{+/-}$ mice
Variable recombination efficiency of floxed alleles due to chromatin structure and epigenetic factors	Specific to *Gnaq*$^{fl/fl}$*;Gna11*$^{-/-}$ mice

The actual amount of tamoxifen ingested via tamoxifen-containing chow can vary between animals due to variable oral intake, and the mesenchymal $G_{\alpha q/11}$ knockdown in *Pdgfrb-Cre/ERT2*$^{+/-}$*;Gnaq*$^{fl/fl}$*;Gna11*$^{-/-}$ mice given tamoxifen may have been incomplete. Intraperitoneal (IP) injection of tamoxifen may have been a more reliable method of administration, and has successfully been used with *Pdgfrb-Cre/ERT2*$^{+/-}$ mice (272). While IP tamoxifen administration is more practical in studies of very young mice that may not reliably eat tamoxifen-laced chow, embryonic development, or of very short developmental stages (272, 408), IP injections do cause stress to the animals and can have rare but life-threatening complications such as abdominal organ damage. Furthermore, tamoxifen-containing show has been found to have equal

efficacy to IP 4-hydroxytamoxifen (411). Given the small numbers of *Pdgfrb-Cre/ERT2*$^{+/-}$*;Gnaq*$^{fl/fl}$*;Gna11*$^{-/-}$ mice produced by this breeding strategy, tamoxifen-containing chow was chosen to minimise procedure-related adverse effects.

Cre^{ERT2} models can be limited by Cre "leakiness", where Cre recombinase is expressed in cell types that do not express the Cre-driving gene, in this case *Pdgfrb*, or in the absence of tamoxifen (422, 423). While the localisation of Cre expression was not investigated in this study, the original work that generated these mice confirmed Cre-mediated gene recombination in embryonic, postnatal and adult PDGFRβ+ cells, and Cre recombinase activity has been found in lung pericytes in *Pdgfrb-Cre/ERT2*$^{+/-}$ mice following tamoxifen administration in newborn mice (272, 409). The cell types affected may be age-specific, therefore the location of Cre recombinase activity should be assessed as part of ongoing optimisation of this work.

In this study, *Gna11*$^{-/-}$ mice that received tamoxifen were used as controls, rather than *Pdgfrb-Cre/ERT2*$^{-/-}$*;Gna11*$^{-/-}$*;Gnaq*$^{fl/fl}$ mice that did not receive tamoxifen. While the latter option would have had the benefit of matching the genotypes exactly and facilitating the identification of Cre recombinase activity in the absence of tamoxifen (423), this approach would have required more animals in an already challenging breeding programme. Ideally, *Pdgfrb-Cre/ERT2*$^{-/-}$*;Gna11*$^{-/-}$*;Gnaq*$^{fl/fl}$ mice that did not receive tamoxifen would be included as a second control group, but this was not feasible and was beyond the scope of this study.

8.7 Conclusion

Mesenchymal cell $G_{\alpha q/11}$ is important for lung homeostasis, but short-term mesenchymal $G_{\alpha q/11}$ knockdown does not cause the same kidney abnormalities as those seen in germline mesenchymal $G_{\alpha q/11}$ knockout mice. Mice lacking mesenchymal $G_{\alpha q/11}$ and $G_{\alpha 12/13}$ may be suitable for use in disease models such as the bleomycin model of pulmonary fibrosis, however more work is required to confirm the role of these transgenic mice in disease models.

9 General discussion

9.1 Main findings

The aims of this work were to investigate the roles of mesenchymal cell $G_{\alpha q/11}$ and $G_{\alpha 12/13}$ signalling in the pathogenesis of pulmonary fibrosis, and to understand the potential consequences of inhibiting these G proteins *in vivo*. This work identified a number of roles of $G_{\alpha q/11}$ and $G_{\alpha 12/13}$ in detecting and propagating chemical and profibrotic stimuli, in particular by mediating activation of the profibrotic cytokine TGFβ. However, whether inhibition of mesenchymal cell $G_{\alpha q/11}$ of $G_{\alpha 12/13}$ signalling is a feasible therapeutic strategy remains unclear, as these molecules clearly play important roles in normal development and tissue homeostasis.

The main findings of this thesis on the roles of mesenchymal $G_{\alpha q/11}$ and $G_{\alpha 12/13}$ can be divided into roles in normal development, fibrosis, and tissue homeostasis. These findings are summarised below:

Development

- $G_{\alpha q/11}$ signalling in mesenchymal (*Pdgfrb*-expressing) cells is essential for normal alveologenesis via several processes, including ECM protein production, control of myofibroblast and epithelial cell differentiation, and control of cellular proliferation.
- Mesenchymal cell $G_{\alpha q/11}$ and $G_{\alpha 12/13}$ mediate LPA-induced TGFβ signalling, which may be important in development.

- Breathing-related cyclical stretch may promote normal alveologenesis through protease-mediated TGFβ2 activation.
- Mesenchymal cell $G_{\alpha q/11}$ signalling is important for TGFβ2 production and deposition in the ECM.
- Mesenchymal cell $G_{\alpha 12/13}$ is also likely to play a key role in development, although the mechanisms and manifestations remain undetermined.

Fibrosis

- The response to and generation of mechanical signals by lung fibroblasts is exaggerated in IPF, with increased stretch-induced TGFβ activation and cellular contractility.
- Fibroblast $G_{\alpha q/11}$ is involved in the response to mechanical signals, such as cyclical stretch or matrix stiffness, whereas $G_{\alpha 12/13}$ is involved in mechanical signal generation, via cellular contraction-induced ECM organisation and stiffening.
- $G_{\alpha q/11}$ and $G_{\alpha 12/13}$ both mediate LPA-induced TGFβ signalling in fibroblasts, but this is likely to occur via contraction-independent and –dependent mechanisms, respectively.
- Fibroblast $G_{\alpha q/11}$ is important for the production of ECM components that form the fibrotic matrix such as collagen, but does not play a role in contraction-induced ECM organisation.
- The breeding of mice for tamoxifen-inducible genetic inhibition of $G_{\alpha q/11}$ and $G_{\alpha 12/13}$ is feasible, but the potential antifibrotic

effects and toxic consequences of this approach have not been fully determined.

Tissue Homeostasis

- Mesenchymal cell $G_{\alpha q/11}$ signalling maintains tissue homeostasis in the lungs and other organs.

9.2 Study Hypotheses

There were two hypotheses underlying the work presented in this thesis:

Mesenchymal cell $G_{\alpha q/11}$ and $G_{\alpha 12/13}$ play central roles in the pathogenesis of pulmonary fibrosis, and this may occur via different molecular mechanisms.

Inhibition of mesenchymal cell $G_{\alpha q/11}$ and $G_{\alpha 12/13}$ in vivo may be protective against experimental pulmonary fibrosis, but this approach may be associated with adverse effects.

These hypotheses will be addressed in the following sections.

9.3 Mesenchymal cell $G_{\alpha q/11}$ and $G_{\alpha 12/13}$ play distinct roles in the pathogenesis of pulmonary fibrosis

In recent years mechanical signals such as stretch and increased matrix stiffness have been determined to be important driving factors in the pathogenesis of pulmonary fibrosis, in addition to the more well-established profibrotic chemical mediators. While the role of increased matrix stiffness in promoting fibroblast-to-myofibroblast differentiation, and the contribution of resulting myofibroblasts to the stiff ECM, is well-

established (53, 167, 170, 424), the role of G proteins as mechanosensors had not been previously investigated. Furthermore, although stretch of fibrotic lung tissue is known to activate TGFβ (113), the contribution of lung fibroblasts and the role of fibroblast G proteins to this response was unknown prior to this work. Finally, while LPA is known to be a key pathogenic driver in IPF, the role of G proteins in LPA-induced TGFβ signalling in fibroblasts had not been reported previously. This study has identified distinct and complementary roles for mesenchymal cell $G_{\alpha q/11}$ and $G_{\alpha 12/13}$ in the pathogenesis of pulmonary fibrosis.

Signalling by both $G_{\alpha q/11}$ and $G_{\alpha 12/13}$ increase TGFβ activation in response to the profibrotic phospholipid LPA. Interestingly, the wrinkling assay revealed that this is likely to occur via contraction-independent and –dependent mechanisms, respectively, as LPA-induced contraction was dramatically reduced in $G_{\alpha 12/13}$-deficient, but not $G_{\alpha q/11}$-deficient, cells. The fact that ROCK inhibition only partially inhibited the LPA-induced TGFβ signalling response in wild-type cells supports the existence of contraction-independent pathways in LPA-induced TGFβ signalling in fibroblasts, but the exact mechanisms have not been determined by this study.

This work confirmed that two aspects of mechanical signalling, stretch-mediated TGFβ signalling and fibroblast contraction, are altered in IPF, as human lung fibroblasts from donors with IPF exhibited exaggeration to both of these responses. In addition, this study found unique roles for mesenchymal cell $G_{\alpha q/11}$ and $G_{\alpha 12/13}$ in mechanical signalling. Only $G_{\alpha q/11}$

was involved in stretch-induced TGFβ signalling and in reducing the myofibroblast phenotype in response to softer environments. Furthermore, only $G_{\alpha 12/13}$ was important for fibroblast contraction, which contributes to ECM stiffness and TGFβ activation (161, 168, 322). These unique roles for $G_{\alpha q/11}$ and $G_{\alpha 12/13}$ in profibrotic mechanical signalling highlight several areas where novel therapeutics could inhibit fibrogenesis. However, further work is required to elucidate the exact molecular mechanisms underlying $G_{\alpha q/11}$ mechanical signal detection and $G_{\alpha 12/13}$-mediated mechanical signal generation to identify these therapeutic targets.

The roles of $G_{\alpha q/11}$ and $G_{\alpha 12/13}$ in profibrotic signal detection and generation were established from *in vitro* experiments. While each experiment of a single stimulus on isolated cells revealed a profibrotic pathway that could act as a promising therapeutic target, it is likely that these pathways interact. For example, traction force generation by valvular interstitial cells is reduced by cyclical stretch (425), suggesting that stretched cells may have altered contractility in the lung. Other work has suggested a role for cyclical stretch in reducing the expression of myofibroblast-associated genetic markers(190), again suggesting that stretch could reduce contractility, by reducing the differentiation of the most contractile cells. This study did not assess the effect of cyclical stretch on lung fibroblast contractility, but it could be hypothesised that contractile cells within the most highly scarred areas of lung experience less cyclical stretch because of the increased stiffness of the

environment. Furthermore, as responses to mechanical stress can be sensitised by chemical stimuli such as LPA (426), it is possible that increased LPA levels in the IPF lung further enhance profibrotic responses to cyclical stretch. Future work should investigate the roles of G protein signalling in the interactions between mechanical and chemical profibrotic stimuli in pulmonary fibrosis.

9.4 Mesenchymal $G_{\alpha q/11}$ signalling is important for normal alveolar development and tissue homeostasis

9.4.1 $G_{\alpha q/11}$ represents a shared component of developmental and profibrotic signalling

While the *in vitro* studies presented in this thesis provide evidence of a role for mesenchymal cell $G_{\alpha q/11}$ in a number of profibrotic pathways relevant to pulmonary fibrosis, the two mouse models gave important insights into the role of $G_{\alpha q/11}$ in lung development and homeostasis. In particular, they indicated that $G_{\alpha q/11}$ signalling may represent a shared pathway between physiological and pathophysiological processes.

Mice lacking mesenchymal cell $G_{\alpha q/11}$ exhibited significant lung abnormalities that suggested defective alveolarisation. The lung scarring characteristic of IPF occurs secondary to uncontrolled activation and continuation of wound healing responses. The dysregulated reactivation of developmental and regenerative processes is a key component of this abnormal wound healing response (26), and several developmental signalling pathways have been found to be overactive in IPF. It is thought that the very different results of organogenesis and fibrogenesis occur

due to different basal environmental conditions, such as cellular senescence, mechanical constraints, and the microbiome in the developing organism compared with fibrotic tissue, in addition to the nature of the profibrotic injury (26). Establishment of the exact $G_{\alpha q/11}$-mediated signalling pathways that are essential for normal alveolarisation and fibrogenesis, could reveal signalling pathways that could be manipulated for numerous therapeutic purposes.

A number of developmental signalling pathways are shared between normal lung development and the pathogenesis of IPF, including Wnt, Shh, TGFβ, and FGF signalling (26, 282), and TGFβ, WNT, FGF, and BMP signalling have all been reported to be dysregulated in BPD (282). While TGFβ signalling is likely to be a central player in the antifibrotic and developmental roles of mesenchymal $G_{\alpha q/11}$ signalling (discussed in the section below), the Frizzled receptors for Wnt ligands are GPCRs, some of which signal via $G_{\alpha q/11}$ (289). It is likely that $G_{\alpha q/11}$ knockout disturbs a number of GPCR-mediated signalling pathways with complex interactions, and it is beyond the scope of this study to determine the individual pathways involved in the phenotypes observed in the mouse models generated here.

In addition to ligand-mediated signalling, mechanical signals are also important in both normal lung development and IPF. For example, Yes-associated protein (YAP) and transcriptional co-activator with PDZ-binding protein (TAZ) signalling is essential for normal alveolarisation (427), in addition to other developmental processes (428), and the

pathogenesis of IPF (60). Relevant to the data presented in this thesis, TGFβ, YAP/TAZ, and Wnt signalling all converge and interact in pulmonary fibrosis (60), and it is possible that all are involved in the pathological manifestations observed in mesenchymal $G_{\alpha q/11}$-deficient mice. Importantly, YAP/TAZ is a mechanosensitive signalling pathway (429, 430), demonstrating that mechanical signalling pathways are important in both normal lung development and pulmonary fibrosis. This study is the first to propose mesenchymal $G_{\alpha q/11}$ as a mechanosensitive signalling pathway in both alveologenesis and IPF, adding to the existing literature in this area.

A key difference between normal lung development and the pathophysiological processes in IPF is control and timing (26). Normal lung development is characterised by tight spatiotemporal control of several signalling pathways, and the coordinated and controlled response of various cell types at particular timepoints. Any disturbance to the timing or control of these pathways can result in abnormal lung development. In IPF, developmental signalling pathways are activated in an unregulated and chaotic manner (26), explaining the differences in structural manifestations between IPF and the developing lung. The data from this study suggest that, while inhibition of mesenchymal $G_{\alpha q/11}$ signalling may have antifibrotic effects, inhibition of this pathway from conception results in disturbance to normal lung developmental pathways. This data necessitated the attempted to knockout mesenchymal $G_{\alpha q/11}$ signalling in adult mice in later experiments.

9.4.2 Mesenchymal $G_{\alpha q/11}$ signalling maintains the balance between tissue fibrosis and homeostasis

The tamoxifen-inducible model of mesenchymal $G_{\alpha q/11}$ knockout revealed that mice subject to $G_{\alpha q/11}$ knockdown in adulthood developed emphysema and mononuclear cellular infiltrates, suggesting a role for this G protein family in lung homeostasis. The evidence for mesenchymal $G_{\alpha q/11}$ signalling in tissue homeostasis was further supported by the neoplastic renal tubular epithelial proliferation observed in the germline mesenchymal $G_{\alpha q/11}$ knockout mice. Similar to the shared pathways between IPF and normal lung development discussed above, dysregulated TGFβ, WNT, FGF, and BMP signalling have all been reported in COPD, a disease that includes the pathological finding of emphysema (282).

While TGFβ signalling was the focus of this study, an alternative explanation for the abnormal lung appearances in mice lacking mesenchymal $G_{\alpha q/11}$ is altered protease activity. This study found that stretch-mediated TGFβ activation occurs via serine protease activity, and a number of proteases have been reported to regulate alveolarisation and lung growth, including MMPs (390-392), and the serine proteases neutrophil elastase (396) and chymotrypsin-like elastase (393). These enzymes are also important in ECM remodelling in fibrosis, as well as tissue destruction in emphysema (431, 432). It is therefore possible that $G_{\alpha q/11}$ regulates protease activity, although more work is required to confirm this.

Protease activity is also key to ECM remodelling, a process that is central to the development of emphysema, fibrosis, and lung development. Some data presented in this thesis suggest that mesenchymal $G_{\alpha q/11}$ is required for the production of the ECM proteins elastin, collagen I, and collagen III. As ECM proteins themselves drive a number of developmental, physiological, and fibrogenic processes, the possibility of the ECM generated by $G_{\alpha q/11}$-defiicent fibroblasts being less fibrogenic, or less supportive for normal alveolarisation, should not be ignored.

9.5 TGFβ activation is central to the effects of $G_{\alpha q/11}$ deficiency

Overall, the data from the animal studies suggest that mesenchymal $G_{\alpha q/11}$ signalling is required to balance tissue repair and homeostasis, as well as playing key roles in alveolar development and tumour suppression. Should mesenchymal $G_{\alpha q/11}$ signalling become uncontrolled, fibrosis may result. However, interruption of mesenchymal $G_{\alpha q/11}$ signalling as a treatment for fibrosis could cause wide ranging adverse effects, including impaired wound healing, tissue destruction, and malignancy.

TGFβ is well established as a central player in fibrogenesis, normal development, and tissue homeostasis (26, 433), while dysregulated TGFβ signalling has been described in IPF, emphysema, and BPD (282). The data presented in this study suggest that mesenchymal $G_{\alpha q/11}$ signalling may control the balance between these processes via the control of TGFβ signalling, and that loss of control of mesenchymal $G_{\alpha q/11}$

signalling can lead to a variety of manifestations driven by TGFβ. More work is required to establish the exact mechanisms of this control, and how this could be manipulated to therapeutic potential.

9.6 Mesenchymal $G_{\alpha 12/13}$ signalling is profibrotic

This study found that mesenchymal $G_{\alpha 12/13}$ signalling is also important for multiple IPF-driving pathways. Fibroblast contractility, which was increased in human lung fibroblasts from IPF donors, was dramatically reduced by $G_{\alpha 12/13}$ knockdown, and $G_{\alpha 12/13}$-deficient fibroblasts had attenuated LPA-induced TGFβ activation. Unfortunately, mice with germline deletion of $G_{\alpha 12/13}$ were not born in sufficient numbers to study, suggesting a significant developmental defect in these animals. This may be due to altered contraction-mediated ECM remodelling in these animals, as this is essential for a number of developmental as well as fibrogenic processes (21). Further work is required to confirm this hypothesis.

The breeding of tamoxifen-inducible mesenchymal $G_{\alpha 12/13}$ knockout mice did not progress to tamoxifen studies, therefore any potential adverse effects of interrupting this signalling pathway postnatally remain undetermined. Although the *in vitro* data show promise for $G_{\alpha 12/13}$ inhibition in mesenchymal cells as an antifibrotic strategy, significant further study is required to confirm this.

9.7 Working hypothesis

This study has found that $G_{\alpha q/11}$ and $G_{\alpha 12/13}$ in mesenchymal cells play overlapping and distinct roles in detecting chemical and physical stimuli, and contributing to the mechanical environment within the lungs. These pathways include TGFβ signalling, ECM generation and organisation, contraction, and cellular migration. Tight control of these pathways is important for normal lung development and tissue homeostasis, and if there is a loss of control of wound-healing signalling in mesenchymal cells, fibrosis or tissue destruction may result.

With further dissection of these pathways, novel therapeutic targets could be identified with potential uses in fibrotic, neoplastic, and developmental diseases.

9.8 Strengths of this work

The main strengths of this work relate to the generation of the novel germline and tamoxifen-inducible mesenchymal G protein knockout transgenic mice, which contributed new data to the field on the role of mesenchymal $G_{\alpha q/11}$ and $G_{\alpha 12/13}$ in developmental processes that have not previously been described. Although further work is required, the data from this thesis consistently converge on $G_{\alpha q/11}$ and $G_{\alpha 12/13}$ as being regulators of TGFβ signalling, which is consistent with a plethora of previous studies.

These studies are also the first to describe an isoform-specific role for TGFβ2 in mammalian alveologenesis, a role of $G_{\alpha q/11}$ in stretch-driven

fibrogenesis as well as tissue homeostasis, to demonstrate that $G_{\alpha 12/13}$ is essential for fibroblast contraction, and that both $G_{\alpha q/11}$ and $G_{\alpha 12/13}$ drive LPA-induced TGFβ signalling in fibroblasts. These findings are likely to be of interest not only to the fibrosis research community which was the primary aim of this study, but also to researchers studying malignancy and lung development. The findings of this work are therefore widely applicable and may lead to significant discoveries and impact on the lives of patients in future.

9.9 Limitations

Although the findings of this study are far-reaching, this study also has several limitations. Many of these have been discussed in the individual results chapters, but some general issues are discussed here.

Due to the broad nature of the findings presented in this study, the precise molecular mechanisms governed by $G_{\alpha q/11}$ and $G_{\alpha 12/13}$ were not always established by this work. For example, the signalling pathway components up- and downstream of $G_{\alpha q/11}$ and $G_{\alpha 12/13}$, which could include integrins, ROCK, transcription factors, second messengers, and proteases, as well as the role of mesenchymal-epithelial interactions in the observations made, were not determined by this study. It is likely that the work presented in this thesis will lead to numerous further studies, in which the exact molecular mechanisms of the processes described here will be established.

Finally, the fundamental hypothesis underlying this study was that inhibition of mesenchymal $G_{\alpha q/11}$ and $G_{\alpha 12/13}$ signalling would be protective against pulmonary fibrosis. While the *in vitro* data support this assertion, it was not possible to complete experimental pulmonary fibrosis studies *in vivo* due to the abnormal phenotype of the germline mesenchymal $G_{\alpha q/11}$ and $G_{\alpha 12/13}$-knockout mice, and COVID-19 pandemic related constraints on animal breeding, which halted the tamoxifen-inducible studies. These *in vivo* models are essential to confirm the conclusions drawn from the *in vitro* studies presented here.

9.10 Proposed further work

Numerous research questions have been raised by this work, which should be addressed by future studies. These include:

- How might deletion of mesenchymal cell $G_{\alpha q/11}$ or $G_{\alpha 12/13}$ in adult mice affect the development of experimental pulmonary fibrosis?
- How do the $G_{\alpha q/11}$- and $G_{\alpha 12/13}$- related stretch, contraction, and GPCR agonist signalling pathways interact?
- What is the role of $G_{\alpha q/11}$ and $G_{\alpha 12/13}$ in generating and maintaining the fibrotic and physiological ECM?
- What is the role of individual TGFβ isoforms in lung development?
- How do $G_{\alpha q/11}$ and $G_{\alpha 12/13}$ affect the epithelial-mesenchymal interactions that regulate fibrogenesis and lung development?

It is expected that the data presented in this thesis will form the basis of some of these proposed studies.

10 Conclusion

10.1 Conclusion

Mesenchymal cell $G_{\alpha q/11}$ and $G_{\alpha 12/13}$ play key roles in the pathogenesis of pulmonary fibrosis by mediating both chemical and mechanical profibrotic signals to induce TGFβ signalling. Many of these pathways are also likely to play important roles in normal mammalian development and tissue homeostasis, making the findings of this work applicable to diseases of lung development and malignancy. Inhibition of mesenchymal cell $G_{\alpha q/11}$ and $G_{\alpha 12/13}$ may inhibit fibrogenesis, however this approach could also be associated with significant homeostatic dysregulation. More work is therefore required to clarify the therapeutic role of $G_{\alpha 12/13}$ and $G_{\alpha q/11}$ inhibition in pulmonary fibrosis.

11 Appendices

11.1 Materials list

11.1.1 Transgenic mice and *in vivo* study materials

Mouse genotype	**Source**
Pdgfrb-Cre$^{+/-}$	A gift from Prof Neil Henderson, University of Edinburgh
Pdgfrb-Cre/ERT2$^{+/-}$	Jackson Laboratories, Cat # 029684
Gnaq$^{fl/fl}$*;Gna11*$^{-/-}$	Gifts from Prof Stefan Offermanns, Max Planck Institute for Heart and Lung Research, Bad Nauheim, Germany
Gna12$^{-/-}$*;Gna13*$^{fl/fl}$	
Tamoxifen-containing chow (400mg/kg tamoxifen citrate)	Envigo Cat# TD.55125.1

11.1.2 *In vitro* experiment materials and reagents

Product	**Supplier**	**Catalogue number**
5 x siRNA buffer	Dharmacon	B-002000-UB-100
AEBSF (serine protease inhibitor	Sigma	SBR00015
Collagen I –coated Bioflex® six well tissue culture plates	Dunn Labortechnik	BF-3001C
Complete mini protease inhibitor tablets	Sigma-Aldrich	04693124001
CWHM-12	Gift from Dr David Griggs	n/a

Control siRNA - ON-TARGET-plus non-targeting pool	Dharmacon	D-001810-10-05
DharmaFECT 1 transfection reagent	Dharmacon	T-200010-01
Dulbecco's Modified Eagle's Medium	Sigma-Aldrich	D5671
Foetal calf serum	Thermo-Fisher	11573397
G418	VWR	E859-1G
Gelatin	Sigma	G1393
GM6001 (MMP inhibitor)	Sigma	CC1010
GNAQ ON-TARGET-plus SMARTpool siRNA	Dharmacon	L-008562-00-0005
GNA11 ON-TARGET-plus SMARTpool siRNA	Dharmacon	L-010860-00-0005
GNA12 ON-TARGET-plus SMARTpool siRNA	Dharmacon	J-008435-00-0005
GNA13 ON-TARGET-plus SMARTpool siRNA	Dharmacon	L-009948-00-0005
L-glutamine	Sigma-Aldrich	G7513-100ML
Lysophosphatidic acid	Sigma	L7260
NOTT199SS	School of Chemistry at the University of Nottingham	n/a
Penicillin/ Streptomycin	Sigma	P4333

Phenylmethylsulfonyl fluoride (PMSF)	Sigma	78830
Phos-stop phosphatase inhibitor tablets	Sigma-Aldrich	04906837001
Protein lysis buffer	Cell Signaling Technology	9803
Reporter lysis buffer	Promega	4030
SB-525334 (Alk5 inhibitor)	Sigma-Aldrich	S8822
TGFβ1 (recombinant)	R&D Systems	240-B-010
Trypsin/ EDTA	Sigma-Aldrich	T4049
Y-27632 (ROCK inhibitor)	Sigma	Y-0503
YM254890	Wako	257-00631

11.1.3 Western blot materials and reagents

Product	**Supplier**	**Catalogue number**
Amersham ECL Western Blotting Detection Reagent	GE Healthcare	RPN2134
Ammonium persulphate	Sigma-Aldrich	A3678
Blotto non-fat dry milk	Santa Cruz	SC-2325
Carestream® Kodak® autoradiography GBX fixer/replenisher	Sigma-Aldrich	P7167

Carestream® Kodak® autoradiography GBX developer/replenisher	Sigma-Aldrich	P7042
Clarity western blotting ECL reagent	Bio-Rad	1705061
Full range molecular weight marker (rainbow)	Amersham	GERPN800E
Hyperfilm for western blots	GE Healthcare	10752067
Polyvinylidine membrane	Bio-Rad	162-0177
ProtoGel (30%) 37.5:1 Acrylamide to Bisacrylamide solution	Thermo-Fisher	12381469
Western Restore stripping buffer	Thermo-Fisher	21059

11.1.4 Materials and reagents for molecular biology work

Product	**Supplier**	**Catalogue number**
100 basepair ladder	New England Biosciences	N3231S
Agarose ultra-pure	Thermo-Fisher	16500500
dNTPs (dATP, dCTP, dGTP, dTTP)	Promega	U120A, U121A, U122A, U123A
Ethidium Bromide	Sigma-Aldrich	E1510

Green GoTaq Flexi Buffer (5x) and Go Taq enzyme	Promega	M7805
Kapa SYBR Fast Taq polymerase	Kapa Biosystems	KK4618
Nuclease-free water	Qiagen	129114
Oligo-dt primer	Sigma-Aldrich	10814270001
Primers for PCR and qPCR	Eurofins	Custom ordered
Proteinase K	Sigma-Aldrich	P2308
RNasin	Promega	N2115

11.1.5 Histology materials and reagents

Product	**Supplier**	**Catalogue number**
DPX mountant for microscopy	VWR	360292F
Eosin, 1%	VWR	RAYLLAMB/100-D
Goat serum	Sigma	G9023
Mayers haematoxylin	Thermo-Fisher	12698616
SIGMAFAST(TM) 3,3'-Diaminobenzidine tablets	Sigma	D4418
Superfrost glass slides	Thermo-Fisher	10149870

11.1.6 Antibodies and immunofluorescence materials

Product	Supplier	Catalogue number
Anti-phalloidin Alexa Fluor 488	Invitrogen	10125092
DAPI	Invitrogen	D1306
Goat anti-mouse IgG2a-TRITC	Southern Biotech	1080-03
Rabbit anti-phospho-Smad2 (pSmad2)	Cell Signaling Technology	3808L
Rabbit anti-Smad2/3	Cell Signaling Technology	3102
Rabbit anti-α-smooth muscle actin (αSMA)	Abcam	ab5694
Rabbit anti-GAPDH	Abcam	ab181603
Rabbit anti-TGFβ1	Abcam	ab92486
Mouse anti-TGFβ2	Abcam	ab36495
Mouse IgG2a anti αSMA	Sigma	A5228
Rabbit anti $G_{\alpha 11}$	Abcam	ab153951
Goat anti-$G_{\alpha q}$	Abcam	ab128060
HRP-conjugated goat-anti-rabbit	Agilent	P044801-2
HRP-conjugated rabbit-anti-goat	Agilent	P016002-2
HRP-conjugated rabbit anti-mouse	Agilent	P0260022-2
Rabbit anti-CD31	Abcam	ab182981
Rabbit anti-ki67	Abcam	ab15580

Rabbit anti-pro-surfactant protein C	Sigma	Ab3786
Rabbit anti-TGFβ2	Proteintech	19999-1-AP
Biotinylated goat anti-rabbit IgG	Vector	BA1000

11.1.7 Commercial kits

Product	**Supplier**	**Catalogue number**
Nucleospin RNA preparation kit (Machery-Nagel)	Thermo-Fisher	12373368
Superscript IV	ThermoFisher	18090050
Periodic Acid Schiff staining kit	Abcam	ab150680
Avidin-Biotin complex kit	Vector	SP2001
BCA protein assay kit	Thermo-Fisher	10678484
Luciferase assay system	Promega	E1501

11.1.8 Chemicals

Product	**Supplier**	**Catalogue number**
Acid fuschin	Sigma	F8129
Direct red 80	Sigma	365548
Ferric chloride (Iron(III) chloride)	Sigma	157740

Formalin Buffered 10%	VWR	11699404
Glycerol	Sigma-Aldrich	G5516
Haematoxylin	Sigma	H3136
Heparin 500 units/ml	Wockhardt	FP1083
Hydrogen peroxide	VWR	23619.264
Iodine	Sigma	326143
MTT (3-(4,5-Dimethylthiazol-2-yl)-2,5-Diphenyltetrazolium Bromide)	Sigma	M5655
Paraformaldehyde	Sigma	P6148
Phosphate buffered saline	Sigma-Aldrich	P4417
Picric acid (in aqueous solution)	VWR	84512.260
Potassium iodide	Sigma	03124
Sodium dodecyl sulphate	Sigma-Aldrich	L3771
Sodium thiosulphate	Scientific Laboratory Supplies	72049
Tetramethylethylenediamine (Temed)	Sigma-Aldrich	T9281
Tween20	Sigma-Aldrich	P1379-500ML

11.1.9 Software

Software	**Publisher**
MxPro	Stratagene
Image J	National Institute of Health (NIH)

GeneSnap	Syngene
NIS Elements 3.2	Nikon
Micro Manager 1.4	National Institute of Health (NIH)
Case Viewer 3.2	3D Histech
Primer BLAST	National Institute of Health (NIH)
GraphPad Prism 8.2	GraphPad
Zen 2.5	Zeiss
Omega	BMG Labtech

11.2 Western blot buffer recipes

11.2.1 4x Lamellae Buffer

Reagent	**Amount**
0.5M tris HCL pH 6.8	5ml
100% glycerol	4ml
10% SDS	4ml
Bromophenol blue	40mg
dH_2O	7ml
Just before use add 60µl/ml β-mercaptoethanol	

11.2.2 Buffer 1

Reagent	**Amount**
Tris base	18.5g
ddH_2O	50ml
10% SDS`	4ml
Adjust pH to 8.8, then add ddH_2O to 100ml. Store at 4°C	

11.2.3 Buffer 2

Reagent	**Amount**
Tris base	6g
ddH_2O	60ml
10% SDS	4ml
Adjust pH to 6.8. Adjust volume to 100ml with ddH_2O	

11.2.4 10x Running buffer

Reagent	**Amount**
Tris base	24.2g
Glycine	144g
SDS	10g

dH_2O	1000ml
Dilute 1:10 with dH_2O before use	

11.2.5 10x Transfer buffer

Reagent	**Amount**
Tris base	24.4g
Glycine	144g
dH_2O	1000ml

11.2.6 1x Transfer buffer

Reagent	**Amount**
10x transfer buffer	200ml
Methanol	400ml
dH_2O	1400ml

11.2.7 10x Tris buffered saline/ Tween (TBST)

Reagent	**Amount**
Tris base	24.4g
Sodium chloride	87.6g
dH_2O	1000ml
Tween20	10ml
Adjust pH to 7.4-7.6 **Dilute 1:10 with dH_2O before use**	

11.3 Western blot gel recipes

11.3.1 Resolving gel

Reagent	**Amount**
30% Bis/Acrylamide	6.66 ml
Buffer 1	5.2 ml
dH_20	7.92 ml
10% ammonium persulphate	200 µl
Tetramethylenediamine (Temed)	20 µl

11.3.2 Stacking gel

Reagent	**Amount**
30% Bis/Acrylamide	1.3 ml
Buffer 2	2.5 ml
dH_20	6.1 ml
10% ammonium persulphate	50 µl
Tetramethylenediamine (Temed)	10 µl

11.4 Buffers used for mouse genotyping

11.4.1 Tail lysis buffer

100mM NaCl

10mM Tris pH 8

25mM EDTA

0.5% SDS

0.15µg/µl proteinase K (added just before use)

11.4.2 50 x Tris Acetate EDTA (TAE)

Reagent	**Amount**
Tris base	242g
Glacial acetic acid	57.1ml
0.5M EDTA pH 8.0	57.1ml
Adjust volume to 1000ml with ddH_2O	

11.4.3 1% agarose gel

Reagent	**Amount**
Agarose	1.5g
1 x TAE	150ml
Ethidium bromide	7µl

11.5 Histology buffer recipes

Solution	Components
Weigert's iodine solution	2g Potassium iodide 1g Iodine 100ml Distilled water
Verhoeff's solution	20ml 5% alcoholic hematoxylin 8ml 10% ferric chloride 8ml Weigert's iodine solution
Van Gieson's solution	5ml aqueous acid fuchsin 100ml Saturated aqueous picric acid
Picro-Sirius Red solution	Direct Red 80 (Sigma 365548) 0.5 g Saturated aqueous solution of picric acid 500 ml
Weigert's haematoxylin	1:1 ratio of Weigert's solution A and Weigert's solution B
Weigert's solution A	1% haematoxylin in 100% ethanol
Weigert's solution B	4ml 30% ferric chloride 1ml 12N hydrochloric acid 95ml water
Acidified water	5 ml glacial acetic acid 1 litre distilled water
Acid/ alcohol solution	70% ethanol, 0.1% hydrochloric acid
0.5% Diastase solution	0.25g α-amylase from porcine pancreas (Sigma A3176) 50ml distilled water

12 References

1. Navaratnam V, Fleming KM, West J, Smith CJ, Jenkins RG, Fogarty A, Hubbard RB. The rising incidence of idiopathic pulmonary fibrosis in the u.K. *Thorax* 2011;66(6):462-467.
2. Hutchinson JP, McKeever TM, Fogarty AW, Navaratnam V, Hubbard RB. Increasing global mortality from idiopathic pulmonary fibrosis in the twenty-first century. *Annals of the American Thoracic Society* 2014;11(8):1176-1185.
3. Gribbin J, Hubbard RB, Le Jeune I, Smith CJ, West J, Tata LJ. Incidence and mortality of idiopathic pulmonary fibrosis and sarcoidosis in the uk. *Thorax* 2006;61(11):980-985.
4. Navaratnam V, Hubbard RB. The mortality burden of idiopathic pulmonary fibrosis in the united kingdom. *Am J Respir Crit Care Med* 2019;200(2):256-258.
5. Goodwin AT, Jenkins G. Molecular endotyping of pulmonary fibrosis. *Chest* 2016;149(1):228-237.
6. Kuhn C, McDonald JA. The roles of the myofibroblast in idiopathic pulmonary fibrosis. Ultrastructural and immunohistochemical features of sites of active extracellular matrix synthesis. *The American journal of pathology* 1991;138(5):1257-1265.
7. Tsou PS, Haak AJ, Khanna D, Neubig RR. Cellular mechanisms of tissue fibrosis. 8. Current and future drug targets in fibrosis: Focus on rho gtpase-regulated gene transcription. *American Journal of Physiology - Cell Physiology* 2014;307(1):C2-13.
8. Chanda D, Otoupalova E, Smith SR, Volckaert T, De Langhe SP, Thannickal VJ. Developmental pathways in the pathogenesis of lung fibrosis. *Mol Aspects Med* 2019;65:56-69.
9. Pakshir P, Noskovicova N, Lodyga M, Son DO, Schuster R, Goodwin A, Karvonen H, Hinz B. The myofibroblast at a glance. *J Cell Sci* 2020;133(13).
10. Varma R, Soleas JP, Waddell TK, Karoubi G, McGuigan AP. Current strategies and opportunities to manufacture cells for modeling human lungs. *Adv Drug Deliv Rev* 2020;161-162:90-109.
11. Donahoe PK, Longoni M, High FA. Polygenic causes of congenital diaphragmatic hernia produce common lung pathologies. *Am J Pathol* 2016;186(10):2532-2543.
12. Bhatt AJ, Pryhuber GS, Huyck H, Watkins RH, Metlay LA, Maniscalco WM. Disrupted pulmonary vasculature and decreased vascular endothelial growth factor, flt-1, and tie-2 in human infants dying with bronchopulmonary dysplasia. *Am J Respir Crit Care Med* 2001;164(10 Pt 1):1971-1980.
13. Surate Solaligue DE, Rodriguez-Castillo JA, Ahlbrecht K, Morty RE. Recent advances in our understanding of the mechanisms of late lung development and bronchopulmonary dysplasia. *Am J Physiol Lung Cell Mol Physiol* 2017;313(6):L1101-l1153.
14. Beauchemin KJ, Wells JM, Kho AT, Philip VM, Kamir D, Kohane IS, Graber JH, Bult CJ. Temporal dynamics of the developing lung transcriptome in three common inbred strains of laboratory mice reveals multiple stages of postnatal alveolar development. *PeerJ* 2016;4:e2318.
15. Schittny JC. Development of the lung. *Cell Tissue Res* 2017;367(3):427-444.

16. Li C, Li M, Li S, Xing Y, Yang CY, Li A, Borok Z, De Langhe S, Minoo P. Progenitors of secondary crest myofibroblasts are developmentally committed in early lung mesoderm. *Stem Cells* 2015;33(3):999-1012.
17. Branchfield K, Li R, Lungova V, Verheyden JM, McCulley D, Sun X. A three-dimensional study of alveologenesis in mouse lung. *Dev Biol* 2016;409(2):429-441.
18. Chung MI, Hogan BLM. Ager-creer(t2): A new genetic tool for studying lung alveolar development, homeostasis, and repair. *Am J Respir Cell Mol Biol* 2018.
19. Opitz L, Kling KM, Brandenberger C, Mühlfeld C. Lipid-body containing interstitial cells (lipofibroblasts) in the lungs of various mouse strains. *J Anat* 2017;231(6):970-977.
20. Torday JS, Rehan VK. On the evolution of the pulmonary alveolar lipofibroblast. *Exp Cell Res* 2016;340(2):215-219.
21. Bonnans C, Chou J, Werb Z. Remodelling the extracellular matrix in development and disease. *Nat Rev Mol Cell Biol* 2014;15(12):786-801.
22. Zhou Y, Horowitz JC, Naba A, Ambalavanan N, Atabai K, Balestrini J, Bitterman PB, Corley RA, Ding BS, Engler AJ, et al. Extracellular matrix in lung development, homeostasis and disease. *Matrix Biol* 2018;73:77-104.
23. Kim N, Vu TH. Parabronchial smooth muscle cells and alveolar myofibroblasts in lung development. *Birth Defects Res C Embryo Today* 2006;78(1):80-89.
24. Kugler MC, Loomis CA, Zhao Z, Cushman JC, Liu L, Munger JS. Sonic hedgehog signaling regulates myofibroblast function during alveolar septum formation in murine postnatal lung. *Am J Respir Cell Mol Biol* 2017;57(3):280-293.
25. Barron L, Gharib SA, Duffield JS. Lung pericytes and resident fibroblasts: Busy multitaskers. *Am J Pathol* 2016;186(10):2519-2531.
26. Froidure A, Marchal-Duval E, Homps-Legrand M, Ghanem M, Justet A, Crestani B, Mailleux A. Chaotic activation of developmental signalling pathways drives idiopathic pulmonary fibrosis. *Eur Respir Rev* 2020;29(158).
27. Rodriguez-Castillo JA, Perez DB, Ntokou A, Seeger W, Morty RE, Ahlbrecht K. Understanding alveolarization to induce lung regeneration. *Respir Res* 2018;19(1):148.
28. Boucherat O, Franco-Montoya ML, Thibault C, Incitti R, Chailley-Heu B, Delacourt C, Bourbon JR. Gene expression profiling in lung fibroblasts reveals new players in alveolarization. *Physiol Genomics* 2007;32(1):128-141.
29. Patel RM, Kandefer S, Walsh MC, Bell EF, Carlo WA, Laptook AR, Sanchez PJ, Shankaran S, Van Meurs KP, Ball MB, et al. Causes and timing of death in extremely premature infants from 2000 through 2011. *N Engl J Med* 2015;372(4):331-340.
30. Collaco JM, McGrath-Morrow SA. Respiratory phenotypes for preterm infants, children, and adults: Bronchopulmonary dysplasia and more. *Ann Am Thorac Soc* 2018.
31. Collaco JM, Romer LH, Stuart BD, Coulson JD, Everett AD, Lawson EE, Brenner JI, Brown AT, Nies MK, Sekar P, et al. Frontiers in pulmonary hypertension in infants and children with bronchopulmonary dysplasia. *Pediatr Pulmonol* 2012;47(11):1042-1053.
32. Bolton CE, Bush A, Hurst JR, Kotecha S, McGarvey L. Lung consequences in adults born prematurely. *Thorax* 2015;70(6):574-580.
33. Cristea AI, Carroll AE, Davis SD, Swigonski NL, Ackerman VL. Outcomes of children with severe bronchopulmonary dysplasia who were ventilator dependent at home. *Pediatrics* 2013;132(3):e727-734.

34. Hurst JR, Beckmann J, Ni Y, Bolton CE, McEniery CM, Cockcroft JR, Marlow N. Respiratory and cardiovascular outcomes in survivors of extremely preterm birth at 19 years. *Am J Respir Crit Care Med* 2020.
35. Um-Bergstrom P, Hallberg J, Pourbazargan M, Berggren-Brostrom E, Ferrara G, Eriksson MJ, Nyren S, Gao J, Lilja G, Linden A, et al. Pulmonary outcomes in adults with a history of bronchopulmonary dysplasia differ from patients with asthma. *Respir Res* 2019;20(1):102.
36. Blencowe H, Cousens S, Oestergaard MZ, Chou D, Moller AB, Narwal R, Adler A, Vera Garcia C, Rohde S, Say L, et al. National, regional, and worldwide estimates of preterm birth rates in the year 2010 with time trends since 1990 for selected countries: A systematic analysis and implications. *Lancet* 2012;379(9832):2162-2172.
37. Ehrenkranz RA, Walsh MC, Vohr BR, Jobe AH, Wright LL, Fanaroff AA, Wrage LA, Poole K. Validation of the national institutes of health consensus definition of bronchopulmonary dysplasia. *Pediatrics* 2005;116(6):1353-1360.
38. Jensen EA, Dysart K, Gantz MG, McDonald S, Bamat NA, Keszler M, Kirpalani H, Laughon MM, Poindexter BB, Duncan AF, et al. The diagnosis of bronchopulmonary dysplasia in very preterm infants. An evidence-based approach. *Am J Respir Crit Care Med* 2019;200(6):751-759.
39. Northway WH, Jr., Rosan RC, Porter DY. Pulmonary disease following respirator therapy of hyaline-membrane disease. Bronchopulmonary dysplasia. *N Engl J Med* 1967;276(7):357-368.
40. Coalson JJ. Pathology of bronchopulmonary dysplasia. *Semin Perinatol* 2006;30(4):179-184.
41. Lal CV, Ambalavanan N. Biomarkers, early diagnosis, and clinical predictors of bronchopulmonary dysplasia. *Clin Perinatol* 2015;42(4):739-754.
42. D'Angio CT, Ambalavanan N, Carlo WA, McDonald SA, Skogstrand K, Hougaard DM, Shankaran S, Goldberg RN, Ehrenkranz RA, Tyson JE, et al. Blood cytokine profiles associated with distinct patterns of bronchopulmonary dysplasia among extremely low birth weight infants. *J Pediatr* 2016;174:45-51.e45.
43. Ambalavanan N, Cotten CM, Page GP, Carlo WA, Murray JC, Bhattacharya S, Mariani TJ, Cuna AC, Faye-Petersen OM, Kelly D, et al. Integrated genomic analyses in bronchopulmonary dysplasia. *J Pediatr* 2015;166(3):531-537.e513.
44. Jenkins G, Goodwin A. Novel approaches to pulmonary fibrosis. *Clin Med (Lond)* 2014;14 Suppl 6:s45-49.
45. Xie T, Wang Y, Deng N, Huang G, Taghavifar F, Geng Y, Liu N, Kulur V, Yao C, Chen P, et al. Single-cell deconvolution of fibroblast heterogeneity in mouse pulmonary fibrosis. *Cell Rep* 2018;22(13):3625-3640.
46. Endale M, Ahlfeld S, Bao E, Chen X, Green J, Bess Z, Weirauch MT, Xu Y, Perl AK. Temporal, spatial, and phenotypical changes of pdgfrα expressing fibroblasts during late lung development. *Dev Biol* 2017;425(2):161-175.
47. Choi CW. Lung interstitial cells during alveolarization. *Korean J Pediatr* 2010;53(12):979-984.
48. Henderson NC, Arnold TD, Katamura Y, Giacomini MM, Rodriguez JD, McCarty JH, Pellicoro A, Raschperger E, Betsholtz C, Ruminski PG, et al. Targeting of alphav integrin identifies a core molecular pathway that regulates fibrosis in several organs. *Nat Med* 2013;19(12):1617-1624.
49. Salter DM, Griffin M, Muir M, Teo K, Culley J, Smith JR, Gomez-Cuadrado L, Matchett K, Sims AH, Hayward L, et al. Development of mouse models of angiosarcoma driven by p53. *Dis Model Mech* 2019;12(7).

50. Hinz B, Phan SH, Thannickal VJ, Prunotto M, Desmouliere A, Varga J, De Wever O, Mareel M, Gabbiani G. Recent developments in myofibroblast biology: Paradigms for connective tissue remodeling. *The American journal of pathology* 2012;180(4):1340-1355.
51. Habiel DM, Hogaboam CM. Heterogeneity of fibroblasts and myofibroblasts in pulmonary fibrosis. *Curr Pathobiol Rep* 2017;5(2):101-110.
52. Lee JH, Rawlins EL. Developmental mechanisms and adult stem cells for therapeutic lung regeneration. *Dev Biol* 2018;433(2):166-176.
53. Balestrini JL, Chaudhry S, Sarrazy V, Koehler A, Hinz B. The mechanical memory of lung myofibroblasts. *Integrative biology : quantitative biosciences from nano to macro* 2012;4(4):410-421.
54. Harrell CR, Simovic Markovic B, Fellabaum C, Arsenijevic A, Djonov V, Volarevic V. Molecular mechanisms underlying therapeutic potential of pericytes. *J Biomed Sci* 2018;25(1):21.
55. Foo SS, Turner CJ, Adams S, Compagni A, Aubyn D, Kogata N, Lindblom P, Shani M, Zicha D, Adams RH. Ephrin-b2 controls cell motility and adhesion during blood-vessel-wall assembly. *Cell* 2006;124(1):161-173.
56. Hung C, Linn G, Chow YH, Kobayashi A, Mittelsteadt K, Altemeier WA, Gharib SA, Schnapp LM, Duffield JS. Role of lung pericytes and resident fibroblasts in the pathogenesis of pulmonary fibrosis. *Am J Respir Crit Care Med* 2013;188(7):820-830.
57. Minutti CM, Modak RV, Macdonald F, Li F, Smyth DJ, Dorward DA, Blair N, Husovsky C, Muir A, Giampazolias E, et al. A macrophage-pericyte axis directs tissue restoration via amphiregulin-induced transforming growth factor beta activation. *Immunity* 2019;50(3):645-654.e646.
58. Dünker N, Krieglstein K. Targeted mutations of transforming growth factor-beta genes reveal important roles in mouse development and adult homeostasis. *Eur J Biochem* 2000;267(24):6982-6988.
59. Bartram U, Speer CP. The role of transforming growth factor beta in lung development and disease. *Chest* 2004;125(2):754-765.
60. Piersma B, Bank RA, Boersema M. Signaling in fibrosis: Tgf-beta, wnt, and yap/taz converge. *Front Med (Lausanne)* 2015;2:59.
61. Shull MM, Ormsby I, Kier AB, Pawlowski S, Diebold RJ, Yin M, Allen R, Sidman C, Proetzel G, Calvin D, et al. Targeted disruption of the mouse transforming growth factor-beta 1 gene results in multifocal inflammatory disease. *Nature* 1992;359(6397):693-699.
62. Tatler AL, Jenkins G. Tgf-beta activation and lung fibrosis. *Proc Am Thorac Soc* 2012;9(3):130-136.
63. Sanford LP, Ormsby I, Gittenberger-de Groot AC, Sariola H, Friedman R, Boivin GP, Cardell EL, Doetschman T. Tgfbeta2 knockout mice have multiple developmental defects that are non-overlapping with other tgfbeta knockout phenotypes. *Development* 1997;124(13):2659-2670.
64. Kaartinen V, Voncken JW, Shuler C, Warburton D, Bu D, Heisterkamp N, Groffen J. Abnormal lung development and cleft palate in mice lacking tgf-beta 3 indicates defects of epithelial-mesenchymal interaction. *Nat Genet* 1995;11(4):415-421.
65. Dabovic B, Chen Y, Choi J, Vassallo M, Dietz HC, Ramirez F, von Melchner H, Davis EC, Rifkin DB. Dual functions for ltbp in lung development: Ltbp-4 independently modulates elastogenesis and tgf-beta activity. *J Cell Physiol* 2009;219(1):14-22.

66. Goodwin A, Jenkins G. Role of integrin-mediated tgfbeta activation in the pathogenesis of pulmonary fibrosis. *Biochem Soc Trans* 2009;37(Pt 4):849-854.
67. Tatler AL, Porte J, Knox A, Jenkins G, Pang L. Tryptase activates tgfbeta in human airway smooth muscle cells via direct proteolysis. *Biochemical and biophysical research communications* 2008;370(2):239-242.
68. Jenkins G. The role of proteases in transforming growth factor-beta activation. *Int J Biochem Cell Biol* 2008;40(6-7):1068-1078.
69. Sime PJ, Xing Z, Graham FL, Csaky KG, Gauldie J. Adenovector-mediated gene transfer of active transforming growth factor-beta1 induces prolonged severe fibrosis in rat lung. *The Journal of clinical investigation* 1997;100(4):768-776.
70. Hong KM, Belperio JA, Keane MP, Burdick MD, Strieter RM. Differentiation of human circulating fibrocytes as mediated by transforming growth factor-beta and peroxisome proliferator-activated receptor gamma. *The Journal of biological chemistry* 2007;282(31):22910-22920.
71. Coker RK, Laurent GJ, Shahzeidi S, Lympany PA, du Bois RM, Jeffery PK, McAnulty RJ. Transforming growth factors-beta 1, -beta 2, and -beta 3 stimulate fibroblast procollagen production in vitro but are differentially expressed during bleomycin-induced lung fibrosis. *The American journal of pathology* 1997;150(3):981-991.
72. Coker RK, Laurent GJ, Jeffery PK, du Bois RM, Black CM, McAnulty RJ. Localisation of transforming growth factor beta1 and beta3 mrna transcripts in normal and fibrotic human lung. *Thorax* 2001;56(7):549-556.
73. Bonniaud P, Margetts PJ, Kolb M, Schroeder JA, Kapoun AM, Damm D, Murphy A, Chakravarty S, Dugar S, Higgins L, et al. Progressive transforming growth factor beta1-induced lung fibrosis is blocked by an orally active alk5 kinase inhibitor. *American journal of respiratory and critical care medicine* 2005;171(8):889-898.
74. Xu MY, Porte J, Knox AJ, Weinreb PH, Maher TM, Violette SM, McAnulty RJ, Sheppard D, Jenkins G. Lysophosphatidic acid induces alphavbeta6 integrin-mediated tgf-beta activation via the lpa2 receptor and the small g protein g alpha(q). *Am J Pathol* 2009;174(4):1264-1279.
75. Weinreb PH, Simon KJ, Rayhorn P, Yang WJ, Leone DR, Dolinski BM, Pearse BR, Yokota Y, Kawakatsu H, Atakilit A, et al. Function-blocking integrin alphavbeta6 monoclonal antibodies: Distinct ligand-mimetic and nonligand-mimetic classes. *J Biol Chem* 2004;279(17):17875-17887.
76. Serra R, Pelton RW, Moses HL. Tgf beta 1 inhibits branching morphogenesis and n-myc expression in lung bud organ cultures. *Development* 1994;120(8):2153-2161.
77. Zhao J, Shi W, Chen H, Warburton D. Smad7 and smad6 differentially modulate transforming growth factor beta -induced inhibition of embryonic lung morphogenesis. *J Biol Chem* 2000;275(31):23992-23997.
78. Zhao J, Crowe DL, Castillo C, Wuenschell C, Chai Y, Warburton D. Smad7 is a tgf-beta-inducible attenuator of smad2/3-mediated inhibition of embryonic lung morphogenesis. *Mech Dev* 2000;93(1-2):71-81.
79. Hu-Lowe DD, Chen E, Zhang L, Watson KD, Mancuso P, Lappin P, Wickman G, Chen JH, Wang J, Jiang X, et al. Targeting activin receptor-like kinase 1 inhibits angiogenesis and tumorigenesis through a mechanism of action complementary to anti-vegf therapies. *Cancer Res* 2011;71(4):1362-1373.
80. Bhaskaran M, Kolliputi N, Wang Y, Gou D, Chintagari NR, Liu L. Trans-differentiation of alveolar epithelial type ii cells to type i cells involves autocrine

signaling by transforming growth factor beta 1 through the smad pathway. *J Biol Chem* 2007;282(6):3968-3976.
81. Xing Y, Li C, Li A, Sridurongrit S, Tiozzo C, Bellusci S, Borok Z, Kaartinen V, Minoo P. Signaling via alk5 controls the ontogeny of lung clara cells. *Development* 2010;137(5):825-833.
82. Schmid P, Cox D, Bilbe G, Maier R, McMaster GK. Differential expression of tgf beta 1, beta 2 and beta 3 genes during mouse embryogenesis. *Development* 1991;111(1):117-130.
83. Pelton RW, Saxena B, Jones M, Moses HL, Gold LI. Immunohistochemical localization of tgf beta 1, tgf beta 2, and tgf beta 3 in the mouse embryo: Expression patterns suggest multiple roles during embryonic development. *J Cell Biol* 1991;115(4):1091-1105.
84. Liu J, Tseu I, Wang J, Tanswell K, Post M. Transforming growth factor beta2, but not beta1 and beta3, is critical for early rat lung branching. *Dev Dyn* 2000;217(4):343-360.
85. Bragg AD, Moses HL, Serra R. Signaling to the epithelium is not sufficient to mediate all of the effects of transforming growth factor beta and bone morphogenetic protein 4 on murine embryonic lung development. *Mech Dev* 2001;109(1):13-26.
86. Stenmark KR, Abman SH. Lung vascular development: Implications for the pathogenesis of bronchopulmonary dysplasia. *Annu Rev Physiol* 2005;67:623-661.
87. Belcastro R, Lopez L, Li J, Masood A, Tanswell AK. Chronic lung injury in the neonatal rat: Up-regulation of tgfβ1 and nitration of igf-r1 by peroxynitrite as likely contributors to impaired alveologenesis. *Free Radic Biol Med* 2015;80:1-11.
88. Nakanishi H, Sugiura T, Streisand JB, Lonning SM, Roberts JD, Jr. Tgf-beta-neutralizing antibodies improve pulmonary alveologenesis and vasculogenesis in the injured newborn lung. *Am J Physiol Lung Cell Mol Physiol* 2007;293(1):L151-161.
89. Chen H, Sun J, Buckley S, Chen C, Warburton D, Wang XF, Shi W. Abnormal mouse lung alveolarization caused by smad3 deficiency is a developmental antecedent of centrilobular emphysema. *Am J Physiol Lung Cell Mol Physiol* 2005;288(4):L683-691.
90. Chen H, Zhuang F, Liu YH, Xu B, Del Moral P, Deng W, Chai Y, Kolb M, Gauldie J, Warburton D, et al. Tgf-beta receptor ii in epithelia versus mesenchyme plays distinct roles in the developing lung. *Eur Respir J* 2008;32(2):285-295.
91. Sterner-Kock A, Thorey IS, Koli K, Wempe F, Otte J, Bangsow T, Kuhlmeier K, Kirchner T, Jin S, Keski-Oja J, et al. Disruption of the gene encoding the latent transforming growth factor-beta binding protein 4 (ltbp-4) causes abnormal lung development, cardiomyopathy, and colorectal cancer. *Genes Dev* 2002;16(17):2264-2273.
92. Pieretti AC, Ahmed AM, Roberts JD, Jr., Kelleher CM. A novel in vitro model to study alveologenesis . *Am J Respir Cell Mol Biol* 2014;50(2):459-469.
93. Deng S, Zhang H, Han W, Guo C, Deng C. Transforming growth factor-β-neutralizing antibodies improve alveolarization in the oxygen-exposed newborn mouse lung. *J Interferon Cytokine Res* 2019;39(2):106-116.
94. Gauldie J, Galt T, Bonniaud P, Robbins C, Kelly M, Warburton D. Transfer of the active form of transforming growth factor-beta 1 gene to newborn rat lung induces changes consistent with bronchopulmonary dysplasia. *Am J Pathol* 2003;163(6):2575-2584.
95. Vicencio AG, Lee CG, Cho SJ, Eickelberg O, Chuu Y, Haddad GG, Elias JA. Conditional overexpression of bioactive transforming growth factor-beta1 in

neonatal mouse lung: A new model for bronchopulmonary dysplasia? *Am J Respir Cell Mol Biol* 2004;31(6):650-656.
96. Alejandre-Alcázar MA, Michiels-Corsten M, Vicencio AG, Reiss I, Ryu J, de Krijger RR, Haddad GG, Tibboel D, Seeger W, Eickelberg O, et al. Tgf-beta signaling is dynamically regulated during the alveolarization of rodent and human lungs. *Dev Dyn* 2008;237(1):259-269.
97. Bonniaud P, Kolb M, Galt T, Robertson J, Robbins C, Stampfli M, Lavery C, Margetts PJ, Roberts AB, Gauldie J. Smad3 null mice develop airspace enlargement and are resistant to tgf-beta-mediated pulmonary fibrosis. *J Immunol* 2004;173(3):2099-2108.
98. Li A, Ma S, Smith SM, Lee MK, Fischer A, Borok Z, Bellusci S, Li C, Minoo P. Mesodermal alk5 controls lung myofibroblast versus lipofibroblast cell fate. *BMC Biol* 2016;14:19.
99. Mager EM, Renzetti G, Auais A, Piedimonte G. Growth factors gene expression in the developing lung. *Acta Paediatr* 2007;96(7):1015-1020.
100. Dabovic B, Robertson IB, Zilberberg L, Vassallo M, Davis EC, Rifkin DB. Function of latent tgfβ binding protein 4 and fibulin 5 in elastogenesis and lung development. *J Cell Physiol* 2015;230(1):226-236.
101. Bultmann-Mellin I, Dinger K, Debuschewitz C, Loewe KMA, Melcher Y, Plum MTW, Appel S, Rappl G, Willenborg S, Schauss AC, et al. Role of ltbp4 in alveolarization, angiogenesis, and fibrosis in lungs. *Am J Physiol Lung Cell Mol Physiol* 2017;313(4):L687-l698.
102. Oak P, Hilgendorff A. The bpd trio? Interaction of dysregulated pdgf, vegf, and tgf signaling in neonatal chronic lung disease. *Mol Cell Pediatr* 2017;4(1):11.
103. Lecart C, Cayabyab R, Buckley S, Morrison J, Kwong KY, Warburton D, Ramanathan R, Jones CA, Minoo P. Bioactive transforming growth factor-beta in the lungs of extremely low birthweight neonates predicts the need for home oxygen supplementation. *Biol Neonate* 2000;77(4):217-223.
104. Ganguly S, Saxena R, Chattopadhyay A. Reorganization of the actin cytoskeleton upon g-protein coupled receptor signaling. *Biochim Biophys Acta* 2011;1808(7):1921-1929.
105. Kamato D, Mitra P, Davis F, Osman N, Chaplin R, Cabot PJ, Afroz R, Thomas W, Zheng W, Kaur H, et al. Gaq proteins: Molecular pharmacology and therapeutic potential. *Cellular and molecular life sciences : CMLS* 2016.
106. Xiang SY, Dusaban SS, Brown JH. Lysophospholipid receptor activation of rhoa and lipid signaling pathways. *Biochim Biophys Acta* 2013;1831(1):213-222.
107. Offermanns S. In vivo functions of heterotrimeric g-proteins: Studies in galpha-deficient mice. *Oncogene* 2001;20(13):1635-1642.
108. Offermanns S, Toombs CF, Hu YH, Simon MI. Defective platelet activation in g alpha(q)-deficient mice. *Nature* 1997;389(6647):183-186.
109. Offermanns S, Hashimoto K, Watanabe M, Sun W, Kurihara H, Thompson RF, Inoue Y, Kano M, Simon MI. Impaired motor coordination and persistent multiple climbing fiber innervation of cerebellar purkinje cells in mice lacking galphaq. *Proc Natl Acad Sci U S A* 1997;94(25):14089-14094.
110. Strathmann M, Simon MI. G protein diversity: A distinct class of alpha subunits is present in vertebrates and invertebrates. *Proc Natl Acad Sci U S A* 1990;87(23):9113-9117.
111. Stoddard NC, Chun J. Promising pharmacological directions in the world of lysophosphatidic acid signaling. *Biomolecules & therapeutics* 2015;23(1):1-11.

112. Singh I, Knezevic N, Ahmmed GU, Kini V, Malik AB, Mehta D. Galphaq-trpc6-mediated ca2+ entry induces rhoa activation and resultant endothelial cell shape change in response to thrombin. *The Journal of biological chemistry* 2007;282(11):7833-7843.
113. Froese AR, Shimbori C, Bellaye PS, Inman M, Obex S, Fatima S, Jenkins G, Gauldie J, Ask K, Kolb M. Stretch-induced activation of transforming growth factor-beta1 in pulmonary fibrosis. *American journal of respiratory and critical care medicine* 2016;194(1):84-96.
114. Kamato D, Thach L, Bernard R, Chan V, Zheng W, Kaur H, Brimble M, Osman N, Little PJ. Structure, function, pharmacology, and therapeutic potential of the g protein, galpha/q,11. *Front Cardiovasc Med* 2015;2:14.
115. Strathmann MP, Simon MI. G alpha 12 and g alpha 13 subunits define a fourth class of g protein alpha subunits. *Proc Natl Acad Sci U S A* 1991;88(13):5582-5586.
116. Mikelis CM, Palmby TR, Simaan M, Li W, Szabo R, Lyons R, Martin D, Yagi H, Fukuhara S, Chikumi H, et al. Pdz-rhogef and larg are essential for embryonic development and provide a link between thrombin and lpa receptors and rho activation. *The Journal of biological chemistry* 2013;288(17):12232-12243.
117. Gu JL, Muller S, Mancino V, Offermanns S, Simon MI. Interaction of g alpha(12) with g alpha(13) and g alpha(q) signaling pathways. *Proc Natl Acad Sci U S A* 2002;99(14):9352-9357.
118. Yu OM, Brown JH. G protein-coupled receptor and rhoa-stimulated transcriptional responses: Links to inflammation, differentiation, and cell proliferation. *Mol Pharmacol* 2015;88(1):171-180.
119. Huang X, Yang N, Fiore VF, Barker TH, Sun Y, Morris SW, Ding Q, Thannickal VJ, Zhou Y. Matrix stiffness-induced myofibroblast differentiation is mediated by intrinsic mechanotransduction. *American Journal of Respiratory Cell & Molecular Biology* 2012;47(3):340-348.
120. Htwe SS, Cha BH, Yue K, Khademhosseini A, Knox AJ, Ghaemmaghami AM. Role of rock isoforms in regulation of stiffness induced myofibroblast differentiation in lung fibrosis. *American journal of respiratory cell and molecular biology* 2017.
121. Sakai N, Chun J, Duffield JS, Wada T, Luster AD, Tager AM. Lpa1-induced cytoskeleton reorganization drives fibrosis through ctgf-dependent fibroblast proliferation. *FASEB journal : official publication of the Federation of American Societies for Experimental Biology* 2013;27(5):1830-1846.
122. Sandbo N, Dulin N. Actin cytoskeleton in myofibroblast differentiation: Ultrastructure defining form and driving function. *Transl Res* 2011;158(4):181-196.
123. Zhou Y, Huang X, Hecker L, Kurundkar D, Kurundkar A, Liu H, Jin TH, Desai L, Bernard K, Thannickal VJ. Inhibition of mechanosensitive signaling in myofibroblasts ameliorates experimental pulmonary fibrosis. *Journal of Clinical Investigation* 2013;123(3):1096-1108.
124. Shimizu Y, Dobashi K, Iizuka K, Horie T, Suzuki K, Tukagoshi H, Nakazawa T, Nakazato Y, Mori M. Contribution of small gtpase rho and its target protein rock in a murine model of lung fibrosis. *American journal of respiratory and critical care medicine* 2001;163(1):210-217.
125. Knipe RS, Probst CK, Lagares D, Franklin A, Spinney JJ, Brazee PL, Grasberger P, Zhang L, Black KE, Sakai N, et al. The rho kinase isoforms rock1 and rock2 each contribute to the development of experimental pulmonary fibrosis. *Am J Respir Cell Mol Biol* 2017.

126. Jenkins RG, Su X, Su G, Scotton CJ, Camerer E, Laurent GJ, Davis GE, Chambers RC, Matthay MA, Sheppard D. Ligation of protease-activated receptor 1 enhances alpha(v)beta6 integrin-dependent tgf-beta activation and promotes acute lung injury. *The Journal of clinical investigation* 2006;116(6):1606-1614.
127. Tager AM, LaCamera P, Shea BS, Campanella GS, Selman M, Zhao Z, Polosukhin V, Wain J, Karimi-Shah BA, Kim ND, et al. The lysophosphatidic acid receptor lpa1 links pulmonary fibrosis to lung injury by mediating fibroblast recruitment and vascular leak. *Nature Medicine* 2008;14(1):45-54.
128. Scotton CJ, Krupiczojc MA, Konigshoff M, Mercer PF, Lee YC, Kaminski N, Morser J, Post JM, Maher TM, Nicholson AG, et al. Increased local expression of coagulation factor x contributes to the fibrotic response in human and murine lung injury. *J Clin Invest* 2009;119(9):2550-2563.
129. Funke M, Zhao Z, Xu Y, Chun J, Tager AM. The lysophosphatidic acid receptor lpa1 promotes epithelial cell apoptosis after lung injury. *American Journal of Respiratory Cell & Molecular Biology* 2012;46(3):355-364.
130. Saleh D, Furukawa K, Tsao MS, Maghazachi A, Corrin B, Yanagisawa M, Barnes PJ, Giaid A. Elevated expression of endothelin-1 and endothelin-converting enzyme-1 in idiopathic pulmonary fibrosis: Possible involvement of proinflammatory cytokines. *Am J Respir Cell Mol Biol* 1997;16(2):187-193.
131. Fabre A, Marchal-Sommé J, Marchand-Adam S, Quesnel C, Borie R, Dehoux M, Ruffié C, Callebert J, Launay JM, Hénin D, et al. Modulation of bleomycin-induced lung fibrosis by serotonin receptor antagonists in mice. *Eur Respir J* 2008;32(2):426-436.
132. Tan WSD, Liao W, Zhou S, Mei D, Wong WF. Targeting the renin-angiotensin system as novel therapeutic strategy for pulmonary diseases. *Curr Opin Pharmacol* 2018;40:9-17.
133. Shea BS, Tager AM. Role of the lysophospholipid mediators lysophosphatidic acid and sphingosine 1-phosphate in lung fibrosis. *Proc Am Thorac Soc* 2012;9(3):102-110.
134. Black KE, Berdyshev E, Bain G, Castelino FV, Shea BS, Probst CK, Fontaine BA, Bronova I, Goulet L, Lagares D, et al. Autotaxin activity increases locally following lung injury, but is not required for pulmonary lysophosphatidic acid production or fibrosis. *FASEB journal : official publication of the Federation of American Societies for Experimental Biology* 2016;30(6):2435-2450.
135. Aikawa S, Hashimoto T, Kano K, Aoki J. Lysophosphatidic acid as a lipid mediator with multiple biological actions. *J Biochem* 2015;157(2):81-89.
136. Montesi SB, Mathai SK, Brenner LN, Gorshkova IA, Berdyshev EV, Tager AM, Shea BS. Docosatetraenoyl lpa is elevated in exhaled breath condensate in idiopathic pulmonary fibrosis. *BMC Pulmonary Medicine* 2014;14:5.
137. Tatler AL, John AE, Jolly L, Habgood A, Porte J, Brightling C, Knox AJ, Pang L, Sheppard D, Huang X, et al. Integrin alphavbeta5-mediated tgf-beta activation by airway smooth muscle cells in asthma. *J Immunol* 2011;187(11):6094-6107.
138. Lee DJ, Ho CH, Grinnell F. Lpa-stimulated fibroblast contraction of floating collagen matrices does not require rho kinase activity or retraction of fibroblast extensions. *Exp Cell Res* 2003;289(1):86-94.
139. Ikeda H, Yatomi Y, Yanase M, Satoh H, Nishihara A, Kawabata M, Fujiwara K. Effects of lysophosphatidic acid on proliferation of stellate cells and hepatocytes in culture. *Biochemical & Biophysical Research Communications* 1998;248(2):436-440.
140. Huang LS, Fu P, Patel P, Harijith A, Sun T, Zhao Y, Garcia JG, Chun J, Natarajan V. Lysophosphatidic acid receptor-2 deficiency confers protection against bleomycin-

induced lung injury and fibrosis in mice. *American Journal of Respiratory Cell & Molecular Biology* 2013;49(6):912-922.
141. Swaney JS, Chapman C, Correa LD, Stebbins KJ, Bundey RA, Prodanovich PC, Fagan P, Baccei CS, Santini AM, Hutchinson JH, et al. A novel, orally active lpa(1) receptor antagonist inhibits lung fibrosis in the mouse bleomycin model. *British Journal of Pharmacology* 2010;160(7):1699-1713.
142. Funke M, Knudsen L, Lagares D, Ebener S, Probst CK, Fontaine BA, Franklin A, Kellner M, Kuhnel M, Matthieu S, et al. Lysophosphatidic acid signaling through the lysophosphatidic acid-1 receptor is required for alveolarization. *Am J Respir Cell Mol Biol* 2016;55(1):105-116.
143. Offermanns S, Zhao LP, Gohla A, Sarosi I, Simon MI, Wilkie TM. Embryonic cardiomyocyte hypoplasia and craniofacial defects in g alpha q/g alpha 11-mutant mice. *The EMBO journal* 1998;17(15):4304-4312.
144. Offermanns S, Mancino V, Revel JP, Simon MI. Vascular system defects and impaired cell chemokinesis as a result of galpha13 deficiency. *Science (New York, NY)* 1997;275(5299):533-536.
145. Haak AJ, Ducharme MT, Diaz Espinosa AM, Tschumperlin DJ. Targeting gpcr signaling for idiopathic pulmonary fibrosis therapies. *Trends Pharmacol Sci* 2020;41(3):172-182.
146. King TE, Jr., Behr J, Brown KK, du Bois RM, Lancaster L, de Andrade JA, Stähler G, Leconte I, Roux S, Raghu G. Build-1: A randomized placebo-controlled trial of bosentan in idiopathic pulmonary fibrosis. *Am J Respir Crit Care Med* 2008;177(1):75-81.
147. King TE, Jr., Brown KK, Raghu G, du Bois RM, Lynch DA, Martinez F, Valeyre D, Leconte I, Morganti A, Roux S, et al. Build-3: A randomized, controlled trial of bosentan in idiopathic pulmonary fibrosis. *Am J Respir Crit Care Med* 2011;184(1):92-99.
148. Raghu G, Million-Rousseau R, Morganti A, Perchenet L, Behr J. Macitentan for the treatment of idiopathic pulmonary fibrosis: The randomised controlled music trial. *Eur Respir J* 2013;42(6):1622-1632.
149. Raghu G, Behr J, Brown KK, Egan JJ, Kawut SM, Flaherty KR, Martinez FJ, Nathan SD, Wells AU, Collard HR, et al. Treatment of idiopathic pulmonary fibrosis with ambrisentan: A parallel, randomized trial. *Ann Intern Med* 2013;158(9):641-649.
150. Palmer SM, Snyder L, Todd JL, Soule B, Christian R, Anstrom K, Luo Y, Gagnon R, Rosen G. Randomized, double-blind, placebo-controlled, phase 2 trial of bms-986020, a lysophosphatidic acid receptor antagonist for the treatment of idiopathic pulmonary fibrosis. *Chest* 2018;154(5):1061-1069.
151. Khalil N, Manganas H, Ryerson CJ, Shapera S, Cantin AM, Hernandez P, Turcotte EE, Parker JM, Moran JE, Albert GR, et al. Phase 2 clinical trial of pbi-4050 in patients with idiopathic pulmonary fibrosis. *Eur Respir J* 2019;53(3).
152. Medicine UNLo. Clinicaltrials.Gov.
153. Couluris M, Kinder BW, Xu P, Gross-King M, Krischer J, Panos RJ. Treatment of idiopathic pulmonary fibrosis with losartan: A pilot project. *Lung* 2012;190(5):523-527.
154. Wright CE, Fraser SD, Brindle K, Morice AH, Hart SP, Crooks MG. Inhaled beclomethasone/formoterol in idiopathic pulmonary fibrosis: A randomised controlled exploratory study. *ERJ Open Res* 2017;3(4).
155. Deng X, Mercer PF, Scotton CJ, Gilchrist A, Chambers RC. Thrombin induces fibroblast ccl2/je production and release via coupling of par1 to galphaq and

cooperation between erk1/2 and rho kinase signaling pathways. *Molecular biology of the cell* 2008;19(6):2520-2533.
156. Flock T, Hauser AS, Lund N, Gloriam DE, Balaji S, Babu MM. Selectivity determinants of gpcr-g-protein binding. *Nature* 2017;545(7654):317-322.
157. Jansen KA, Atherton P, Ballestrem C. Mechanotransduction at the cell-matrix interface. *Semin Cell Dev Biol* 2017;71:75-83.
158. Asano S, Ito S, Takahashi K, Furuya K, Kondo M, Sokabe M, Hasegawa Y. Matrix stiffness regulates migration of human lung fibroblasts. *Physiol Rep* 2017;5(9).
159. Jansen KA, Donato DM, Balcioglu HE, Schmidt T, Danen EH, Koenderink GH. A guide to mechanobiology: Where biology and physics meet. *Biochimica et Biophysica Acta* 2015;1853(11 Pt B):3043-3052.
160. Yi E, Sato S, Takahashi A, Parameswaran H, Blute TA, Bartolak-Suki E, Suki B. Mechanical forces accelerate collagen digestion by bacterial collagenase in lung tissue strips. *Frontiers in physiology* 2016;7:287.
161. Hinz B. The extracellular matrix and transforming growth factor-beta1: Tale of a strained relationship. *Matrix Biology* 2015;47:54-65.
162. Liu F, Mih JD, Shea BS, Kho AT, Sharif AS, Tager AM, Tschumperlin DJ. Feedback amplification of fibrosis through matrix stiffening and cox-2 suppression. *The Journal of cell biology* 2010;190(4):693-706.
163. Liu F, Lagares D, Choi KM, Stopfer L, Marinkovic A, Vrbanac V, Probst CK, Hiemer SE, Sisson TH, Horowitz JC, et al. Mechanosignaling through yap and taz drives fibroblast activation and fibrosis. *American journal of physiology Lung cellular and molecular physiology* 2015;308(4):L344-357.
164. Goffin JM, Pittet P, Csucs G, Lussi JW, Meister JJ, Hinz B. Focal adhesion size controls tension-dependent recruitment of alpha-smooth muscle actin to stress fibers. *The Journal of cell biology* 2006;172(2):259-268.
165. Arora PD, Narani N, McCulloch CA. The compliance of collagen gels regulates transforming growth factor-beta induction of alpha-smooth muscle actin in fibroblasts. *The American journal of pathology* 1999;154(3):871-882.
166. Southern BD, Grove LM, Rahaman SO, Abraham S, Scheraga RG, Niese KA, Sun H, Herzog EL, Liu F, Tschumperlin DJ, et al. Matrix-driven myosin ii mediates the pro-fibrotic fibroblast phenotype. *The Journal of biological chemistry* 2016;291(12):6083-6095.
167. Marinkovic A, Liu F, Tschumperlin DJ. Matrices of physiologic stiffness potently inactivate idiopathic pulmonary fibrosis fibroblasts. *Am J Respir Cell Mol Biol* 2013;48(4):422-430.
168. Wipff PJ, Rifkin DB, Meister JJ, Hinz B. Myofibroblast contraction activates latent tgf-beta1 from the extracellular matrix. *Journal of Cell Biology* 2007;179(6):1311-1323.
169. Zhou C, Jin S, Willing R. Simulation of extracellular matrix remodeling by fibroblast cells in soft three-dimensional bioresorbable scaffolds. *Biomechanics and modeling in mechanobiology* 2016;15(6):1685-1698.
170. Klingberg F, Chow ML, Koehler A, Boo S, Buscemi L, Quinn TM, Costell M, Alman BA, Genot E, Hinz B. Prestress in the extracellular matrix sensitizes latent tgf-beta1 for activation. *Journal of Cell Biology* 2014;207(2):283-297.
171. Carmona-Rosas G, Alfonzo-Mendez MA, Hernandez-Espinosa DA, Romero-Avila MT, Garcia-Sainz JA. A549 cells as a model to study endogenous lpa1 receptor signaling and regulation. *Eur J Pharmacol* 2017;815:258-265.

172. Carloni A, Poletti V, Fermo L, Bellomo N, Chilosi M. Heterogeneous distribution of mechanical stress in human lung: A mathematical approach to evaluate abnormal remodeling in ipf. *J Theor Biol* 2013;332:136-140.
173. Martin C, Papazian L, Payan MJ, Saux P, Gouin F. Pulmonary fibrosis correlates with outcome in adult respiratory distress syndrome. A study in mechanically ventilated patients. *Chest* 1995;107(1):196-200.
174. Watanabe A, Kawaharada N, Higami T. Postoperative acute exacerbation of ipf after lung resection for primary lung cancer. *Pulmonary medicine* 2011;2011:960316.
175. Sakamoto S, Homma S, Mun M, Fujii T, Kurosaki A, Yoshimura K. Acute exacerbation of idiopathic interstitial pneumonia following lung surgery in 3 of 68 consecutive patients: A retrospective study. *Internal medicine (Tokyo, Japan)* 2011;50(2):77-85.
176. Knudsen L, Lopez-Rodriguez E, Berndt L, Steffen L, Ruppert C, Bates JHT, Ochs M, Smith BJ. Alveolar micromechanics in bleomycin-induced lung injury. *Am J Respir Cell Mol Biol* 2018.
177. Albert RK, Smith B, Perlman CE, Schwartz DA. Is progression of pulmonary fibrosis due to ventilation-induced lung injury? *Am J Respir Crit Care Med* 2019.
178. Gunther A, Schmidt R, Nix F, Yabut-Perez M, Guth C, Rosseau S, Siebert C, Grimminger F, Morr H, Velcovsky HG, et al. Surfactant abnormalities in idiopathic pulmonary fibrosis, hypersensitivity pneumonitis and sarcoidosis. *Eur Respir J* 1999;14(3):565-573.
179. Cabrera-Benitez NE, Parotto M, Post M, Han B, Spieth PM, Cheng WE, Valladares F, Villar J, Liu M, Sato M, et al. Mechanical stress induces lung fibrosis by epithelial-mesenchymal transition. *Critical Care Medicine* 2012;40(2):510-517.
180. O'Callaghan CJ, Williams B. Mechanical strain-induced extracellular matrix production by human vascular smooth muscle cells: Role of tgf-beta(1). *Hypertension (Dallas, Tex : 1979)* 2000;36(3):319-324.
181. Black SM, Grobe A, Mata-Greenwood E, Noskina Y. Cyclic stretch increases vegf expression in pulmonary arterial smooth muscle cells via tgf-1 and reactive oxygen species: A requirement for nad(p)h oxidase. *Conf Proc IEEE Eng Med Biol Soc* 2004;7:5053-5056.
182. Mohamed JS, Boriek AM. Stretch augments tgf-beta1 expression through rhoa/rock1/2, ptk, and pi3k in airway smooth muscle cells. *American journal of physiology Lung cellular and molecular physiology* 2010;299(3):L413-424.
183. Ohno S, Tanaka N, Ueki M, Honda K, Tanimoto K, Yoneno K, Ohno-Nakahara M, Fujimoto K, Kato Y, Tanne K. Mechanical regulation of terminal chondrocyte differentiation via rgd-cap/beta ig-h3 induced by tgf-beta. *Connective tissue research* 2005;46(4-5):227-234.
184. Xu H, Zhang X, Wang H, Zhang Y, Shi Y. Continuous cyclic mechanical tension increases ank expression in endplate chondrocytes through the tgf-beta1 and p38 pathway. *European journal of histochemistry : EJH* 2013;57(3):e28.
185. Liton PB, Liu X, Challa P, Epstein DL, Gonzalez P. Induction of tgf-beta1 in the trabecular meshwork under cyclic mechanical stress. *J Cell Physiol* 2005;205(3):364-371.
186. Guo F, Carter DE, Leask A. Mechanical tension increases ccn2/ctgf expression and proliferation in gingival fibroblasts via a tgfbeta-dependent mechanism. *PloS one* 2011;6(5):e19756.

187. Peters AS, Brunner G, Krieg T, Eckes B. Cyclic mechanical strain induces tgfbeta1-signalling in dermal fibroblasts embedded in a 3d collagen lattice. *Arch Dermatol Res* 2015;307(2):191-197.
188. Sato M, Muragaki Y, Saika S, Roberts AB, Ooshima A. Targeted disruption of tgf-beta1/smad3 signaling protects against renal tubulointerstitial fibrosis induced by unilateral ureteral obstruction. *Journal of Clinical Investigation* 2003;112(10):1486-1494.
189. Sakata R, Ueno T, Nakamura T, Ueno H, Sata M. Mechanical stretch induces tgf-beta synthesis in hepatic stellate cells. *Eur J Clin Invest* 2004;34(2):129-136.
190. Blaauboer ME, Smit TH, Hanemaaijer R, Stoop R, Everts V. Cyclic mechanical stretch reduces myofibroblast differentiation of primary lung fibroblasts. *Biochemical & Biophysical Research Communications* 2011;404(1):23-27.
191. Breen EC. Mechanical strain increases type i collagen expression in pulmonary fibroblasts in vitro. *Journal of applied physiology (Bethesda, Md : 1985)* 2000;88(1):203-209.
192. Lutz R, Sakai T, Chiquet M. Pericellular fibronectin is required for rhoa-dependent responses to cyclic strain in fibroblasts. *Journal of cell science* 2010;123(Pt 9):1511-1521.
193. Foolen J, Janssen-van den Broek MW, Baaijens FP. Synergy between rho signaling and matrix density in cyclic stretch-induced stress fiber organization. *Acta biomaterialia* 2014;10(5):1876-1885.
194. Vining KH, Mooney DJ. Mechanical forces direct stem cell behaviour in development and regeneration. *Nat Rev Mol Cell Biol* 2017;18(12):728-742.
195. Li J, Wang Z, Chu Q, Jiang K, Tang N. The strength of mechanical forces determines the differentiation of alveolar epithelial cells. *Dev Cell* 2018;44(3):297-312.e295.
196. Mizikova I, Morty RE. The extracellular matrix in bronchopulmonary dysplasia: Target and source. *Front Med (Lausanne)* 2015;2:91.
197. Filipovic N, Gibney BC, Kojic M, Nikolic D, Isailovic V, Ysasi A, Konerding MA, Mentzer SJ, Tsuda A. Mapping cyclic stretch in the postpneumonectomy murine lung. *Journal of applied physiology (Bethesda, Md : 1985)* 2013;115(9):1370-1378.
198. Breen EC, Fu Z, Normand H. Calcyclin gene expression is increased by mechanical strain in fibroblasts and lung. *American journal of respiratory cell and molecular biology* 1999;21(6):746-752.
199. Chen Y, Ju L, Rushdi M, Ge C, Zhu C. Receptor-mediated cell mechanosensing. *Mol Biol Cell* 2017;28(23):3134-3155.
200. Storch U, Mederos y Schnitzler M, Gudermann T. G protein-mediated stretch reception. *American Journal of Physiology - Heart & Circulatory Physiology* 2012;302(6):H1241-1249.
201. Gasparski AN, Beningo KA. Mechanoreception at the cell membrane: More than the integrins. *Archives of Biochemistry & Biophysics* 2015;586:20-26.
202. Shen B, Delaney MK, Du X. Inside-out, outside-in, and inside-outside-in: G protein signaling in integrin-mediated cell adhesion, spreading, and retraction. *Current opinion in cell biology* 2012;24(5):600-606.
203. Sun Z, Guo SS, Fassler R. Integrin-mediated mechanotransduction. *The Journal of cell biology* 2016;215(4):445-456.
204. Chen Y, Lee H, Tong H, Schwartz M, Zhu C. Force regulated conformational change of integrin alphavbeta3. *Matrix biology : journal of the International Society for Matrix Biology* 2016.

205. Kong F, Li Z, Parks WM, Dumbauld DW, Garcia AJ, Mould AP, Humphries MJ, Zhu C. Cyclic mechanical reinforcement of integrin-ligand interactions. *Molecular cell* 2013;49(6):1060-1068.
206. Li Z, Kong F, Zhu C. A model for cyclic mechanical reinforcement. *Sci Rep* 2016;6:35954.
207. Hamzeh MT, Sridhara R, Alexander LD. Cyclic stretch-induced tgf-beta1 and fibronectin expression is mediated by beta1-integrin through c-src- and stat3-dependent pathways in renal epithelial cells. *American Journal of Physiology - Renal Physiology* 2015;308(5):F425-436.
208. Elosegui-Artola A, Oria R, Chen Y, Kosmalska A, Perez-Gonzalez C, Castro N, Zhu C, Trepat X, Roca-Cusachs P. Mechanical regulation of a molecular clutch defines force transmission and transduction in response to matrix rigidity. *Nature cell biology* 2016;18(5):540-548.
209. Sunyer R, Conte V, Escribano J, Elosegui-Artola A, Labernadie A, Valon L, Navajas D, Garcia-Aznar JM, Munoz JJ, Roca-Cusachs P, et al. Collective cell durotaxis emerges from long-range intercellular force transmission. *Science (New York, NY)* 2016;353(6304):1157-1161.
210. Yasuda N, Miura S, Akazawa H, Tanaka T, Qin Y, Kiya Y, Imaizumi S, Fujino M, Ito K, Zou Y, et al. Conformational switch of angiotensin ii type 1 receptor underlying mechanical stress-induced activation. *EMBO reports* 2008;9(2):179-186.
211. Mederos YSM, Storch U, Gudermann T. Mechanosensitive gq/11 protein-coupled receptors mediate myogenic vasoconstriction. *Microcirculation (New York, NY : 1994)* 2016;23(8):621-625.
212. Mederos y Schnitzler M, Storch U, Meibers S, Nurwakagari P, Breit A, Essin K, Gollasch M, Gudermann T. Gq-coupled receptors as mechanosensors mediating myogenic vasoconstriction. *The EMBO journal* 2008;27(23):3092-3103.
213. Zou Y, Akazawa H, Qin Y, Sano M, Takano H, Minamino T, Makita N, Iwanaga K, Zhu W, Kudoh S, et al. Mechanical stress activates angiotensin ii type 1 receptor without the involvement of angiotensin ii. *Nature cell biology* 2004;6(6):499-506.
214. Schleifenbaum J, Kassmann M, Szijarto IA, Hercule HC, Tano JY, Weinert S, Heidenreich M, Pathan AR, Anistan YM, Alenina N, et al. Stretch-activation of angiotensin ii type 1a receptors contributes to the myogenic response of mouse mesenteric and renal arteries. *Circ Res* 2014;115(2):263-272.
215. Hong K, Zhao G, Hong Z, Sun Z, Yang Y, Clifford PS, Davis MJ, Meininger GA, Hill MA. Mechanical activation of angiotensin ii type 1 receptors causes actin remodelling and myogenic responsiveness in skeletal muscle arterioles. *The Journal of physiology* 2016;594(23):7027-7047.
216. Nishida M, Sato Y, Uemura A, Narita Y, Tozaki-Saitoh H, Nakaya M, Ide T, Suzuki K, Inoue K, Nagao T, et al. P2y6 receptor-galpha12/13 signalling in cardiomyocytes triggers pressure overload-induced cardiac fibrosis. *The EMBO journal* 2008;27(23):3104-3115.
217. Takefuji M, Kruger M, Sivaraj KK, Kaibuchi K, Offermanns S, Wettschureck N. Rhogef12 controls cardiac remodeling by integrating g protein- and integrin-dependent signaling cascades. *The Journal of experimental medicine* 2013;210(4):665-673.
218. Ziembicki J, Tandon R, Schelling JR, Sedor JR, Miller RT, Huang C. Mechanical force-activated phospholipase d is mediated by galpha12/13-rho and calmodulin-dependent kinase in renal epithelial cells. *American journal of physiology Renal physiology* 2005;289(4):F826-834.

219. John AE, Wilson MR, Habgood A, Porte J, Tatler AL, Stavrou A, Miele G, Jolly L, Knox AJ, Takata M, et al. Loss of epithelial gq and g11 signaling inhibits tgfbeta production but promotes il-33-mediated macrophage polarization and emphysema. *Science signaling* 2016;9(451):ra104.
220. Moore BB, Hogaboam CM. Murine models of pulmonary fibrosis. *Am J Physiol Lung Cell Mol Physiol* 2008;294(2):L152-160.
221. Mouratis MA, Aidinis V. Modeling pulmonary fibrosis with bleomycin. *Curr Opin Pulm Med* 2011;17(5):355-361.
222. Moeller A, Ask K, Warburton D, Gauldie J, Kolb M. The bleomycin animal model: A useful tool to investigate treatment options for idiopathic pulmonary fibrosis? *Int J Biochem Cell Biol* 2008;40(3):362-382.
223. Tatler AL, Habgood A, Porte J, John AE, Stavrou A, Hodge E, Kerama-Likoko C, Violette SM, Weinreb PH, Knox AJ, et al. Reduced ets domain-containing protein elk1 promotes pulmonary fibrosis via increased integrin alphavbeta6 expression. *J Biol Chem* 2016;291(18):9540-9553.
224. Kohan DE. Progress in gene targeting: Using mutant mice to study renal function and disease. *Kidney Int* 2008;74(4):427-437.
225. Mobley AK, McCarty JH. Use of cre-lox technology to analyze integrin functions in astrocytes. *Methods Mol Biol* 2012;814:555-570.
226. Sauer B. Inducible gene targeting in mice using the cre/lox system. *Methods* 1998;14(4):381-392.
227. Wettschureck N, van der Stelt M, Tsubokawa H, Krestel H, Moers A, Petrosino S, Schutz G, Di Marzo V, Offermanns S. Forebrain-specific inactivation of gq/g11 family g proteins results in age-dependent epilepsy and impaired endocannabinoid formation. *Mol Cell Biol* 2006;26(15):5888-5894.
228. Zywietz A, Gohla A, Schmelz M, Schultz G, Offermanns S. Pleiotropic effects of pasteurella multocida toxin are mediated by gq-dependent and -independent mechanisms. Involvement of gq but not g11. *J Biol Chem* 2001;276(6):3840-3845.
229. Abe M, Harpel JG, Metz CN, Nunes I, Loskutoff DJ, Rifkin DB. An assay for transforming growth factor-beta using cells transfected with a plasminogen activator inhibitor-1 promoter-luciferase construct. *Analytical biochemistry* 1994;216(2):276-284.
230. Pegg DE. Principles of cryopreservation. *Methods Mol Biol* 2007;368:39-57.
231. Dana H, Chalbatani GM, Mahmoodzadeh H, Karimloo R, Rezaiean O, Moradzadeh A, Mehmandoost N, Moazzen F, Mazraeh A, Marmari V, et al. Molecular mechanisms and biological functions of sirna. *Int J Biomed Sci* 2017;13(2):48-57.
232. Jensen EC. The basics of western blotting. *Anat Rec (Hoboken)* 2012;295(3):369-371.
233. Walker JM. The bicinchoninic acid (bca) assay for protein quantitation. *Methods Mol Biol* 1994;32:5-8.
234. Tan SC, Yiap BC. Dna, rna, and protein extraction: The past and the present. *J Biomed Biotechnol* 2009;2009:574398.
235. Bustin SA, Benes V, Nolan T, Pfaffl MW. Quantitative real-time rt-pcr--a perspective. *J Mol Endocrinol* 2005;34(3):597-601.
236. Moers A, Nieswandt B, Massberg S, Wettschureck N, Grüner S, Konrad I, Schulte V, Aktas B, Gratacap MP, Simon MI, et al. G13 is an essential mediator of platelet activation in hemostasis and thrombosis. *Nat Med* 2003;9(11):1418-1422.
237. Laboratory J. 029684 - b6.Cg-tg(pdgfrb-cre/ert2)6096rha/j (jax.Org). 21st January 2021].

238. Stellwagen NC. Electrophoresis of dna in agarose gels, polyacrylamide gels and in free solution. *Electrophoresis* 2009;30 Suppl 1(Suppl 1):S188-195.
239. Percival KR, Radi ZA. A modified verhoeff's elastin histochemical stain to enable pulmonary arterial hypertension model characterization. *Eur J Histochem* 2016;60(1):2588.
240. Fu DA, Campbell-Thompson M. Periodic acid-schiff staining with diastase. *Methods Mol Biol* 2017;1639:145-149.
241. Lattouf R, Younes R, Lutomski D, Naaman N, Godeau G, Senni K, Changotade S. Picrosirius red staining: A useful tool to appraise collagen networks in normal and pathological tissues. *J Histochem Cytochem* 2014;62(10):751-758.
242. Ramos-Vara JA. Principles and methods of immunohistochemistry. *Methods Mol Biol* 2017;1641:115-128.
243. Offermanns S, Simon MI. Genetic analysis of mammalian g-protein signalling. *Oncogene* 1998;17(11 Reviews):1375-1381.
244. Wettschureck N, Rutten H, Zywietz A, Gehring D, Wilkie TM, Chen J, Chien KR, Offermanns S. Absence of pressure overload induced myocardial hypertrophy after conditional inactivation of galphaq/galpha11 in cardiomyocytes. *Nat Med* 2001;7(11):1236-1240.
245. Moers A, Wettschureck N, Gruner S, Nieswandt B, Offermanns S. Unresponsiveness of platelets lacking both galpha(q) and galpha(13). Implications for collagen-induced platelet activation. *J Biol Chem* 2004;279(44):45354-45359.
246. Murray IR, Gonzalez ZN, Baily J, Dobie R, Wallace RJ, Mackinnon AC, Smith JR, Greenhalgh SN, Thompson AI, Conroy KP, et al. Alphav integrins on mesenchymal cells regulate skeletal and cardiac muscle fibrosis. *Nat Commun* 2017;8(1):1118.
247. Chen YT, Chang FC, Wu CF, Chou YH, Hsu HL, Chiang WC, Shen J, Chen YM, Wu KD, Tsai TJ, et al. Platelet-derived growth factor receptor signaling activates pericyte-myofibroblast transition in obstructive and post-ischemic kidney fibrosis. *Kidney Int* 2011;80(11):1170-1181.
248. Ikura Y, Morimoto H, Ogami M, Jomura H, Ikeoka N, Sakurai M. Expression of platelet-derived growth factor and its receptor in livers of patients with chronic liver disease. *Journal of gastroenterology* 1997;32(4):496-501.
249. Coin PG, Lindroos PM, Bird GS, Osornio-Vargas AR, Roggli VL, Bonner JC. Lipopolysaccharide up-regulates platelet-derived growth factor (pdgf) alpha-receptor expression in rat lung myofibroblasts and enhances response to all pdgf isoforms. *Journal of immunology (Baltimore, Md : 1950)* 1996;156(12):4797-4806.
250. Patel JA, Shen L, Hall SM, Benyahia C, Norel X, McAnulty RJ, Moledina S, Silverstein AM, Whittle BJ, Clapp LH. Prostanoid ep_2 receptors are up-regulated in human pulmonary arterial hypertension: A key anti-proliferative target for treprostinil in smooth muscle cells. *Int J Mol Sci* 2018;19(8).
251. Costantini F, Kopan R. Patterning a complex organ: Branching morphogenesis and nephron segmentation in kidney development. *Dev Cell* 2010;18(5):698-712.
252. Babwah AV, Navarro VM, Ahow M, Pampillo M, Nash C, Fayazi M, Calder M, Elbert A, Urbanski HF, Wettschureck N, et al. Gnrh neuron-specific ablation of galphaq/11 results in only partial inactivation of the neuroendocrine-reproductive axis in both male and female mice: In vivo evidence for kiss1r-coupled galphaq/11-independent gnrh secretion. *J Neurosci* 2015;35(37):12903-12916.
253. Broicher T, Wettschureck N, Munsch T, Coulon P, Meuth SG, Kanyshkova T, Seidenbecher T, Offermanns S, Pape HC, Budde T. Muscarinic ach receptor-mediated control of thalamic activity via g(q)/g (11)-family g-proteins. *Pflugers Arch* 2008;456(6):1049-1060.

254. Wettschureck N, Moers A, Hamalainen T, Lemberger T, Schutz G, Offermanns S. Heterotrimeric g proteins of the gq/11 family are crucial for the induction of maternal behavior in mice. *Mol Cell Biol* 2004;24(18):8048-8054.
255. Coulon P, Kanyshkova T, Broicher T, Munsch T, Wettschureck N, Seidenbecher T, Meuth SG, Offermanns S, Pape HC, Budde T. Activity modes in thalamocortical relay neurons are modulated by g(q)/g(11) family g-proteins - serotonergic and glutamatergic signaling. *Front Cell Neurosci* 2010;4:132.
256. Dettlaff-Swiercz DA, Wettschureck N, Moers A, Huber K, Offermanns S. Characteristic defects in neural crest cell-specific galphaq/galpha11- and galpha12/galpha13-deficient mice. *Dev Biol* 2005;282(1):174-182.
257. Gangadharan V, Selvaraj D, Kurejova M, Njoo C, Gritsch S, Skoricova D, Horstmann H, Offermanns S, Brown AJ, Kuner T, et al. A novel biological role for the phospholipid lysophosphatidylinositol in nociceptive sensitization via activation of diverse g-protein signalling pathways in sensory nerves in vivo. *Pain* 2013;154(12):2801-2812.
258. Hoyer DP, Gronke S, Frank KF, Addicks K, Wettschureck N, Offermanns S, Erdmann E, Reuter H. Diabetes-related defects in sarcoplasmic ca2+ release are prevented by inactivation of g(alpha)11 and g(alpha)q in murine cardiomyocytes. *Mol Cell Biochem* 2010;341(1-2):235-244.
259. Kero J, Ahmed K, Wettschureck N, Tunaru S, Wintermantel T, Greiner E, Schutz G, Offermanns S. Thyrocyte-specific gq/g11 deficiency impairs thyroid function and prevents goiter development. *J Clin Invest* 2007;117(9):2399-2407.
260. Li YQ, Shrestha Y, Pandey M, Chen M, Kablan A, Gavrilova O, Offermanns S, Weinstein LS. G(q/11)alpha and g(s)alpha mediate distinct physiological responses to central melanocortins. *J Clin Invest* 2016;126(1):40-49.
261. Ogata N, Shinoda Y, Wettschureck N, Offermanns S, Takeda S, Nakamura K, Segre GV, Chung UI, Kawaguchi H. G alpha(q) signal in osteoblasts is inhibitory to the osteoanabolic action of parathyroid hormone. *J Biol Chem* 2011;286(15):13733-13740.
262. Rieken S, Herroeder S, Sassmann A, Wallenwein B, Moers A, Offermanns S, Wettschureck N. Lysophospholipids control integrin-dependent adhesion in splenic b cells through g(i) and g(12)/g(13) family g-proteins but not through g(q)/g(11). *J Biol Chem* 2006;281(48):36985-36992.
263. Sassmann A, Gier B, Grone HJ, Drews G, Offermanns S, Wettschureck N. The gq/g11-mediated signaling pathway is critical for autocrine potentiation of insulin secretion in mice. *J Clin Invest* 2010;120(6):2184-2193.
264. Tappe-Theodor A, Constantin CE, Tegeder I, Lechner SG, Langeslag M, Lepcynzsky P, Wirotanseng RI, Kurejova M, Agarwal N, Nagy G, et al. Galpha(q/11) signaling tonically modulates nociceptor function and contributes to activity-dependent sensitization. *Pain* 2012;153(1):184-196.
265. Wettschureck N, Moers A, Wallenwein B, Parlow AF, Maser-Gluth C, Offermanns S. Loss of gq/11 family g proteins in the nervous system causes pituitary somatotroph hypoplasia and dwarfism in mice. *Mol Cell Biol* 2005;25(5):1942-1948.
266. Wettschureck N, Lee E, Libutti SK, Offermanns S, Robey PG, Spiegel AM. Parathyroid-specific double knockout of gq and g11 alpha-subunits leads to a phenotype resembling germline knockout of the extracellular ca2+ -sensing receptor. *Mol Endocrinol* 2007;21(1):274-280.
267. Ricard N, Tu L, Le Hiress M, Huertas A, Phan C, Thuillet R, Sattler C, Fadel E, Seferian A, Montani D, et al. Increased pericyte coverage mediated by endothelial-

derived fibroblast growth factor-2 and interleukin-6 is a source of smooth muscle-like cells in pulmonary hypertension. *Circulation* 2014;129(15):1586-1597.
268. Armulik A, Genove G, Betsholtz C. Pericytes: Developmental, physiological, and pathological perspectives, problems, and promises. *Developmental cell* 2011;21(2):193-215.
269. Mecham RP. Elastin in lung development and disease pathogenesis. *Matrix Biol* 2018;73:6-20.
270. Barkauskas CE, Cronce MJ, Rackley CR, Bowie EJ, Keene DR, Stripp BR, Randell SH, Noble PW, Hogan BL. Type 2 alveolar cells are stem cells in adult lung. *J Clin Invest* 2013;123(7):3025-3036.
271. Desai TJ, Brownfield DG, Krasnow MA. Alveolar progenitor and stem cells in lung development, renewal and cancer. *Nature* 2014;507(7491):190-194.
272. Kato K, Dieguez-Hurtado R, Park DY, Hong SP, Kato-Azuma S, Adams S, Stehling M, Trappmann B, Wrana JL, Koh GY, et al. Pulmonary pericytes regulate lung morphogenesis. *Nat Commun* 2018;9(1):2448.
273. Bowers SL, Norden PR, Davis GE. Molecular signaling pathways controlling vascular tube morphogenesis and pericyte-induced tube maturation in 3d extracellular matrices. *Adv Pharmacol* 2016;77:241-280.
274. Cheng HY, Dong A, Panchatcharam M, Mueller P, Yang F, Li Z, Mills G, Chun J, Morris AJ, Smyth SS. Lysophosphatidic acid signaling protects pulmonary vasculature from hypoxia-induced remodeling. *Arterioscler Thromb Vasc Biol* 2012;32(1):24-32.
275. Li R, Bernau K, Sandbo N, Gu J, Preissl S, Sun X. Pdgfra marks a cellular lineage with distinct contributions to myofibroblasts in lung maturation and injury response. *Elife* 2018;7.
276. Schlondorff D, Banas B. The mesangial cell revisited: No cell is an island. *Journal of the American Society of Nephrology : JASN* 2009;20(6):1179-1187.
277. Zou X, Ramachandran P, Kendall TJ, Pellicoro A, Dora E, Aucott RL, Manwani K, Man TY, Chapman KE, Henderson NC, et al. 11beta-hydroxysteroid dehydrogenase-1 deficiency or inhibition enhances hepatic myofibroblast activation in murine liver fibrosis. *Hepatology* 2018;67(6):2167-2181.
278. Herroeder S, Reichardt P, Sassmann A, Zimmermann B, Jaeneke D, Hoeckner J, Hollmann MW, Fischer KD, Vogt S, Grosse R, et al. Guanine nucleotide-binding proteins of the g12 family shape immune functions by controlling cd4+ t cell adhesiveness and motility. *Immunity* 2009;30(5):708-720.
279. Moers A, Nurnberg A, Goebbels S, Wettschureck N, Offermanns S. Galpha12/galpha13 deficiency causes localized overmigration of neurons in the developing cerebral and cerebellar cortices. *Mol Cell Biol* 2008;28(5):1480-1488.
280. Rieken S, Sassmann A, Herroeder S, Wallenwein B, Moers A, Offermanns S, Wettschureck N. G12/g13 family g proteins regulate marginal zone b cell maturation, migration, and polarization. *J Immunol* 2006;177(5):2985-2993.
281. Gofflot F, Hall M, Morriss-Kay GM. Genetic patterning of the developing mouse tail at the time of posterior neuropore closure. *Developmental dynamics : an official publication of the American Association of Anatomists* 1997;210(4):431-445.
282. Ota C, Baarsma HA, Wagner DE, Hilgendorff A, Königshoff M. Linking bronchopulmonary dysplasia to adult chronic lung diseases: Role of wnt signaling. *Mol Cell Pediatr* 2016;3(1):34.
283. Hung CF, Mittelsteadt KL, Brauer R, McKinney BL, Hallstrand TS, Parks WC, Chen P, Schnapp LM, Liles WC, Duffield JS, et al. Lung pericyte-like cells are functional interstitial immune sentinel cells. *Am J Physiol Lung Cell Mol Physiol* 2017;312(4):L556-l567.

284. Adissu HA, Estabel J, Sunter D, Tuck E, Hooks Y, Carragher DM, Clarke K, Karp NA, Newbigging S, Jones N, et al. Histopathology reveals correlative and unique phenotypes in a high-throughput mouse phenotyping screen. *Dis Model Mech* 2014;7(5):515-524.
285. Jokinen V, Suvanto P, Franssila S. Oxygen and nitrogen plasma hydrophilization and hydrophobic recovery of polymers. *Biomicrofluidics* 2012;6(1):16501-1650110.
286. www.lungmap.net. Lungmap consortium. Www.Lungmap.Net. 2020 [cited 2020 04/08/2020].
287. www.ipfcellatlas.com. Ipf cell atlas researchers. Www.Ipfcellatlas.Com. Kaminski/rosas dataset. 2020 [cited 2020 05/09/2020].
288. Adams TS, Schupp JC, Poli S, Ayaub EA, Neumark N, Ahangari F, Chu SG, Raby BA, Deluliis G, Januszyk M, et al. Single-cell rna-seq reveals ectopic and aberrant lung-resident cell populations in idiopathic pulmonary fibrosis. *Sci Adv* 2020;6(28):eaba1983.
289. GPCRdb. Https://gpcrdb.Org/ gpcr-g protein couplings. [cited 2020 12/11/2020].
290. Szekeres M, Nadasy GL, Turu G, Soltesz-Katona E, Benyo Z, Offermanns S, Ruisanchez E, Szabo E, Takats Z, Batkai S, et al. Endocannabinoid-mediated modulation of gq/11 protein-coupled receptor signaling-induced vasoconstriction and hypertension. *Mol Cell Endocrinol* 2015;403:46-56.
291. Sava P, Ramanathan A, Dobronyi A, Peng X, Sun H, Ledesma-Mendoza A, Herzog EL, Gonzalez AL. Human pericytes adopt myofibroblast properties in the microenvironment of the ipf lung. *JCI Insight* 2017;2(24).
292. Wilson CL, Stephenson SE, Higuero JP, Feghali-Bostwick C, Hung CF, Schnapp LM. Characterization of human pdgfr-beta-positive pericytes from ipf and non-ipf lungs. *Am J Physiol Lung Cell Mol Physiol* 2018;315(6):L991-l1002.
293. Tokumura A, Carbone LD, Yoshioka Y, Morishige J, Kikuchi M, Postlethwaite A, Watsky MA. Elevated serum levels of arachidonoyl-lysophosphatidic acid and sphingosine 1-phosphate in systemic sclerosis. *International Journal of Medical Sciences* 2009;6(4):168-176.
294. Tsutsumi T, Adachi M, Nikawadori M, Morishige J, Tokumura A. Presence of bioactive lysophosphatidic acid in renal effluent of rats with unilateral ureteral obstruction. *Life Sciences* 2011;89(5-6):195-203.
295. Cong C, Mao L, Zhang Y, Zhao Z, Xu X, Zhao J. Regulation of silicosis formation by lysophosphatidic acid and its receptors. *Experimental Lung Research* 2014;40(7):317-326.
296. Geng H, Lan R, Singha PK, Gilchrist A, Weinreb PH, Violette SM, Weinberg JM, Saikumar P, Venkatachalam MA. Lysophosphatidic acid increases proximal tubule cell secretion of profibrotic cytokines pdgf-b and ctgf through lpa2- and galphaq-mediated rho and alphavbeta6 integrin-dependent activation of tgf-beta. *American Journal of Pathology* 2012;181(4):1236-1249.
297. Takefuji M, Wirth A, Lukasova M, Takefuji S, Boettger T, Braun T, Althoff T, Offermanns S, Wettschureck N. G(13)-mediated signaling pathway is required for pressure overload-induced cardiac remodeling and heart failure. *Circulation* 2012;126(16):1972-1982.
298. Zhao J, Chen Q, Li H, Myerburg M, Spannhake EW, Natarajan V, Zhao Y. Lysophosphatidic acid increases soluble st2 expression in mouse lung and human bronchial epithelial cells. *Cell Signal* 2012;24(1):77-85.

299. Zhang T, Gong T, Xie J, Lin S, Liu Y, Zhou T, Lin Y. Softening substrates promote chondrocytes phenotype via rhoa/rock pathway. *ACS Appl Mater Interfaces* 2016;8(35):22884-22891.
300. Hoon JL, Tan MH, Koh CG. The regulation of cellular responses to mechanical cues by rho gtpases. *Cells* 2016;5(2).
301. Li CX, Talele NP, Boo S, Koehler A, Knee-Walden E, Balestrini JL, Speight P, Kapus A, Hinz B. Microrna-21 preserves the fibrotic mechanical memory of mesenchymal stem cells. *Nat Mater* 2017;16(3):379-389.
302. Chen H, Qu J, Huang X, Kurundkar A, Zhu L, Yang N, Venado A, Ding Q, Liu G, Antony VB, et al. Mechanosensing by the alpha6-integrin confers an invasive fibroblast phenotype and mediates lung fibrosis. *Nat Commun* 2016;7:12564.
303. Eckes B, Zweers MC, Zhang ZG, Hallinger R, Mauch C, Aumailley M, Krieg T. Mechanical tension and integrin alpha 2 beta 1 regulate fibroblast functions. *Journal of Investigative Dermatology Symposium Proceedings* 2006;11(1):66-72.
304. Fiore VF, Strane PW, Bryksin AV, White ES, Hagood JS, Barker TH. Conformational coupling of integrin and thy-1 regulates fyn priming and fibroblast mechanotransduction. *Journal of Cell Biology* 2015;211(1):173-190.
305. Tschumperlin DJ, Ligresti G, Hilscher MB, Shah VH. Mechanosensing and fibrosis. *J Clin Invest* 2018;128(1):74-84.
306. Burgess JK, Mauad T, Tjin G, Karlsson JC, Westergren-Thorsson G. The extracellular matrix - the under-recognized element in lung disease? *J Pathol* 2016;240(4):397-409.
307. Mammoto T, Jiang E, Jiang A, Mammoto A. Extracellular matrix structure and tissue stiffness control postnatal lung development through the lipoprotein receptor-related protein 5/tie2 signaling system. *Am J Respir Cell Mol Biol* 2013;49(6):1009-1018.
308. Hartman CD, Isenberg BC, Chua SG, Wong JY. Extracellular matrix type modulates cell migration on mechanical gradients. *Exp Cell Res* 2017;359(2):361-366.
309. Hartmann J, Blum R, Kovalchuk Y, Adelsberger H, Kuner R, Durand GM, Miyata M, Kano M, Offermanns S, Konnerth A. Distinct roles of galpha(q) and galpha11 for purkinje cell signaling and motor behavior. *J Neurosci* 2004;24(22):5119-5130.
310. El-Mohri H, Wu Y, Mohanty S, Ghosh G. Impact of matrix stiffness on fibroblast function. *Mater Sci Eng C Mater Biol Appl* 2017;74:146-151.
311. Gan L, Xue JX, Li X, Liu DS, Ge Y, Ni PY, Deng L, Lu Y, Jiang W. Blockade of lysophosphatidic acid receptors lpar1/3 ameliorates lung fibrosis induced by irradiation. *Biochemical & Biophysical Research Communications* 2011;409(1):7-13.
312. Ninou I, Kaffe E, Müller S, Budd DC, Stevenson CS, Ullmer C, Aidinis V. Pharmacologic targeting of the atx/lpa axis attenuates bleomycin-induced pulmonary fibrosis. *Pulm Pharmacol Ther* 2018;52:32-40.
313. Castelino FV, Seiders J, Bain G, Brooks SF, King CD, Swaney JS, Lorrain DS, Chun J, Luster AD, Tager AM. Amelioration of dermal fibrosis by genetic deletion or pharmacologic antagonism of lysophosphatidic acid receptor 1 in a mouse model of scleroderma. *Arthritis & Rheumatism* 2011;63(5):1405-1415.
314. Ohashi T, Yamamoto T. Antifibrotic effect of lysophosphatidic acid receptors lpa1 and lpa3 antagonist on experimental murine scleroderma induced by bleomycin. *Experimental Dermatology* 2015;24(9):698-702.
315. Pradere JP, Klein J, Gres S, Guigne C, Neau E, Valet P, Calise D, Chun J, Bascands JL, Saulnier-Blache JS, et al. Lpa1 receptor activation promotes renal

interstitial fibrosis. *Journal of the American Society of Nephrology* 2007;18(12):3110-3118.
316. van der Aar E, Desrivot J, Dupont S, Heckmann B, Fieuw A, Stutvoet S, Fagard L, Van de Wal K, Helmer E. Safety, pharmacokinetics, and pharmacodynamics of the autotaxin inhibitor glpg1690 in healthy subjects: Phase 1 randomized trials. *J Clin Pharmacol* 2019;59(10):1366-1378.
317. Maher TM, van der Aar EM, Van de Steen O, Allamassey L, Desrivot J, Dupont S, Fagard L, Ford P, Fieuw A, Wuyts W. Safety, tolerability, pharmacokinetics, and pharmacodynamics of glpg1690, a novel autotaxin inhibitor, to treat idiopathic pulmonary fibrosis (flora): A phase 2a randomised placebo-controlled trial. *Lancet Respir Med* 2018;6(8):627-635.
318. Olianas MC, Dedoni S, Onali P. Antidepressants induce profibrotic responses via the lysophosphatidic acid receptor lpa(1). *Eur J Pharmacol* 2020;873:172963.
319. Miki H, Mio T, Nagai S, Hoshino Y, Nagao T, Kitaichi M, Izumi T. Fibroblast contractility: Usual interstitial pneumonia and nonspecific interstitial pneumonia. *Am J Respir Crit Care Med* 2000;162(6):2259-2264.
320. Fireman E, Shahar I, Shoval S, Messer G, Dvash S, Grief J. Morphological and biochemical properties of alveolar fibroblasts in interstitial lung diseases. *Lung* 2001;179(2):105-117.
321. Hinz B, Celetta G, Tomasek JJ, Gabbiani G, Chaponnier C. Alpha-smooth muscle actin expression upregulates fibroblast contractile activity. *Mol Biol Cell* 2001;12(9):2730-2741.
322. Fiore VF, Wong SS, Tran C, Tan C, Xu W, Sulchek T, White ES, Hagood JS, Barker TH. Alphavbeta3 integrin drives fibroblast contraction and strain stiffening of soft provisional matrix during progressive fibrosis. *JCI Insight* 2018;3(20).
323. Bochaton-Piallat ML, Gabbiani G, Hinz B. The myofibroblast in wound healing and fibrosis: Answered and unanswered questions. *F1000Res* 2016;5.
324. Buscemi L, Ramonet D, Klingberg F, Formey A, Smith-Clerc J, Meister JJ, Hinz B. The single-molecule mechanics of the latent tgf-beta1 complex. *Curr Biol* 2011;21(24):2046-2054.
325. Chennupati R, Wirth A, Favre J, Li R, Bonnavion R, Jin YJ, Wietelmann A, Schweda F, Wettschureck N, Henrion D, et al. Myogenic vasoconstriction requires g(12)/g(13) and larg to maintain local and systemic vascular resistance. *Elife* 2019;8.
326. Kauffenstein G, Tamareille S, Prunier F, Roy C, Ayer A, Toutain B, Billaud M, Isakson BE, Grimaud L, Loufrani L, et al. Central role of p2y6 udp receptor in arteriolar myogenic tone. *Arterioscler Thromb Vasc Biol* 2016;36(8):1598-1606.
327. Dér B, Molnár PJ, Ruisanchez É, Őrsy P, Kerék M, Faragó B, Nyirády P, Offermanns S, Benyó Z. Nk2 receptor-mediated detrusor muscle contraction involves g(q/11)-dependent activation of voltage-dependent ca(2+) channels and the rhoa-rho kinase pathway. *Am J Physiol Renal Physiol* 2019;317(5):F1154-f1163.
328. Wirth A, Wang S, Takefuji M, Tang C, Althoff TF, Schweda F, Wettschureck N, Offermanns S. Age-dependent blood pressure elevation is due to increased vascular smooth muscle tone mediated by g-protein signalling. *Cardiovasc Res* 2016;109(1):131-140.
329. Gohla A, Schultz G, Offermanns S. Role for g(12)/g(13) in agonist-induced vascular smooth muscle cell contraction. *Circ Res* 2000;87(3):221-227.
330. Somlyo AP, Somlyo AV. Ca2+ sensitivity of smooth muscle and nonmuscle myosin ii: Modulated by g proteins, kinases, and myosin phosphatase. *Physiol Rev* 2003;83(4):1325-1358.

331. Wirth A, Benyo Z, Lukasova M, Leutgeb B, Wettschureck N, Gorbey S, Orsy P, Horvath B, Maser-Gluth C, Greiner E, et al. G12-g13-larg-mediated signaling in vascular smooth muscle is required for salt-induced hypertension. *Nat Med* 2008;14(1):64-68.
332. Chiba Y, Misawa M. Increased expression of g12 and g13 proteins in bronchial smooth muscle of airway hyperresponsive rats. *Inflamm Res* 2001;50(6):333-336.
333. Lee SJ, Lee WH, Ki SH, Kim YM, Lee CH, Kim SG. Galpha13 regulates methacholine-induced contraction of bronchial smooth muscle via phosphorylation of mlc20. *Biochem Pharmacol* 2009;77(9):1497-1505.
334. Yoo EJ, Cao G, Koziol-White CJ, Ojiaku CA, Sunder K, Jude JA, Michael JV, Lam H, Pushkarsky I, Damoiseaux R, et al. Gα(12) facilitates shortening in human airway smooth muscle by modulating phosphoinositide 3-kinase-mediated activation in a rhoa-dependent manner. *Br J Pharmacol* 2017;174(23):4383-4395.
335. Nurnberg A, Brauer AU, Wettschureck N, Offermanns S. Antagonistic regulation of neurite morphology through gq/g11 and g12/g13. *J Biol Chem* 2008;283(51):35526-35531.
336. Dancs PT, Ruisanchez E, Balogh A, Panta CR, Miklos Z, Nusing RM, Aoki J, Chun J, Offermanns S, Tigyi G, et al. Lpa1 receptor-mediated thromboxane a2 release is responsible for lysophosphatidic acid-induced vascular smooth muscle contraction. *Faseb j* 2017;31(4):1547-1555.
337. Tomasek JJ, Vaughan MB, Kropp BP, Gabbiani G, Martin MD, Haaksma CJ, Hinz B. Contraction of myofibroblasts in granulation tissue is dependent on rho/rho kinase/myosin light chain phosphatase activity. *Wound Repair Regen* 2006;14(3):313-320.
338. Hinz B, Gabbiani G. Mechanisms of force generation and transmission by myofibroblasts. *Curr Opin Biotechnol* 2003;14(5):538-546.
339. Goulimari P, Kitzing TM, Knieling H, Brandt DT, Offermanns S, Grosse R. Galpha12/13 is essential for directed cell migration and localized rho-dia1 function. *J Biol Chem* 2005;280(51):42242-42251.
340. Ohanian V, Gatfield K, Ohanian J. Role of the actin cytoskeleton in g-protein-coupled receptor activation of pyk2 and paxillin in vascular smooth muscle. *Hypertension* 2005;46(1):93-99.
341. Gohla A, Offermanns S, Wilkie TM, Schultz G. Differential involvement of galpha12 and galpha13 in receptor-mediated stress fiber formation. *J Biol Chem* 1999;274(25):17901-17907.
342. Jin J, Togo S, Kadoya K, Tulafu M, Namba Y, Iwai M, Watanabe J, Nagahama K, Okabe T, Hidayat M, et al. Pirfenidone attenuates lung fibrotic fibroblast responses to transforming growth factor-β1. *Respir Res* 2019;20(1):119.
343. Huang X, Gai Y, Yang N, Lu B, Samuel CS, Thannickal VJ, Zhou Y. Relaxin regulates myofibroblast contractility and protects against lung fibrosis. *American Journal of Pathology* 2011;179(6):2751-2765.
344. Seibold JR, Korn JH, Simms R, Clements PJ, Moreland LW, Mayes MD, Furst DE, Rothfield N, Steen V, Weisman M, et al. Recombinant human relaxin in the treatment of scleroderma. A randomized, double-blind, placebo-controlled trial. *Ann Intern Med* 2000;132(11):871-879.
345. Khanna D, Clements PJ, Furst DE, Korn JH, Ellman M, Rothfield N, Wigley FM, Moreland LW, Silver R, Kim YH, et al. Recombinant human relaxin in the treatment of systemic sclerosis with diffuse cutaneous involvement: A randomized, double-blind, placebo-controlled trial. *Arthritis Rheum* 2009;60(4):1102-1111.

346. Fernandez-Sanchez ME, Brunet T, Roper JC, Farge E. Mechanotransduction's impact on animal development, evolution, and tumorigenesis. *Annual Review of Cell & Developmental Biology* 2015;31:373-397.
347. Hume S. Development of a novel device for high-throughput screening of cell contraction. Institute of Biomaterial and Biomedical Engineering. Toronto, Canada: University of Toronto;2014.
348. Hinz B. Mechanical aspects of lung fibrosis: A spotlight on the myofibroblast. *Proc Am Thorac Soc* 2012;9(3):137-147.
349. Fujita H, Hida M, Kanemoto K, Fukuda K, Nagata M, Awazu M. Cyclic stretch induces proliferation and tgf-beta1-mediated apoptosis via p38 and erk in ureteric bud cells. *Am J Physiol Renal Physiol* 2010;299(3):F648-655.
350. Furumatsu T, Matsumoto E, Kanazawa T, Fujii M, Lu Z, Kajiki R, Ozaki T. Tensile strain increases expression of ccn2 and col2a1 by activating tgf-beta-smad2/3 pathway in chondrocytic cells. *J Biomech* 2013;46(9):1508-1515.
351. Maeda T, Sakabe T, Sunaga A, Sakai K, Rivera AL, Keene DR, Sasaki T, Stavnezer E, Iannotti J, Schweitzer R, et al. Conversion of mechanical force into tgf-beta-mediated biochemical signals. *Curr Biol* 2011;21(11):933-941.
352. Russo TA, Stoll D, Nader HB, Dreyfuss JL. Mechanical stretch implications for vascular endothelial cells: Altered extracellular matrix synthesis and remodeling in pathological conditions. *Life Sci* 2018;213:214-225.
353. Shynlova O, Tsui P, Dorogin A, Langille BL, Lye SJ. The expression of transforming growth factor beta in pregnant rat myometrium is hormone and stretch dependent. *Reproduction* 2007;134(3):503-511.
354. Wang BW, Wu GJ, Cheng WP, Shyu KG. Mechanical stretch via transforming growth factor-beta1 activates microrna-208a to regulate hypertrophy in cultured rat cardiac myocytes. *J Formos Med Assoc* 2013;112(10):635-643.
355. Aldrich S. Y27632 dihydrochloride. [cited 2020 20th January 2020].
356. Hinz B. It has to be the alphav: Myofibroblast integrins activate latent tgf-beta1. Nat med. United States;2013. p. 1567-1568.
357. Wipff PJ, Hinz B. Integrins and the activation of latent transforming growth factor beta1 - an intimate relationship. *Eur J Cell Biol* 2008;87(8-9):601-615.
358. Tschumperlin DJ, Margulies SS. Alveolar epithelial surface area-volume relationship in isolated rat lungs. *J Appl Physiol (1985)* 1999;86(6):2026-2033.
359. Murata N, Ito S, Furuya K, Takahara N, Naruse K, Aso H, Kondo M, Sokabe M, Hasegawa Y. Ca2+ influx and atp release mediated by mechanical stretch in human lung fibroblasts. *Biochemical & Biophysical Research Communications* 2014;453(1):101-105.
360. Heise RL, Stober V, Cheluvaraju C, Hollingsworth JW, Garantziotis S. Mechanical stretch induces epithelial-mesenchymal transition in alveolar epithelia via hyaluronan activation of innate immunity. *Journal of Biological Chemistry* 2011;286(20):17435-17444.
361. Banerjee I, Carrion K, Serrano R, Dyo J, Sasik R, Lund S, Willems E, Aceves S, Meili R, Mercola M, et al. Cyclic stretch of embryonic cardiomyocytes increases proliferation, growth, and expression while repressing tgf-beta signaling. *J Mol Cell Cardiol* 2015;79:133-144.
362. van Wamel AJ, Ruwhof C, van der Valk-Kokshoorn LJ, Schrier PI, van der Laarse A. Stretch-induced paracrine hypertrophic stimuli increase tgf-beta1 expression in cardiomyocytes. *Mol Cell Biochem* 2002;236(1-2):147-153.

363. Hirakata M, Kaname S, Chung UG, Joki N, Hori Y, Noda M, Takuwa Y, Okazaki T, Fujita T, Katoh T, et al. Tyrosine kinase dependent expression of tgf-beta induced by stretch in mesangial cells. *Kidney Int* 1997;51(4):1028-1036.
364. Bouffard NA, Cutroneo KR, Badger GJ, White SL, Buttolph TR, Ehrlich HP, Stevens-Tuttle D, Langevin HM. Tissue stretch decreases soluble tgf-beta1 and type-1 procollagen in mouse subcutaneous connective tissue: Evidence from ex vivo and in vivo models. *J Cell Physiol* 2008;214(2):389-395.
365. Hamzeh MT, Sridhara R, Alexander LD. Cyclic stretch-induced tgf-beta1 and fibronectin expression is mediated by beta1-integrin through c-src- and stat3-dependent pathways in renal epithelial cells. *Am J Physiol Renal Physiol* 2015;308(5):F425-436.
366. Jones ER, Jones GC, Legerlotz K, Riley GP. Cyclical strain modulates metalloprotease and matrix gene expression in human tenocytes via activation of tgfbeta. *Biochim Biophys Acta* 2013;1833(12):2596-2607.
367. Li JH, Huang XR, Zhu HJ, Oldfield M, Cooper M, Truong LD, Johnson RJ, Lan HY. Advanced glycation end products activate smad signaling via tgf-beta-dependent and independent mechanisms: Implications for diabetic renal and vascular disease. *Faseb j* 2004;18(1):176-178.
368. Tatler AL, Goodwin AT, Gbolahan O, Saini G, Porte J, John AE, Clifford RL, Violette SM, Weinreb PH, Parfrey H, et al. Amplification of tgfbeta induced itgb6 gene transcription may promote pulmonary fibrosis. *PLoS One* 2016;11(8):e0158047.
369. Coghlan MA, Shifren A, Huang HJ, Russell TD, Mitra RD, Zhang Q, Wegner DJ, Cole FS, Hamvas A. Sequencing of idiopathic pulmonary fibrosis-related genes reveals independent single gene associations. *BMJ Open Respir Res* 2014;1(1):e000057.
370. Kropski JA, Pritchett JM, Zoz DF, Crossno PF, Markin C, Garnett ET, Degryse AL, Mitchell DB, Polosukhin VV, Rickman OB, et al. Extensive phenotyping of individuals at risk for familial interstitial pneumonia reveals clues to the pathogenesis of interstitial lung disease. *Am J Respir Crit Care Med* 2015;191(4):417-426.
371. Nathan N, Giraud V, Picard C, Nunes H, Dastot-Le Moal F, Copin B, Galeron L, De Ligniville A, Kuziner N, Reynaud-Gaubert M, et al. Germline sftpa1 mutation in familial idiopathic interstitial pneumonia and lung cancer. *Hum Mol Genet* 2016;25(8):1457-1467.
372. Kropski JA, Blackwell TS, Loyd JE. The genetic basis of idiopathic pulmonary fibrosis. *Eur Respir J* 2015;45(6):1717-1727.
373. Wipff PJ, Hinz B. Myofibroblasts work best under stress. *J Bodyw Mov Ther* 2009;13(2):121-127.
374. Manuyakorn W, Smart DE, Noto A, Bucchieri F, Haitchi HM, Holgate ST, Howarth PH, Davies DE. Mechanical strain causes adaptive change in bronchial fibroblasts enhancing profibrotic and inflammatory responses. *PLoS One* 2016;11(4):e0153926.
375. Huang JW, Pan HJ, Yao WY, Tsao YW, Liao WY, Wu CW, Tung YC, Lee CH. Interaction between lung cancer cell and myofibroblast influenced by cyclic tensile strain. *Lab Chip* 2013;13(6):1114-1120.
376. Zheng L, Paik WY, Cesnjaj M, Balla T, Tomic M, Catt KJ, Stojilkovic SS. Effects of the phospholipase-c inhibitor, u73122, on signaling and secretion in pituitary gonadotrophs. *Endocrinology* 1995;136(3):1079-1088.
377. Zapf-Colby A, Eichhorn J, Webster NJ, Olefsky JM. Inhibition of plc-gamma1 activity converts nerve growth factor from an anti-mitogenic to a mitogenic signal in cho cells. *Oncogene* 1999;18(35):4908-4919.

378. Shah BH, Lashari I, Rana S, Saeed O, Rasheed H, Arshad Saeed S. Synergistic interaction of adrenaline and histamine in human platelet aggregation is mediated through activation of phospholipase, map kinase and cyclo-oxygenase pathways. *Pharmacol Res* 2000;42(5):479-483.
379. Mohamed JS, Lopez MA, Boriek AM. Mechanical stretch up-regulates microrna-26a and induces human airway smooth muscle hypertrophy by suppressing glycogen synthase kinase-3beta. *J Biol Chem* 2010;285(38):29336-29347.
380. Giacomini MM, Travis MA, Kudo M, Sheppard D. Epithelial cells utilize cortical actin/myosin to activate latent tgf-beta through integrin alpha(v)beta(6)-dependent physical force. *Exp Cell Res* 2012;318(6):716-722.
381. Menou A, Duitman J, Crestani B. The impaired proteases and anti-proteases balance in idiopathic pulmonary fibrosis. *Matrix Biol* 2018;68-69:382-403.
382. Howell DC, Goldsack NR, Marshall RP, McAnulty RJ, Starke R, Purdy G, Laurent GJ, Chambers RC. Direct thrombin inhibition reduces lung collagen, accumulation, and connective tissue growth factor mrna levels in bleomycin-induced pulmonary fibrosis. *Am J Pathol* 2001;159(4):1383-1395.
383. Bogatkevich GS, Ludwicka-Bradley A, Nietert PJ, Akter T, van Ryn J, Silver RM. Antiinflammatory and antifibrotic effects of the oral direct thrombin inhibitor dabigatran etexilate in a murine model of interstitial lung disease. *Arthritis Rheum* 2011;63(5):1416-1425.
384. Kobayashi H, Gabazza EC, Taguchi O, Wada H, Takeya H, Nishioka J, Yasui H, Kobayashi T, Hataji O, Suzuki K, et al. Protein c anticoagulant system in patients with interstitial lung disease. *Am J Respir Crit Care Med* 1998;157(6 Pt 1):1850-1854.
385. Yasui H, Gabazza EC, Tamaki S, Kobayashi T, Hataji O, Yuda H, Shimizu S, Suzuki K, Adachi Y, Taguchi O. Intratracheal administration of activated protein c inhibits bleomycin-induced lung fibrosis in the mouse. *Am J Respir Crit Care Med* 2001;163(7):1660-1668.
386. Yasui H, Gabazza EC, Taguchi O, Risteli J, Risteli L, Wada H, Yuda H, Kobayashi T, Kobayashi H, Suzuki K, et al. Decreased protein c activation is associated with abnormal collagen turnover in the intraalveolar space of patients with interstitial lung disease. *Clin Appl Thromb Hemost* 2000;6(4):202-205.
387. Chua F, Dunsmore SE, Clingen PH, Mutsaers SE, Shapiro SD, Segal AW, Roes J, Laurent GJ. Mice lacking neutrophil elastase are resistant to bleomycin-induced pulmonary fibrosis. *Am J Pathol* 2007;170(1):65-74.
388. Shimbori C, Upagupta C, Bellaye PS, Ayaub EA, Sato S, Yanagihara T, Zhou Q, Ognjanovic A, Ask K, Gauldie J, et al. Mechanical stress-induced mast cell degranulation activates tgf-beta1 signalling pathway in pulmonary fibrosis. *Thorax* 2019;74(5):455-465.
389. Abman SH, Sun X. Mechanistic insights into lethal lung developmental disorders: The rare informs the common. *Am J Respir Crit Care Med* 2019.
390. Gill SE, Pape MC, Leco KJ. Absence of tissue inhibitor of metalloproteinases 3 disrupts alveologenesis in the mouse. *Dev Growth Differ* 2009;51(1):17-24.
391. Ambalavanan N, Nicola T, Li P, Bulger A, Murphy-Ullrich J, Oparil S, Chen YF. Role of matrix metalloproteinase-2 in newborn mouse lungs under hypoxic conditions. *Pediatr Res* 2008;63(1):26-32.
392. Atkinson JJ, Holmbeck K, Yamada S, Birkedal-Hansen H, Parks WC, Senior RM. Membrane-type 1 matrix metalloproteinase is required for normal alveolar development. *Dev Dyn* 2005;232(4):1079-1090.

393. Joshi R, Liu S, Brown MD, Young SM, Batie M, Kofron JM, Xu Y, Weaver TE, Apsley K, Varisco BM. Stretch regulates expression and binding of chymotrypsin-like elastase 1 in the postnatal lung. *Faseb j* 2016;30(2):590-600.
394. Jesudason R, Black L, Majumdar A, Stone P, Suki B. Differential effects of static and cyclic stretching during elastase digestion on the mechanical properties of extracellular matrices. *J Appl Physiol (1985)* 2007;103(3):803-811.
395. Jesudason R, Sato S, Parameswaran H, Araujo AD, Majumdar A, Allen PG, Bartolak-Suki E, Suki B. Mechanical forces regulate elastase activity and binding site availability in lung elastin. *Biophys J* 2010;99(9):3076-3083.
396. Hilgendorff A, Parai K, Ertsey R, Juliana Rey-Parra G, Thebaud B, Tamosiuniene R, Jain N, Navarro EF, Starcher BC, Nicolls MR, et al. Neonatal mice genetically modified to express the elastase inhibitor elafin are protected against the adverse effects of mechanical ventilation on lung growth. *Am J Physiol Lung Cell Mol Physiol* 2012;303(3):L215-227.
397. Mao X, Said R, Louis H, Max JP, Bourhim M, Challande P, Wahl D, Li Z, Regnault V, Lacolley P. Cyclic stretch-induced thrombin generation by rat vascular smooth muscle cells is mediated by the integrin alphavbeta3 pathway. *Cardiovasc Res* 2012;96(3):513-523.
398. Trepat X, Puig F, Gavara N, Fredberg JJ, Farre R, Navajas D. Effect of stretch on structural integrity and micromechanics of human alveolar epithelial cell monolayers exposed to thrombin. *Am J Physiol Lung Cell Mol Physiol* 2006;290(6):L1104-1110.
399. Shin JY, Beckett JD, Bagirzadeh R, Creamer TJ, Shah AA, McMahan Z, Paik JJ, Sampedro MM, MacFarlane EG, Beer MA, et al. Epigenetic activation and memory at a tgfb2 enhancer in systemic sclerosis. *Sci Transl Med* 2019;11(497).
400. Blomme B, Deroanne C, Hulin A, Lambert C, Defraigne JO, Nusgens B, Radermecker M, Colige A. Mechanical strain induces a pro-fibrotic phenotype in human mitral valvular interstitial cells through rhoc/rock/mrtf-a and erk1/2 signaling pathways. *J Mol Cell Cardiol* 2019.
401. Guo T, Guo L, Fan Y, Fang L, Wei J, Tan Y, Chen Y, Fan X. Aqueous humor levels of tgfbeta2 and sfrp1 in different types of glaucoma. *BMC Ophthalmol* 2019;19(1):170.
402. Pelton RW, Dickinson ME, Moses HL, Hogan BL. In situ hybridization analysis of tgf beta 3 rna expression during mouse development: Comparative studies with tgf beta 1 and beta 2. *Development* 1990;110(2):609-620.
403. Diatchuk V, Lotan O, Koshkin V, Wikstroem P, Pick E. Inhibition of nadph oxidase activation by 4-(2-aminoethyl)-benzenesulfonyl fluoride and related compounds. *J Biol Chem* 1997;272(20):13292-13301.
404. Browe DM, Baumgarten CM. Angiotensin ii (at1) receptors and nadph oxidase regulate cl- current elicited by beta1 integrin stretch in rabbit ventricular myocytes. *J Gen Physiol* 2004;124(3):273-287.
405. Patel RK, Prasad N, Kuwar R, Haldar D, Abdul-Muneer PM. Transforming growth factor-beta 1 signaling regulates neuroinflammation and apoptosis in mild traumatic brain injury. *Brain Behav Immun* 2017;64:244-258.
406. Tanaka T, Saito Y, Matsuda K, Kamio K, Abe S, Kubota K, Azuma A, Gemma A. Cyclic mechanical stretch-induced oxidative stress occurs via a nox-dependent mechanism in type ii alveolar epithelial cells. *Respir Physiol Neurobiol* 2017;242:108-116.

407. Jahn HM, Kasakow CV, Helfer A, Michely J, Verkhratsky A, Maurer HH, Scheller A, Kirchhoff F. Refined protocols of tamoxifen injection for inducible dna recombination in mouse astroglia. *Sci Rep* 2018;8(1):5913.
408. Chen Q, Zhang H, Liu Y, Adams S, Eilken H, Stehling M, Corada M, Dejana E, Zhou B, Adams RH. Endothelial cells are progenitors of cardiac pericytes and vascular smooth muscle cells. *Nat Commun* 2016;7:12422.
409. Sheikh AQ, Misra A, Rosas IO, Adams RH, Greif DM. Smooth muscle cell progenitors are primed to muscularize in pulmonary hypertension. *Sci Transl Med* 2015;7(308):308ra159.
410. Gerl K, Miquerol L, Todorov VT, Hugo CP, Adams RH, Kurtz A, Kurt B. Inducible glomerular erythropoietin production in the adult kidney. *Kidney Int* 2015;88(6):1345-1355.
411. Kiermayer C, Conrad M, Schneider M, Schmidt J, Brielmeier M. Optimization of spatiotemporal gene inactivation in mouse heart by oral application of tamoxifen citrate. *Genesis* 2007;45(1):11-16.
412. Li M, Krishnaveni MS, Li C, Zhou B, Xing Y, Banfalvi A, Li A, Lombardi V, Akbari O, Borok Z, et al. Epithelium-specific deletion of tgf-β receptor type ii protects mice from bleomycin-induced pulmonary fibrosis. *J Clin Invest* 2011;121(1):277-287.
413. Hersh CP, Hansel NN, Barnes KC, Lomas DA, Pillai SG, Coxson HO, Mathias RA, Rafaels NM, Wise RA, Connett JE, et al. Transforming growth factor-beta receptor-3 is associated with pulmonary emphysema. *Am J Respir Cell Mol Biol* 2009;41(3):324-331.
414. Celedón JC, Lange C, Raby BA, Litonjua AA, Palmer LJ, DeMeo DL, Reilly JJ, Kwiatkowski DJ, Chapman HA, Laird N, et al. The transforming growth factor-beta1 (tgfb1) gene is associated with chronic obstructive pulmonary disease (copd). *Hum Mol Genet* 2004;13(15):1649-1656.
415. Bierie B, Moses HL. Transforming growth factor beta (tgf-beta) and inflammation in cancer. *Cytokine Growth Factor Rev* 2010;21(1):49-59.
416. Dong M, Blobe GC. Role of transforming growth factor-beta in hematologic malignancies. *Blood* 2006;107(12):4589-4596.
417. Piotrowski WJ, Kiszałkiewicz J, Pastuszak-Lewandoska D, Antczak A, Górski P, Migdalska-Sęk M, Górski W, Czarnecka K, Nawrot E, Domańska D, et al. Tgf-β and smads mrna expression in pulmonary sarcoidosis. *Adv Exp Med Biol* 2015;852:59-69.
418. Jenkins RG, Moore BB, Chambers RC, Eickelberg O, Konigshoff M, Kolb M, Laurent GJ, Nanthakumar CB, Olman MA, Pardo A, et al. An official american thoracic society workshop report: Use of animal models for the preclinical assessment of potential therapies for pulmonary fibrosis. *Am J Respir Cell Mol Biol* 2017;56(5):667-679.
419. Hershberger KA, Abraham DM, Liu J, Locasale JW, Grimsrud PA, Hirschey MD. Ablation of sirtuin5 in the postnatal mouse heart results in protein succinylation and normal survival in response to chronic pressure overload. *J Biol Chem* 2018;293(27):10630-10645.
420. Korecki AJ, Hickmott JW, Lam SL, Dreolini L, Mathelier A, Baker O, Kuehne C, Bonaguro RJ, Smith J, Tan CV, et al. Twenty-seven tamoxifen-inducible icre-driver mouse strains for eye and brain, including seventeen carrying a new inducible-first constitutive-ready allele. *Genetics* 2019;211(4):1155-1177.
421. Andersson KB, Winer LH, Mørk HK, Molkentin JD, Jaisser F. Tamoxifen administration routes and dosage for inducible cre-mediated gene disruption in mouse hearts. *Transgenic Res* 2010;19(4):715-725.

422. Sinha M, Lowell CA. Efficiency and specificity of gene deletion in lung epithelial doxycycline-inducible cre mice. *Am J Respir Cell Mol Biol* 2017;57(2):248-257.
423. O'Neal WK. Lung cell-specific cre deleter mouse strains: Going back to move forward. *Am J Respir Cell Mol Biol* 2017;57(2):149-150.
424. Hinz B. Masters and servants of the force: The role of matrix adhesions in myofibroblast force perception and transmission. *Eur J Cell Biol* 2006;85(3-4):175-181.
425. Cirka H, Monterosso M, Diamantides N, Favreau J, Wen Q, Billiar K. Active traction force response to long-term cyclic stretch is dependent on cell pre-stress. *Biophys J* 2016;110(8):1845-1857.
426. Ohata H, Aizawa H, Momose K. Lysophosphatidic acid sensitizes mechanical stress-induced ca2+ response via activation of phospholipase c and tyrosine kinase in cultured smooth muscle cells. *Life Sciences* 1997;60(15):1287-1295.
427. Mitani A, Nagase T, Fukuchi K, Aburatani H, Makita R, Kurihara H. Transcriptional coactivator with pdz-binding motif is essential for normal alveolarization in mice. *Am J Respir Crit Care Med* 2009;180(4):326-338.
428. Kim J, Kim YH, Kim J, Park DY, Bae H, Lee DH, Kim KH, Hong SP, Jang SP, Kubota Y, et al. Yap/taz regulates sprouting angiogenesis and vascular barrier maturation. *J Clin Invest* 2017;127(9):3441-3461.
429. Dupont S, Morsut L, Aragona M, Enzo E, Giulitti S, Cordenonsi M, Zanconato F, Le Digabel J, Forcato M, Bicciato S, et al. Role of yap/taz in mechanotransduction. *Nature* 2011;474(7350):179-183.
430. Mohri Z, Del Rio Hernandez A, Krams R. The emerging role of yap/taz in mechanotransduction. J thorac dis. China;2017. p. E507-e509.
431. Kononov S, Brewer K, Sakai H, Cavalcante FS, Sabayanagam CR, Ingenito EP, Suki B. Roles of mechanical forces and collagen failure in the development of elastase-induced emphysema. *Am J Respir Crit Care Med* 2001;164(10 Pt 1):1920-1926.
432. Xu B, Chen H, Xu W, Zhang W, Buckley S, Zheng SG, Warburton D, Kolb M, Gauldie J, Shi W. Molecular mechanisms of mmp9 overexpression and its role in emphysema pathogenesis of smad3-deficient mice. *Am J Physiol Lung Cell Mol Physiol* 2012;303(2):L89-96.
433. Gauldie J, Kolb M, Ask K, Martin G, Bonniaud P, Warburton D. Smad3 signaling involved in pulmonary fibrosis and emphysema. *Proc Am Thorac Soc* 2006;3(8):696-702.